Faculty of Science and Engineering
Department of Civil Engineering

Development of an Advanced Fatigue Model of a Cement-Treated Base Material Based on Continuum Damage Mechanics

Korakod Nusit

This thesis is presented for the Degree of
Doctor of Philosophy
of
Curtin University

December 2016

DECLARATION

To the best of my knowledge and belief this thesis contains no material previously published by any other person except where due acknowledge has been made.

This thesis contains no material which has been accepted for the award of any other degree or diploma in any university.

Signature: 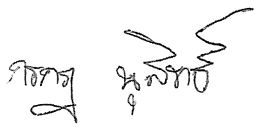

Date: December 2016

LIST OF PUBLICATION

The following publications have resulted from the works carried out for this degree.

Journal Papers

1. Nusit, K., Jitsangiam, P., Kodikara, J., Bui, H. H., & Leung, G. L. M., (2016). Advanced Characteristics of Cement-Treated Materials with respect to Strength Performance and Damage Evolution. *Journal of Materials in Civil Engineering*, 04016255. doi:10.1061/(ASCE)MT.1943-5533.0001772.

2. Jitsangiam, P., Nusit, K., Chummuneerat, S., Chindaprasirt, P., & Pichayapan, P., (2016). Fatigue Assessment of Cement-Treated Base for Roads: An Examination of Beam-Fatigue Tests. *Journal of Materials in Civil Engineering*, 04016095. doi:10.1061/(ASCE)MT.1943-5533.0001601.

3. Nusit, K., Jitsangiam, P., Kodikara, J., Bui, H. H., & Leung, G. L. M., (2015). Dynamic Modulus Measurements of Bound Cement-Treated Base Materials. *Geotechnical Testing Journal*, 38(3), 275-289. doi:10.1520/GTJ20140233.

Conference Papers

1. Nusit, K., & Jitsangiam, P., (2016). Damage Behaviour of Cement-Treated Base Material. *Procedia Engineering*, 143, 161-169.

2. Nusit, K., Jitsangiam, P., Kodikara, J., & Bui, H. H., (2015). Cyclic Loading Responses of Cement-Stabilised Base Materials: An Investigation on Moduli for Pavement Design. *The 12th Australia New Zealand Conference on Geomechanics*, Wellington, NZ, 22nd – 25th February.

3. Nusit, K., Jitsangiam, P., Nikraz, H., & Hewa Thalagahage, R. D., (2014). Dynamic Modulus Characteristics of Bound Cement-Treated Crushed Rock Base Course. *The International Conference on Advances in Civil Engineering for Sustainable Development*, Suranaree University of Technology, Thailand, 27th – 29th August.

DEVELOPMENT OF AN ADVANCED FATIGUE MODEL OF A CEMENT-TREATED BASE MATERIAL BASED ON CONTINUUM DAMAGE MECHANICS

ABSTRACT

The stabilisation of road pavement base or subbase materials is becoming a more common method of obtaining superior-performance in road pavement structures. In this research, conventional road base material is stabilised by adding Portland cement and compacting it at optimum moisture conditions to create Cement-Treated Base (CTB) material. In doing this, the strength and durability of road pavement structure can be significantly improved. However, recent literature has shown that there are still uncertainties around mechanistic-empirical design procedures for road pavement with CTB layers. Accordingly, this research aims to achieve improved CTB characterisation and design procedures, which could result in more economical application and greater reliability in the use of CTB materials. To achieve the objective, the characteristics of CTB material were examined through conventional and sophisticated testing platforms. The modified mix design framework was developed based on the strength performance of CTB to incorporate the effects of CTB mix proportion variation, which may be encountered during construction. The performance tests revealed that an appropriate amount of cement binder for CTB should stay within the soil-cement interaction zone of the strength development curve. The cyclic four-point bending test platforms and Asphalt Mixture Performance Tester (AMPT) were used to simulate traffic loading conditions. Consequently, the real responses of CTB in-situ can now be investigated using the aforementioned cyclic loading tests. The cyclic flexural modulus determined from the four-point bending test seemed to be very close to the dynamic modulus measured by the AMPT. However, specimen preparation for flexural tests is cumbersome and this may lead to inaccurate testing results. Accordingly, the dynamic modulus measured by the AMPT should be employed as a design parameter in mechanistic-empirical design for road pavement. Fatigue damage behaviour in CTB is characterised by using the testing protocols for

asphalt concrete and cement-treated material. The test results from both protocols revealed the existence of a fatigue endurance limit for CTB material. The fatigue endurance limit is the material property which indicates the tolerable level of applied stress or strain within the ranges of specified loading cycles. Finally, the fatigue damage evolution model of CTB was developed based on the framework of Continuum Damage Mechanics (CDM). The model was also calibrated with field fatigue damage which was tested by the Accelerated Loading Facility (ALF) from previous research. Therefore, material deterioration in the field under real traffic loads can now be explained using the damage characteristics of laboratory CTB. Moreover, field fatigue damage can be progressively monitored and forecast using the framework developed in this research.

ACKNOWLEDGEMENTS

I would like to thank the Australian Research Council (ARC) and the project partners of the Queensland Department of Transportation and Main Roads, IPC Global, Golders Associates and Hong Kong Road Research Laboratory (HKRRL) for their financial support of this research project, and their in-kind contributions are also gratefully acknowledged. I would also like to acknowledge the Royal Thai Government (RTG) for providing me with a scholarship to continue my Ph.D. at Curtin University.

I would like to express my deepest appreciation to my supervisor, Dr. Peerapong Jitsangiam, for his patience and guidance throughout this challenging journey. His encouragement and the opportunities provided by him make this thesis possible. I am also deeply thankful to my co-supervisor, Professor Hamid Nikraz, my associate supervisors, Professor Jayantha Kodikara, and Dr. Ha H. Bui, for their valuable comments, supports, and guidance throughout the course.

I appreciate Dr. Suphat Chummuneerat for his precious guidance on material testing, and his support and contributions to my publications. I wold like to extend my thanks to Arooran Sounthararajah, and Nhu Nguyen, for their time and effort in our research projects.

I thank all the technicians and staff at the Geomechanics laboratory who helped me in experimental work, in particular, Mark Whittaker and Darren Isaac. I also thank the administrative staff and secretary at the School of Civil and Mechanical Engineering for their support in administrative matters.

Special thanks to all my friends, Dr. Hyuk Lee, Pengloy Chow, Chi Zhang, and their family members, Dr. Pham Minh Thong, Dr. Suphat Chummuneerat, Sawitchaya Tippaya, Sarayoot Kumlai, and Dr. Pakdee Khobklang, for a wonderful time at Curtin University.

Finally, and perhaps most importantly, I thank my wife, my daughter, my parents, and my sister, who supported me to overcome every difficult task in my life.

TABLE OF CONTENTS

LIST OF FIGURES

LIST OF TABLES

CHAPTER 1

INTRODUCTION

1.1 Background

The construction of modern road pavement requires the use of superior performance road pavement materials. This is due to a significant increase in demand from the population and the fact that heavier and more frequent loads are being transported across regions. As such, more-effective road networks with a longer service life and less maintenance are required. One alternative option for enhancing road performance is the application of a cement-stabilisation technique to improve the engineering properties of the pavement base. The base consists of the layers underneath the pavement surface, such as asphalt or concrete, known as the base course and/or subbase course layers. Based on the technique, a substance known as Cement-Stabilised Base (CSB) or Cement-Treated Base (CTB) is used in a specific way in road pavement construction. The cement-stabilisation technique is already used in road construction, employing poorly-graded or sub-standard materials for the pavement base, due to well-graded materials being very expensive or unavailable. CTB is essentially a mixture of a standard road base material, a prescribed amount of cement (less than approximately 15% by mass of normal concrete), and water. The main objective in adding cement to a pavement base is to increase the strength of the road structure. In Australia, the stabilisation of pavement base using cement was introduced in the early 1950's and has been widely used since then. However, the ambiguous characteristics of these materials have led to further investigation. Y.S. Yeo (2011) reported a comprehensive review on cement-treated crushed rock base and its application in Western Australia. In his work, significant limitations around the cement-stabilised technique were found and summarised. These included ambiguous mechanistic classification, fatigue and shrinkage cracking problems, and in-situ-stabilised pavement bases which were not fully utilised. It can be summarised from Yeo's studies that cement is a major additive which is generally used to improve the properties of pavement base in Western Australia.

In Australia, CTB material is normally categorised by the degree of binding substances it contains. Therefore, it can be classified into:

(1) Modified or unbound CTB, in which a small amount of cement is added to the mixture to improve its moisture sensitivity and strength, and

(2) Stabilised or bound CTB, where the aim is to obtain improved performance (e.g. tensile strength resistance) in the road base material by adding a greater amount of cement.

In addition to the amount of the additive substance, the Unconfined Compressive Strength (UCS) of the cylindrical sample, and the modulus of elasticity are used in Australia as classification parameters. However, the delineation point between unbound and bound pavement bases is still unclear. This classification issue is of fundamental importance, as it provides guidelines to the designers as to the performance and behaviour of the material.

The conventional mix design for CTB materials is usually based on the trial-and-error method. The percentage of cement content per dry weight of parent material (e.g. crushed rock, aggregate, sand) is initially assigned according to the design guideline's recommendations. The Optimum Moisture Content (OMC), which is specified as the designed amount of water to use for the CTB mixture, is then determined from the compaction test. At a later stage, the compacted CTB specimens, prepared using the amount of water at OMC and cured for a specific duration, are tested to find the UCS. The cement content of the CTB material can then be designed based on the strength and durability criteria suggested by the design guidelines. A single set of design values of cement content and water content is commonly provided by the mix design process. However, the amount of water and cement employed in the field usually fluctuates around the design values. The variations in mix proportion certainly influence the performance of road structures. Yet, the effects of the variation in mix proportion are not always properly considered during the mix design process for CTB materials. Therefore, the long-term performance of road pavement cannot realistically be forecast using the design values determined by the conventional mix design process.

Despite improving the structural performance of road pavement, CTB has also been plagued by problems in its field application. Shrinkage cracking that generally occurs during the hardening process of CTB layer is unavoidable. The shrinkage cracks may propagate to the asphalt surface and consequently cause a reduction in the road's structural performance. Some problems associated with CTB characteristics have previously been addressed by some researchers. The behaviour of CTB associated with shrinkage cracking was previously investigated by George (1990) and Kodikara and Chakrabarti (2001). Furthermore, road distress relating to durability and the loss of the surface integrity of CTB layers was examined by Wen et al. (2014) and Li, Metcalf, Romanoschi, and Rasoulian (1999), respectively. De Beer (1990) and Li et al. (1999) studied the fatigue behaviour of CTB layers based on information obtained from laboratory and full-scale accelerated loading tests.

Stabilised CTB is a stiff material which experiences fatigue failure under repeated loading. Unbound pavement base however, is secured from fatigue failure, but it possesses limited strength and low stiffness which can lead to excessive deformation as its failure mode. Accordingly, the fatigue-life of CTB needs to be addressed during the design period to maximise the potential use of such material. Fatigue failure is one of the most significant problems in stabilised pavement base. Typically, fatigue failure is defined as material failure caused by damage accumulated under cyclic loading. To date, most of the fatigue models for cement-treated base have been developed based on empirical formulations. The "*fatigue life*", or a certain number of load cycles to failure is commonly estimated from these empirical formulations and used in the serviceability design. However, high uncertainty around the predicted fatigue life is often encountered due to the common limitations in empirical formulations. It can be said that the fatigue behaviour of CTB is complicated by, and not well-explained, using top-down empirical models. Therefore, bottom-up constitutive equations for CTB are preferable for a precise prediction of fatigue life and a better understanding of fatigue behaviour.

To design a road pavement with CTB, the estimated fatigue life from empirical formulations is usually multiplied by the "*shift factor*" to obtain the service lifetime of road pavement. The shift factor is comparable to the bias factor which incorporates all the sources of uncertainty encountered during the construction of the road pavement.

Nevertheless, the fatigue damage development of field CTB cannot be forecast by employing a single shift factor. The damage development of field CTB under traffic loading conditions provides more accurate information to pavement engineers. This because the performance of in-situ road pavement can be monitored using damage development trends under progressive traffic loads. However, this information is rarely available during the design period and not well forecast using a single shift factor.

Besides the limitations of the cement-stabilised technique reported by Y.S. Yeo (2011), it can be seen that there is still uncertainty around the mix design framework and performance prediction model for CTB materials. This study aims to examine the engineering characteristics and damage characteristics of CTB materials to gain more understanding of the material's performance. Accordingly, the gaps in knowledge should be filled, allowing CTB to be fully utilised in the field with confidence.

1.2 Objectives and Scope

This research focuses on the development of the fatigue damage evolution model for CTB utilising extensive and intensive theoretical and experimental studies to overcome the shortcomings of the currently used fatigue model for pavement design and analysis. The research aims to achieve improved CTB characterisation and design procedures, which should result in economical application and highly reliable use of CTB materials. Therefore, the research objectives are to:

(1) Evaluate the basic geotechnical and mechanical properties of CTB through fundamental and sophisticated laboratory testing.

(2) Investigate the parameters influencing the performance of CTB, e.g. mix-proportion, curing time, gradation of parent materials, and loading rate (frequency).

(3) Suggest a simple method for CTB mix design which incorporate the effects of variation in influential parameters.

(4) Characterise the dynamic behaviour of CTB materials to understand the dynamic responses of CTB under traffic loading conditions. Therefore, the appropriate parameters representing the dynamic responses of CTB can be recommended and implemented into road pavement design guidelines.

(5) Evaluate the fatigue damage behaviour of CTB materials based on the Continuum Damage Mechanics (CDM) framework. This would allow the fatigue damage characteristics of CTB tested in the field and the laboratory to be characterised and compared.

(6) Develop a fatigue life estimation framework based on the damage characteristics of CTB materials.

1.3 Significance

This research is scientifically significant as it conducted a comprehensive investigation into CTB materials. The aim of the research is to reduce the costs of pavement design and construction. As mentioned earlier, the recent mix design process for CTB materials has been performed based on the trial-and-error method. Accordingly, a single set of mix proportions is always reported by the conventional mix design process. However, the mix proportion in the field may fluctuate due to various factors during the construction. The variation in the in-situ mix proportion may affect the performance of the road pavement structure. Therefore, it is necessary to incorporate the influences of field variation in the mix design of CTB materials.

In this research, traffic loading conditions will be simulated in the laboratory, using both conventional and sophisticated tests. The main objective of these tests is to determine the design parameters which represent material responses under traffic loading conditions. It is understood that the responses of cement-treated materials are influenced by loading characteristics, i.e., loading mode, and loading rate or frequency. Accordingly, the appropriate design parameters should be employed for road pavement design based on the mechanistic approach.

A more reliable fatigue damage model for CTB materials will be developed in this research with the aim of benefiting the road and highway construction industry across Australia. Most of the recent fatigue damage models have provided only the fatigue life of road pavement structures. However, the development or evolution of fatigue damage with respect to an increase in the number of traffic loading cycles is of fundamental importance. The performance of road structures can be examined and evaluated throughout their service lifetime using damage evolution characteristics. This will be a highly significant contribution to road pavement rehabilitation plans.

The characteristics and performance of CTB materials for road pavement structures will be examined in this research. The goal is to generate more accurate guidelines to produce an effective mix design framework and improved mechanistic design procedures for CTB materials. Specific focus will be given to producing:

- a more effective mix design framework which incorporates the variation in influencing parameters, i.e., cement content, compacted moisture content, and compacted density,

- an appropriate design parameter which represents the intrinsic response of CTB materials under traffic loading conditions,

- measures of fatigue damage behaviour, along with the damage evolution of CTB material under traffic loading conditions based on the CDM framework,

- a framework to forecast the fatigue damage behaviour and performance of road pavement structures with CTB layers.

1.4 Methodology

Figure 1.1 presents the project methodology overview which comprises the study of basic geotechnical properties of parent material, mechanical characterisation of CTB materials, and examination of CTB performance.

In this research, conventional Crushed Rock Base (CRB) manufactured by a local pit in Western Australia will be used as the parent material for cement-treated road base. The basic properties and engineering properties of CRB will be investigated in the first stage. In the second stage, the mechanical characteristics of CTB materials will be examined. The tests in the second stages are made up of compaction tests, strength tests, shrinkage tests, and tests to investigate the effects of gradation and of the fines content of parent materials on the strength performance of CTB. To fulfil the objectives of this research, the performance tests will be conducted in the third stage. The performance tests can be divided into two categories as follows:

(1) Monotonic loading tests

The strength performances of CTB materials will be initially investigated using monotonic loading tests. Unconfined Compressive Strength (UCS) tests will be employed to determine the compressive strength of CTB materials. The tensile strength of CTB materials will be indirectly measured using the four-point bending test.

(2) Cyclic loading tests

The appropriate design parameters representing the dynamic responses and the fatigue behaviour of CTB materials will be examined using cyclic loading tests. The dynamic modulus of CTB materials will be evaluated by the Asphalt Mixture Performance Tester (AMPT). The cyclic four-point bending tests will be used to determine the dynamic flexural modulus, fatigue life, and fatigue damage characteristics of CTB materials.

The performance tests in this research should deliver three main findings.

(1) Modified mix design framework

The modified mix design framework for CTB materials will be developed based on the strength performance (UCS) of test specimens. The variations in mix proportion, i.e., cement content and moisture content, and the compacted dry density of the specimens will be considered in the proposed mix design framework. CTB specimens prepared from various mix proportions and cured for different durations will be tested using the conventional UCS test.

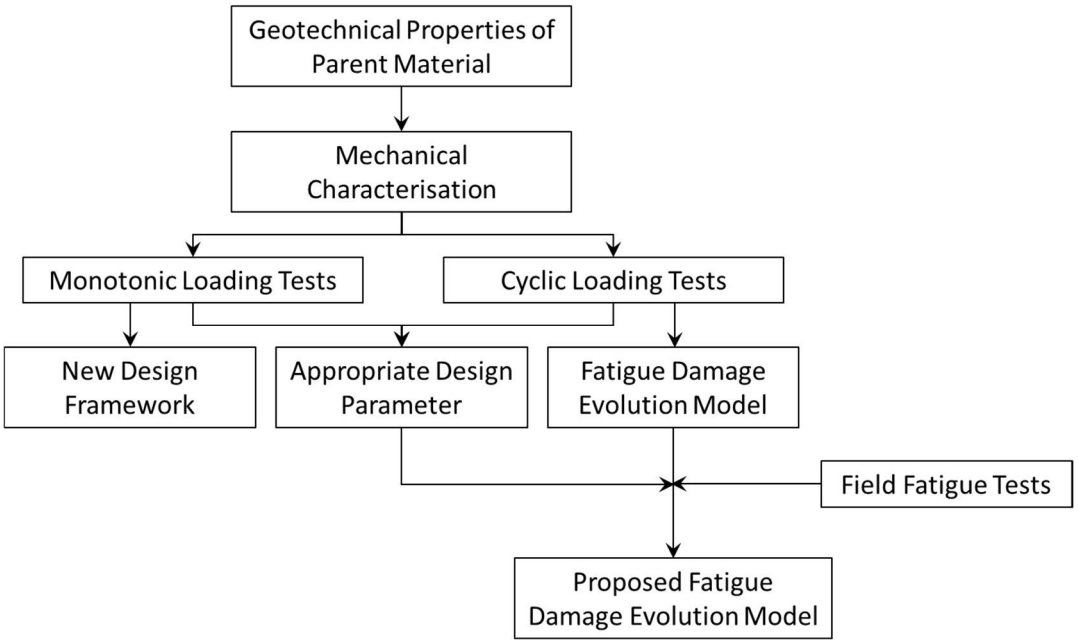

Figure 1.1: Research methodology

(2) Appropriate design parameters represent the dynamic responses of CTB

The design parameters representing the dynamic responses of CTB materials under traffic loading conditions will be determined from the results of both monotonic loading tests and cyclic loading tests. Initially, the behaviour of cylindrical specimens tested under a static loading rate and a dynamic loading rate will be examined using conventional UCS tests. The AMPT will then be employed to characterise the dynamic responses of cylindrical specimens. Finally, the dynamic bending responses of beam specimens will be measured using cyclic four-point bending tests. The effects of cement content, curing time, and loading rate (frequency) on the material responses will also be characterised by these tests.

(3) Fatigue damage evolution model

The main laboratory test in this section consists of the cyclic four-point bending test. Firstly, the fatigue life of the beam specimens will be determined based on stress-controlled and strain-controlled fatigue tests. The influences of applied loading level, applied displacement magnitude, cement content, and applied frequency will be examined. Secondly, the fatigue damage development of CTB specimens under cyclic loading conditions will be

characterised. The damage development of in-situ CTB layers will then be compared with the damage development characterised from the CTB specimens. The objective of these comparisons is to develop a fatigue damage evolution model which can forecast in-the-field damage using laboratory test results. Lastly, a fatigue damage evolution model for road pavement structures with CTB layers will be proposed.

1.5 Thesis organisation

This thesis comprises seven chapters. Chapter 1 provides the overview of the thesis, which includes research background, objectives and scope, significance of the research, and research methodology. Chapter 2 summarises recent developments, designs, and applications of cement-stabilised or cement-treated materials for road pavement construction projects. At the beginning of Chapter 2, the definition of CTB assigned by different road pavement design guidelines is summarised. The possible failure modes of road pavement constructed with CTB layers and mechanical characteristics of CTB are then provided. A comparison of design procedures implemented in different road pavement design guidelines is also given in Chapter 2. Recent developments in service lifetime prediction models for road pavement structures are included in this comparison. In addition, basic knowledge around Continuum Damage Mechanics (CDM) framework is discussed. At the end of Chapter 2, the performance of in-situ CTB layers investigated in previous literature is also highlighted. Chapter 3 provides information on the geotechnical properties of parent materials and the mechanical characteristics of CTB. The mechanical properties characterised in Chapter 3 include compressive strength, flexural strength (indirect tensile strength), and shrinkage behaviour of CTB materials. Moreover, the effects of fines content and gradation of parent material on the strength performance of CTB is investigated. Chapter 3 also includes the development of procedures for a modified mix design framework for CTB materials. The influence of loading rate on the performance of CTB materials is characterised in Chapter 4. The dynamic responses of CTB materials investigated using the AMPT and the cyclic four-point bending tests are summarised in this chapter. The analysis results in Chapter 4 deliver the design parameters which represent the dynamic responses of CTB materials under traffic

loading conditions. Chapter 5 summarises the test results from the cyclic four-point bending tests. In this chapter, the cyclic four-point bending tests are conducted based on two different test platforms. Accordingly, the long-term behaviour and fatigue life of CTB materials under cyclic loading regime are provided. The material responses under cyclic loading conditions are, therefore, used to develop the fatigue damage evolution model in Chapter 6. The developed model is then calibrated using the damage evolution of in-situ CTB layers in road pavement structures. Finally, the thesis conclusion and recommendations for future research are given in Chapter 7.

CHAPTER 2

CEMENT-TREATED MATERIALS FOR ROAD PAVEMENT

This chapter provides the background to cement-treated materials for road pavement, along with current knowledge, and all with regard to the available literature. The applications and classifications of cement-treated materials are explained in the first section. Following this, the possibly observed distress modes of road pavement with a cement-treated base or subbase are illustrated in Section 2.2. Section 2.3 provides the available definitions and tests required for measuring the mechanistic and engineering characteristics of cement-treated materials. These include strength, modulus, Poisson's ratio, dynamic response, and mix design of cement-treated materials. In Section 2.4, the design concept for road pavement with cement-treated layers is briefly explained. Established fatigue models for the service-life estimation of road pavement with cement-treated layers are also presented in this section. In addition, fatigue models developed in different areas around the world, and the parameters required for the models' input, are provided. Finally, the Continuum Damage Mechanics (CDM) concept and the in-field performance of cement-treated layers are illustrated in Sections 2.5 and 2.6.

2.1 Cement-treated materials for road pavement

Cement-treated materials are the products of a soil-cement stabilisation technique for creating a superior road base or subbase material in pavement. They could be theoretically categorised as fully-bound (stabilised) materials, which generally have much better tensile resistance than general-use road base material or unbound granular material (i.e., insignificant tensile-resistant material) (Austroads, 2006b). Roller-Compacted Concrete (RCC) is not classified as cement-treated material, since the engineering properties of RCC are similar to concrete and a higher percentage of cement content is usually required for RCC (Arellano & Thompson, 1998; Thompson, 2001).

This research focuses on cement-bound or stabilised crushed-rock base, classified according to Austroads (2006b). Terminology and classification may change depending on the country being studied (Arellano & Thompson, 1998). In Europe, particularly the United Kingdom (UK), road base material stabilised with various kinds of binder, e.g. lime, fly ash, and cement, is termed Hydraulically Bound Material (HBM). In the US, this group of road base materials is known as cementitiously-stabilised material (Wen et al., 2014). In South Africa, it is called cementitious-stabilised material (SANRAL, 2013). The cement-stabilised crushed rock in this study is comparable to Cement Bound Granular Mixture (CBGM) (Highways Agency, 2009), particularly in the UK, cement-bound base (Shahid, 1997). However, the term cement-stabilised granular has been commonly used in the US (Wen et al., 2014) and South Africa (SANRAL, 2013).

2.1.1 Applications of cement-treated materials

The main aim of the cement-stabilisation technique for road pavement is to increase the strength of the structure of a road, allowing it to withstand more severe traffic and environmental conditions. Y. S. Yeo (2011), reported on a comprehensive review of cement-treated crushed rock base course and its applications in Australia. From this work, significant limitations of cement-treated crushed rock base course were summarised. The summary included ambiguous mechanistic classification, fatigue and shrinkage cracking problems, and in-situ stabilised pavement base course which was not fully utilised to maximize the effective use of the stabilisation technique.

According to Croney and Croney (1998), cement-treated materials can be categorised into three groups based on their applications, which are: (1) soil-cement for the subbase or capping layer, (2) cement-bound granular materials, and (3) lean concrete. It was highlighted by the authors that the soil-cement technique is unnecessary for sandy gravel soil in the UK, as sandy gravel usually has enough strength to be employed as a road subbase layer. Croney and Croney (1998) mentioned that the hand-laid technique is suitable for the application of cement-bound granular materials such as, i.e., the subbase layer. However, a mechanical paver is necessary where cement-bound granular material is employed as the road base layer. The latest update on the

applications of Soil treated by Cement (SC) and Cement Bound Granular Mixture (CBGM) according to UK specifications can be found in Highways Agency (2009).

In South Africa, the aforementioned stabilised material is considered appropriate for use in both base and subbase layers of road pavement (SANRAL, 2013). The suitability of stabilised materials as base or subbase layers is determined based on the type of pavement structure and the required structural capacity (the amount of load repetition calculated in the design).

2.1.2 Categories of cement-treated materials

Cement-treated material is usually classified according to its material performance after treatment. The classification procedure is important in terms of providing guidelines to designers for the selection of the appropriate material for its intended purpose, particularly with regard to performance (Y. S. Yeo, 2011). In Australia, Cement-Treated Base (CTB) can be classified as shown in Table 2.1 (Austroads, 2006b, 2013b). Bound or stabilised CTB is a relatively stiff material which is prone to fatigue deterioration to the point of failure under repeated traffic loading. Unbound pavement base, although not subject to fatigue failure, possesses limited strength and a low modulus which can lead to excessive deformation, resulting in pavement rutting, such is its failure mode. Note that Table 2.1 is a modified version of Austroads (2006b), proposed by Austroads (2013b). The CTB categorised by Australian regional classification criteria can be found in Y. S. Yeo (2011).

In South Africa, cement and hydrated lime are the most common types of binder (SANRAL, 2013) for cement-treated materials. Apart from strength as a marker of stabilised materials, the material class and the engineering properties of the parent material are also employed as classification criteria, as shown in Table 2.2. According to SANRAL (2013), G2 - G3 are categorised as graded crushed stone, while G4 - G6 are in the group of natural gravels. C1 - C2 are classified as cemented crushed stone or gravel, and C3 - C4 are cemented natural gravels. Some South African road authorities also employ indirect tensile strength and a wet-dry durability index as classification criteria.

Table 2.1: Classification of cement-treated materials in Australia (Austroads, 2013b)

Category	Strength criteria	Performance attributes
Modified	UCS < 1 MPa	Improve moisture sensitivity and strength
Bound	UCS > 2 MPa	Obtain better performance, e.g., tensile strength resistance

Note

- UCS is Unconfined Compressive Strength of test specimens.
- UCS values determined from specimen compacted at Optimum Moisture Content (OMC) to 100% standard Maximum Dry Density (MDD), moist cured for 28 days.
- Bound material is submerged in water for 4 hours prior to the UCS test.
- Modified material can be tested without soaking.

Table 2.2: Classification of cement-treated materials in South Africa (SANRAL, 2013)

Class	Parent materials				Stabilised materials	
	Class	Crushing strength	FI	Sand equivalent	UCS (MPa)	PI
C1	G2	ACV (max) 29% 10% FACT (min) 110 kN	Max 35%	Max 30%	6 ≤ UCS ≤ 12	N.A.
C2	G2/G3/G4	ACV (max) 29% 10% FACT (min) 110 kN	Max 35%	Max 30%	3 ≤ UCS ≤ 6	N.A.
C3	G5/G6	N.A.	N.A.	N.A.	3 ≤ UCS ≤ 1.5	Max 6
C4	G5/G6	N.A.	N.A.	N.A.	1.5 ≤ UCS ≤ 0.75	Max 6

Note

ACV:	Aggregate Crushing Value
10% FACT:	10% Fines Aggregate Crushing Value
FI:	Flakiness index
Sand equivalent:	For any sand added to correct the grading
UCS:	Unconfined Compressive Strength at 100% MDD, cured for 7 days
PI:	Plasticity Index
Max:	Maximum value
Min:	Minimum value
N.A.:	Not applicable

According to the Highways Agency (2009), Cement Bound Granular Mixture (CBGM) is a sub-category of Hydraulically Bound Material (HBM) for road

pavement. In the UK, the qualities of parent materials are preliminarily employed as classification criteria. Therefore, CBGM can be classified as CBGM A, CBGM B, and CBGM C (Highways Agency, 2009). These CBGMs can be categorised further based on (1) compressive strength, and (2) tensile strength and modulus of elasticity (BS, 2004b). The strength and modulus employed as UK classification parameters are the values obtained from 28-day specimens. The CBGM categorised according to compressive strength comprises eight groups: C0, C1.5/2, C3/4, C5/6, C8/10, C12/15, C16/20, and C20/15; the letter C representing the CBGM. The first number in the group indicates the 28-day strength (MPa) of a cylindrical specimen with a height to diameter ratio (H/D) equal to two; while the latter is the 28-day strength of cylindrical or cube specimens with H/D varying from 0.8 to 1.21. On the other hand, five groups of CBGM are classified based on tensile strength and modulus of elasticity according to BS (2004b); these are T1, T2, T3, T4, and T5. After the category of CBGM has been specified, e.g. CBGM B – C8/10 (or T3), the design thickness of CBGM layers for road structure can subsequently be determined from the design charts recommended by the Highways Agency (2006).

In the US, Wen et al. (2014) recommended the employment of the 7-day Unconfined Compressive Strength (UCS) of 1.38 MPa (200 psi) as the delineation line between lightly stabilised materials and heavily stabilised materials (See Table 2.3). However, PCA (1992) recommended a minimum 7-day strength of 2.07 MPa (300 psi) for the mix design criteria of cement-treated materials. Another recommendation for the minimum 7-day strength was that it be equal to 5.17 MPa (750 psi) for flexible road pavement (NCHRP, 2004). This is the same criteria specified by the Department of the Army; the Navy and the Air Force (1994).

2.2 Distress modes of road pavement with stabilised layers

In this section, the possible distress modes of road pavement with cement-treated layers are highlighted. Generally speaking, the cracks in pavement layers which are generated by traffic loads tend to reduce the performance of road pavement structures. The failure of one pavement layer may also cause distress in other layers. Consequently, the performance or service life of the road pavement is rapidly reduced.

Therefore, an understanding of the material's characteristics and its possible distress modes is necessary prior to engineers designing any road pavement with a cement-treated layer. In this chapter, "*stabilised materials*" refer to the materials used for road pavement prepared from various types of binder.

Table 2.3: Classification of cement-treated materials in the US (Wen et al., 2014)

Category	UCS	Mixture examples
Lightly stabilised materials	< 1.38 MPa	Sand treated with cement lower than 5%.
Heavily stabilised materials	≥ 1.38 MPa	Gravel treated with 3% cement and higher, Sand treated with 5% cement and higher, Silt treated with 8% cement and higher, Clay treated with 10% cement and higher.
Note: • 7-day UCS • Mixture examples were obtained from Wen et al. (2014)		

2.2.1 Shrinkage cracking

Shrinkage of concrete consists of autogenous shrinkage, drying shrinkage, and thermal shrinkage (Wen et al., 2014). This assumption is also valid for concrete-like materials such as cement-treated materials. Autogenous shrinkage is caused by the hydration process; while the loss in moisture and change in temperature are the main sources of drying shrinkage and temperature shrinkage, respectively. However, autogenous shrinkage is characterised as drying shrinkage in some literature (Y. S. Yeo, 2011). For pavement structure where a cement-treated layer is overlaid by an asphalt layer, cracks may occur and can be observed on the asphalt surface. This is usually due to the unequal movement of the two layers during the drying process. For thin asphalt surfaces with a cement treated layer underneath, block cracking is usually encountered (Wang, 2013). Block cracking usually originates from the shrinkage of the cement-treated layer and later extends to the asphalt surface. The shrinkage of cement-treated layers is influenced by many factors, i.e., moisture in-the-field, binder content, curing time, characteristics of parent material, fines content, and degree of compaction (Chakrabarti & Kodikara, 2005; George, 2002; van-Blerk & Scullion, 1995).

Moreover, a compaction moisture content higher than the OMC is also the reason for excessive shrinkage cracking of cement-treated layers (George, 1990).

It is known that shrinkage behaviour in cement-treated materials is inevitable, and therefore, mitigation methods are necessary (Y. S. Yeo, 2011). Examples of mitigation methods are: (1) specifying adequate amounts of binder content, (2) employing special binders, (3) designing construction and curing techniques, and (4) altering the physical factors (Adaska & Luhr, 2004; Cho, Lee, & Ryu, 2006; George, 2002).

Chummuneerat (2014) undertook tests on the drying shrinkage behaviours of cement-treated crushed rock in Western Australia. The shrinkage tests, according to AS 1012.13 (Standard Australia, 1992) indicated that the drying shrinkage of 4%, 5%, and 6% cement specimens reached 80% of their maximum values after 21 days of drying. The rise in the percentage of drying shrinkage was insignificant after 90 days of drying. The drying shrinkage of 4% cement specimens was found to be smaller than the drying shrinkage of other specimens where the cement content varied from 2% - 5%.

Wen et al. (2014) conducted comprehensive tests in the US on the shrinkage characteristics of cement-treated materials. The thermal strain, drying shrinkage strain, and other relevant parameters were determined from laboratory studies. Accordingly, efficient mathematical equations were developed for estimating the shrinkage spacing and shrinkage crack width of cement-treated layers.

2.2.2 Bottom-up fatigue cracking

There are two types of fatigue cracking that can be observed from a stabilised pavement layer in the field, i.e., bottom-up and top-down fatigue cracking (Wen et al., 2014). Bottom-up fatigue cracking is caused by the tensile strain at the bottom of a stabilised layer exceeding its breaking strain. Tensile strain is generally produced by repeated traffic loads on top of pavement structures. Little, Scullion, Kota, and Bhuiyan (1995) discovered that bottom-up fatigue failure is usually observed in a thin layer of heavily stabilised base. Further information on this phenomenon is provided later in this chapter.

2.2.3 Top-down fatigue cracking

Top-down fatigue cracking, or crushing fatigue occurs due to the compressive strain at the top of a stabilised layer exceeding its tolerable limit (De Beer, 1990). The crushing failure on top of a stabilised layer may lead to the rutting distress of an asphalt pavement layer. This type of distress mode is typically observed in relatively thick and lightly stabilised layers. The present top-down fatigue model is available in SANRAL (2013) and in research by Wen et al. (2014).

2.2.4 Reflective cracking

For asphalt pavement with stabilised base layers, reflective cracks on the asphalt surface may be initiated by cracks in the stabilised base layers (Adaska & Luhr, 2004; Wen et al., 2014; Y. S. Yeo, 2011). According to Adaska and Luhr (2004), the following three conditions must be met for reflective cracks to appear on the asphalt surface;

- The crack width in the stabilised base layer must be wide enough to induce stress concentration at the bottom of the asphalt layer,
- A mitigation method to prevent the induced stress concentration is not available, and
- The asphalt layer is thin and brittle enough for the cracks to propagate through the surface.

Wen et al. (2014) researched reflective cracking modes observed from asphalt road pavement with stabilised-base layers. Their comprehensive reviews of previously existing literature showed that the shrinkage cracking in a stabilised base layer is the cause of block cracking and transverse cracking occurred on the asphalt surface. Longitudinal cracks along the wheel path may be observed on the asphalt surface if the stabilised based layer fails from top-down fatigue. Bottom-up fatigue cracking of a stabilised base layer leads to the forming of alligator cracks. To date, a reflective cracking prediction model for pavement with a stabilised base layer is still unavailable (Wen et al., 2014).

2.2.5 Deterioration of stabilised materials

Changes in environmental conditions, i.e., freeze-thaw and wet-dry, usually affect the performance of stabilised materials. Wen et al. (2014) conducted comprehensive tests to investigate the effects of freeze-thaw and wet-dry cycles on laboratory-prepared specimens. The test results indicated that the strength and modulus of stabilised material is significantly reduced due to freeze-thaw and wet-dry cycles (Su, 2012; Wen et al., 2014). Moreover, the UCS test of stabilised specimens obtained from sites revealed that strength of the stabilised materials was reduced by 10% from its original strength after 7 years of service (Wen & Ramme, 2008). According to the mix design guidelines for cement-stabilised materials, durability tests (Department of the Army; the Navy and the Air Force, 1994; PCA, 1956) and swell and erodibility tests (Austroads, 2006b) must be compulsory in design. The prediction models for strength reduction caused by freeze-thaw and wet-dry cycles were developed and provided by Wen et al. (2014).

2.3 Mechanical and engineering characteristics of cement-treated materials

In this section, the literature relating to properties of cement-treated materials which relate to and influence the behaviours of road pavement structure is examined.

2.3.1 Strength of cement-treated materials

The first section of this chapter showed that UCS is usually employed as the classification index for cement-treated material. However, the UCS obtained from monotonic compression tests alone may not accurately represent the field performance of the materials. This is because the cement-treated layers of a road structure are usually subjected to repeated traffic loads. In addition, there are other aspects of strength parameters of cement-treated material to be considered. These have been examined and investigated in previous literature and include flexural strength (modulus of rupture), indirect tensile strength, and direct tensile strength.

UCS

The UCS test for cement-treated materials is usually performed on specimens in a saturated state. As such, the test specimens must be submerged in water for 4 hours

prior to the beginning of the test (ASTM, 2000; Standard Australia, 2008b). A 7-day strength period is required by the material classification system in the US and South Africa. However, in Australia and the UK, a 28-day strength period is employed. Figure 2.1 illustrates a UCS test on a cement-treated crush rock specimen. During a UCS test, load and displacement are continuously monitored until the maximum load is reached. Accordingly, the UCS of the test specimen can be calculated as shown in Eq. 2.1.

$$UCS = \frac{P}{A} \tag{2.1}$$

in which, P is the maximum applied load, and A is the cross-sectional area of the test specimen.

The UCS test is the simplest of the strength parameter tests and is used by most road authorities. However, the simplicity of the test does not allow for the effective simulation of the responses of materials in the field. It should be highlighted that cement-treated materials in the field usually fail due to tension (Y. S. Yeo, 2011). However, a direct tension test is difficult to perform. Accordingly, the UCS test is still extensively employed as the index parameter for cement-treated material. Numerous studies have attempted to correlate the UCS with other strength parameters, particularly the tensile strength parameter. Arellano and Thompson (1998) and Shahid (1997) reviewed past literature that correlated the UCS of cement-treated materials with other strength parameters, i.e., flexural strength, indirect tensile strength, and direct tensile strength. Recent studies have focused on the relationship between UCS and flexural strength (Arulrajah, Disfani, Haghighi, Mohammadinia, & Horpibulsuk, 2015; Disfani, Arulrajah, Haghighi, Mohammadinia, & Horpibulsuk, 2014; Wen et al., 2014). Wen et al. (2014) established relationship equations between UCS and splitting tensile strength (indirect tensile strength). The estimation equation for the direct tensile strength of cement-treated material based on UCS values was developed by Shahid (1997). Mohammadinia et al. (2015) have also reported on the relationship between UCS and the secant modulus at 0.5 × UCS of cement-treated specimens prepared from construction and demolition (C&D) materials. Additional relationship equations

between the UCS, static modulus, and the dynamic modulus of cement-treated recycled materials can be found in Xuan (2012).

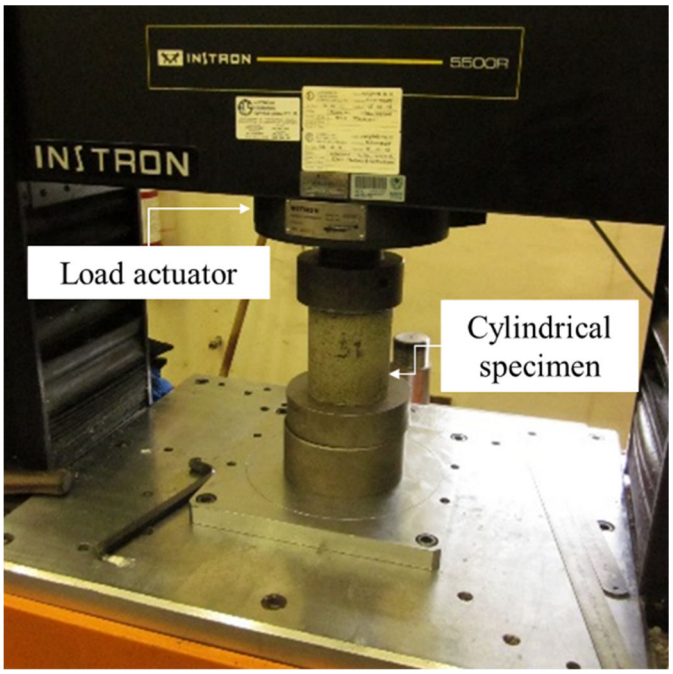

Figure 2.1: The UCS test of a cement-treated crush rock specimen

Direct tensile strength

Shahid (1997) established a relationship between the fatigue life of cement-treated materials and their direct tensile strength. His laboratory test results revealed that the tensile strength measured from the direct tension test (direct tensile strength) was more reliable than the tensile strength obtained from the splitting test and the beam bending test (indirect tensile strength). This is due to the fact that the tensile strength results achieved from the splitting test and the beam bending test make a great deal of assumptions. Moreover, stress distribution occurring in the splitting test and beam bending test specimens is usually complex. However, the direct tensile test also has limitations (Neville, 1998; Planas, Guinea, & Elices, 1992; Reinhardt, Cornelissen, & Hordijk, 1986; Wen et al., 2014). The two major limitations of the direct tensile test are: (1) the application of uniform tension force to the test specimen is difficult, and (2) high stress concentration is hard to avoid at the specimen grips (Neville, 1998). The indirect measurement of tensile strength is therefore preferable (Planas et al., 1992). Figure 2.2 illustrates the direct tension test for cement-treated materials, as designed by Shahid (1997). Shahid (1997) also established a relationship between the

direct tensile strength of cement-treated materials and the flexural strength, splitting strength, and compressive strength measured from both cube and cylindrical specimens.

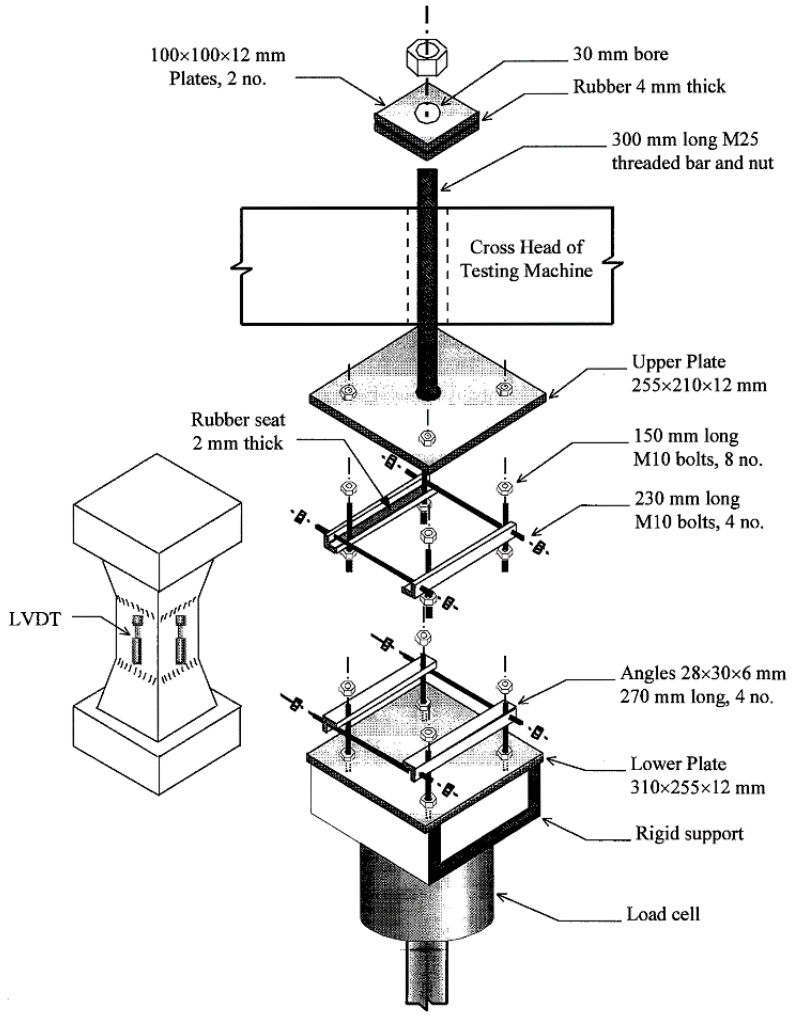

Figure 2.2: Direct tension test for cement-treated materials (Shahid, 1997)

Splitting tensile strength

The first indirect measurement method for tensile strength shown in this section is the splitting method. Wen et al. (2014) developed the splitting tensile strength testing protocol for cement-treated material based on an Australian method (Austroads, 2008a). Note that in the original literature, Wen et al. (2014) defined the splitting test as an Indirect Tensile Strength (IDT) test. The four-point bending test mentioned in Austroads (2008a) was termed the "*simple beam with third-point loading test"* by Wen

et al. (2014). Figure 2.3 shows the configurations of the splitting tensile strength test. During the test, a cylindrical specimen (Figure 2.3a) is loaded with compressive load strips located on the opposite side, across the centre of the specimen (Figure 2.3b). The compressive loads are increased until the specimen is split into two semi-cylindrical pieces along the loading plane. Accordingly, the splitting tensile strength can be calculated from Eq. 2.2.

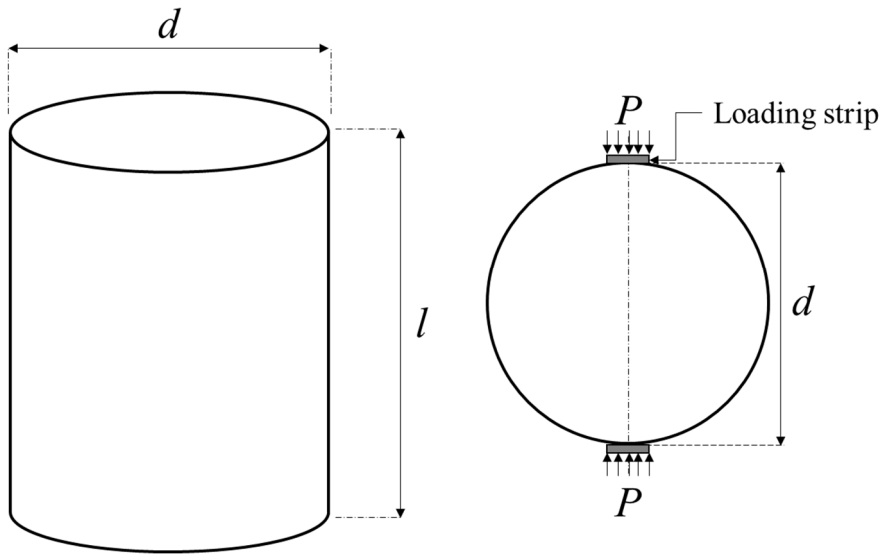

Figure 2.3: (a) splitting tensile strength specimen (b) test configuration

$$STS = \frac{2P}{\pi l d} \tag{2.2}$$

in which, *STS* is the splitting tensile strength, *P* is the maximum applied load, *l* is the height of the specimen, and *d* is the diameter of the specimen.

Flexural strength

The flexural strength, or the Modulus of Rupture (MOR) is the indirect tensile strength of a prismatic beam specimen. The measure is obtained from monotonic three-point or four-point bending tests. Figure 2.4 shows the flexural strength measured by a four-point bending apparatus. The flexural strength of cement-treated materials is currently measured under the test standard for concrete beams (ASTM, 2012a). However, flexural strength test protocols for cement-treated materials are currently only in development in a few countries (Austroads, 2014a; Mandal, Tinjum, Gokce, & Edil,

2016; Wen et al., 2014). Flexural strength is a very important parameter in road pavement design. This is due to the cement-treated layer in the field behaving in a similar way to the beam specimen in the four-point bending apparatus test (Austroads, 2014b). Past literature demonstrates that traffic-induced cracking of a cement-treated layer in the field is strongly correlated with its flexural strength (Thompson, 2001). Certain fatigue models were established based on the ratio between the maximum tensile stress at the bottom of a cement-treated layer and its flexural strength. Examples include the fatigue model developed by NCHRP (2004) and Wen et al. (2014).

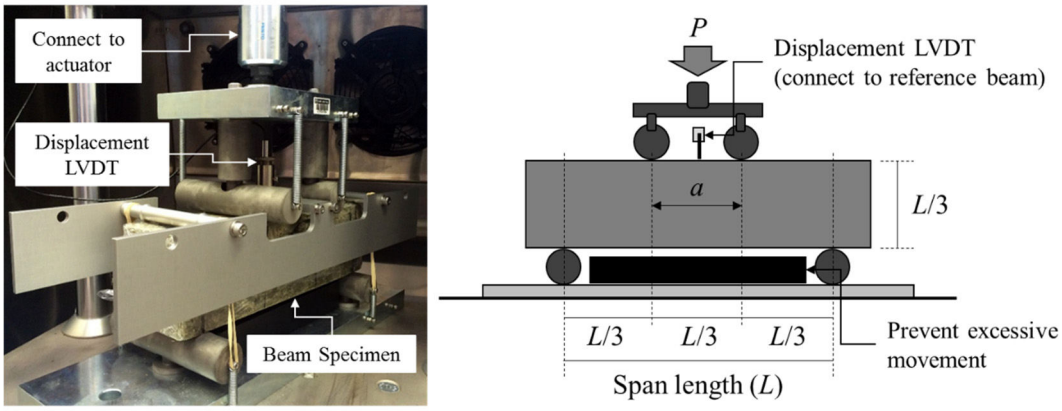

Figure 2.4: Four-point bending test (a) during the test (b) test configuration

During the flexural strength test, applied load measurements and displacement of bending beam specimen measurements are collected from the load actuator and displacement Linear Variable Differential Transformer (LVDT) (see Figure 2.4), respectively. The flexural strength or MOR of tested specimen can be calculated based on Eq. 2.3.

$$FS = \frac{PL}{bd^2} \tag{2.3}$$

in which, *FS* is the flexural strength (kPa), *P* is the maximum applied load (N), *L* is the span length of a specimen (mm), *b* is the width of the specimen (*L*/3) (mm), and *d* is the depth of the specimen (*L*/3) (mm). Austroads (2014a) recommend calculating the breaking strain at 95% of flexural strength (see Eq. 2.4).

$$\varepsilon_b = \frac{12d\delta}{(3L^2-4a^2)} \tag{2.4}$$

in which, ε_b is the breaking strain at the bottom fibre of a beam specimen, δ is the mid-span displacement at a load equal to 95% of the maximum applied load (mm), and a is the distance between the inner rollers (mm).

2.3.2 Modulus of cement-treated materials

The modulus of the materials is defined as the ratio between stress and strain measured with specific tests. It is also used to represent the response of materials in road pavement design. The characteristics of the material modulus are governed by the measurement methods. NCHRP (2004) initially recommended the elastic modulus for road pavement design in the US be determined by a monotonic compressive loading test of a cylindrical specimen (ASTM, 2010). According to ASTM (2010), the compressive strains employed for the elastic modulus calculation were 0.0050% and the strain at 40% of UCS. In later literature, the indirect tensile modulus determined from a cylindrical specimen was proposed as a pavement design parameter by Wen et al. (2014). Prior to the indirect tensile modulus test, the indirect tensile strength or *STS* is required as the reference parameter. Following this, 30% of *STS* is applied repeatedly, using a haversine-shaped load pulse of 0.1 s duration followed by a rest period of 0.9 s. A total number of 100 load repetitions is recommended, but only the last 10 cycles are used to calculate the indirect tensile modulus. The equations for tensile stress, strain, and indirect tensile modulus (E_{IDT}) are shown in Eqs. 2.5 - 2.7.

$$\sigma_t = \frac{2P}{\pi l d} \tag{2.5}$$

$$\varepsilon_t = U\frac{\gamma_1+\gamma_2\nu}{\gamma_3+\gamma_4\nu} \tag{2.6}$$

$$E_{IDT} = \frac{\sigma_t}{\varepsilon_t} \tag{2.7}$$

in which, σ_t is the tensile stress (Pa), ε_t is the tensile strain, U is the horizontal displacement (m) measured from the displacement LVDT, ν is the Poisson's ratio (assuming a value of 0.2), P is the maximum applied load (N), l is the height of the specimen (m), d is the diameter of the specimen (m), and γ_1, γ_2, γ_3, γ_4 are the parameters dependent on the diameter of the specimen, the gauge length, and the bearing block width (Wen et al., 2014). Similar to Austroads (2014a), Wen et al. (2014) developed a test protocol for determining the flexural modulus of cement-treated materials based

on a four-point bending test platform (see Figure 2.4). A recommended applied load of 20% - 40% of *FS* is employed under the haversine-shaped load for a duration of 250 ms followed by a rest period of 750 ms. In 100 cycles of loading, the last 50 cycles are used in the determination of the flexural modulus, as seen in Eq. 2.8.

$$E_{flex} = \frac{23PL^2}{108bd^3\delta} \times 1{,}000 \tag{2.8}$$

in which, E_{flex} is the flexural modulus (MPa), P is the maximum applied load (N), L is the span length (mm), b is the width of the specimen (mm), d is the depth of the specimen, and δ is the peak mid-span displacement (mm).

Shahid (1997) developed correlational equations between the modulus and the strength parameters of the cement bound base. These were obtained from the direct tensile test, and the UCS test. Brown (1979) established a relationship equation between flexural modulus and flexural strength. Similarly, the relationship equation between flexural strength and flexural modulus, and the relationship equation between splitting tensile strength and splitting modulus can be found in a study by Wen et al. (2014).

2.3.3 Poisson's ratio

Poisson's ratio of cement-treated materials can be determined by both static and dynamic methods Shahid (1997). It is defined as the ratio of the lateral to longitudinal strain developed during the monotonic compressive loading test of a cylindrical specimen (ASTM, 2010). Wen et al. (2014) recommended the value of Poisson's ratio for cementitiously bound material as equivalent to 0.20. Table 2.4 provides the range of Poisson's ratios reported in previous literature.

2.3.4 Dynamic responses of cement-treated materials

Croney and Croney (1998) developed a correlational curve between the static modulus and the dynamic modulus of cement-treated materials. The dynamic modulus in their study referred to the dynamic modulus measured by the ultrasonic pulse method (BS, 1986). The dynamic modulus was generally higher than the static modulus measured according to the monotonic compression test (BS, 1983). Accordingly, the average value of the dynamic and static modulus was recommended as a design parameter

(Croney & Croney, 1998). More importantly, the authors suggested performing a dynamic loading test, which models real traffic loading on cement-treated materials, to investigate the actual dynamic responses of materials. Kolias and Williams (1980) also determined the relationship between the static and the dynamic modulus of cement-treated materials. The impact resonance test was used to determine the dynamic modulus in their study. The variations in the density and strength of cement-treated materials were also considered. The test results revealed that the dynamic modulus was greater than the static modulus by a magnitude of 5 GN/m^2 where the dynamic modulus was higher than 15 GN/m^2. It should be emphasised that the static modulus obtained from compressive loading tests, e.g. UCS test, generally involves material strains greater than those experienced in pavement. On the other hand, the dynamic modulus measured by the ultrasonic pulse method and impact resonance tests is calculated based on strains that are less than those induced by traffic (Croney & Croney, 1998; Kolias & Williams, 1980).

Table 2.4: Poisson's ratio of cement-treated materials reported in previous literature

Materials	Poisson's ratio	Literatures
• Cement bound base with granular aggregate • Fine grained soil cement	0.15-0.20 0.33	Kolias and Williams (1978)
• Cement stabilised aggregate (including lean concrete)	0.10-0.20	NCHRP (2004)
• Base material with 4% - 5% cement • Subbase crushed rock with 3% - 4% cement • Subbase natural gravel with 4% - 5% cement	0.10-0.30	Austroads (2014a)
• Stabilised material	0.35	SANRAL (2013)

In Australia, the dynamic flexural modulus measurement guidelines for cement-treated materials were first developed by Austroads (2008a). Paul and Gnanendran (2016) later characterised the flexural dynamic modulus behaviour of lightly stabilised granular base. The 28-day dynamic flexural modulus was approximately twice the value of the 28-day static flexural modulus. In the aforementioned study, the dynamic

flexural moduli were measured by the application of sinusoidal waveform loading with a frequency of 3 Hz. However, test guidelines developed in Australia (Austroads, 2008a, 2014a) and the US (Mandal et al., 2016) recommended a dynamic load with a haversine waveform loading of 1 Hz for the measurement of the dynamic flexural modulus.

2.3.5 Factors influencing characteristics of cement-treated materials

As with concrete materials, the strength of cement-treated materials is usually influenced by the characteristics of the parent material, cement content, curing time, moisture content, and compaction energy (Arellano & Thompson, 1998; Austroads, 2014a; Horpibulsuk, Katkan, Sirilerdwattana, & Rachan, 2006; Z. Zhang & Tao, 2008). Compaction moisture content is another factor that affects the characteristics of cement-treated materials. The cement-treated materials moulded using water equivalent to Optimum Moisture Content (OMC) provided the highest strength (Horpibulsuk et al., 2006; Horpibulsuk, Miura, & Nagaraj, 2003). Similar to concrete materials, the modulus and strength of cement-treated materials depend on the material's density (Austroads, 2014a; Horpibulsuk et al., 2006). Croney and Croney (1998) established relationship curves between specimen size and UCS in cement-treated materials, measured by the Transport and Road Research Laboratory (TRRL) in the UK.

Paul and Gnanendran (2016) investigated the effects of applied stress ratio to the flexural dynamic moduli of lightly stabilised granular base. In their study, the applied stress ratio was the ratio of the applied bending stress amplitude to the flexural strength of materials. The results showed that the dynamic flexural modulus decreased with the increase in the applied stress ratio. Therefore, the dynamic flexural modulus measured at 50% of the stress ratio was selected as the representative value. Moffatt, Jameson, and Young (2012) examined the effects of different groups of axle load, i.e., single, tandem, triaxle, and quad-axle, on the flexural moduli and fatigue characteristics of cement-treated materials. Similar to the study results of Austroads (2014b) and Paul and Gnanendran (2016), the dynamic flexural stiffness of cement-treated materials usually decreased when the applied load level increased. However, the flexural stiffness was not affected by the shape or duration of the load pulse. Mbaraga, Jenkins,

and Van De Ven (2014) studied the effects of beam geometry and aggregate size on the flexural strength and modulus of cement-treated materials. The study results indicated that maximum aggregate particle size, beam depth, and loading span significantly affected the flexural strength of the cement-treated materials.

For concrete materials, the strength and modulus of materials are significantly influenced by the rate of loading (Bischoff & Perry, 1991; O. Xiao, Li, & Lin, 2008; S. Xiao, Li, & Monteiro, 2011). Both strength and modulus normally increase with the rise in loading rate. Bischoff and Perry (1991) recommended the strain rates expected for various loads, as shown in Figure 2.5.

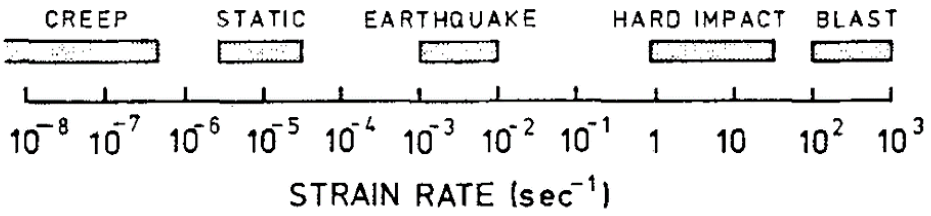

Figure 2.5: Magnitude of strain rates expected for different loads (Bischoff & Perry, 1991)

According to Destrebecq (2010), the fatigue characteristics of concrete are influenced by the same parameters that affect its static strength. These parameters are: types of parent material, gradations of parent material, cement content, water-cement ratio, porosity, and method of casting. Medeiros, Zhang, Ruiz, Yu, and Velasco (2015) found that loading frequency also affects the fatigue behaviour of plain and reinforced concrete. The consideration of loading frequency was merged with the well-known Aas-Jakobsen's fatigue life prediction equation by B. Zhang, Phillips, and Wu (1996).

2.3.6 Mix design

The appropriate quantities of water and cement required for cement-treated mixtures are generally determined based on mix design procedures (Austroads, 2006b; PCA, 1956). Croney and Croney (1998) recommended determining the required amount of water by performing a compaction (Proctor) test of aggregate alone. The Optimum Moisture Content (OMC) at the Maximum Dry Density (MDD), with approximately

1% of added water was used as the design value. The purpose of the additional water was to ensure that there was enough water to react with the fine particles of cement added to the parent material. This procedure is considerably different to that recommended by the Department of the Army; the Navy and the Air Force (1994) in the US. The cement-stabilised compaction test according to ASTM D558 (ASTM, 2011c) and ASTM D1557 (ASTM, 2012b), requires the aggregates to be mixed thoroughly with the cement prior to performing compaction procedures. Figure 2.6 shows the mix design procedure developed by the Department of the Army; the Navy and the Air Force (1994). As shown, the Unified Soil Classification Group (USCS) (ASTM, 2011a) and Particle Size Distribution (PSD) (ASTM, 2007b) are required prior to defining the initial cement content. Compaction tests then determine the OMC and MDD of the cement-treated material with initial cement content. Following this, a series of UCS tests (ASTM, 2000) was conducted using varying cement content (see Figure 2.6). The target UCS value recommended by the guidelines (see Section 2.1.2) was used to define the optimum cement content of cement-treated materials. It should be emphasised that test specimens in the mix design process were generally prepared at OMC based on the compaction test (Austroads, 2006b; PCA, 1956). Additional tests were prepared for specimens with an optimum cement content. These included the durability test (ASTM, 2015a, 2015b), and the swell and erodibility test (Austroads, 2006b). These tests were compulsory. The specimens for the UCS test and the durability test were prepared according to ASTM D1632 (ASTM, 2007a).

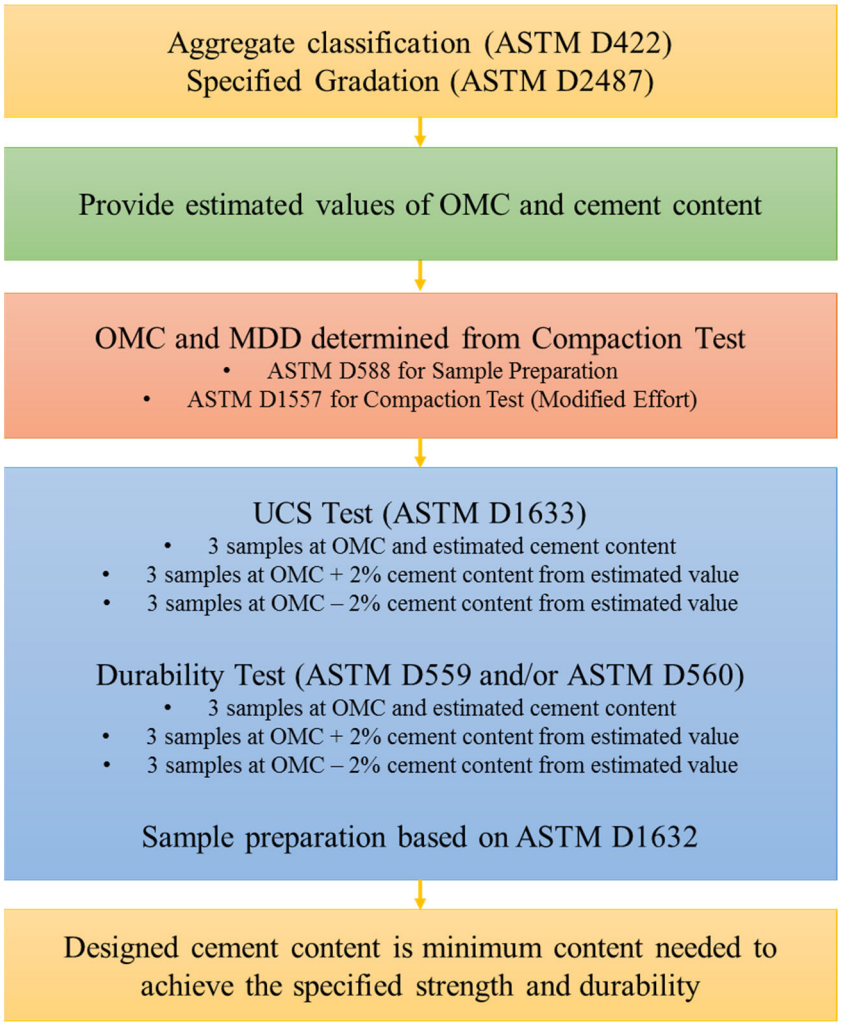

Figure 2.6: Mix design procedure for stabilised base course, as recommended by the Department of the Army; the Navy and the Air Force (1994)

2.4 Road pavement design with Cement-Treated Base (CTB) layer

Presently, the fatigue distress model of cement-treated material contains the essential criteria for pavement with a CTB layer, according to the design guidelines for road pavement. To design road pavement in Australia, the thickness of each pavement material is usually estimated in the early design stage (Austroads, 2010b). The stresses and strains at critical locations (see Figure 2.7) are then calculated according to linear elastic theory, with the application of standard loads on top of the pavement structure. The number of load repetitions or the life of individual pavement layers, in accordance with possible distress modes, is then estimated. This allows the approximate life of a pavement structure to be estimated from the minimum values of those estimated

numbers of load repetitions. For example, the service life of the road structure shown in Figure 2.7 is the minimum value of the number of load repetitions calculated from the distress models of asphalt, cement-treated materials, and subgrade (Austroads, 2010b).

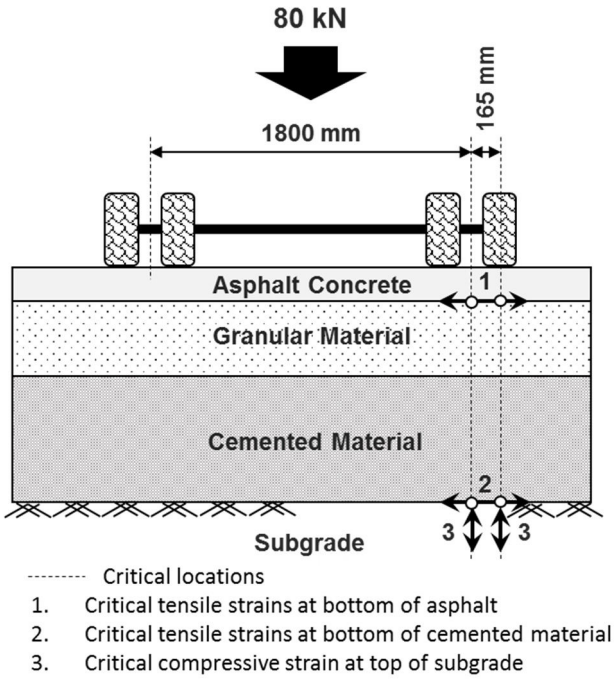

Figure 2.7: Pavement with CTB model and locations of critical strain (adapted from Austroads (2010b))

It should be emphasised that the actual life of road structures with a CTB layer is not terminated immediately after the cemented layer fails from fatigue. The failed CTB layer usually breaks into blocks and behaves similarly to granular material after failure (Austroads, 2010b; SANRAL, 2013). Therefore, the total service life of pavement structures with CTB layers is the summation of load repetitions estimated before the CTB fails from fatigue and after the fatigue failure (granular-like material behaviour) itself. The long-term behaviour of CTB is provided in the following section.

2.4.1 Behaviour of CTB under repeated traffic loading

Powell, Potter, Mayhew, and Nunn (1984) conducted an intensive program of field investigations to characterise traffic-induced cracking of cement-treated road base (refer to lean concrete road base in Powell et al. (1984)). Figure 2.8 illustrates the

relationship of traffic-induced and temperature induced stress to the 28-day flexural strength of a cement-treated beam. It is evident from the Figure 2.8 that longitudinal cracking is generally observed when the induced stresses are greater than the 28-day flexural strengths. The investigations by Powell et al. (1984) were performed after the pavement had carried traffic from 8 to 20 Million Standard Axles (MSA).

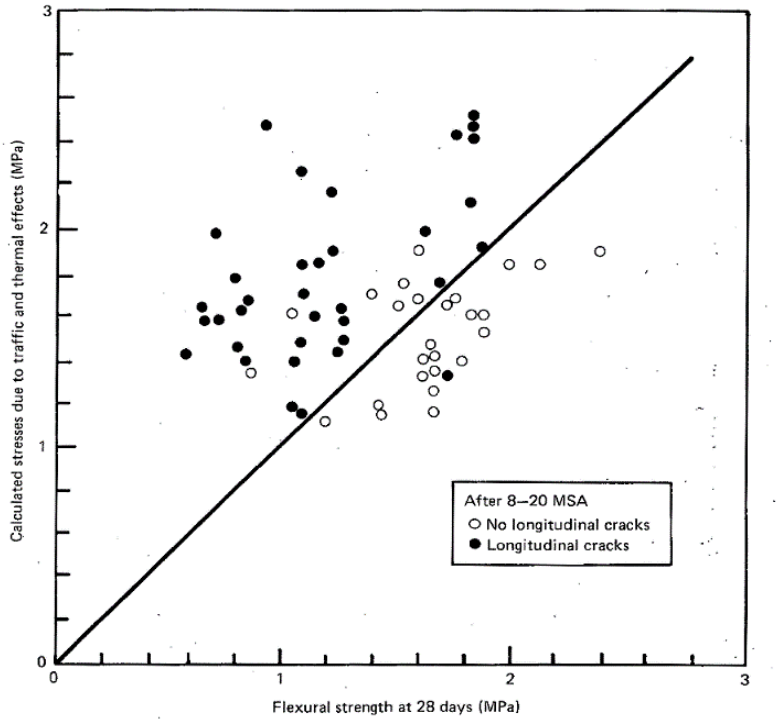

Figure 2.8: Flexural strength as an indicator of ability to resist longitudinal cracking (Powell et al., 1984)

It is well understood that the fatigue mechanisms of CTB can be explained by the modulus reductions of CTB which are mainly caused by repeated traffic loads (Austroads, 2014b). Figure 2.9 presents the long-term behaviour of a lightly treated CTB layer subjected to repeated traffic loads in the field, as outlined by Theyse, De Beer, and Rust (2014).

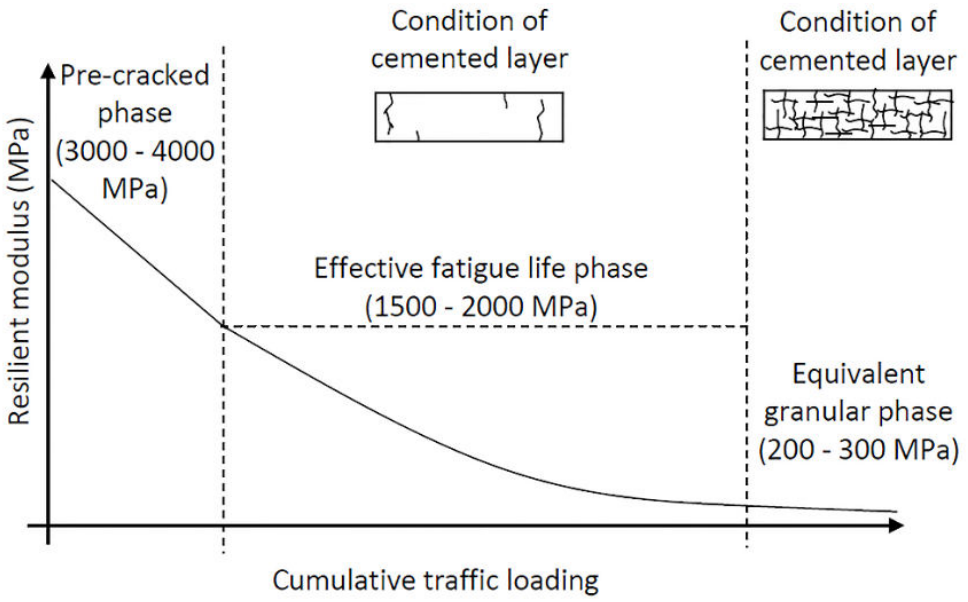

Figure 2.9: Long-term behaviour of lightly treated cement material outlined by Theyse et al. (2014) (reproduced by Y. S. Yeo (2011))

According to Figure 2.9, the behaviour of lightly treated cement material can be divided into three phases (Theyse et al., 2014): The pre-cracked phase represents the stage where there is a rapid reduction in the material modulus. During the effective fatigue-life phase, the cement-treated material is further broken down into block-like material with the size usually less than the thickness of the layer. Finally, the modulus of the cement-treated material reduces to the minimum value in the equivalent granular phase; this is the phase where the lightly treated cement layer typically behaves in a similar fashion to a granular layer.

Similar to the field behaviour of a CTB layer (described by Theyse et al. (2014)), Austroads (2010a) demonstrated the characteristics of CTB prismatic beam specimens subjected to repeated loads, as shown in Figure 2.10. A rapid reduction in flexural modulus was observed in the first phase, defined as the bedding-in phase by Austroads (2010a). The flexural modulus was then gradually reduced in the second phase by repeated loads at a constant rate. When the flexural modulus was reduced to 80% of the initial flexural modulus, the reduction was accelerated by repeated loads until finally, failure occurred. Austroads (2010a) defined the initial flexural modulus as the average value of the calculated flexural modulus during the first 50 cycles of applied loading.

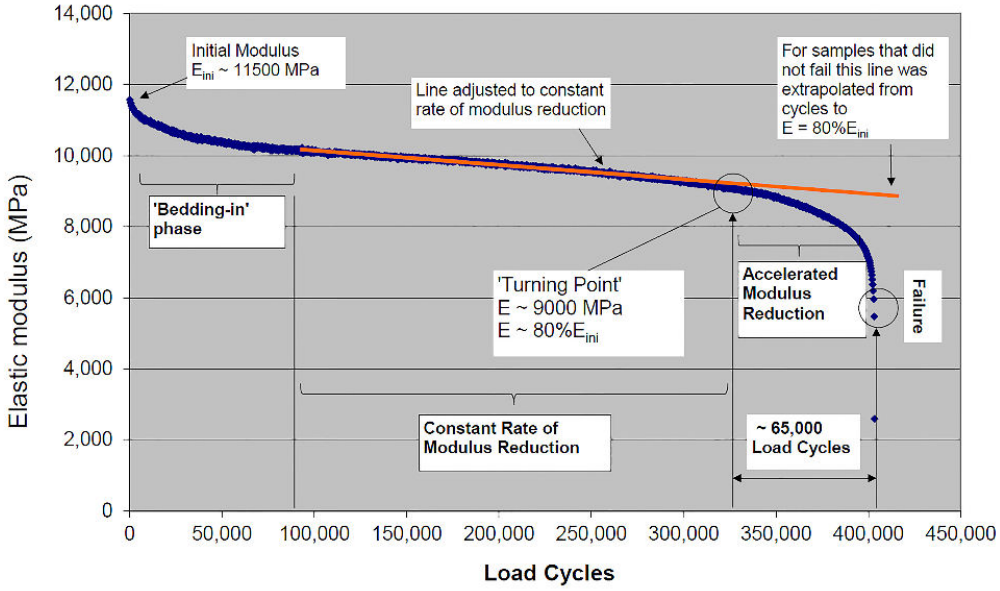

Figure 2.10: Flexural modulus reductions induced by cyclic loading of CTB prismatic specimens tested by the cyclic four-point bending method (Austroads, 2010a)

2.4.2 Fatigue distress models for pavement design

Europe

The Highways Agency (2006) has developed design charts for road bases in the UK using flexible composite pavement with Hydraulically Bound Material (HBM). The design charts were originally developed based on field data collected by Powell et al. (1984). This data included 39 sections of tested pavement (Thompson, 2001). Similar to most pavement design charts, the thickness of the asphalt layer and HBM road base in the y-axis of the design is simply determined based on the design traffic in the x-axis. In addition, the design charts provided by the Highways Agency (2006) also recommend a suitable HBM category for the road structure design. There are no considerations of fatigue life estimated from the fatigue distress model in the UK road pavement design guidelines (Thompson, 2001). However, examples of the HBM fatigue distress model developed in the UK can be found in Shahid (1997), and Thompson (2001). Shahid (1997) developed a fatigue prediction model for Cement Bound Material (CBM) based on cyclic direct tensile test results. In addition, Thompson (2001) employed results from the cyclic four-point bending test for the

development of a fatigue model. It should be emphasised that these fatigue models are stress-based equations. In Europe, France has probably carried out the most research on HBM (Thompson, 2001). Approximately 45% of the French state-managed network and country primary network is pavement with cement-treated or slag-treated bases (Corte & Goux, 1996). The French fatigue prediction model shown in Table 2.5 (LCPC, 1997) was calibrated from the trapezoidal fatigue test results, and the data from a full-scale accelerated loading carousel (R. Yeo, 2012). Similar to the fatigue models developed in the UK, critical stress in cement-treated layers, and flexural strength are generally used as the input parameters for fatigue life estimation in the French model.

Table 2.5: Fatigue prediction models for road pavement with cement-treated layer in different countries

Country	Fatigue prediction equation	Input parameters	Reference
France	$\log N = \frac{1}{\beta}\left[\frac{\sigma_t}{FS} - 1\right]$	σ_t = critical tensile stress FS = flexural strength β = regression parameter	LCPC (1997)
South Africa	$\log N = SF \times c\left[1 - \frac{\varepsilon_t}{d \times \varepsilon_b}\right]$	ε_t = critical tensile strain ε_b = braking strain c, d = regression parameters SF = shift factor	SANRAL (2013)
United States	$\log N = \frac{0.972\beta_{c1} - \left({}^{\sigma_t}/_{FS}\right)}{0.0825\beta_{c2}}$	σ_t = critical tensile stress FS = flexural strength β_{c1}, β_{c2} = field calibration factors	NCHRP (2004)
Australia	$N = RF\left[\frac{{}^{113000}/_{E_{Flex}^{0.804}} + 191}{\varepsilon_t}\right]^{12}$	ε_t = critical tensile strain E_{Flex} = flexural modulus RF = reliability factor	Austroads (2010b)

South Africa

The current South African fatigue prediction model for cement-treated layers was recommended by the South African Pavement Engineering Manual (SANRAL, 2013). According to the reviews by Theyse et al. (2014), the South African Mechanistic Design Method (SAMDM) was first published in 1974. However, the development of cement-treated material fatigue criteria was only available from 1977. The distress modes considered by the South African method for lightly treated cement layers are

crushing and effective fatigue failures. Crushing failure on top of the cement-treated layers due to excessive vertical stress was discovered by De Beer (1990) and based on Accelerated Pavement Testing (APT) results. However, SAMDM does not recommend crushing failure as the termination criteria for road pavement design (SANRAL, 2013; Theyse et al., 2014).

The South African life prediction model, based on the fatigue failure of cement-treated layers, can be found in Table 2.5. Evidence shows that the fatigue life of a cement-treated layer is estimated from the maximum tensile strain at the bottom of the layer (ε_t) and the strain at the break (ε_b). According to Theyse et al. (2014), the long-term behaviour of a lightly treated cement layer can be broken down into three phases, as shown in Figure 2.9. It should be noted that the fatigue life of the pre-cracked phase is not taken into consideration by the SAMDM, as it is very short compared to the other phases (effective fatigue life and equivalent granular phases). After the effective fatigue cracking phase, the cement-treated layer is broken down into small blocks from repeated traffic loads. The properties of the cement-treated layer in this phase are equivalent to those of granular material, and the remaining life is estimated based on the properties of equivalent granular material (Theyse et al., 2014). The shift factor is multiplied by the fatigue life, estimated from the South African prediction equation, to consider the effects of layer thickness variation (SANRAL, 2013). Theyse (2008) recommended a new set of input parameters for fatigue life prediction, but these inputs are not yet in popular use in South Africa (SANRAL, 2013).

United States

The official United States road pavement design guidelines, according to the Mechanistic-Empirical (M-E) design method, were originally published in NCHRP (2004). The American bottom-up fatigue life prediction model shown in Table 2.5 was recommended for semi-rigid road pavement design only. According to NCHRP (2004), semi-rigid pavement is pavement with a cementitiously stabilised layer, i.e., an asphalt-treated material and a cement-treated material as a base course layer. Table 2.5 illustrates that the American fatigue life prediction equation is the function of critically induced tensile stress (σ_t), from traffic, 28-day flexural strength (*FS*), and field calibration factors (β_{c1}, β_{c2}). In addition, a prediction equation was recommended

by the NCHRP (2004) for the damaged modulus of a cement-treated layer and cracks in the cement-treated layer based on the damage level (*D*). However, details of the damage level calculations were not available in the guidelines. The bottom-up fatigue prediction model and damaged modulus prediction equation developed by the NCHRP (2004) were later implemented in the American *M-E pavement design guide (interim edition)* (AASHTO, 2008). The prediction equations for Hot Mix Asphalt (HMA) reflective cracking and cement-treated layer fatigue cracking were also proposed in the above guide. However, the guide states that the recommended fatigue distress model and damage model should not be employed until such time as the model parameters have been accurately calibrated. Note that this recommendation still appears in the current version of the American M-E pavement design guide, AASHTO (2015). Saxena, Tompkins, Khazonovich, and Balbo (2010) completed extensive reviews on the performance modelling of cement-treated layers suggested by the *M-E pavement design guide (interim edition)* (AASHTO, 2008). The major drawback of the American M-E pavement design guide is that the test standards for obtaining the model parameters are not yet available. Moreover, Saxena et al. (2010) advised that other cement-treated layer distress models, i.e., those concerned with shrinkage, durability, transverse and block cracking, should be implemented in the design guidelines. These drawbacks were later addressed by Wen et al. (2014) in the NCHRP project 04-36. The authors modified the bottom-up fatigue model by independently applying the model parameters calibrated from laboratory test results and field measurement data (Eq. 2.11). The top-down fatigue model, durability (effects of freeze-thaw and wet-dry processes) prediction equation, and shrinkage prediction equation were also developed. Top-down fatigue cracking usually occurs when a lightly stabilised layer is overlaid by a thin asphalt layer (Wen et al., 2014). In fact the bottom-up fatigue model and top-down fatigue model proposed by Wen et al. (2014) are respectively comparable to the effective fatigue model and crushing prediction model recommended by SANRAL (2013) in South Africa. Significantly, testing protocols for model parameter determination were also developed by Wen et al. (2014), and these included:

- Modulus of rupture measurement using a simple beam with third-point loading,
- Flexural modulus measurement using a simple beam with third-point loading,
- Indirect tensile strength test,

- Indirect tensile modulus test,
- Coefficient of thermal expansion test, and
- Shear strength test.

Australia

In Australia, only the bottom-up fatigue model has been developed and recommended for road pavement design with a cement-treated layer. Austroads (2014b) refers to the fatigue distress model which was first developed and proposed in the Austroads Pavement Design Guide of 1987 (NAASRA, 1987). The predicted fatigue life of a cement-treated layer was calculated from only two model parameters, namely the modulus of cement-treated material and tolerable strain ($\mu\varepsilon$). This tolerable strain is the expected maximum tensile strain that occurs in the cement-treated layer during service. However, studies from past works have proven that the modulus of the material and the tolerable strain are inadequate as predictions of the fatigue life of cement-treated layers (Austroads, 2014b; Baran & Aubrey, 1987; Litwinowicz, 1986; Otte, Salvage, & Monismith, 1982). The earliest version of the Australian fatigue model has an exponent value of 18. In 1992, Jameson, Sharp, and Yeo (1992) adopted the 8th power relationship of a fatigue prediction equation, based on the analysis results obtained from both laboratory and field tests. However, the proposed equation of Jameson et al. (1992) was not widely employed in Australian road design, since it was based on only one type of cement-treated material. The fatigue distress model was changed to a 12th power relationship in the 1997 version of the design guide (Austroads, 2014b), based on the study completed by Jameson, Dash, Tharan, and Vertessy (1995). The present Australian fatigue prediction model (see Table 2.5) was originally presented in the Pavement Design Guide of 2004 (Austroads, 2014b), and has been employed as the design criteria for road pavement with cement-treated layers ever since. The modulus of the cement-treated layer in the Australian fatigue prediction model represents the flexural modulus of a 28-day beam specimen. Improvements to the Australian fatigue model have since been proposed by Austroads (2014a) and Austroads (2014b). In the newly-proposed fatigue prediction model, the numerator term ($113000/E_{Flex}^{0.804} + 191$), as shown in Table 2.5, was reduced to a single factor "*k*". This newly-proposed fatigue prediction model is expressed in Eq. 2.9. The *k*-factor can be obtained from three approaches: (1) a laboratory testing program, (2)

an estimation of the empirical relationship equation, and (3) employing presumptive values in the calculation (Austroads, 2014b). It should be emphasised that the maximum tensile strain (ε_t) for the newly-proposed fatigue prediction model should be predicted from the design flexural modulus, which is defined as one-third of the flexural modulus measured from a 90-day laboratory prepared specimen. In addition, Austroads (2014b) also recommended employing the *"shift factor"* in the fatigue life estimation of cement-treated layers. The shift factor allows consideration of the effects of low modulus micro-crack areas in the field (pre-cracked or weak zone). Further to these specifications, the delineation point in the Australian Pavement Design Guide between modified CTB and stabilised CTB was reviewed and an amendment suggested by Austroads (2013b).

2.4.3 Testing for fatigue prediction model parameters

Previous sections have summarised the fatigue life prediction equations for road pavement structures based on road design guidelines developed in different countries. Various model parameters were required as inputs for those prediction equations (see Table 2.5). In this section, testing and approaches to obtain the input parameters for fatigue life prediction models are reviewed.

In Australia, critical tensile strain (ε_t) occurring in cement-treated layers and measured in micro-strains ($\mu\varepsilon$), has usually been estimated as outlined in Section 2.4 (see Figure 2.7). The modulus (E_{Flex}) in the fatigue prediction equation represents the 28-day flexural modulus measured from the four-point bending test. According to Austroads (2010b), the flexural modulus can be obtained from both monotonic and repeated (cyclic) loading tests. However, the flexural modulus determined from the repeat loading test was cautioned in the guidelines as its values are measured at the low strain range and are normally higher than the values measured from the monotonic loading test. For the repeated loading flexural beam test (refer to the dynamic test in Austroads (2010b)), Austroads (2008a) recommends the use of the haversine loading function. An applied peak load of less than 40% of flexural strength with a loading duration of 250 ms and a rest period of 750 ms is suggested. The peak load is limited to 40% of flexural strength to ensure that the load-deflection curve is still within the elastic range. The flexural modulus measurement is completed after 100 loading cycles. The flexural

modulus of an individual loading cycle can be calculated as shown in Eq. 2.8. Initially, the flexural modulus or the design modulus was deemed as the average flexural modulus of the *first* 50 cycles. However, as explained in Section 2.3.2, Austroads (2014a) changed this average value to the *last* 50 cycles of the repeated load. Moreover, Austroads (2014b) suggested adjusting the flexural modulus measured from the repeated load four-point bending test to represent the design modulus or field flexural modulus. The adjustment is required due to the fact that the in-field flexural modulus is usually lower than the laboratory flexural modulus. The difference in the flexural modulus is caused by a variation in the modulus at different field locations and the difference in density between laboratory and field CTB. Therefore, Austroads (2014b) recommended reducing the laboratory flexural modulus measurement by three times to represent the field or design flexural modulus.

In the US, Wen et al. (2014) and Mandal et al. (2016) proposed testing protocols for measuring the flexural strength, flexural modulus, and fatigue failure of cement-treated materials using the four-point bending test. Thus the modulus of rupture or flexural strength (*FS*) can be measured from the flexural strength test. The critical tensile strain (σ_t) at the bottom of a cement-treated layer can be determined by a similar procedure, detailed in Section 2.4. At this estimation stage, the design modulus is also required. It should be emphasised that the design modulus for heavily stabilised materials is the flexural modulus, while the resilient modulus is recommended for lightly stabilised materials (Wen et al., 2014). Moreover, Wen et al. (2014) also suggested adding the field calibration factor to the original US fatigue prediction model, as shown in Table 2.5 (see Eq. 2.11).

The breaking strain (ε_b) of cement-treated layers in the South African prediction model can be defined based on the recommended values of SANRAL (2013). The shift factor (*SF*) and constant parameters (*c* and *d*) are also provided by the guidelines. In France, the flexural strength from that prediction model is determined from the beam bending test.

2.4.4 Recent fatigue model development and fatigue testing

Cement-treated materials

Current developments in fatigue testing guidelines and CTB fatigue life prediction procedures in Australia can be found in Austroads (2014a) and Austroads (2014b). The testing guidelines for measuring the fatigue life of CTB were developed based on the four-point bending test framework. Different from the flexural modulus measurement, a haversine loading function with a frequency of 2 Hz is recommended for fatigue life determination. Therefore, the duration of the applied load is 250 ms with a rest period of 250 ms. A constant peak load of greater than 60% but less than 90% of flexural strength is applied throughout the fatigue test. This applied stress range is equivalent to 50 $\mu\varepsilon$ – 120 $\mu\varepsilon$ at the bottom fibre of the test beam (Austroads, 2014a). The repeated load is usually continued until the flexural modulus decreases to one half of the initial value or until fatigue failure is observed. For CTB fatigue life prediction procedure, Austroads (2014b) developed three approaches for fatigue characterisation.

- **Method 1**: develop a fatigue life prediction equation from laboratory test results; then apply the shift factor and design reliability factor to estimate the in-service fatigue life.

- **Method 2**: predict the fatigue life of CTB based on the design flexural moduli and measured flexural strengths; then apply the shift factor and design reliability factor to estimate the in-service fatigue life.

- **Method 3**: employ the presumptive design flexural moduli and flexural strengths as the inputs for Method 2.

The fatigue life of CTB estimated by method 1 can be written in the form of Eq. 2.9.

$$N = RF\left(\frac{SF \times k}{\varepsilon_t}\right)^{12} \tag{2.9}$$

in which N is the in-service fatigue life, RF is the reliability factor (equal to 1 for a reliability equal to 95%), ε_t is the load-induced tensile strain at the base of the CTB

layer ($\mu\varepsilon$), *SF* is the laboratory-to-field shift factor, and *k* is the fatigue constant obtained from four-point bending test data (method 1 only). Based on Austroads (2014b), a presumptive value of 1.8 is recommended for *SF*. For methods 2 and 3, the fatigue constant (*k*) can be estimated by Eq. 2.10.

$$k = 164FS + \frac{6288000}{E_{Flex}} - 195 \tag{2.10}$$

in which, *FS* is the flexural strength measured from the four-point bending test (method 2) or as recommended by the guidelines (method 3), and E_{Flex} is the flexural modulus measured from the four-point bending test (method 2) or as recommended by the guidelines (method 3).

In the US, current work on the fatigue characteristics of CTB has been undertaken by Wen et al. (2014). The main objective of their study is to develop performance-related procedures to characterise the Cementitiously Stabilised Layer (CSL) of a road pavement structure. The authors' analysis included four parent materials, i.e., clay, silt, sand and gravel. These parent materials were then mixed with four binders to form cementitiously stabilised materials; the binders being cement, lime, Class F, and Class C fly ash. As mentioned in the previous section, testing guidelines for fatigue life measurement based on the four-point bending test were also developed and proposed by the authors. Different from other cementitiously stabilised materials, stabilised gravel specimens were prepared based on a modified compaction effort (Mandal et al., 2016; Wen et al., 2014). From the test results, Wen et al. (2014) developed a bottom-up fatigue model, as shown in Eq. 2.11.

$$LogN = k_1 \left(\frac{k_2 - \frac{\sigma_t}{FS}}{k_3} \right) \tag{2.11}$$

in which, k_1 is the parameter used for field calibration (1.0 for laboratory test), and k_2, and k_3 are the regression parameters.

In the UK, Thompson (2001) carried out dynamic four-point bending tests on Cement Bound Materials (CBM) and Fibre Reinforced Cement Bound Base (FRCBM) specimens. In his study, low and high strength gravels were employed as the parent

materials. The percentages of cement content per dry weight of aggregate were 4.5% and 8.5% for low and high strength gravels, respectively. During the fatigue tests, the test specimens were subjected to 6 Hz of sinusoidal loading waveform. The fatigue life estimation model developed, based on the test results by Thompson (2001), is shown in Eq. 2.12.

$$\frac{\sigma_{max}}{FS} = 95 - 1.5Ln(N) \tag{2.12}$$

in which, σ_{max} is the maximum applied load, and *FS* is the flexural strength. In addition, the minimum applied load (σ_{min}) was assigned at 10% of *FS* for every fatigue test.

Concrete for structural applications

The procedures for the flexural strength test of CTB have been modified from the standard test methods for concrete, AS 1012.11 (Standard Australia, 2000a) by Austroads (2008a), and ASTM D1635 (ASTM, 2012a) by Mandal et al. (2016). The four-point bending test of CTB is actually developed from the standard test methods for concrete materials. Consequently, developments on fatigue models and fatigue testing for concrete have also been provided in this section.

Fatigue analysis of concrete members for structural applications can be carried out based on empirical approaches and constitutive relations (Ameen & Szymanski, 2006). In the empirical approach, fatigue behaviours of concrete are usually described by the ratio between the constant amplitude of applied stress and the number of applied loading cycles to failure, or a Wöhler's curve (Ameen & Szymanski, 2006; Destrebecq, 2010). Figure 2.11 shows a classic Wöhler's curve, illustrated by Destrebecq (2010). From the figure, three different stages of fatigue behaviour can be categorised, based on the number of cycles to failure.

- Stage (1): low cycle fatigue represents the number of cycles to failure less than 10^3 cycles.

- Stage (2): large or high cycle fatigue represents the number of cycles to failure, varying between 10^3 and 10^7 cycles.

- Stage (3): very large cycle fatigue represents the number of cycles to failure greater than 10^7 cycles.

According to Destrebecq (2010), stage 2 of the Wöhler's curve can be estimated by the straight line shown in Eq. 2.13.

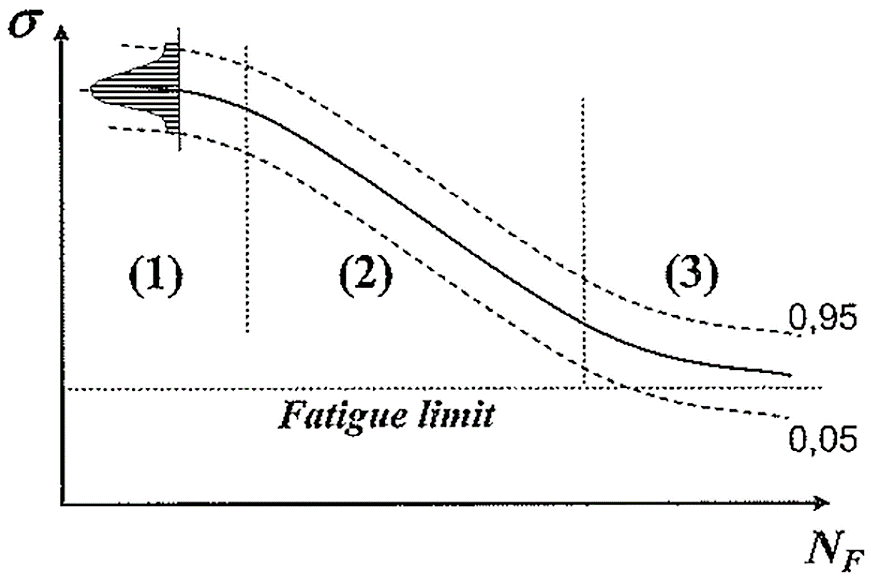

Figure 2.11: Classic Wöhler's curve, illustrated by Destrebecq (2010)

$$\sigma = \alpha - \beta LogN \tag{2.13}$$

in which, σ is the mean or maximum applied stress amplitude, N is the number of applied loading cycles to failure (N_F in Figure 2.11), and α and β are the fitting curve parameters. On the other hand, σ in Eq. 2.13 is also defined as *"endurance"* or *"fatigue strength"* in some literature (Destrebecq, 2010). However, the application of the fatigue relationship represented by Eq. 2.13 is constrained by the age and characteristics of the concrete specimens. Due to this, the effects of the concrete's strength were normalised and represented in terms of the ratio between the applied stress and the flexural strength of concrete ($S = \sigma/FS$). Accordingly, the fatigue curve of concrete is only influenced by the loading amplitude.

In 1970, Aas-Jakobsen developed a fatigue equation for concrete based on Wöhler's curve (Destrebecq, 2010; B. Zhang et al., 1996). The linear relationship equation known as Aas-Jakobsen's formula can be written as shown in Eq. 2.14.

$$\frac{\sigma_{max}}{FS} = 1 - \beta(1 - R)LogN \tag{2.14}$$

in which, σ_{max} is the maximum applied stress, FS is the flexural strength, β is the material constant and equal to 0.0685, R is the ratio between σ_{min} and σ_{max} or loading ratio, σ_{min} is the minimum applied stress, and N is the number of applied loading cycles to failure. This equation has been widely used and accepted by both researchers and practical engineering designers. However, the effects of loading frequency were neglected in the estimation. B. Zhang et al. (1996) later modified the Aas-Jakobsen's formula to incorporate the effects of loading frequency and stress reversal ($R < 1$).

It can be seen that the fatigue curves of concrete (S-N curve) develop based on the constant applied loading amplitude. However, in reality, variable loading amplitudes are usually anticipated (Ameen & Szymanski, 2006). To define the number of loading cycles to failure in cases of varying load amplitude, one way is to develop fatigue curves that match with the real loading spectrum expected in the field. However, this approach is very costly and rarely employed (Destrebecq, 2010). An alternative approach is to employ an analysis based on the rule of damage accumulation. The most popularly used method is the linear cumulative Palmgren-Miner law (Ameen & Szymanski, 2006; Destrebecq, 2010; Shah, 1984). According to the assumptions of linear Palmgren-Miner law, the loading set comprises several sequences of cycle sets (i), each set having n_i loading cycles of constant loading level S (σ_{max}/FS), and the number of cycles to failure for each constantly applied loading level S is N_i. Therefore, the cumulative fatigue damage induced by a set of loading cycles can be represented in Eq. 2.15.

$$\sum_i \delta_i = \sum_i \frac{n_i}{N_i} = 1 \tag{2.15}$$

in which, δ_i is the cycle ratios to failure. It can be seen that the maximum value of cycle ratios to failure is one. On the other hand, the fatigue failure of concrete occurs

if the summation of δ_i is one. The linear Palmgren-Miner law is therefore similar to the rule of damage accumulation; that the damage parameters vary from zero for the intact state, to one at the time of failure (Destrebecq, 2010). However, where the applied loading level (S_i) changes, δ_i is usually greater than one when the successive loading level (S_2) is increased. On the other hand, δ_i is generally less than one when the successive loading level (S_2) is reduced (see Figure 2.12). This can be expressed in terms of Palmgren-Miner's law, as shown in Eq. 2.16.

$$S_2 > S_1 \Longrightarrow \frac{n_1}{N_1} + \frac{n_2}{N_2} \geq 1 \tag{2.16a}$$

$$S_2 < S_1 \Longrightarrow \frac{n_1}{N_1} + \frac{n_2}{N_2} \leq 1 \tag{2.16b}$$

in which, S_1 and S_2 are the loading levels of loading sequence one and two respectively; n_1 and n_2 are the numbers of applied loading cycles for the loading levels S_1 and S_2, respectively, and N_1 and N_2 are the number of cycles to failure for loading levels S_1 and S_2, respectively.

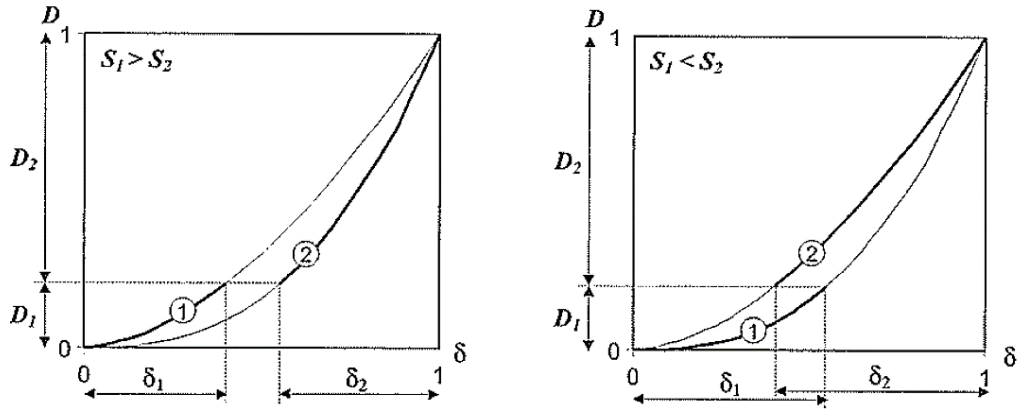

Figure 2.12: Non-linear accumulation of the cycle ratio to failure (Destrebecq, 2010)

2.4.5 Conclusions on recent fatigue prediction models

Presently, the bottom-up fatigue prediction model seems to be the only distress model that widely employs termination criteria for designing road pavement with cement-treated layers. Table 2.5 illustrates the fatigue prediction models that have been implemented in road pavement design guidelines developed by many different

countries around the world. From Table 2.5, the most significant advantages and limitations of the current fatigue models can be summarised as follows:

- All the fatigue prediction equations shown in Table 2.5 are empirical. This means that regression parameters must be calibrated to obtain reasonable prediction results. Accordingly, a series of laboratory tests and field data are usually required in the calibration process.

- To predict the in-service fatigue life of cement-treated layers, the South African Pavement Engineering Manual (SANRAL, 2013) proposed the application of the shift factor in the estimation, to account for layer thickness. For Wen et al. (2014), a fatigue life prediction equation was developed, incorporating a regression parameter which was calibrated from field data (to account for crack propagation). Austroads (2014b) advised reducing the design modulus to one-third of the flexural modulus, measured from laboratory-prepared specimens. In addition, a strain shift factor was introduced to account for low modulus micro-cracking in the CTB layer.

- Fatigue prediction equations for road pavement design with cement-treated layers in Australia, France, and South Africa were calibrated using results from an Accelerated Loading Facility (ALF) (R. Yeo, 2012). However, fatigue prediction equations employed in the US were calibrated using field measurement data (Wen et al., 2014).

- Wen et al. (2014) developed a prediction equation for the damage (or current) modulus in the field based on the linear Palmgren-Miner law. However, there is no verification of this in the literature.

- An Australian fatigue prediction equation was developed based on the equation of Exponent 12 (Austroads, 2014b). However, all other fatigue prediction equations were established in the form of logarithmic functions. A high exponent may be the source of large-scale errors in estimating the fatigue life of cement-treated layers.

2.5 Continuum Damage Mechanics (CDM) for fatigue modelling

CDM is a discipline in which internal damage variables are used on a macroscopic scale to quantify microscopic damage to a material (W. Zhang & Cai, 2010). Consequently, a damage variable (D), has generally been employed to represent damage levels. The minimum value of D (D = 0) indicates that the material is in its original state without any damage. Conversely, where D attains a maximum value of D = 1, the specified material is said to have reached a fully damaged state. In this context, the stress-strain constitutive law with regard to material damage (Mai, Le-Corre, Foret, & Nedjar, 2012) can be applied, as shown in Eq. 2.17.

$$\boldsymbol{\sigma} = (1 - D)\boldsymbol{C}\colon \boldsymbol{\varepsilon} \tag{2.17}$$

in which, $\boldsymbol{C}$ is a fourth-order undamaged Hooke's elasticity tensor, $\boldsymbol{\sigma}$ is a second-order stress tensor, $\boldsymbol{\varepsilon}$ is a second-order strain tensor, D is the damage variable, and the symbol ":" represents a double tensor contraction. In a one-dimensional problem, $\boldsymbol{C}$ is equivalent to Young's modulus of a material. Note that inelastic strain and time-dependent dynamic effects have been excluded from the stress-strain relationship in Eq. 2.17. It can be observed from Eq. 2.17 that D is the only additional parameter to the conventional elastic stress-strain relationship equation. Previous studies on the damage evolution characterisation of concrete material can be found in various literature (Rogge & Thiele, 2012; Shah, 1984; Sukontasukkul, Nimityongsakul, & Mindess, 2004; Vega, Bhatti, & Nixon, 1995; S. Xiao et al., 2011).

CDM has been used as a tool for the modelling of the fatigue behaviour of concrete and Asphalt Concrete (AC) for more than a decade. CDM is a discipline which quantifies the microscopic damage of material on a macroscopic scale by using internal damage variables (W. Zhang & Cai, 2010). Consequently, the damage variable (D) has generally been used to indicate the level of material damage. The fundamental Kachnov-Rabotonov theory shown in Eq. 2.18 is usually applied and has recently been used as a prototype for CDM model development (Marukami, 2012).

$$\dot{D} = A\left[\frac{\sigma}{1-D}\right]^{m} \tag{2.18a}$$

$$\dot{\varepsilon} = B\left[\frac{\sigma}{1-D}\right]^n \tag{2.18b}$$

in which, ($\dot{}$) denotes the time derivative, ε is the strain, σ is the stress, D is the damage variable, and A, B, m and n are the material constants. CDM was successfully applied to model the behaviour of Asphalt Concrete (AC) under cyclic loading by Kim and Little (1990). In their studies, the accumulated damage due to applied cyclic loading on AC was mainly caused by fatigue and viscoelastic relaxation. Internal state variables being pseudo strain, maximum pseudo strain in past history, and damage parameters, were carefully defined based on established assumptions. However, the work was limited to modelling the behaviour of AC when elastic and viscoelastic behaviour predominated. This model was further developed by Chehub (2002) to consider viscoplasticity behaviour in a constitutive model (VEPCD model).

Ameen and Szymanski (2006) stated that Paris' law is often used for fatigue analysis in concrete. Paris's law characterises the crack growth induced by external forces using the relationship equation shown in Eq. 2.19.

$$\frac{da}{dN} = C(\Delta K)^m \tag{2.19}$$

in which, *da/dN* is the crack growth per one load cycle, ΔK is the stress intensity range during the same load cycle, and C and m are the material constants. Vega et al. (1995) developed a non-linear fatigue damage model for concrete in tension, based on CDM. The prediction equation for damage to concrete due to crack propagation was established as a function of the tensile strength of concrete, with maximum, and minimum applied stresses. The proposed model was then validated by results from flexural fatigue tests. Alliche (2004) developed a 3-Dimensional (3D) damage model for fatigue loading of concrete based on CDM. However, the model's validity was tested only under uniaxial fatigue loading. On the other hand, Mai et al. (2012) verified their developed 3D fatigue model using results from a flexural fatigue test. In addition, a new concept for interpreting damage evolution; the bi-power law function, was introduced by the authors. The proposed damage evolution function proved a good fit with the experimental data. Raad (1981) developed a mechanistic model for the fatigue characterisation of cement-treated soil based, on the Griffith failure theory. The

damage to cement-treated soil was considered with regard to Miner's sum, in accordance with Palmgren-Miner's law.

2.6 Field performance of CTB in Australia

In order to incorporate developed fatigue prediction models into road pavement design guidelines, model verification is essential. Wen et al. (2014) calibrated their developed top-down and bottom-up fatigue models using a back-calculated modulus collected consecutively from fieldwork. These models were proposed for incorporation into the M-E pavement design guide developed in the US. As mentioned earlier, the fatigue models developed in France, South Africa and Australia were validated using data collected from Accelerated Loading Facilities (ALF) (Theyse et al., 2014; R. Yeo, 2012). This section presents some of the ALF results collected in Australia that relate to the performance of CTB layers.

R. Yeo (2012) conducted ALF experiments on test pavement sections where two cement-treated materials were used as the road base. These cement-treated materials were prepared from two different parent materials, Hornfels and Siltstone. The test pavement sections were loaded continuously with rolling half-axle wheel loads. The load capacity range of the Australian ALF was 40 kN to 80 kN. During the test, a rolling wheel travelled one way on 12-m strips of pavement section and was lifted off by its supporting frame at the end of each cycle. According to R. Yeo (2012), three thicknesses of CTB layer (100 mm, 150 mm, and 200 mm), three different design moduli (2,000 MPa, 5,000 MPa, and 10,000 MPa), and two maximum amplitude wheel loads (40 kN, and 80 kN) were employed during the design of the ALF test sections. Prior to the application of the ALF loads, the CTB layers were cured for at least 220 days and 400 days for Siltstone and Hornfels CTB, respectively. Plastic sheets were initially used to cover the compacted CTB layer for curing; primed and surfaced thin asphalt layers were then added. Prior to the asphalt layer coverage, shrinkage cracks on the CTB surface were investigated. The final thicknesses of the CTB layers after construction varied from 120 mm to 160 mm. The field density of CTB was 94% to 95% of the modified compaction density. The performance of test sections was determined based on surface cracking, deformation, and surface deflection. R. Yeo

(2012) assumed that the changes in deflection measured at various loading cycles represented changes in the material performance of CTB. This was due to the ALF experiments being conducted in an enclosed environment.

During the ALF loading, cracks on the pavement surface were investigated by visual inspection. Pavement deformations on the surface and deflections at different depths were monitored by a Transverse Profile (TP) and Multi-Depth Deflectometer (MDD), respectively. In addition, a Falling Weight Deflectometer (FWD) was also used to collect pavement deflections at regular stages of loading. Four axle load levels (40 kN, 50 kN, 60 kN, and 80 kN) were applied to the Siltstone CTB, while three axle load levels were used for testing on Hornfels CTB.

The back-calculated moduli of the cement-treated layers were obtained from the FWD data based on a linear elastic assumption. This assumption was employed for the CTB layers prior to the commencement of cracks or ALF loading. After the ALF loading commenced, cracked CTB material was modelled as a weakened linear elastic layer (Austroads, 2010b). The equivalent modulus approach was therefore used instead, after the layers had been wheel-loaded (R. Yeo, 2012). Accordingly, the fatigue prediction models developed from Australian ALF experiments for Hornfels and Siltstone CTB are presented in Eqs. 2.20 and 2.21, respectively.

$$LogN = -4.9Log(\varepsilon_i) + 14; n = 27, R^2 = 0.73 \quad (2.20)$$

$$LogN = -6.1Log(\varepsilon_i) + 17; n = 32, R^2 = 0.46 \quad (2.21)$$

in which, N is the number of applied loading cycles, ε_i is the initial tensile strain ($\mu\varepsilon$), n is the number of data points for fatigue equation development, and R^2 is the coefficient of variation. The mean initial moduli for Hornfels and Siltstone CTB are 12,000 MPa and 11,000 MPa, respectively.

CHAPTER 3

MECHANICAL CHARACTERSITICS OF BOUND CTB

3.1 Introduction and background

In Australia, the current design guidelines for pavement structure with Cement-Treated Base (CTB) were developed by the association of Australasian road transport and traffic agencies, Austroads (Austroads, 2010b). Recent literature indicates that the structural performance of CTB is essentially influenced by cement content, moisture content, aggregate, age, and degree of compaction (Arellano & Thompson, 1998; Austroads, 2014a; Croney & Croney, 1998; Horpibulsuk, Katkan, Sirilerdwattana, & Rachan, 2006; Wen et al., 2014; R. Yeo, 2012). Based on Austroads design guidelines (Austroads, 2013b), different types of CTB are classified according to their Unconfined Compressive Strength (UCS). Some Australian road authorities, such as the Queensland Department of Transport and Main Roads, and Main Roads Western Australia have used the elastic modulus as another classification index of CTB (Y. S. Yeo, 2011). To design pavement with a CTB layer, Austroads (2010b) recommends that the flexural modulus of CTB is to be used as the design input parameter to determine pavement layer thicknesses and estimate pavement life. The flexural modulus of CTB can be measured based on the flexural beam test method (Austroads, 2014a) that is also used to characterise the flexural response of concrete material. However, (Austroads, 2014b) has emphasised the limitation of the flexural beam test and suggested that further studies be undertaken to improve the testing procedure. Limitations include the uncertainty of specimen size, support conditions, preparation methods, and the initial condition of beam specimens (Austroads, 2014b; Walker & Bloem, 1957).

In the US, the elastic modulus, or Young's modulus, derived from the monotonic-compression test is formally employed as a design parameter for a road pavement with CTB (NCHRP, 2004). Later, Wen et al. (2014) suggested changing Young's modulus to the flexural modulus as the flexural beam test could reasonably simulate the material response in a real pavement more appropriately than the response from the monotonic-compression test. In addition, degradation of the material modulus, caused by the

accumulated damage induced by repetitive loading from traffic, can be calculated from a prediction model, as proposed by Wen et al. (2014).

The appropriate quantities of water and cement required for CTB mixtures are generally determined based on mix design procedures (Austroads, 2006b; PCA, 1956). Firstly, the trial value of the assumed amount of cement is used to prepare a CTB test specimen. Then, a series of UCS tests of CTB test specimens with varying cement content is conducted. The target UCS value recommended by the guidelines (Austroads, 2013b; NCHRP, 2004) is used to define the optimum cement content of CTB (Austroads, 2006b; Croney & Croney, 1998; Department of the Army; the Navy and the Air Force, 1994; PCA, 1956). It should be emphasised that CTB test specimens in the mix design process are generally prepared at Optimum Moisture Content (OMC) based on the compaction test (Austroads, 2006b; PCA, 1956). Thereafter, additional tests are required on CTB test specimens prepared at an optimum cement content — i.e., the durability test (Department of the Army; the Navy and the Air Force, 1994; PCA, 1956), and the swell and erodibility test (Austroads, 2006b).

It can be seen that the characteristics of CTB were typically investigated from test specimens prepared at OMC for relatively dense conditions. Therefore, the behaviour of CTB in less dense conditions would be less predictable. Horpibulsuk et al. (2006) investigated the effects of compaction moisture content (moulding moisture content) on the strength of cement-stabilised materials. Lateritic soils and crushed rock obtained from local pits in Thailand were used as the parent materials in the study. Test results revealed that the strength of cement-stabilised materials can be estimated based on two parameters: namely, water-cement ratio (*w/c*) and curing time. At a given age, the strength and material responses (in terms of stress-strain relationship) of specimens prepared at the same *w/c* are nearly identical, although compaction, moisture content, cement content, and compaction energy are different. Furthermore, the strength of field-prepared cement-stabilised specimens was correlated with that of laboratory-prepared specimens by Horpibulsuk et al. (2006). Different strength values of field-prepared and laboratory-prepared specimens resulted from the difference in non-uniform mixing in the field, and from the difference between curing and compaction methods in the laboratory and in the field.

Based on comparisons between past and recent developments in cement-treated materials, it could be said that to obtain more-effective CTB (the cement-treated material for pavement), more in-depth studies of CTB are required. The study in this chapter was carried out with the primary aim of characterising CTB with respect to its strength performance and shrinkage behaviour. Furthermore, a modified mix design concept for CTB, based on more rational mix design parameters and processes, was also developed. Standard crushed rock (CRB) from a local pit in Western Australia was used as the parent material for the CTB test specimens. Despite this, it is still the case that the gradations of parent material employed in the field may differ from those used in the laboratory. Previous literature demonstrates that road base performance is influenced by the gradation of parent materials (Y. Xiao, Tutumluer, Qian, & Siekmeier, 2012) and the amount of fines content (Davis, Warr, Burns, & Hoppe, 2007). The gradation and fines content of standard CRB were therefore varied for purpose of the investigation. The effects of crushed rock gradation and the effects of the amount of fines content on the performances of CTB were also examined in this chapter.

3.2 Materials

3.2.1 Parent material

Crushed Rock Base (CRB) from a local quarry (Gosnells) in Western Australia was employed as the parent material for CTB test specimens. The selected CRB was classified as granite/diorite. Table 3.1 presents the geotechnical properties of CRB used in this research. The particle size distribution curve of CRB is presented in Figure 3.1. This CRB can be categorised as a suitable material for roadway construction and it is used to produce CTB (Austroads, 2006b; Department of the Army; the Navy and the Air Force, 1994).

Table 3.1: Geotechnical properties of parent material (CRB)

Geotechnical properties	**Test standards/Sources**	
Particle density: coarse (g/cm^3)	AS 1141.6.1 (Standard Australia, 2000b)	2.75
Particle density: fines (g/cm^3)	AS 1141.5 (Standard Australia, 2000c)	2.59
Particle density: average (g/cm^3)	AS 1141.6.1 (Standard Australia, 2000b)	2.67
Water absorption: coarse (%)	AS 1141.6.1 (Standard Australia, 2000b)	0.61
Water absorption: fines (%)	AS 1141.5 (Standard Australia, 2000c)	10.83
Water absorption: average (%)	AS 1141.6.1 (Standard Australia, 2000b)	5.58
Fines content (%)	ASTM D422 (ASTM, 2007b)	8.12
Sand content (%)	ASTM D422 (ASTM, 2007b)	40.83
Gravel content (%)	ASTM D422 (ASTM, 2007b)	51.05
Coefficient of uniformity (C_u)	ASTM D422 (ASTM, 2007b)	70.00
Coefficient of curvature (C_c)	ASTM D422 (ASTM, 2007b)	3.66
Liquid limit (%)	Jitsangiam and Nikraz (2009)	22.40
Plastic limit (%)	Jitsangiam and Nikraz (2009)	17.60
Plastic index (%)	Jitsangiam and Nikraz (2009)	4.80
Linear shrinkage (%)	Jitsangiam and Nikraz (2009)	1.50
Flakiness index (%)	Jitsangiam and Nikraz (2009)	22.50
CBR	Jitsangiam and Nikraz (2009)	180.00
USCS	ASTM D2487 (ASTM, 2011a)	GP-GM /GP-GC
Maximum dry density (g/cm^3)	ASTM D1557 (ASTM, 2012b)	2.27
Optimum moisture content (%)	ASTM D1557 (ASTM, 2012b)	6.50
CBR = California Bearing Ratio USCS = Unified Soil Classification System		

3.2.2 Cement

General Purpose (GP) cement manufactured by Cockburn Cement was selected as the binder substance for CTB in this research. All essential properties of cement used in this research comply with AS 3972 (Standard Australia, 2010). During testing, the GP cement was stored in a cool, dry place and completely sealed.

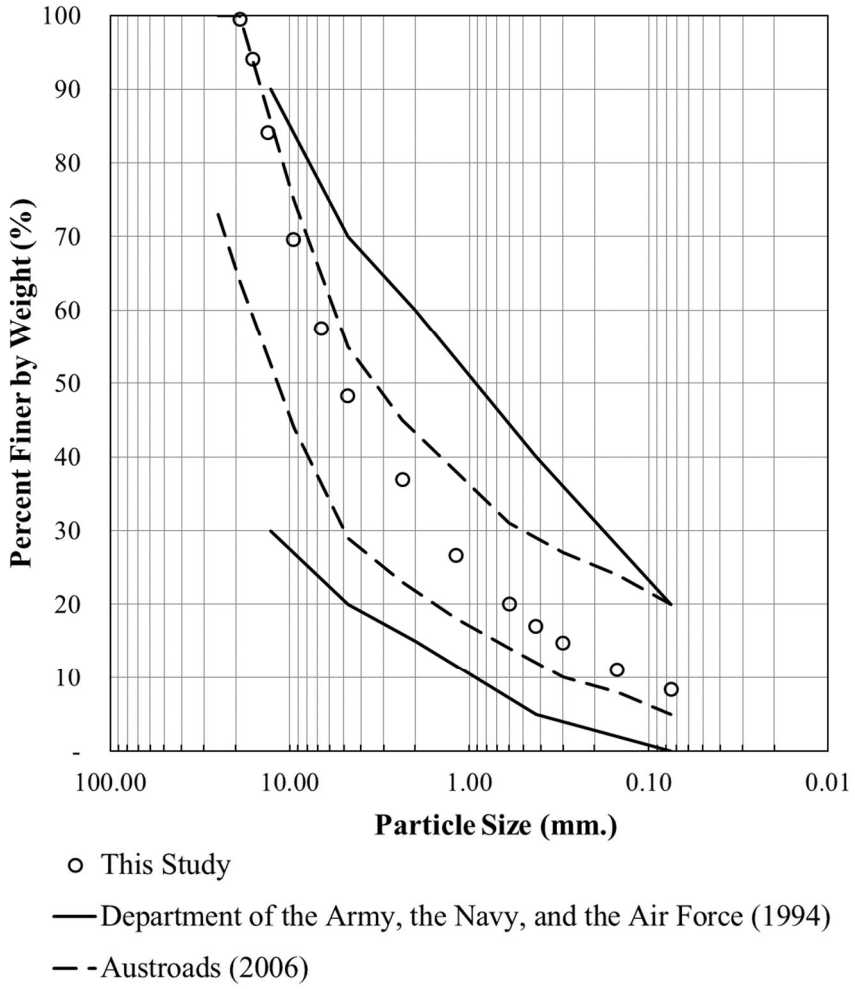

Figure 3.1: Particle Size Distribution (PSD) of parent material used for CTB preparation

3.2.3 Cement-Treated Base (CTB)

According to Austroads (2006b), CTB can be categorised into two types: modified and stabilised materials. Unlike stabilised materials, modified material behaviour is influenced by material grain interlocking (Y. S. Yeo, 2011). This particle interlocking leads to complex behaviour in a modified material. The test results from this research demonstrate that stabilised materials, under cyclic loading with a strain amplitude ranging between 45 and 105 $\mu\varepsilon$ (micro-strains), behave as elastic materials (see Chapter 4). This finding agrees with the assumption regarding multi-layered pavement design in which a cement-treated layer is presumed to be an elastic material. Austroads (2006b) recommended that the minimum cement content required for stabilised material is 3%. However, a cement content of 10% is considered as the maximum

value for economic use in road construction (NAASRA, 1970). Accordingly, the cement content of CTB test specimens in this research was limited to a minimum value of 3% and a maximum value of 10% for the UCS test. A few tests on a modified material (cement content less than 3%) were also conducted to fully complete the strength development curves. For the flexural strength test and shrinkage test, specimens with cement content varying from 3% to 6% were employed in this research.

3.3 Test specimen preparation

3.3.1 Specimens for UCS test

To prepare the CTB specimens for the UCS test, fresh CRB from the quarry was dried in an oven overnight. The process of oven-drying CRB differed from the standard procedure AS 5101.2.2 (Standard Australia, 2008a) and ASTM D558 (ASTM, 2011c), in which air drying is recommended. However, the moisture content of CTB in this preparation process could be controlled perfectly when completely dried CRB was employed in the specimen preparation. After oven-dried CRB had cooled to room temperature, aggregates larger than 19 mm were removed from the CRB by sieving. The CRB was then subdivided by passing it through a sample splitter. This process was performed to ensure uniformity in the gradation of subdivided CRB. Following this, a specified amount of CRB was mixed with water and kept in a sealed container for at least 24 hours. Prior to compaction, moist CRB was thoroughly mixed by hand with a prescribed amount of GP cement. Finally, the CRB and cement mixture were compacted in accordance with ASTM D1557 (ASTM, 2012b). According to the standard design procedure, the OMC and Maximum Dry Density (MDD) of the aggregates (Croney & Croney, 1998) for cement-treated materials (Department of the Army; the Navy and the Air Force, 1994) are two prerequisite parameters for road pavement design with a CTB layer. In summary, the parent material preparation process and the CTB mixing procedure of ASTM D558 (ASTM, 2011c) were followed in this research. The CRB and CTB cylindrical specimens for UCS tests were moulded following the modified compaction effort in accordance with ASTM D1557 (ASTM, 2012b).

Additional CTB test specimens with a moisture content of 0.8, 1.2, and 1.4 times the OMC were prepared for the UCS tests. Five layers of CTB were compacted manually in a mould; 100 mm in diameter and 115 mm in height, using a modified compaction effort. For every specimen, 95% of a specific MDD was assigned as a target degree of compaction. Compacted CTB test specimens were later extruded from a compaction mould and stored in a moist chamber for curing. A temperature of 23.0 °C ± 1.7 °C, and a relative humidity of not less than 96% were employed in specimen curing. In this research, the curing durations for CTB test specimens were set at 7, 14, 28, and 60 days after compaction. To investigate the effects of *w/c* ratio on strength development, CTB test specimens with a cement content of approximately 0.5% to 10% were prepared for the UCS tests. The mix proportions for each CTB specimen are summarised in Table 3.2.

3.3.2 Specimens for flexural strength test

Two sizes of prismatic beam specimen were employed for the flexural strength tests in this research. These included beams with dimensions of 63.5×50×400 mm^3 and 100×100×400 mm^3. Small-sized beams were prepared in accordance with the testing protocol for asphalt concrete (Austroads, 2005). CTB slabs, with dimensions of 400×300 mm^2 and a thickness of 75 mm, were made from the mixture of CRB, with the specified amount of cement and water at OMC. The mixtures were then compacted to achieve at least 95% of the MDD using a roller compactor (see Figure 3.2a). The material compaction proceeded according to AG:PT/T220 (Austroads, 2005). Each CTB slab was cured for at least seven days to gain sufficient strength before cutting. Three prismatic beams - 400 mm in length, 63.5 mm wide, and 50 mm thick - were then cut from each compacted slab, as shown in Figures 3.2b and c. All specimens were cured at 25°C for 28 days (after compaction) prior to the flexural strength tests.

Table 3.2: Mix design and UCS test results of CTB specimens

No.	Cement		Water		Water-Cement Ratio	UCS (MPa)	Curing (Days)
	(%)[a]	(g)	(%)[b]	(g)			
Specimens tested under static loading rate							
1	-	-	6.50	182.00	-	0.18	-
2	10.00	280.00	5.00	154.00	0.55	8.98	7
3	10.00	280.00	5.00	154.00	0.55	11.84	14
4	10.00	280.00	5.00	154.00	0.55	9.67	28
5	10.00	280.00	5.00	154.00	0.55	13.07	60
6	10.00	280.00	6.20	190.96	0.68	11.07	7
7	10.00	280.00	6.20	190.96	0.68	14.58	14
8	10.00	280.00	6.20	190.96	0.68	15.75	28
9	10.00	280.00	6.20	190.96	0.68	18.78	60
10	10.00	280.00	7.40	227.92	0.81	11.15	7
11	10.00	280.00	7.40	227.92	0.81	13.38	14
12	10.00	280.00	7.40	227.92	0.81	13.56	28
13	10.00	280.00	7.40	227.92	0.81	15.84	60
14	10.00	280.00	8.00	246.40	0.88	9.38	7
15	10.00	280.00	8.00	246.40	0.88	11.32	14
16	10.00	280.00	8.00	246.40	0.88	12.12	28
17	10.00	280.00	8.00	246.40	0.88	13.79	60
18, 19, 20	6.00	168.00	6.40	189.95	1.13	9.77, 10.08, 8.93	7
21, 22, 23	6.00	168.00	6.40	189.95	1.13	9.71, 9.60, 10.31	7
24, 25, 26	6.00	168.00	6.40	189.95	1.13	10.82, 11.67, 9.19	14
27, 28, 29	6.00	168.00	6.40	189.95	1.13	12.73, 12.71, 12.18	28
30	5.00	140.00	5.00	147.00	1.05	7.46	7
31	5.00	140.00	5.00	147.00	1.05	8.64	14
32	5.00	140.00	5.00	147.00	1.05	9.03	28
33	5.00	140.00	5.00	147.00	1.05	8.67	60
34, 35, 36	5.00	140.00	6.00	176.40	1.26	7.64, 7.41, 8.93	7
37, 38, 39	5.00	140.00	6.00	176.40	1.26	11.23, 10.11, 10.11	28
40	5.00	140.00	6.20	182.28	1.30	8.12	7
41	5.00	140.00	6.20	182.28	1.30	9.85	14
42	5.00	140.00	6.20	182.28	1.30	10.42	28
43	5.00	140.00	6.20	182.28	1.30	10.49	60

No.	Cement		Water		Water-Cement Ratio	UCS (MPa)	Curing (Days)
	(%)[a]	(g)	(%)[b]	(g)			
44	5.00	140.00	7.40	217.56	1.55	5.54	7
45	5.00	140.00	7.40	217.56	1.55	5.81	14
46	5.00	140.00	7.40	217.56	1.55	6.85	28
47	5.00	140.00	7.40	217.56	1.55	7.96	60
48	5.00	140.00	8.00	235.20	1.68	4.08	7
49	5.00	140.00	8.00	235.20	1.68	5.12	14
50	5.00	140.00	8.00	235.20	1.68	5.39	28
51	5.00	140.00	8.00	235.20	1.68	5.74	60
52, 53, 54	4.00	112.00	6.20	180.54	1.61	6.33, 7.09, 6.80	7
55, 56, 57	4.00	112.00	6.20	180.54	1.61	8.36, 6.82, 7.85	28
58	2.07	57.96	6.20	177.19	3.00	3.47	7
59	2.50	70.00	7.40	212.38	3.00	2.83	7
60	1.67	46.76	5.00	142.34	3.00	2.88	7
61	2.07	57.96	6.20	177.19	3.00	4.33	28
62	2.50	70.00	7.40	212.38	3.00	3.98	28
63	1.24	34.72	6.20	175.75	5.00	2.16	7
64	1.50	42.00	7.40	210.31	5.00	1.43	7
65	1.24	34.72	6.20	175.75	5.00	2.56	28
66	1.50	42.00	7.40	210.31	5.00	1.87	28
67	0.78	21.84	6.20	174.95	8.00	1.77	7
68	0.94	26.32	7.40	209.15	8.00	1.07	7
69	0.63	17.64	5.00	140.88	8.00	1.03	7
70	0.78	21.84	6.20	174.95	8.00	1.90	28
71	0.94	26.32	7.40	209.15	8.00	1.54	28
Specimens tested under dynamic loading rate							
72, 73, 74	4.00	112.00	6.20	180.54	1.61	8.08, 8.29, 9.06	7
75, 76, 77	5.00	140.00	6.00	176.40	1.26	9.14, 8.89, 9.62	7
78, 79, 80	6.00	168.00	6.40	189.95	1.13	10.69, 9.40, 11.66	7

(%)[a] = Percentage by weight of dry crushed rock (2,800 g.)

(%)[b] = Percentage by weight of dry mass (crushed rock and cement)

Figure 3.2: Manufacturing of small-sized beams: (a) a roller compactor used for making CTB slabs, (b) a cutting machine, and (c) prismatic beams cut from compacted slabs

For the large-sized beams - 400 mm in length, 100 mm wide, and 100 mm thick - the rectangular steel mould shown in Figure 3.3a was employed for specimen preparation. The CTB mixtures were prepared from dry CRB, cement, and water with an amount equivalent to OMC, using a concrete drum mixer. Following this, two equal thicknesses of CTB layers were immediately compacted in the steel mould to achieve at least 95% of the MDD. The compacted specimens were left in the steel mould for a minimum of 48 hours to gain sufficient strength prior to removal from the mould. The specimens were then cured for 28 days after the compaction was completed, the same period used for the small-sized beam specimens.

Figure 3.3: Manufacturing of large beam specimens: (a) a steel mould, and (b) a large-sized beam

3.3.3 Specimens for shrinkage test

The CTB specimens for the shrinkage test were prepared based on the test standard for concrete materials, AS 1012.13 (Standard Australia, 1992). A rectangular steel mould with dimensions of 75×75×280 mm^3 was used for shrinkage specimen compaction (see Figure 3.4a). In this research, the cement content of shrinkage specimens was varied from 3% to 5%. For the specimen preparation, specified amounts of CRB, cement, and water were thoroughly mixed using the same procedure as used for the UCS specimen preparation. According to the test standard, the mixtures require compaction immediately following the mixing process (Standard Australia, 1992). However, the CTB mixtures in this research were left in a sealed container for specific times prior to compaction, to investigate the effects of delayed compaction time. The delayed times employed in this research were 30 minutes, 1 hour, 2 hours, 3 hours, and 1 day. For every specimen, two equivalent layers were compacted using a tamping bar with distributed tamping strokes of not less than 35 times per layer. The compaction degree of all specimens achieved at least 95% of the MDD. The shrinkage specimens were left in the mould for approximately 48 hours prior to removal. After removal, the specimens were completely sealed with plastic film to prevent moisture loss during the curing process. All specimens were then placed into a curing chamber for 7 days before initial readings were taken. The temperature and relative humidity in the curing chamber were assigned at 23 °C and 96%, respectively. On the 6th day of curing, steel studs were installed at each ends of the specimens, using epoxy, as shown in Figure 3.4b. The stud installation technique using epoxy differed from the standard method (Standard Australia, 1992), and was undertaken in order to avoid specimen failures which can occur during the stud insertion process.

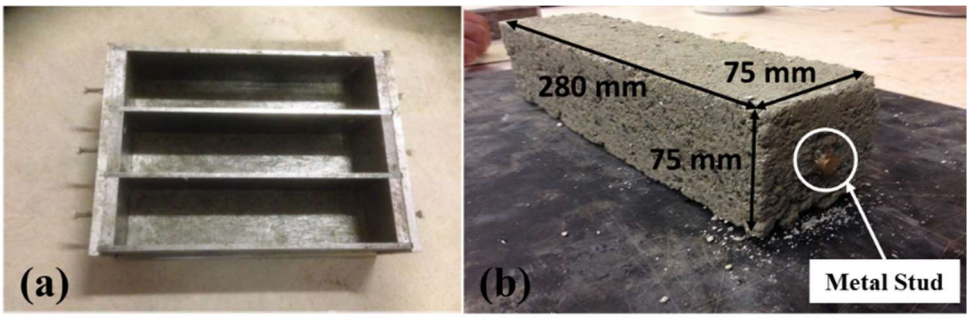

Figure 3.4: (a) Steel mould for shrinkage specimen preparation, and (b) shrinkage specimens with metal studs

3.4 Strength development of compacted CRB and bound CTB

The UCS tests for CTB in this research were conducted based on AS 5101.4 (Standard Australia, 2008b). It should be noted that the test procedure according to AS 5101.4 is similar to ASTM D1633 (ASTM, 2000). When the CTB test specimens had reached their target curing times, they were submerged in water for 4 hours. The water was then allowed to drain out from the specimens for 15 minutes before the UCS tests commenced. The UCS tests were conducted in accordance with AS 5101.4 (Standard Australia, 2008b). The stress-strain values of the materials while testing were also monitored and recorded. Based on the standards for the tests (ASTM, 2000; Standard Australia, 2008b), the recommended compressive loading rate was used, this being 1.0 mm/minute.

3.4.1 Strength development of compacted CRB

Figure 3.5 illustrates the compaction curves of CRB compared to CSB. Based on the test results, the OMC and MDD of CRB were 6.5% and 2.27 g/cm^3, respectively. The strength development and the stress-strain curves of compacted CRB with various moisture content are presented in Figure 3.6.

Figure 3.6a clearly shows that the strength of compacted CRB reduces with an increase in moisture content at the compaction stage while preparing test specimens. Moreover, specimens compacted on the dry-side of OMC are brittle (i.e., steeper curves) than the specimens compacted on the wet-side of OMC (see Figure 3.6). Similar observations can be found in Horpibulsuk et al. (2006) and Leroueil and Hight (2013). The reduction in the strength of CRB, when moulding moisture content increases, is principally caused by suction (Kohgo, Nakaho, & Miyaki, 1993; Leroueil & Hight, 2013). Generally, the suction of typical soils reduces when the moisture content of soil increases. This is because of the changes in soil structure and pore size.

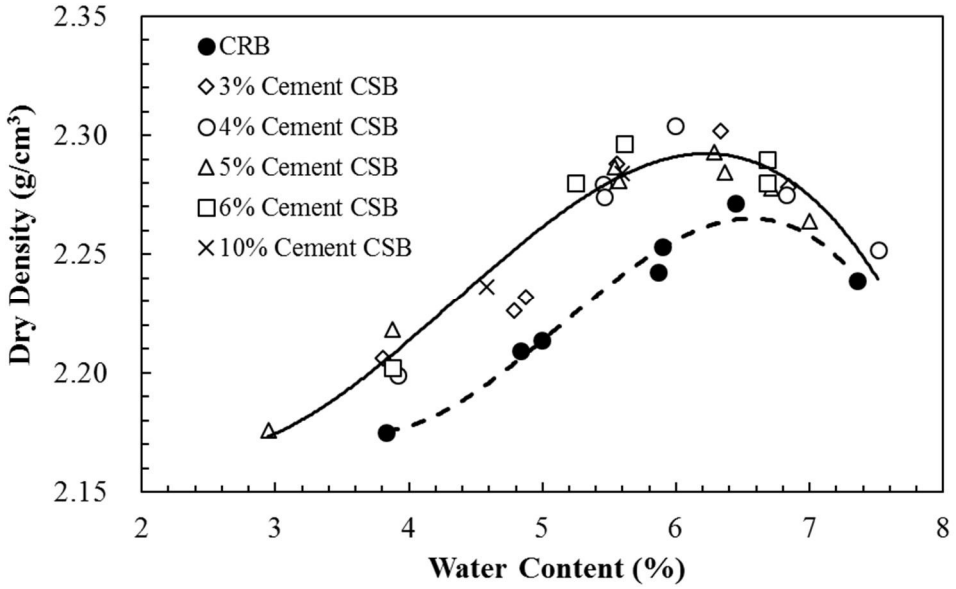

Figure 3.5: Compaction curves of CRB and CTB by modified effort

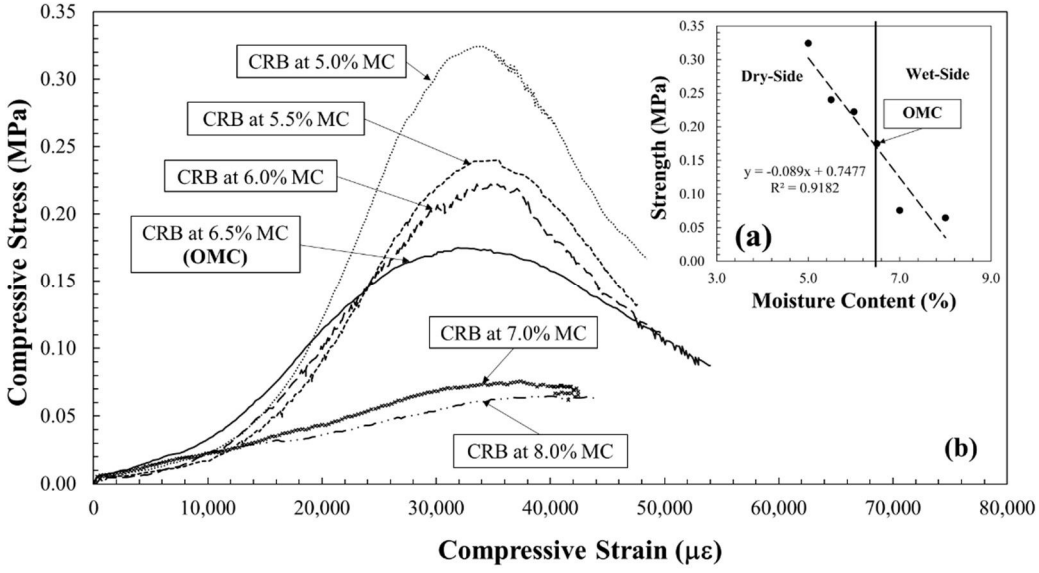

Figure 3.6: (a) Strength, and (b) stress-strain relationships of compacted CRB with varying moisture content

3.4.2 Strength development of CTB

The compaction curves of CTB (see Figure 3.5) reveal that the OMC and MDD of CTB are 6.2% and 2.29 g/cm^3, respectively. The OMC of CTB is slightly lower than that of CRB, but the MDD of CTB is higher. However, the cement content seems to have negligible effect on the compaction curve of CTB. Therefore, identical OMC and

MDD were applied to every CTB test specimen with different cement content. Table 3.2 provides a summary of UCS test results obtained from this research. The strength development of CTB test specimens prepared at OMC is shown in Figure 3.7a. The specimens with cement content of less than 3% were the modified material, while the specimens with cement content greater than 3% and up to 10% were considered to be the stabilised material (Austroads, 2006b). Figure 3.7a clearly shows that specimen strength grows at a slower rate with increases in cement content, when the cement content exceeds approximately 7%. It indicates that adding cement greater than 7% to this CRB would result in minor improvements to its material strength. Similar findings can be found in Horpibulsuk, Miura, and Nagaraj (2003) and Horpibulsuk et al. (2006). Horpibulsuk et al. (2006) described the strength development mechanism of cement-treated laterite soils and recommended dividing the strength development into three different zones (see Figure 3.7b). The soil-cement interaction zone is the area in which strength of CTB dramatically rises when the cement content increases. The rate of strength gain reduces in the transition zone if an amount of cement is continually added to material beyond the boundary line. Finally, the cement-soil interaction zone indicates the proportions of strength rising again after the transition zone. However, the cement content required to achieve this proportion is considerably high. Therefore, this research emphasises that the cement content of CTB should fall within the soil-cement interaction zone for the effective use of a cement additive.

Figure 3.8 demonstrates the strength of 5% and 10% cement CTB prepared with different moisture content. It clearly shows that based on these results, the UCS of CTB is significantly influenced by cement content, moulding moisture content, and curing time. As shown in Figure 3.8, the maximum strength of CTB was observed at OMC for almost every cement content value and curing duration. For CTB test specimens compacted at OMC, the strength of CTB increased by 1.4 – 1.8 times when the cement content was doubled. The increase in the strength of CTB also depended on the curing time. Similar outcomes can be found in Horpibulsuk et al. (2006).

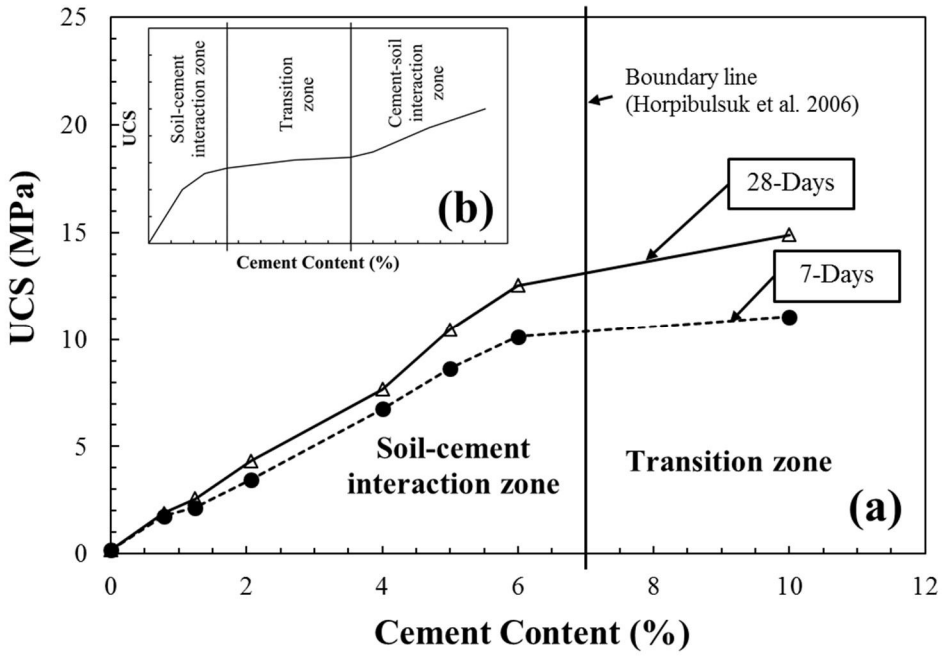

Figure 3.7: (a) Strength development of 7-day and 28-day CTB prepared at OMC, and (b) strength development zones of cement-stabilised materials

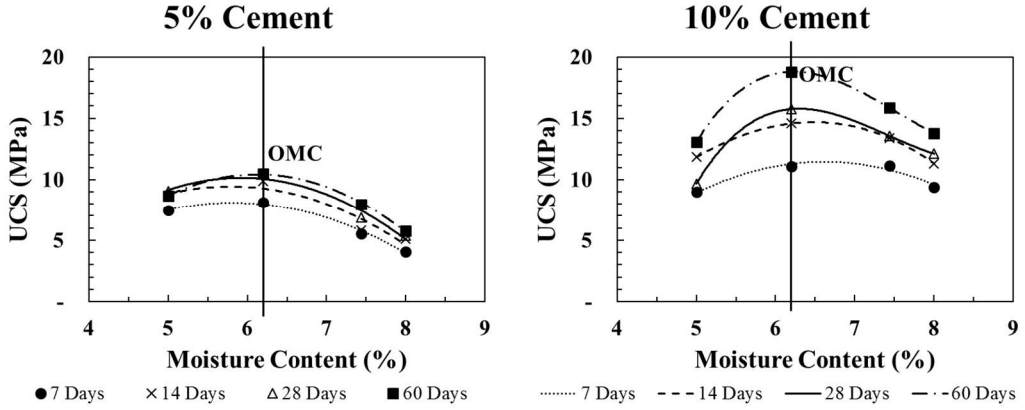

Figure 3.8: Strength development of 7-day and 28-day CTB prepared at OMC

Examples of stress-strain curves summarized from the UCS tests are shown in Figure 3.9. Similar to CRB, CTB appears to have a more brittle response if the specimens are moulded at a relatively low moisture content. In addition to the influence of the moisture content, the cement content also affects the stress-strain relationship of CTB. Figure 3.9 illustrates that CTB with higher cement content is more brittle than CTB with lower cement content, particularly for the less-aged specimens (Figures 3.9a and

c). More importantly, the elastic modulus of CTB seems to be influenced by the moisture content at compaction and the cement content.

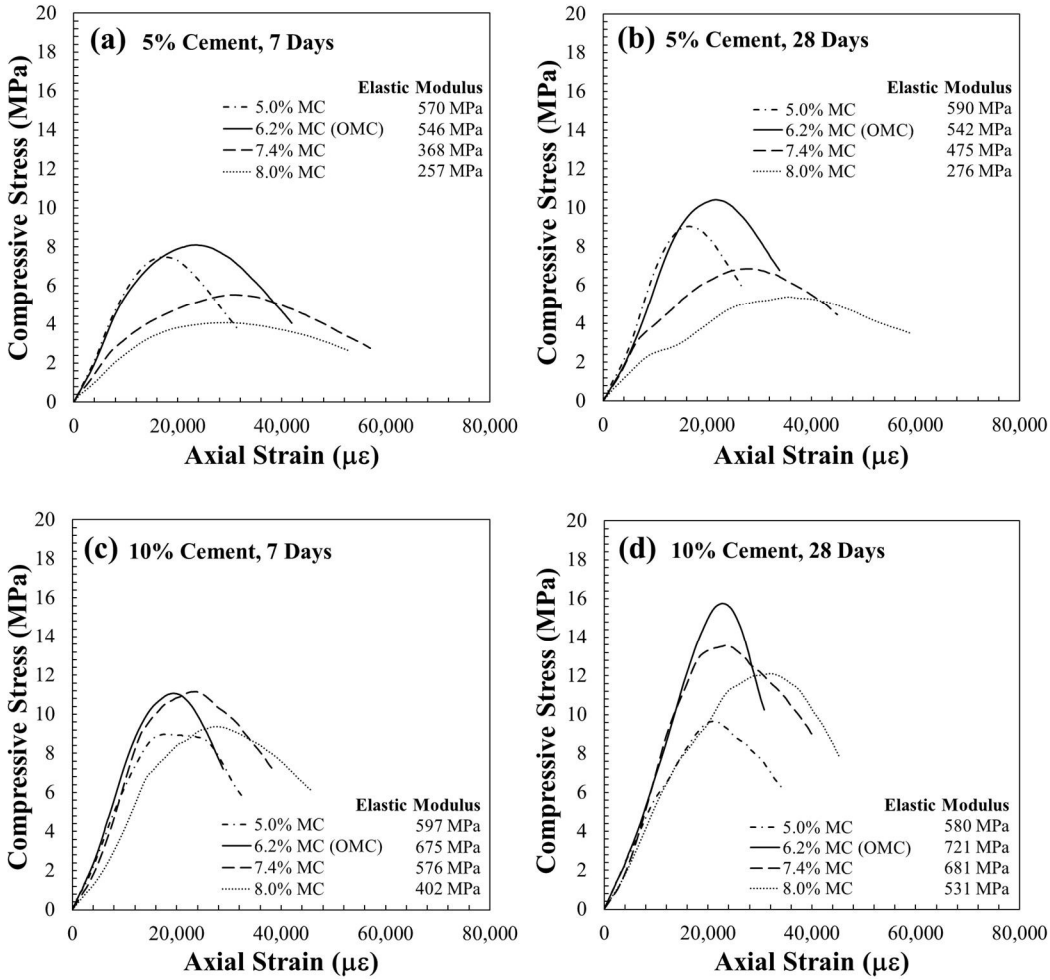

Figure 3.9: Stress-strain relationships of CTB test specimens with (a) 5% cement and 7-day curing, (b) 5% cement and 28-day curing, (c) 10% cement and 7-day curing, and (d) 10% cement and 28-day curing

The elastic moduli of CTB compacted at low moisture content are mostly higher than the elastic moduli of specimens prepared at a high moisture content. Likewise, CTB with high cement content is observed to be generally stiffer than specimens with low cement content. The abovementioned elastic moduli are chord moduli, calculated in accordance with ASTM C469 (ASTM, 2010b). It is important to emphasise that the traffic-induced strain encountered in the field is typically within the small strain range (see Chapter 4). Therefore, it may not be appropriate to apply the elastic modulus

measured from the monotonic-compression test to the design of a road pavement structure.

In summary, Figures 3.8 and 3.9 show that the maximum strength of CTB can be achieved by employing moisture content equal to OMC in the compaction process. Moreover, the CTB appears to be mostly stiffer and more brittle when the moulding moisture content is less than the OMC (specimens with 5% cement content) or equivalent to the OMC (specimens with 10% cement content).

3.5 Development of modified mix design concept for CTB

In soil materials, the compacted dry density is governed by the moisture content in the mould or the moisture content at compaction. The maximum dry density of soils can be achieved by employing moisture content at OMC for moulding the specimens. However, compacting the soil with a degree of moisture content that differs from the OMC leads to a reduction in the dry density (see Figure 3.5). This reduction is caused by a rise in the pore volume of the soil mass (Craig, 2004). In addition to the dry density, the strength of compacted soil is also influenced by the suction force within the pore space of soils. Therefore, the strength of compacted soils at their densest state (at OMC and minimum pore volume) is possibly less than the strength of compacted soil in a looser state, resulting from the effect of suction (see Figure 3.6). In contrast to soils, the maximum strength of CTB is generally found in specimens moulded at OMC (see Figure 3.8). Nevertheless, the strength of concrete-like material is also influenced by pore volume or degree of compaction (Neville, 1998). The increase in pore volume, less so in compaction degree, typically results in decreasing concrete strength. In addition to compaction degree, the water-cement ratio is also an important factor in the mix design of concrete and CTB (Aderibigbe, Akeju, & Orangun, 1985; Horpibulsuk et al., 2006; Yoon & Abu-Farsakh, 2009; Z. Zhang & Tao, 2008). Figure 3.10 illustrates the relationships between the water-cement ratio and the strength of CTB.

Horpibulsuk et al. (2006) formulated the relationship between the strength of cement-stabilised coarse grained soil and water-cement ratio as Eq. 3.1.

$$q_u = A/(w/c)^B \quad (3.1)$$

where q_u is the UCS of the material, *w/c* is the water-cement ratio, and *A* and *B* are empirical constants. The parameters *A* and *B* generally vary across different soil types and curing times. Figure 3.10a illustrates the relationship between the water-cement ratio and the UCS of CTB. This can be drawn by a trend line which connects a set of peak UCS values of test specimens having particular cement content and curing times. A trend line can be clearly observed from the specimens compacted at OMC. Figure 3.10a also shows that the strength of CTB depends significantly on the water-cement ratio. However, the strength of CTB test specimens compacted on the dry-side of optimum (left-hand side of the peak strength) cannot be estimated accurately by the water-cement ratio due to the complex physical-chemical processes among water, cement, and the parent material of CTB (Horpibulsuk et al., 2006; Z. Zhang & Tao, 2008). Strong correlations are observed only from the values corresponding to CTB test specimens compacted at OMC and on the wet-side of OMC. Therefore, the strength development lines of 7-day and 28-day cured CTB were created from the specimens compacted at OMC and on the wet-side of OMC (see Figure 3.10b). The regression equations in this research, such as those illustrated in Figure 3.10, were obtained from the analysis package in Excel. Figure 3.10b shows that the strength of CTBs at different curing durations varies slightly. Previous literature illustrates that the strength of cement-stabilised soil also depends on the dry density of the material (Z. Zhang & Tao, 2008). These characteristics of cement-stabilised soil are similar to the characteristics of concrete for structural applications. Cement-stabilised soils moulded to achieve maximum dry density (compacted at OMC) generally provide the highest strength (Aderibigbe et al., 1985; Yoon & Abu-Farsakh, 2009), as shown in Figures 3.8 and 3.10a.

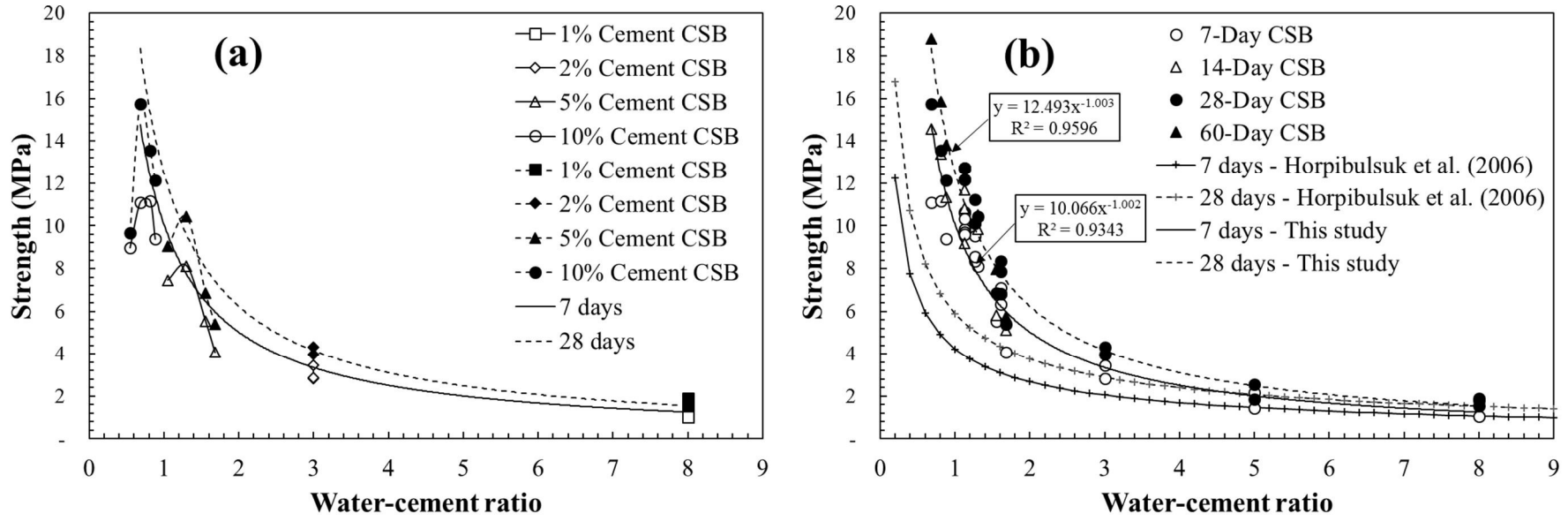

Figure 3.10: Relationship between water-cement ratio and strength of CTB at (a) different cement content, and (b) different curing durations

The American Concrete Institute (2005) defined the water-cement ratio of concrete for structural applications as the ratio of mass of effective water in the aggregate to the mass of cement. Effective water is defined as the amount of water solely involved in the cement hydration process. This includes the amount of water possessed by the products of hydration and the quantity of water left in the void space (Neville, 2006). Former studies on the relationship between the effective water-cement ratio and the strength of concrete can be found in Newman (1959) and Poon, Shui, Lam, Fok, and Kou (2004). The quantity of effective water can be calculated by subtracting the moisture content at the Saturated-Surface Dry (SSD) state from the total moisture content of the aggregate (Mohammadinia et al., 2015; Neville, 2006). Field aggregates are typically in an air-dried or damp (wet) condition and these are different from the conditions in the laboratory test. The aggregate used in the laboratory generally relies on oven-dried or SSD conditions. Therefore, an explicit definition of water quantity in the water-cement ratio should be provided to avoid any confusion (Neville, 1998; Newman, 1959). According to Table 3.1, the capability of oven-dried CRB to absorb water and achieve the SSD condition is 5.58%. The effective water, is therefore calculated by subtracting 5.58% from the moulding moisture content. The average water absorption in Table 3.1 was weighted based on the relative masses of coarse and fine material (Standard Australia, 2000b). Similar to Figure 3.10, the relationship between the strength of CTB and the effective water-cement ratio with different cement content and curing durations is presented in Figure 3.11. Figure 3.11a shows that an amount of water for CTB test specimens compacted on the dry-side may be absorbed completely by oven-dried CRB prior to mixing with cement (effective water is a negative value). Therefore, the amount of water for the hydration process was deficient and led to complications in strength prediction for the case of CTB compacted on the dry-side of optimum. Accordingly, strength development lines with respect to variations in the effective water-cement ratio were drawn from CTB test specimens compacted at OMC and on the wet-side (see Figure 3.11b). However, the values of R^2 were reduced from 0.96 to 0.82 for the 28-day curing CTB and from 0.93 to 0.85 for the 7-day curing CTB, compared to the strength development lines estimated from the water-cement ratio. It can be seen from Figure 3.11 that the correlation between the effective water-cement ratio and the strength of CTB is influenced by the dry density of the material. The strength development lines of

specimens with a dry density equal to MDD (compacted at OMC) can be differentiated from specimens with a dry density lower than MDD (compacted on the wet-side).

Figures 3.12a and b show the strength development lines of the 7-day curing CTB and the 28-day curing CTB, without taking into account the strength of CTB compacted on the dry-side of OMC. The regions of strength development were drawn from two strength development lines that were estimated from CTB test specimens compacted with differing moisture content. The upper boundary lines were created from the strength measurements of specimens compacted at 7.44% moisture content (wet-side), while results from specimens moulded at OMC were used to develop the lower boundary line. Figure 3.12 shows that at the identical value of the effective water-cement ratio, CTB test specimens compacted on the wet-side provided a higher strength value than that of the specimens compacted at OMC. At the point of identical effective water-cement ratio, specimens compacted on the wet-side typically required a higher cement content to attain the same effective water-cement ratio of the specimens compacted at OMC. Therefore, a higher cement content would be a major factor in strength increase in the specimens compacted on the wet-side compared to specimens moulded at OMC. This finding is also in line with the previous assumption that for a set of specimens prepared at the same cement content, greater strength is generally observed from the specimens compacted at OMC (see Figure 3.11a).

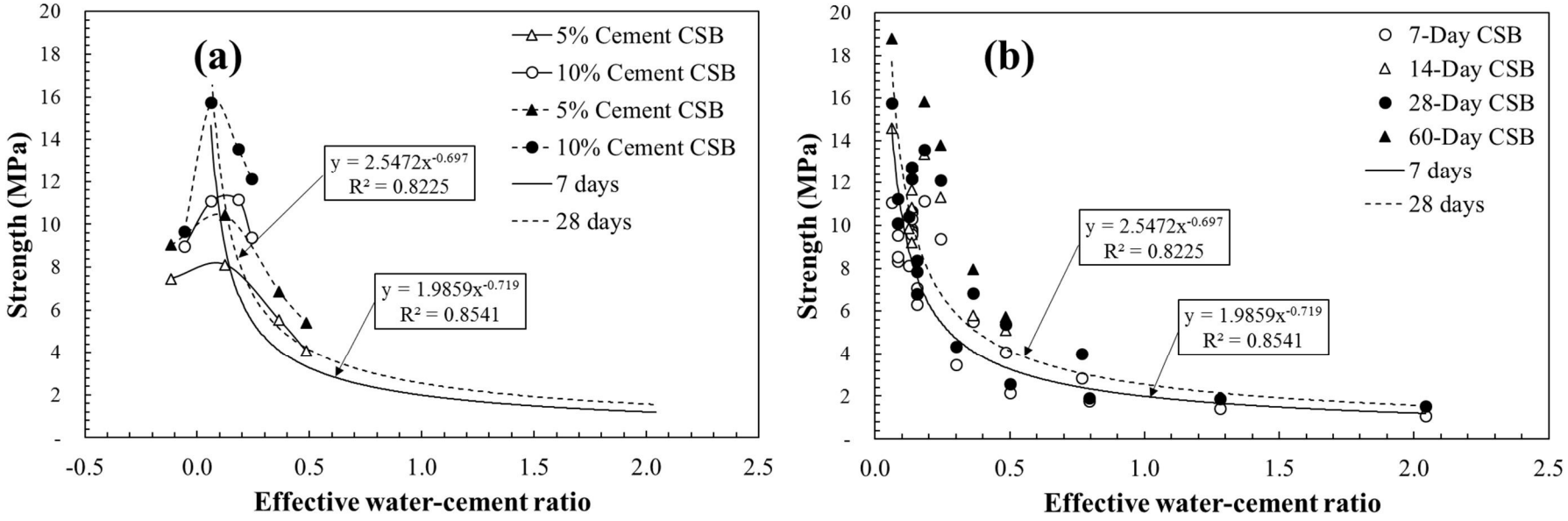

Figure 3.11: Relationships between effective water-cement ratio and strength of CTB at (a) different curing durations, and (b) with varying cement content

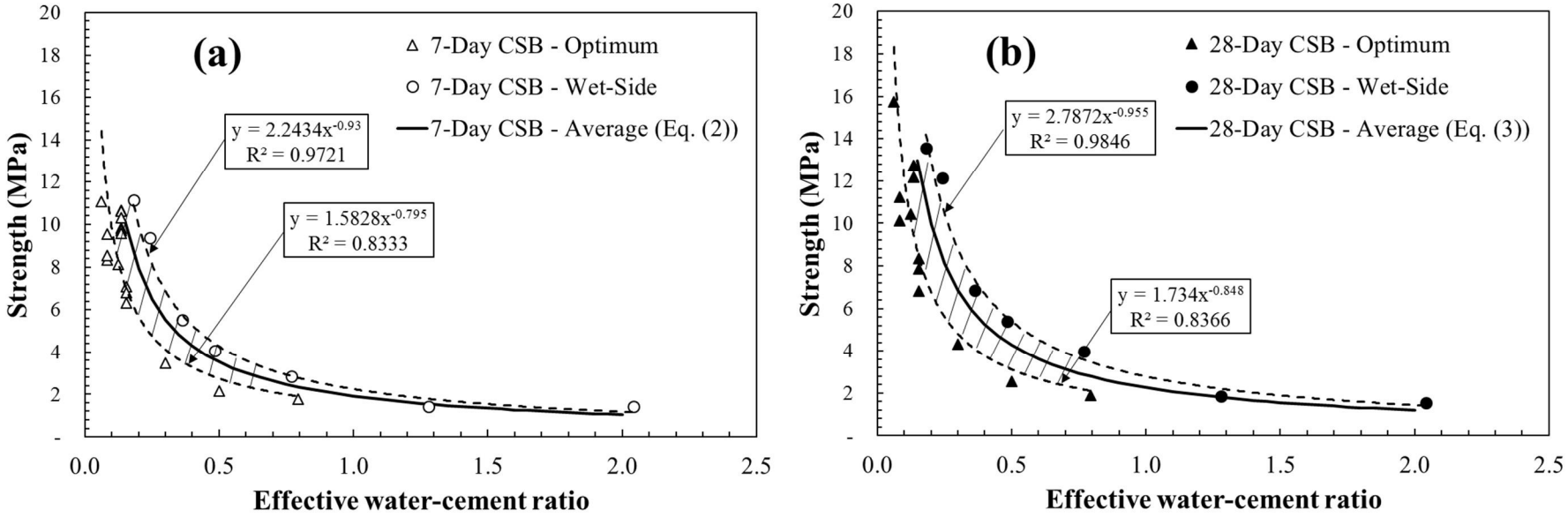

Figure 3.12: Relationship between effective water-cement ratio and strength of CTB at (a) 7 days, and (b) 28 days

The equations for the average strength development lines for 7-day and 28-day curing CSB test specimens are given in Eqs. 3.2 and 3.3, respectively.

$$q_{u,7\ days}(MPa) = 1.9171/(\frac{w_{eff}}{c})^{0.88} \quad (3.2)$$

$$q_{u,28\ days}(MPa) = 2.2635/(\frac{w_{eff}}{c})^{0.92} \quad (3.3)$$

where w_{eff}/c is the effective water-cement ratio. Test results indicate that the strength of CTB from the UCS tests can be estimated from the effective water-cement ratio and the curing duration. Therefore, a new CTB mix design concept, which can incorporate variations in moisture content in the mould, cement content, and curing duration, was developed based on the test outcomes in this research. It is to be noted that the relationship between the UCS and the water-cement ratio is independent of compaction effort, when dynamically compacted with modified compaction effort (Horpibulsuk et al., 2006; Neville, 1998). However, Horpibulsuk et al. (2006) demonstrated that UCS values derived from roller-compacted CTB (field) specimens are generally lower than those of hand-compacted CTB (laboratory) specimens by a magnitude of 0.5 to 1.0 times. The difference in the UCS values of the CTB in the field and in the laboratory is caused by different compaction methods (roller vs hand-compaction), different curing conditions, and the non-uniform mixing of soils with cement in the field.

3.5.1 Proposed mix design procedure for CTB

The mix design procedure for CTB developed in this research is presented below. The design steps are undertaken following the completion of the strength development prediction equation. The equations, for example, Eqs. 3.2 and 3.3, are determined in the laboratory.

- Determine OMC and MDD of the parent material from the compaction test to estimate a target OMC for the CTB mixture. Based on current research, an assumption can be made that the OMC of the parent material is equal to the OMC of a CTB mixture at any percentage of cement content (but less than 10%). However, the assumption of CRB and CTB having an equal OMC may only be true for the parent material used in this research.

- Estimate the strength of CTB material in the field at the 7- and 28-day mark post-construction, using Eqs. 3.2 and 3.3 respectively, based on the effective water-cement ratio. In addition, the effects of dry density on the strength of CTB can be illustrated in the boundary lines, as shown in Figure 3.12.

- Refine the quantities of water and cement appropriate to the moisture content of field conditions and the target UCS value.

3.6 Effects of crushed rock gradation on the strength of bound CTB

Gradation or Particle Size Distribution (PSD) of aggregate significantly influences the material density, void, workability, durability, and other characteristics of concrete (Neville, 1998). Previous literature indicates that the workability of concrete can be improved if the concrete is produced from uniformly distributed aggregates, as opposed to gap-graded aggregates (Arora, Kumar, & Dhoopad, 2015; Golterman, Johansen, & Palbfl, 1997). Y. Xiao et al. (2012) examined the effects of aggregate gradation on the mechanical performance of unbound road base used in Minnesota, US. The study results revealed that the shear strength, resilient modulus, and compaction degree of road base could be correlated with gravel-to-sand ratio (G/S) of aggregate. The gravel-to-sand ratio is defined based on Eq. 3.4 (Y. Xiao et al., 2012).

$$\frac{G}{S} = \frac{p_{75mm} - p_{4.75mm}}{p_{4.75mm} - p_{0.0075mm}} = \frac{(D_{max})^n - 4.75^n}{4.75^n - 0.075^n} \tag{3.4}$$

in which, p_{75mm} is the percentage of material by weight passing a 75-mm opening sieve, $p_{4.75mm}$ is the percentage of material by weight passing a 4.75-mm opening sieve (No. 4), $p_{0.075mm}$ is the percentage of material by weight passing a 75-μm opening sieve (No. 200), D_{max} is the maximum size of the aggregate, and n is the shape factor of the gradation curve. The shape factor of the soil gradation curve can be calculated based on Eq. 3.5 (Sánchez-Leal, 2007).

$$p_i = \left(\frac{D_i}{D_{max}}\right)^n \tag{3.5}$$

in which, D_i is the opening size of any sieve, and p_i is the percentage of soil particles finer than the sieve opening size D_i. In this research, the UCS of CTB specimens prepared from three different gradations of crushed rock was investigated. Standard CRB with the gradation shown in Figure 3.1 was used to produce three modified CRB samples with different gradations (G-1, G-2, and G-3) as shown in Figure 3.13. The UCS specimens were prepared based on the same procedure shown in Section 3.3.1. However, the CTB specimens produced from G-1 crushed rock failed when extruding the CTB specimens from a standard mould—115 mm in length, and 100 mm diameter—as illustrated in Figures 3.14a and b. Therefore, a split mould of 100 mm in diameter and 200 mm in height (see Figure 3.14c) was substituted for the standard mould, for the preparation of CTB specimens moulded from G-1 crushed rock. A standard mould was still employed for the compaction process of CTB specimens moulded from G-2, and G-3 crushed rock. The cement content used for characterising the effects of CRB gradation was 3%, 4%, and 5% of dry CRB weight.

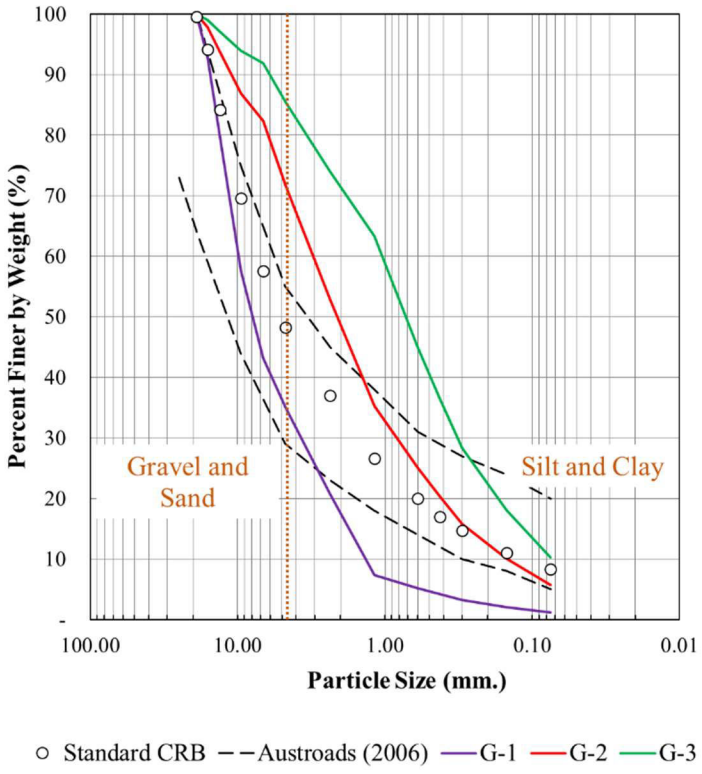

Figure 3.13: Particle Size Distribution (PSD) of modified crushed rock used to examine the effects of gradation on the UCS of CTB specimens

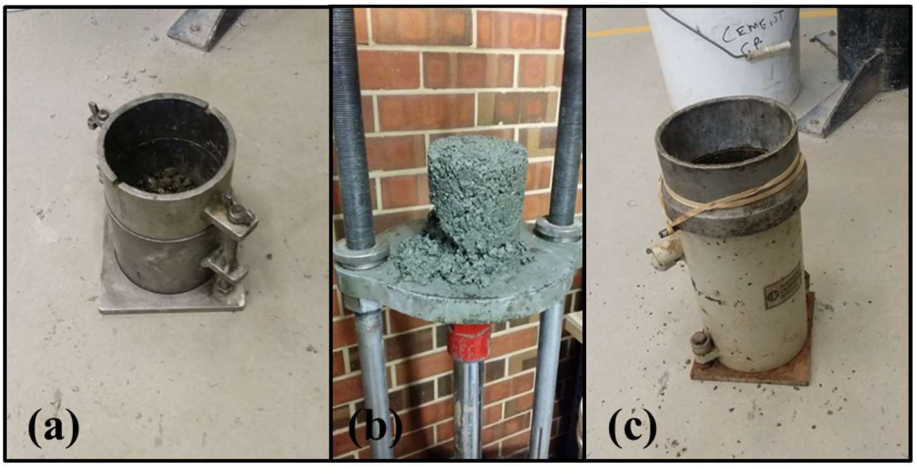

Figure 3.14: (a) Standard compaction mould, (b) failed CTB specimens prepared from G-1 crushed rock, and (c) split compaction mould

To compare the results of the UCS values obtained from different sized specimens, correction factors recommended by ASTM (2013) were multiplied by the UCS of specimens with a length to diameter ratio (L/D) of less than two. The correction factors suggested by ASTM (2013) are presented in Table 3.3. Accordingly, a correction factor equal to 0.903 (L/D = 1.15) was applied to CTB specimens moulded from G-2, and G-3 crushed rocks. The corrected UCS values of CTB prepared from all modified CRB are presented in Figure 3.15.

Figure 3.15 shows that the gradation of the parent material greatly affects the UCS of CTB materials. According to ASTM (2011a), soil particles larger than 4.75 mm are categorised as coarse-grained soil (gravel and sand); whereas soil particles smaller than 4.75 mm are classified as fine-grained soil (silt and clay). It can be seen from Figure 3.15 that the larger UCS values were generally observed in the 7-day and 14-day specimens moulded from crushed rock with a higher amount of coarse-grained particles (G-1 > G-2 > G-3). However, the 28-day specimens behaved differently; the specimens prepared from G-2 crushed rock provided the highest UCS when the specimens were cured for 28 days.

Table 3.3: Correction factors for UCS of concrete based on L/D (ASTM, 2013)

Length to Diameter Ratio (L/D)	Strength Correction Factor
1.75	0.98
1.50	0.96
1.25	0.93
1.00	0.87

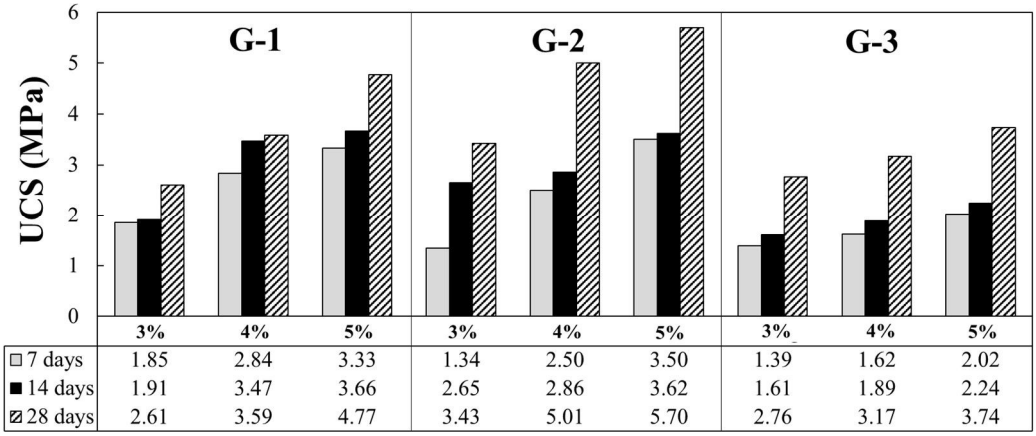

	G-1			G-2			G-3		
	3%	4%	5%	3%	4%	5%	3%	4%	5%
7 days	1.85	2.84	3.33	1.34	2.50	3.50	1.39	1.62	2.02
14 days	1.91	3.47	3.66	2.65	2.86	3.62	1.61	1.89	2.24
28 days	2.61	3.59	4.77	3.43	5.01	5.70	2.76	3.17	3.74

Figure 3.15: UCS of CTB specimens prepared from three different gradations of modified CRB

Figure 3.16 shows the strength development of specimens with 5% cement content, moulded from CRB with different gradations. The UCS obtained from specimens moulded from standard crushed rock was corrected by multiplying the UCS values by 0.903 (L/D = 1.15). Figure 3.16 illustrates that the highest UCS is always observed in CTB specimens prepared from standard crushed rock. However, if the crushed rock gradation falls outside the standard boundary (see Figure 3.13), an increase in the amount of coarse-grained soils (or a reduction in the amount of fine-grained soils) may lead to an increase in the UCS of CTB. This hypothesis is also supported by the findings in the investigation detailed below.

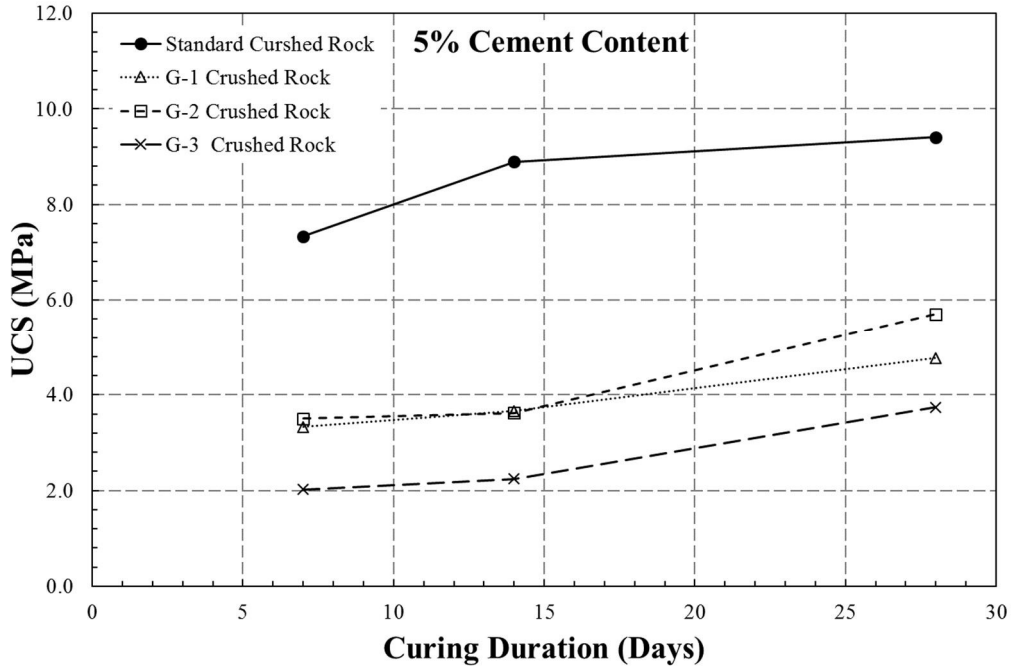

Figure 3.16: Strength development of specimens with 5% cement content prepared from CRB of different gradations

Davis et al. (2007) demonstrated that the changes in the amount of fines content of CRB, slightly influences the UCS of cement-treated aggregates. In this research, crushed rock particles finer than 75 μm were initially extracted from standard CRB, i.e., CRB containing approximately 8% of particles finer than 75 μm, as shown in Figure 3.1. Extracted fine particles were then added back to fresh standard CRB. The percentage of particles finer than 75 μm in the standard crushed rock therefore rose - with increases of 10%, 20%, and 30%.

The UCS of CTB specimens prepared from three modified CRB samples is illustrated in Figure 3.17. The UCS of CTB moulded from CRB with 10% particles finer than 75 μm is higher than the UCS of CTB moulded from CRB with 20% and 30% particles finer than 75 μm. However, the strength development of CTB specimens obtained in this section seems to have little correlation with the specimen curing times. The comparison between the UCS obtained from specimens moulded from standard crushed rock, and that of crushed rock with 10%, 20%, and 30% particles finer than 75 μm is shown in Figure 3.18. It can be seen from Figure 3.18 that an increase in the amount of particles finer than 75 μm may result in a reduction in UCS.

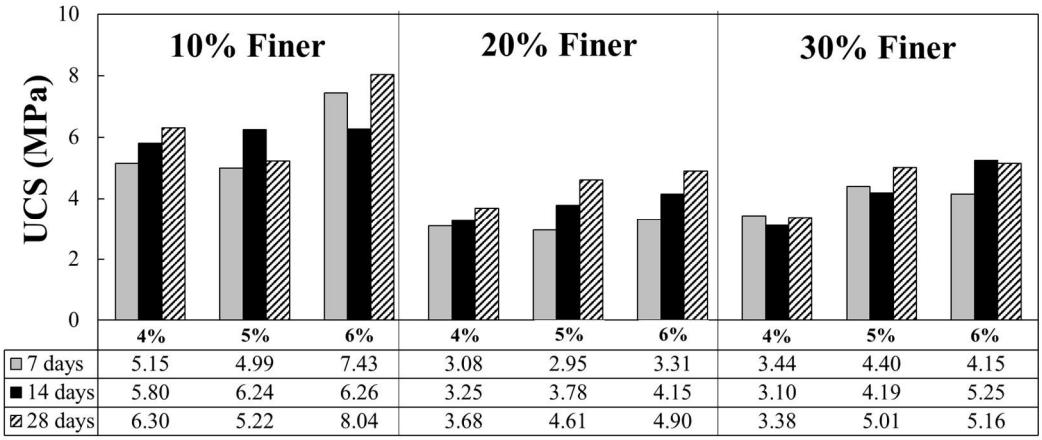

	10% Finer			20% Finer			30% Finer		
	4%	5%	6%	4%	5%	6%	4%	5%	6%
7 days	5.15	4.99	7.43	3.08	2.95	3.31	3.44	4.40	4.15
14 days	5.80	6.24	6.26	3.25	3.78	4.15	3.10	4.19	5.25
28 days	6.30	5.22	8.04	3.68	4.61	4.90	3.38	5.01	5.16

Figure 3.17: UCS test results of CTB specimens prepared from CRB with 10%, 20%, and 30% particles finer than 75 μm

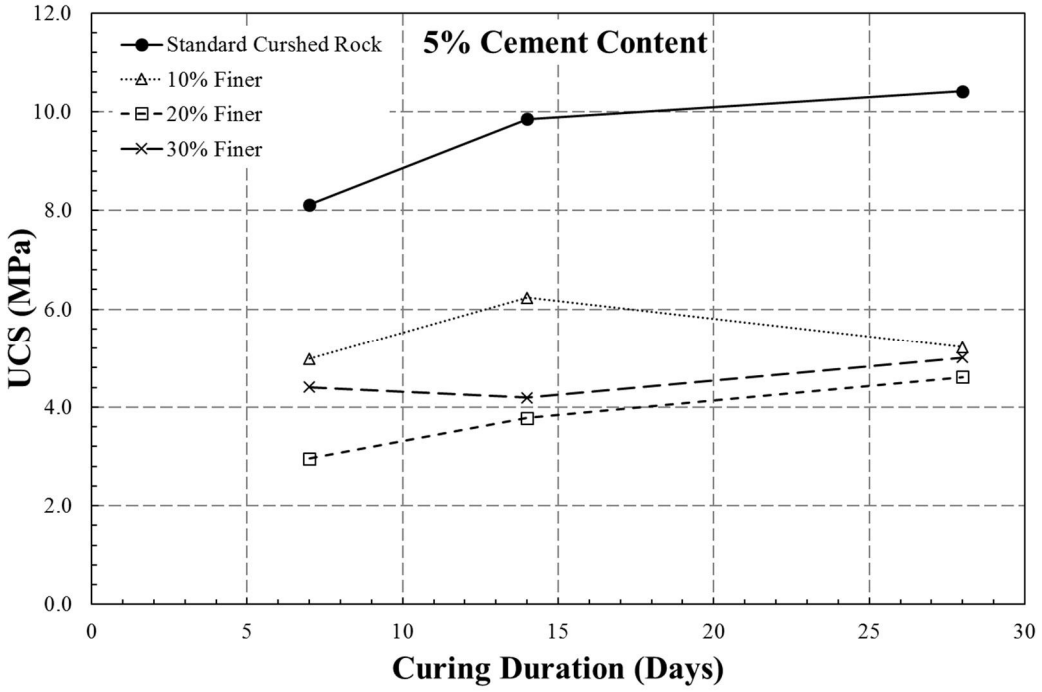

Figure 3.18: Strength development of specimens with 5% cement content prepared from standard CRB, and CRB with 10%, 20%, and 30% particles finer than 75 μm

3.7 Flexural strength of bound CTB

In this research, the flexural strength measurements of CTB material were obtained from two different sizes of CTB specimen. Specimens with dimensions of 63.5×50×400 mm^3 and 100×100×400 mm^3 were tested according to Standard

Australia (2000a) and Austroads (2014a), respectively. For the small specimens, the test standard for concrete material, AS 1012.11 (Standard Australia, 2000a), was adapted to measure the static flexural strength of CTB with a different beam size from the standard. The altered test specimens' dimensions of 63.5×50×400 mm^3, which are the same size as the test specimen of the standard four-point bending test for asphalt concrete (Austroads, 2006a), were used instead. Support span width (L in Figure 2.4b) for the flexural strength measurement was 355.5 mm; the loading span width was 118.5 mm (L/3). The flexural strength measure is the maximum tensile stress at the bottom fiber of the test specimen, as shown in Eq. 2.3. The flexural strength test results of small-sized specimens are summarised in Table 3.4.

Table 3.4: Flexural strength of small-sized beams

Specimen	Cement Content (%)	w_{eff}/c	Curing Time (Days)	FS (MPa)
M-1	5	0.12	28	1.52
M-2	5	0.12	28	1.70
M-3	5	0.12	28	1.36
Average				**1.53**

w_{eff}/c = Effective water to cement ratio
FS = Flexural strength

The flexural strength tests of the large-sized beam or standard sized beam were conducted according to Austroads (2014a). The test results are summarised in Table 3.5.

Table 3.5: Flexural strengths of standard sized beams

Specimen	Cement Content (%)	w_{eff}/c	Curing Time (Days)	FS (MPa)	E_s (MPa)	ε_b ($\mu\varepsilon$)
F-1	4	0.16	28	1.99	22,800	103
F-2	5	0.12	28	2.53	25,000	127
F-3	6	0.10	28	2.87	24,600	148

w_{eff}/c = Effective water to cement ratio
FS = Flexural strength
E_s = Secant flexural modulus calculated at 30% of FS
ε_b = Breaking strain at 95% of FS (Austroads, 2014a)

The relationship curves between the strength of 28-day CTB and cement content are presented in Figure 3.19. The increase in cement content (Figure 3.19a) or decrease in effective water-cement ratio (Figure 3.19b) leads to an increase in both UCS and FS. For the specimens tested in this section, a cement content of 4% to 6% was chosen according to the effective soil-cement interaction zone, as illustrated in Figure 3.7.

3.8 Shrinkage test

Chummuneerat (2014) examined the effects of cement content on the shrinkage characteristics of CTB, based on Standard Australia (1992). In his research, test specimens were prepared with a cement content which varied from 2% to 6%. Crushed rock from the same source used in this research was employed for the CTB specimen preparation. Figure 3.20 presents the shrinkage development of CTB measured by Chummuneerat (2014).

Figure 3.20 indicates that the shrinkage values of most specimens attained 80% of their maximum values after 21 days of drying. After 90 days, the increase in the shrinkage values of all specimens was negligible. Chummuneerat (2014) assumed that the water lost from hydration and evaporation was the major cause of CTB shrinkage. For specimens with a high cement content (5% to 6%), the shrinkage induced by the hydration process was predominant. On the other hand, the shrinkage of specimens with a low cement content (2% to 3%) was mainly attributed to water evaporation during the drying process.

In this research, the initial length of all shrinkage specimens was measured after the 7-day curing point was reached. A horizontal comparator (see Figure 3.21) was used to determine the initial length of the specimens within an accuracy figure of 0.001 mm. To ascertain shrinkage development, the changes in specimen length were continually monitored for up to 40 days of drying.

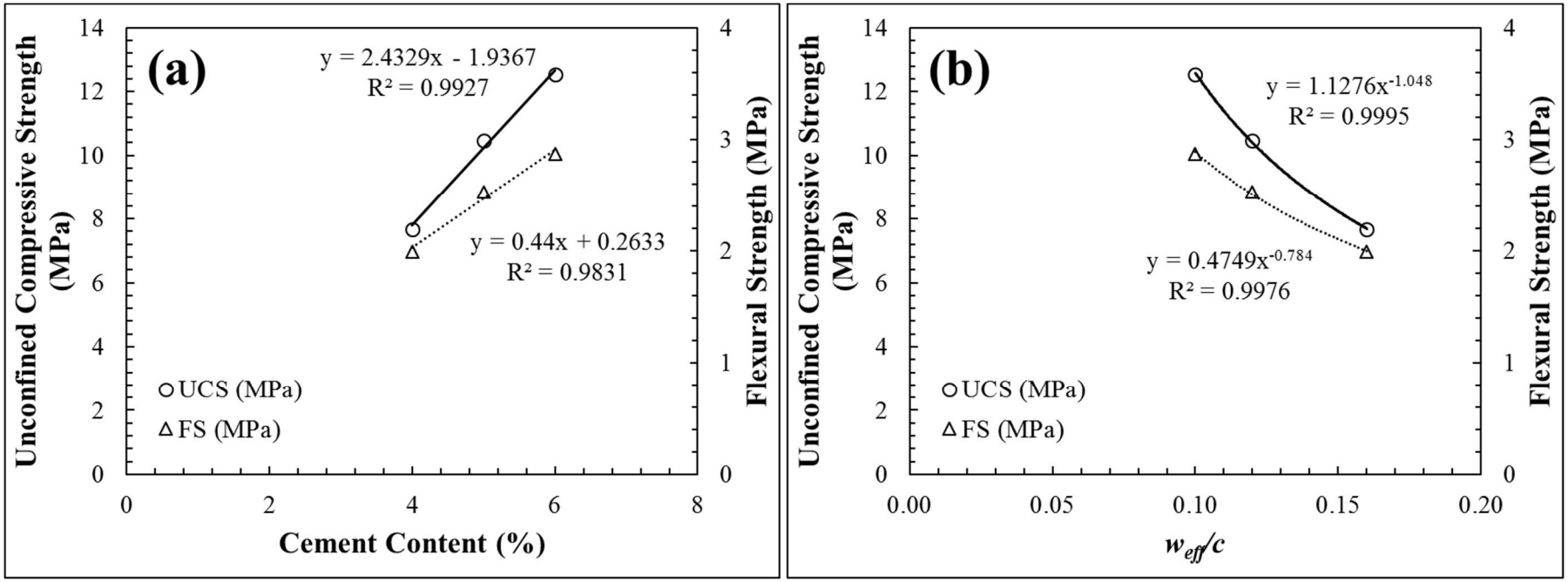

Figure 3.19: UCS and *FS* development of 28-day CTB specimens with respect to (a) cement content, and (b) effective water to cement ratio

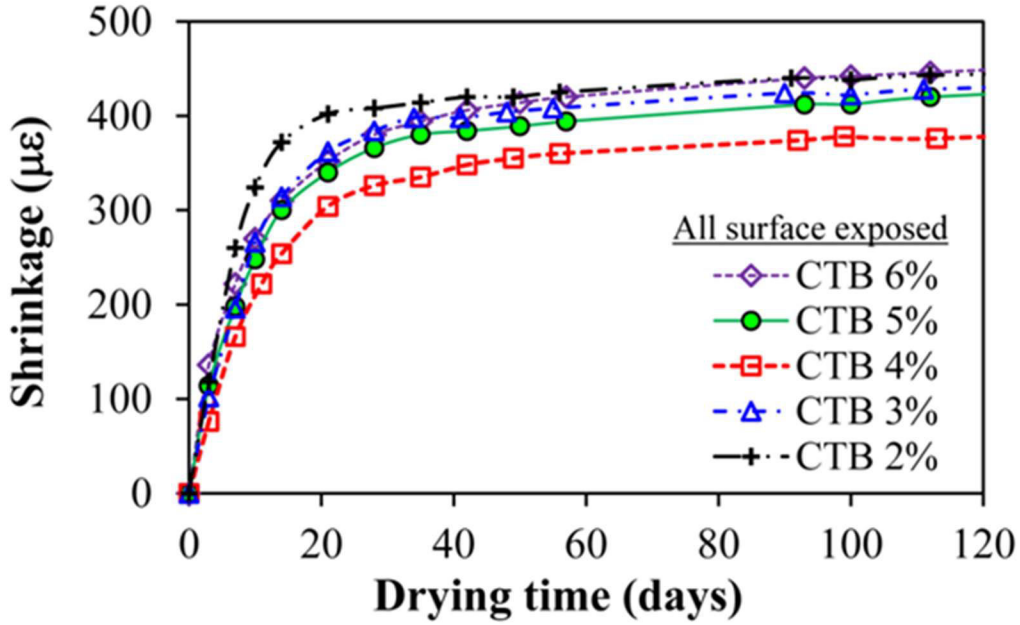

Figure 3.20: Shrinkage values of CTB with cement content varying from 2% to 6% (Chummuneerat, 2014)

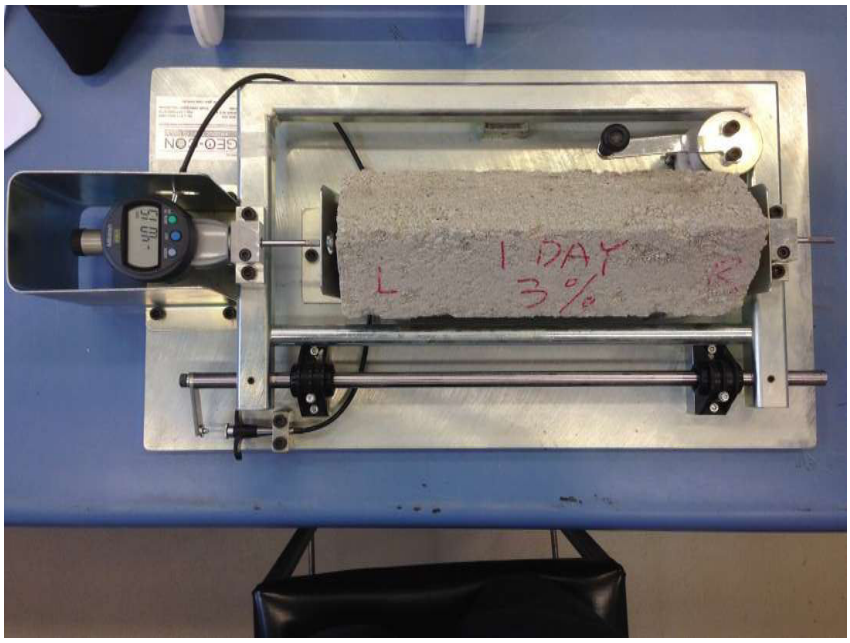

Figure 3.21: Horizontal comparator and shrinkage measurement of CTB specimen

The shrinkage values of delayed compaction specimens are illustrated in Figures 3.22 to 3.24. The shrinkage values of non-delayed compaction specimens measured by Chummuneerat (2014) were also plotted in the figures (0-Hour). Similar to the findings by Chummuneerat (2014), the rate of CTB shrinkage development seemed to reduce

after 21 days of drying. Figures 3.22 and 3.23 show that a delayed compaction time of 3 hours produced the highest shrinkage values for CTB specimens with 3% and 4% cement content. The test results also indicate that shrinkage values may increase up to 2 times if the compaction process is delayed for 3 hours. The specimens with 5% cement content behaved differently to the others (see Figure 3.24). The maximum shrinkage values were observed from a 2-hour delayed specimen and these were larger than the shrinkage of non-delayed specimens by only 1.6 times. According to the test results at this stage, it can be concluded that the shrinkage values of CTB specimens are influenced by delayed compaction time. Longer time gaps between the mixing process and the compacting process may lead to an increase in the shrinkage values of CTB. Shrinkage values may rise from 1.6 – 2 times in the case where CTB mixtures are left for 2 – 3 hours prior to compaction.

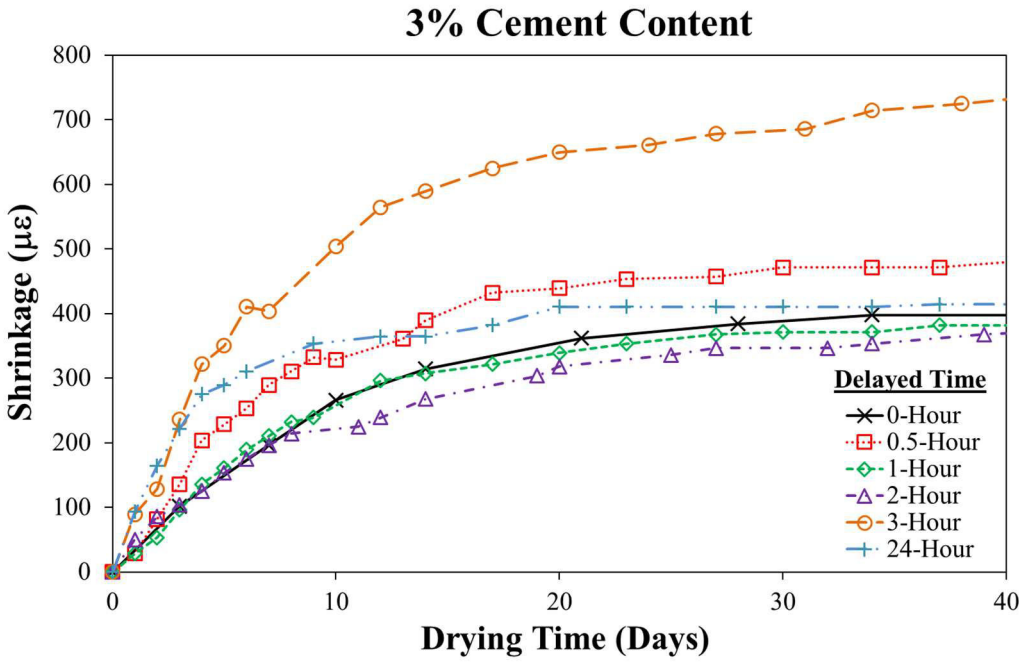

Figure 3.22: The effects of delayed compaction time on the shrinkage values of 3% cement content CTB

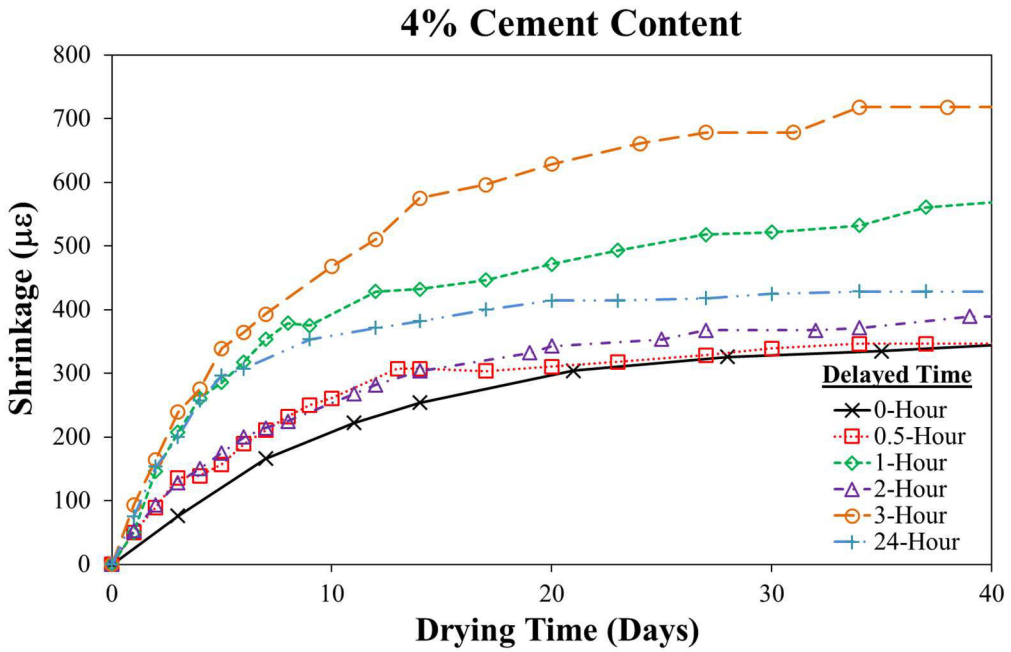

Figure 3.23: The effects of delayed compaction time on the shrinkage values of 4% cement content CTB

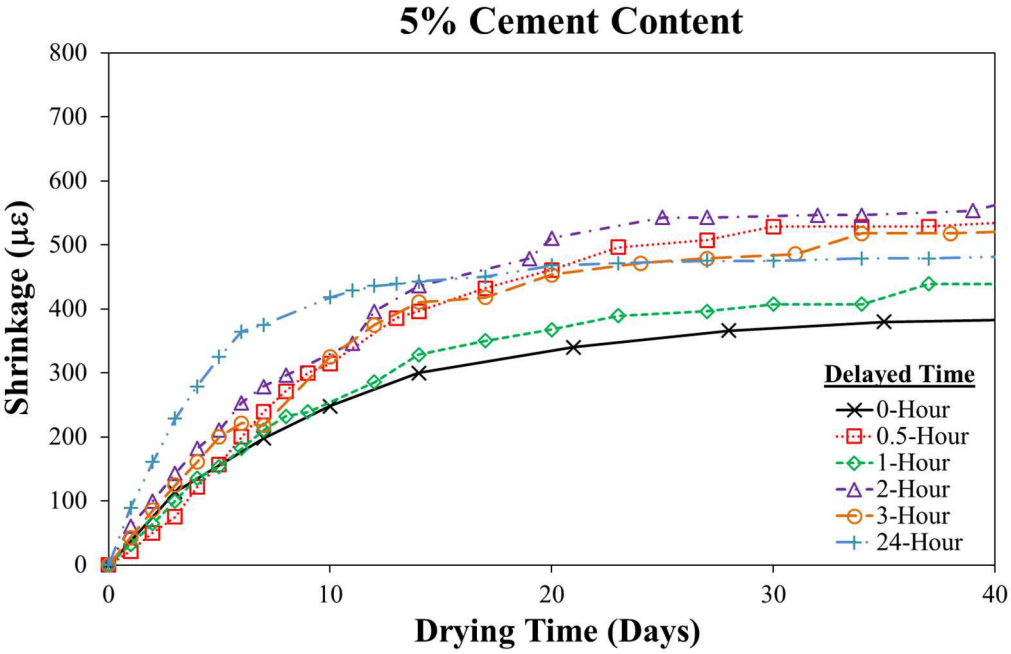

Figure 3.24: The effects of delayed compaction time on the shrinkage values of 5% cement content CTB

In this research, the influence of particles finer than 75 μm contained in the parent material on the shrinkage behaviour of CTB was also investigated. Similar to the UCS

test in Section 3.6, particles finer than 75 μm of standard CRB were increased to 10%, 20%, and 30% of dry crushed rock weight. Figure 3.25 demonstrates the shrinkage development lines averaged from three replicated specimens. The CTB specimens for this investigation were moulded from three modified types of crushed rock and with three different percentages of cement content (4%, 5%, and 6%); the total number of the specimens being 27. It can be seen from Figure 3.25 that the amount of particles finer than 75 μm affects the shrinkage behaviour of CTB. The rise in the amount of particles finer than *75* μm resulted in an increase in shrinkage values of CTB. For the CTB specimens prepared from standard crushed rock, the shrinkage values of 3% to 6% specimens at 40 days were approximately equal to 300 – 400 $\mu\varepsilon$ (see Figure 3.20). The shrinkage values at 21 days and 40 days of specimens moulded from standard and modified are summarised in Table 3.6. The information in Table 3.6 confirms that (1) increases in the amount of particles finer than 75 μm leads to a rise in shrinkage values, and (2) the shrinkage value at 21 days is approximately equivalent to 70% - 80% of the maximum shrinkage value.

Table 3.6: Shrinkage values at 21 days and 40 days of specimens moulded from crushed rock with different amounts of particles finer than 75 μm

Cement Content (%)	**Amount of Particle Finer than 75 μm (%)**	**Shrinkage at 21 days ($\mu\varepsilon$)**	**Shrinkage at 40 days ($\mu\varepsilon$)**
3	8 (Standard Crushed Rock)	362	398
	10	590	700
	20	1,107	1,218
	30	2,082	2,323
4	8 (Standard Crushed Rock)	304	348
	10	791	1,158
	20	937	1,395
	30	2,576	2,832
5	8 (Standard Crushed Rock)	340	384
	10	669	880
	20	837	970
	30	2,175	2,364

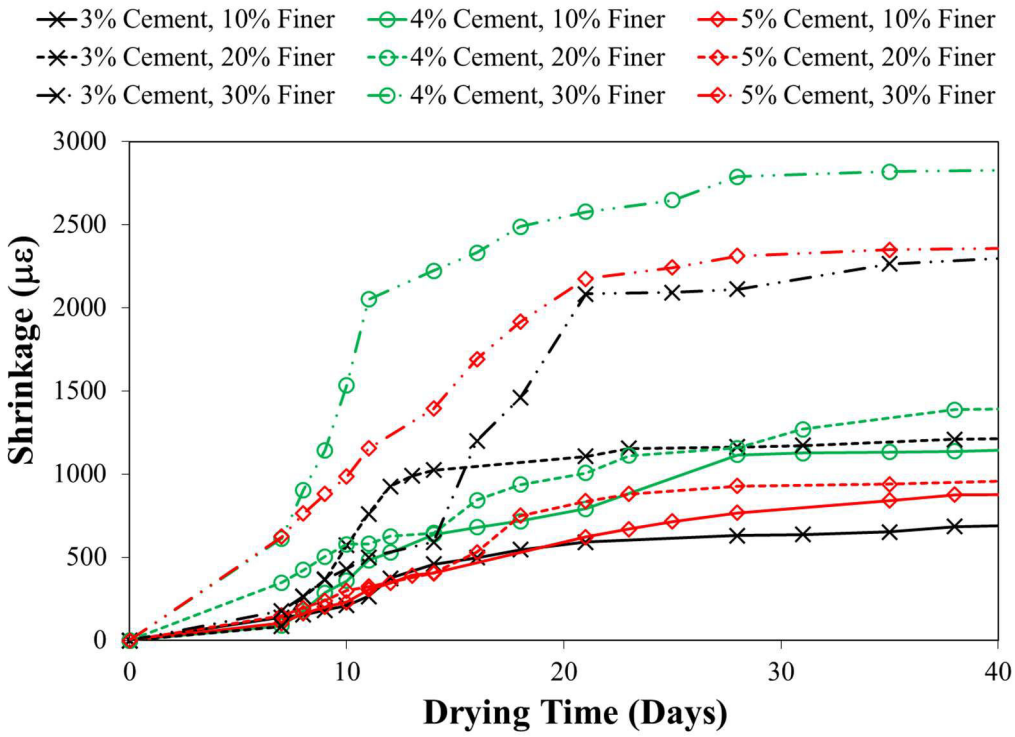

Figure 3.25: The effects of crushed rock particles finer than 75 μm on the shrinkage values of CTB

3.9 Concluding remarks

The characteristics of the CTB test specimens prepared from Western Australian standard crushed rock base were investigated in this chapter. A modified mix design concept for CTB was introduced, based on the test results. The main findings of this research are as follows:

- The strength of CRB and CTB depends on the moisture content in the moulding process, the moisture content at compaction, the dry density and the compaction degree. The maximum UCS of CTB test specimens was observed from the specimens compacted at OMC, while the UCS of CRB test specimens increased with respect to the moulding moisture content.

- The suggested cement content range recommended for CTB prepared from Western Australian standard crushed rock is between 3% and 7%. A maximum value of 7% was defined, based on the boundary line between the soil-cement

interaction zone and the transition zone, established from the test results of this research.

- Test results indicate that the strength of CTB can be estimated from the water-cement ratio (or effective water-cement ratio) and curing durations. However, this statement is valid only for CTB prepared with a moisture content equivalent to OMC and greater. The strength of CTB compacted on the dry-side of OMC cannot be reliably estimated.

- A modified mix design concept for CTB based upon the relationship of strength and the effective water-cement ratio was suggested. The main benefits of this modified mix design concept are (1) the present lengthy trial-and-error process can be dispensed with, and (2) the amount of water and/or cement can be instantly adjusted in-situ to achieve the design strength value.

- The flexural strength of CTB with a cement content of 4% to 6% varied from 1.99 MPa to 2.87 MPa. The values of flexural strength had a very strong correlation with the cement content and the effective water-cement ratio. The flexural strength tests in this research were conducted based on Standard Australia (2000a) and Austroads (2014a).

- The UCS of CTB materials was greatly influenced by the gradation of parent materials. Test results in this research indicate that an increase in the amount of coarse-grained particles, or a reduction in the amount of fine-grained particles, leads to a rise in UCS values.

- The gradation of crushed rock also had a major effect on the shrinkage performance of CTB; the rise in the amount of particles finer than 75 μm of parent materials resulted in an increase in shrinkage values of CTB.

- Delayed compaction time is defined as the time gap between the mixing and the compacting process. The longer delayed compaction time spent during specimen preparation results in greater shrinkage values compared to that of

specimens prepared using a shorter delayed time. Shrinkage values may increase from 1.6 – 2 times if CTB mixtures are left for 2 – 3 hours prior to compaction.

CHAPTER 4

DYNAMIC RESPONSES OF BOUND CTB

4.1 Introduction and background

Road pavement containing a Cement-Treated Base (CTB) layer can be designed using various methods including the empirical, limiting strength, limiting deformation, and mechanistic methods (Huang, 2004). Of these, mechanistic design is becoming more preferable with regard to obtaining reliable outcomes from scientific-based analysis. In mechanistic pavement design, an accurate evaluation of pavement response is required, in terms of stresses and strains induced from moving wheels and axle loads. Therefore, a suitable modulus input parameter, which can represent pavement responses under cyclic (traffic) loading conditions is necessary in mechanistic pavement design for CTB pavement. Austroads (2010b) recommends the flexural modulus as a design modulus input, due to its potential to describe the tensile strength criteria of a CTB layer when subjected to a loading regime in the field. According to the guidelines, the flexural modulus can be obtained from flexural tests conducted on rectangular beam test-specimens which have undergone 28-day moist-curing. Alternatively, the flexural modulus can be empirically predicted from a typical UCS value of a CTB material. This prediction is valid when the UCS of a CTB material is less than 5 MPa. In the US, the National Cooperative Highway Research Program (NCHRP, 2004) does not use the flexural modulus, but suggests the elastic modulus as a design input for mechanistic-empirical pavement design, since pavement response analysis there is usually performed using a linear-elastic assumption. In order to obtain the elastic modulus of a CTB material, a specimen of 28 days curing is required, and this is tested in accordance with ASTM C469 (ASTM, 2010b). In this case, the test specimen can either be a laboratory prepared specimen or a specimen acquired from the field. Alternatively, the elastic modulus of the CTB material can be estimated from the empirical formula recommended by Austroads (2006b).

According to the Guide for Mechanistic-Empirical Design (NCHRP, 2004), ASTM C469 (ASTM, 2010b) is recommended to determine the elastic modulus of CTB

material. However, the testing, in accordance with ASTM C469 (ASTM, 2010b) is only conducted on the basis of monotonic-compression tests. This is vastly different from traffic loading conditions in-service, where pavement structure is subjected to cyclic compressive loads from moving vehicles. Besides the lack of appropriate testing guidelines, test results from previous research reveal that the dynamic moduli of concrete and CTB materials are considerably higher than their elastic moduli measured from monotonic loading tests (Kolias & Williams, 1980; Lee, Kwan, & Zheng, 2013; Mindess & Young, 1981; Neville, 1998). It should be noted that the dynamic moduli considered in the previous literature were measured from either ultrasonic pulse velocity or vibration resonance methods. More details on the electro-dynamic moduli of stabilised material can be found in Williams (1986), and Arellano and Thompson (1998). Bischoff and Perry (1991) characterised the behaviour of concrete under different monotonic loading rates (see Figure 2.5). Based on their study, material strength and modulus are influenced by the strain rate of loading. The strain rates of monotonic loading in between 5×10^{-5} per second and 5×10^{-4} per second were considered as the static loading range. They also suggested the strain rates for earthquakes, or the dynamic loading conditions, which are the strain rates ranging from 1.0×10^{-3} per second to 1.0×10^{-2} per second. Strain rates of loading higher than 1 per second and 1.0×10^{2} per second were considered as impact and blasting load, respectively. It should be highlighted that the parameters obtained from the monotonic-compression test (i.e., under the static loading regime) are recommended in the US (NCHRP, 2004). However, in real pavement conditions, all materials are subjected to cyclic loading from moving vehicles in traffic. Due to this, previous studies recommended measuring road design parameters by using dynamic loading tests which simulate traffic loading (Austroads, 2010b; Croney & Croney, 1998).

The flexural modulus recommended by Austroads (2010b) for pavement response analysis differs from the elastic modulus, according to ASTM C469 (ASTM, 2010b). It could be simply said that the flexural modulus is the modulus of a rectangular beam specimen subjected to a cyclic or monotonic bending force, while the elastic modulus is determined from axial loading in the form of monotonic compression forces on a cylinder test specimen. Austroads (2008a) demonstrated a testing protocol to measure the flexural modulus and fatigue life of a CTB material using four-point bending tests (Austroads, 2008a, 2013a). According to this test protocol, applied loads on a beam

test specimen are in the form of the cyclic haversine loading function. Accordingly, the flexural modulus can be determined from Eq. 2.8. In Eq. 2.8, the flexural modulus can be seen to be simply the ratio between the bending stress and the bending strain at the bottom of the beam. Based on Austroads (Austroads, 2008a, 2013a), the flexural modulus derived from the four-point bending test might be used to represent the elastic modulus of a CTB material for pavement analysis. In other words, the induced stress-strain values at critical parts of a pavement structure could be determined by the flexural modulus. However, in order to calculate a reliable elastic modulus of a beam under bending forces, Timoshenko and Young (1968) recommended taking the effects of shear stress into consideration in the calculations. This is due to the maximum displacement at the mid-span of a beam being the combination of bending deformation and shear deformation. However, rigorous values for shear deformations are difficult to predict precisely. Due to these difficulties, an accurate method of calculation for determining the elastic modulus from a beam under bending forces is not yet available (Iyer, 2005). Moreover, parameters measured from flexural tests are largely based on uncertain or changeable factors such as specimen preparation, handling, curing, beam depth and specimen quality. This obviously produces a significant degree of test result variations (Walker & Bloem, 1957). Therefore, parameters from flexural tests alone may not be consistent enough to be used as design inputs in the quest to obtain a reliable and effective mechanistic pavement design.

It can be seen that there is still uncertainty around the modulus input parameters for a cement-stabilised material (or bound CTB) for mechanistic pavement design. If the elastic modulus and flexural modulus are not accurate enough to describe the dynamic responses of a CTB material in pavement, then more reliable parameters for CTB pavement design and analysis must be sought. Cement-stabilised material for roadways is no longer seen as a choice or an alternative option; it is a vital part of the modern road network which must now bear heavier and more numerous traffic loads, along with contending with the effects of more severe environmental conditions. A reliable parameter is essential in order to capture the cyclic response of a pavement structure under repetitive loading (traffic) conditions. In this chapter, the dynamic responses of CTB specimens subjected to monotonic-compression loads were firstly investigated. The stress-strain curves obtained from ordinary UCS tests in Chapter 3 were used for the determination of the CTB's elastic modulus. The effects of cement

content, curing time, and loading rate on the elastic modulus of CTB were characterised. Furthermore, the modulus reduction caused by damage at different loading rates was also examined in this research. The dynamic flexural modulus of CTB determined by the cyclic four-point bending tests was then analysed. The aforementioned dynamic flexural modulus is defined as "*cyclic flexural modulus*" in this research. The four-point bending tests were performed following the testing protocol developed by Austroads (2014a). The purpose of investigating the dynamic responses of CTB materials is to provide reliable inputs for mechanistic pavement design. This has led to the implementation of Asphalt Mixture Performance Tester (AMPT) in laboratory testing in this research. The tester determines the dynamic responses of CTB material by applying the cyclic load directly onto a test specimen. In addition, compression loading rates and testing temperatures can be controlled under AMPT test conditions. By providing as stable and consistent a testing environment as possible, the results obtained are likely to be more accurate when transferred to the field. In order to produce a comprehensive study, the effects of loading rate, temperature, curing time and cement content were also examined in this research.

4.2 Materials

4.2.1 Parent material and cement

CTB specimens were prepared from Crushed Rock Base (CRB) and General Purpose (GP) cement. These specimens were the same type as those employed in the characteristics study completed in Chapter 3. The geotechnical properties and gradation of selected CRB are summarised in Table 3.1 and Figure 3.1, respectively.

4.2.2 Cement-Treated Base (CTB)

CTB specimens were made by blending 4%, 5%, and 6% GP cement with a prescribed amount of CRB. Cement content of 4%, 5% and 6% cement was selected to ensure that the study material would be maintained at the "*stabilised level*" of the CTB material. The first task of the laboratory work was to produce a fully stabilised or "*bound*" pavement material to detect its behaviour under static and dynamic loading conditions. Due to the belief that such stabilised material is prone to behave as an

elastic material, most of the responses of CTB were able to be captured through the test procedures proposed in this research. With other materials, such as unbound and modified materials which are still governed by a degree of material grain interlocking, it is extremely difficult to measure the intact material modulus directly, given the limitations of the measuring devices and the test protocols available. The elastic response in a multi-layered pavement structure is one of the general assumptions found in most pavement design guidelines (Austroads, 2010b; NCHRP, 2004). The behaviour of "*unbound*" and "*modified*" pavement, as previously mentioned, depends greatly on the interlocking of aggregates (Y.S. Yeo, 2011), and it is this interlocking which may lead to the permanent deformation and complex behaviour of pavement. In addition to the effects of cement content, the characteristics of CTB also depend on the age of the material. According to mechanistic-empirical pavement design guidelines developed by the National Cooperative Highway Research Program (NCHRP, 2004), the UCS and elastic modulus of CTB should be measured when the age of specimens is equal to 7 days and 28 days, respectively. However, Austroads (2006b) recommends conducting four-point bending tests on specimens of 28 days curing only. Accordingly, the elastic moduli of CTB in this research were obtained from the UCS tests of 7-day and 28-day specimens. Additional 14-day specimens were employed for 6% cement CTB only. The cyclic flexural moduli of CTB were determined from the four-point bending test results of 28-day specimens. The specimens used for the dynamic modulus test in this research were selected at curing durations of 7 days, 14 days and 28 days, to allow investigation into the possible effects of the material's age upon the dynamic modulus values.

4.3 Test specimen preparation

The specimens for the UCS test and the four-point bending test were prepared in accordance with the procedures outlined in Section 3.3.1 and 3.3.2, respectively. The dynamic moduli of CTB specimens in this research were measured according to AASHTO TP79 (AASHTO, 2011b) with the only modification being in the applied dynamic strain values. The AMPT was typically developed for asphalt testing standards, therefore its testing parameters are constrained and modification would be limited. Furthermore, both CTB material and asphalt concrete are classified as

pavement materials. Their cyclic responses could possibly be correlated and examined further when both materials are tested under the same standard. The specimens for the dynamic modulus tests were prepared under the same densification conditions as those of the UCS specimens (at least 95% of MDD). Where a cylindrical specimen is to be tested in an AMPT machine, suitable dimensions would be 100 mm in diameter and 150 mm in height. As such, specimens for the dynamic modulus tests were prepared in a mould with a diameter of 100 mm but at a slightly greater than recommended height of 200 mm. Eight layers of crushed rock, mixed with the specified cement binder and water at OMC, were compacted in a mould until a height of 200 mm was reached. The extra height was trimmed to specifications (150 mm) just prior to testing. AASHTO (2011b), specifies that at least two specimens are required for each dynamic modulus measurement. Therefore, six specimens with a cement content equal to 4%, 5%, and 6% were prepared to examine the effects of the cement content. A supplementary six specimens of CTB with 6% cement were prepared to investigate the influence of curing time (two specimens each at 7, 14 and 28 days curing). Table 4.3 illustrates the details for each specimen prepared for the dynamic modulus measurements in this research.

4.4 Dynamic responses of bound CTB under monotonic-compressive load

According to UCS test standards (ASTM, 2000; Standard Australia, 2008b), the recommended compressive loading rate is 1.0 mm/min. Thus, the strain rate of loading is approximately 8.7×10^{-3} per minute or 1.4×10^{-4} per second. This loading rate is slightly higher than the static loading rate recommended by Bischoff and Perry (1991). In this research, an additional loading rate of 1.0×10^{-3} per second was selected to represent the dynamic loading condition. The UCS tests with dynamic loading strain rate were performed with 7-day specimens only. This additional test is the ordinary UCS test with a loading rate equivalent to the dynamic loading rate suggested by Bischoff and Perry (1991).

Average UCS values and average moduli from three replicated specimens, measured at different strain rates of loading, are shown in Figure 4.1. The UCS tested under static loading rate is greatly influenced by curing times and cement content. As per the

method of Croney and Croney (1998), the ratios between strength measured after any curing period and strength at 28 days curing were plotted against curing time. This strength ratio can vary from 0.2 for 1-day specimens to up to 1.7 for a 10,000-day specimen (approximately 27 years). The strength ratio of a 7-day specimen to a 28-day specimen in this research is in-between 0.8 - 0.9 (Figure 4.1), which is slightly higher than shown in the results of Croney and Croney (1998) (0.7). This difference may be caused by the effect of parent material types and cement content. Research on the effects of parent material (soil) types and stabiliser types on the UCS is also given in Croney and Croney (1998).

The strain rates for static loading and dynamic loading in this research were 1.4×10^{-4} per second and 1.0×10^{-3} per second, respectively. It should be understood that the elastic moduli of test specimens were calculated based on the procedure recommended by ASTM C469 (ASTM, 2010b). According to ASTM (2010b), the cylindrical concrete specimen is tested under a compressive load to determine the stress-strain response. Accordingly, the elastic modulus of the test specimen can be calculated from Eq. 4.1.

$$E = \frac{S_2 - S_1}{\varepsilon_2 - 0.000050} \tag{4.1}$$

in which, E is the chord modulus of elasticity (MPa), S_2 is the stress corresponding to 40% of ultimate load (MPa), S_1 is the stress corresponding to a longitudinal strain, ε_1, of 50 $\mu\varepsilon$, and ε_2 is the longitudinal strain induced by stress S_2. It can be seen that the strain rates of loading affect the strength and moduli of CTB (see Figure 4.1). A rise in the strain rate of loading leads to an increase in the strength and elastic modulus. Studies of the effects of loading rates on the response of concrete material can be found in previous studies (Bischoff & Perry, 1991; O. Xiao, Li, & Lin, 2008; S. Xiao, Li, & Monteiro, 2011). Cook and Chindaprasirt (1980) and S. Xiao et al. (2011) examined the effects of loading history on the strength and modulus of concrete. However, the study of the influence of loading rates on the response of CTB materials is very limited.

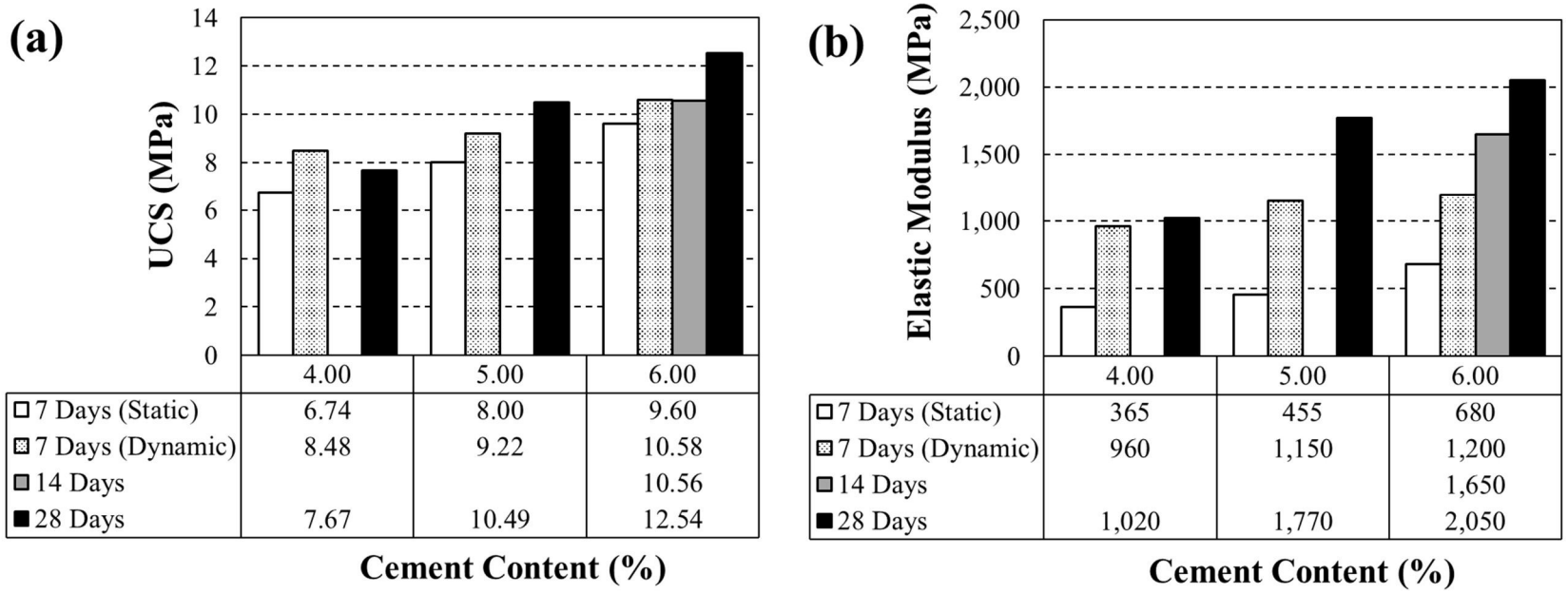

Figure 4.1: (a) Strengths and (b) elastic moduli of CTB measured at different strain rates of loading

Figure 4.2 illustrates the stress-strain response of 5% CTB specimens compacted at OMC and cured for 7 days. The bold lines in the figure represent the average values of three replicated specimens. The average strength and modulus of these specimens is shown in Figure 4.1. Specimens D-1, D-2, and D-3 were tested under dynamic loading, while static loading was applied to specimens S-1, S-2, and S-3. In this chapter, the damage parameter as defined in Eq. 4.2 indicate a reduction in the elastic moduli of CTB specimens induced by the monotonic-compressive load. S. Xiao et al. (2011) define the damage parameter as the degradation of tangent moduli. In their study, the initial tangent modulus is the secant modulus at 5% strain. Therefore, damage parameters can be estimated from Eq. 4.2.

$$D_n = \frac{E_i - E_n}{E_i} \tag{4.2}$$

in which, D_n is the damage parameter at current applied stress, E_i is the initial tangent modulus, and E_n is the tangent modulus at current applied stress. For example, the applied compressive stress to specimen D-1 is approximately equal to 6.5 MPa (stress ratio = 0.8), E_n = 910 MPa and E_i = 1,100 MPa. Therefore, the damage parameter of D-1 at 6.5 MPa can be calculated as follows: (1,100-910)/1,100 = 0.17. The stress ratio in Figure 4.2b is the ratio between the applied stress value and the UCS value (i.e., the maximum value) of a test material. Accordingly, the maximum and minimum values of the damage parameter are one and zero, respectively. A zero value damage parameter indicates that a material is intact or has no damage. The damage parameter is equal to one when the applied stress reaches peak stress (UCS). The comparison between the stress-strain relationship demonstrated in Figure 4.2a and damage induced by a compressive load, shown in Figure 4.2b, leads to a better understanding of the effects of loading rate on material strength. Figure 4.2b shows that at the same stress ratio, under dynamic loading conditions, test specimens exhibit less damage than those under static loading. Similar behaviour can be observed in tests on concrete material (Sukontasukkul, Nimityongsakul, & Mindess, 2004; S. Xiao et al., 2011). The damage growth is relatively dramatic and sudden for specimens subjected to a level of dynamic loading at high stress ratios (i.e., more than 0.8). At low stress ratios, damage evolution is slower. This may be the reason that higher strength and higher elastic moduli can be observed from tests on specimens tested under dynamic loading conditions. The

sudden increase in load-induced damage at high stress ratios may support the reason why there can be sudden failure in test specimens.

Figures 4.1 and 4.2 clearly indicate that the responses of CTB specimens under dynamic loading and under static loading are different. This leads to concerns regarding the employment of parameters derived from the static loading regime in road pavement design as road pavements are usually subjected to the dynamic loading conditions of moving vehicles.

4.5 Cyclic flexural modulus of bound CTB determined from four-point bending test

4.5.1 Methodology

The four-point bending test configuration illustrated in Figure 2.4 was employed for the measurement of the cyclic flexural modulus in this chapter. A beam specimen, 100 mm in height and width, and 400 mm in length, was tested in accordance with Austroads's testing protocol (Austroads, 2014a). According to the testing protocol, a haversine loading waveform with a frequency of 1 Hz (250 ms loading and a 750 ms rest period) was applied to beam specimens for one hundred cycles. The cyclic flexural modulus of CTB was then assigned as the average value of the flexural modulus calculated from the 51^{st} cycle to the 100^{th} cycle. The flexural modulus of the individual loading cycle was determined according to Eq. 2.8. Based on the testing protocol, a suitable applied stress level for cyclic flexural modulus determination is between 20% and 40% of flexural strength (0.20*FS* and 0.40*FS*) (Austroads, 2014a). A maximum applied stress level of 0.40*FS* was recommended to ensure the elastic response of CTB specimen.

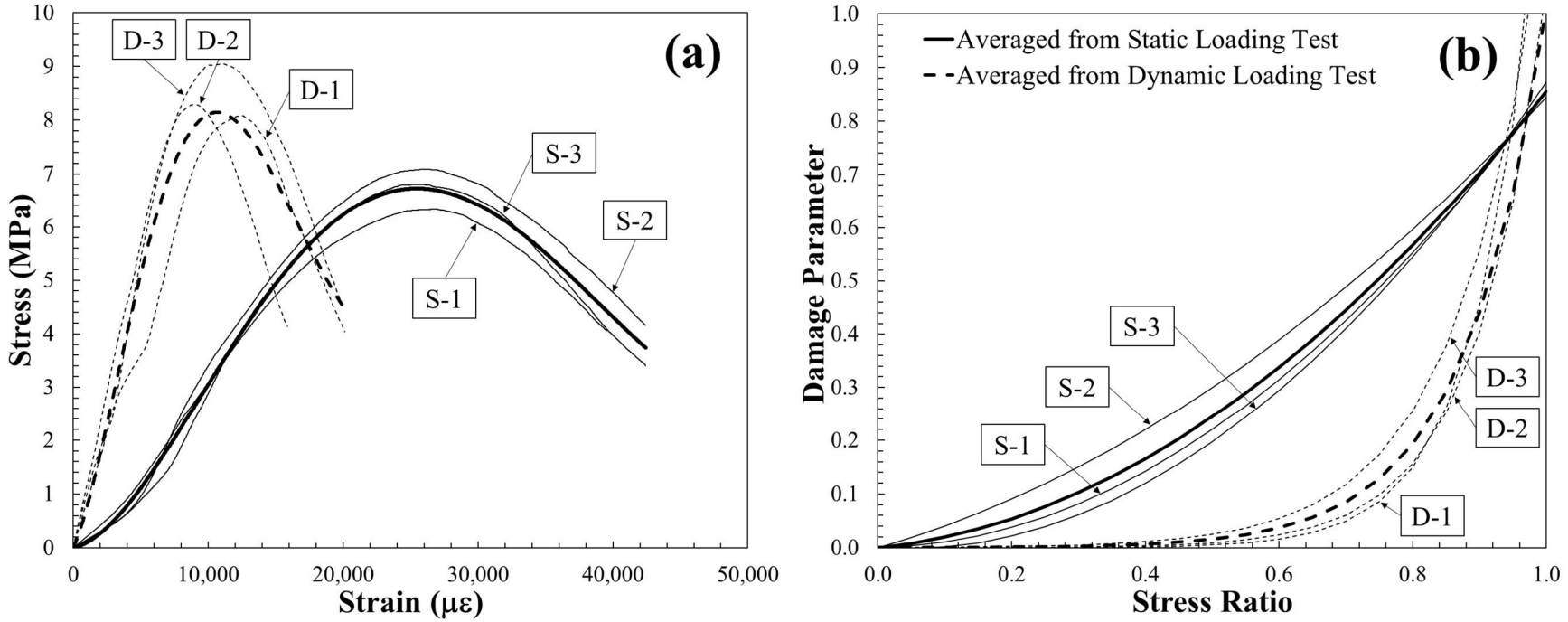

Figure 4.2: (a) Stress-strain relationship and (b) damage development of 5% cement CTB compacted at OMC and 7-day cured

Figure 4.3 shows the hydraulic universal testing machine employed for the four-point bending test. The machine was equipped with a four-point bending jig for the flexural strength test, cyclic flexural modulus measurement, and fatigue test for CTB material in this research. A Linear Variable Differential Transformer (LVDT) was attached to the aluminium frame and located at the centre-top of the beam specimen. Accordingly, the maximum vertical displacement of beam specimens induced by cyclic load were continually monitored by the LVDT and recorded throughout the test.

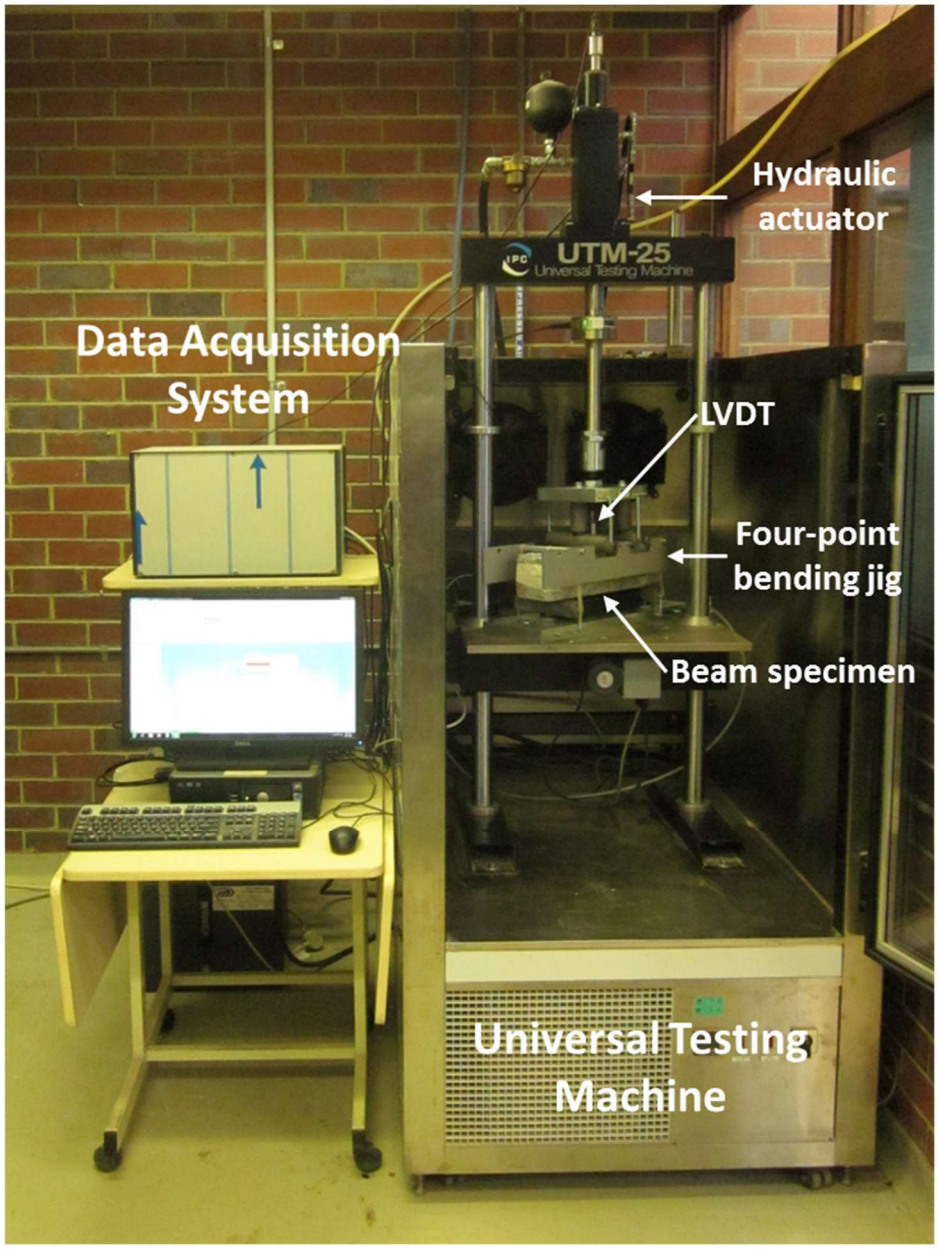

Figure 4.3: Universal testing machine equipped with four-point bending jig

In this research, the cyclic flexural modulus of every CTB specimen was measured prior to the commencement of the fatigue test. An applied stress level of 0.30*FS* was employed for the cyclic flexural modulus measured by a stress-controlled test. The specified stress level generally generated maximum tensile strain at the bottom of the beam fibre equivalent to 30 - 40 $\mu\varepsilon$. This induced strain range accords with the values recommended by Austroads (2014a) if the specimen is to be subsequently tested for fatigue behaviour. During the measurement of the cyclic flexural modulus, the maximum applied loads and maximum vertical displacements were continuously collected until one hundred loading cycles had been completed. The maximum applied tensile stress and maximum tensile strain could then be calculated, using Eqs. 4.3 and 4.4, respectively (Austroads, 2014a; Mandal, Tinjum, Gokce, & Edil, 2016).

$$\sigma_{t,max} = \frac{3(L-a)P}{2bd^2} \tag{4.3}$$

$$\varepsilon_{t,max} = \frac{108d\delta}{23L^2} \tag{4.4}$$

in which, P is the maximum applied load, L is the span length of a specimen, b is the average width of the specimen, d is the average depth of the specimen, δ is the maximum vertical displacement of the beam specimen, and a is the distance between the inner rollers. The flexural modulus of an individual loading cycle was then calculated by dividing the maximum tensile stress by the maximum tensile strain ($\sigma_{t,max}/\varepsilon_{t,max}$), or computed using Eq. 2.8.

4.5.2 Testing

In this chapter, CTB specimens were blended from CRB, with water equal to OMC, and 4%, 5%, and 6% of GP cement by dry weight of crushed rock. The beam specimens were cured in a moist chamber for 25 to 29 days prior to the cyclic flexural modulus measurements. During the cyclic flexural modulus measurement and fatigue test, the beam specimens were sealed in plastic film to prevent moisture loss. Both the cyclic modulus measurements and the fatigue tests in this research were conducted under strain-controlled (constant strain) and stress-controlled (constant stress) testing conditions. The test details for each specific beam are summarised in Table 4.1. According to Table 4.1, the total number of CTB beam specimens tested in this research was 29. The number of specimens tested under stress-controlled testing

conditions alone was 23, while 6 specimens were tested using strain-controlled testing conditions. For the stress-controlled test, the maximum values of applied stress for 4%, 5%, and 6% specimens were 0.60 MPa, 0.76 MPa, and 0.86 MPa, respectively. Therefore, the maximum level of the applied stress ratio (σ_t/FS) was kept at 30% in this research. The values of flexural strength (*FS*) for 4%, 5%, and 6% specimens are summarised in Table 3.5.

Table 4.1: CTB specimens and cyclic flexural modulus measurement results

Specimen	Cement Content (%)	Curing Duration (Days)	Tensile Stress (MPa)	Tensile Strain ($\mu\varepsilon$)	E_{flex} (MPa)
		Stress-Controlled Test			
M-1	5	27	0.76	30	25,118
M-2	5	28	0.76	40	18,802
M-3	5	26	0.76	37	20,291
M-4	5	28	0.76	39	19,510
M-5	5	25	0.76	37	20,424
M-9	5	29	0.76	36	21,079
M-10	5	27	0.76	40	18,724
M-14	5	29	0.76	36	20,958
M-15	5	29	0.76	38	20,175
M-16	5	27	0.76	41	18,488
M-17	5	27	0.76	36	21,125
M-18	5	28	0.76	37	20,425
M-19	5	28	0.76	41	18,525
M-28	5	28	0.76	36	21,309
M-29	5	25	0.76	41	18,503
M-20	4	28	0.60	35	17,336
M-21	4	27	0.60	36	16,557
M-22	4	26	0.60	35	16,957
M-23	4	28	0.60	36	16,606
M-24	6	27	0.86	41	20,778
M-25	6	27	0.86	41	20,805
M-26	6	27	0.86	40	21,368
M-27	6	28	0.86	36	23,997
		Strain-Controlled Test			
M-6	5	26	0.61	33	17,878
M-7	5	29	0.72	34	21,030
M-8	5	26	0.74	34	21,284
M-11	5	29	0.66	34	19,356
M-12	5	27	0.60	34	17,343
M-13	5	29	0.65	34	19,026

To maintain the stress ratio at 30% during the strain-controlled test, a target applied strain level of 35 $\mu\varepsilon$ was estimated and assigned for the cyclic flexural modulus

measurements. However, the real stress ratios achieved during the strain-controlled tests fluctuated between 24% and 29%.

4.5.3 Test results

The cyclic flexural moduli measured from the stress-controlled and strain-controlled tests are summarised in Table 4.1. The variations in cyclic flexural modulus, measured from the stress-controlled test, with respect to the changes in curing time are plotted in Figure 4.4. It can be seen from Figure 4.4 that the curing time, which varied from 25 days to 29 days, seems to have a negligible effect on the cyclic flexural modulus of CTB specimens.

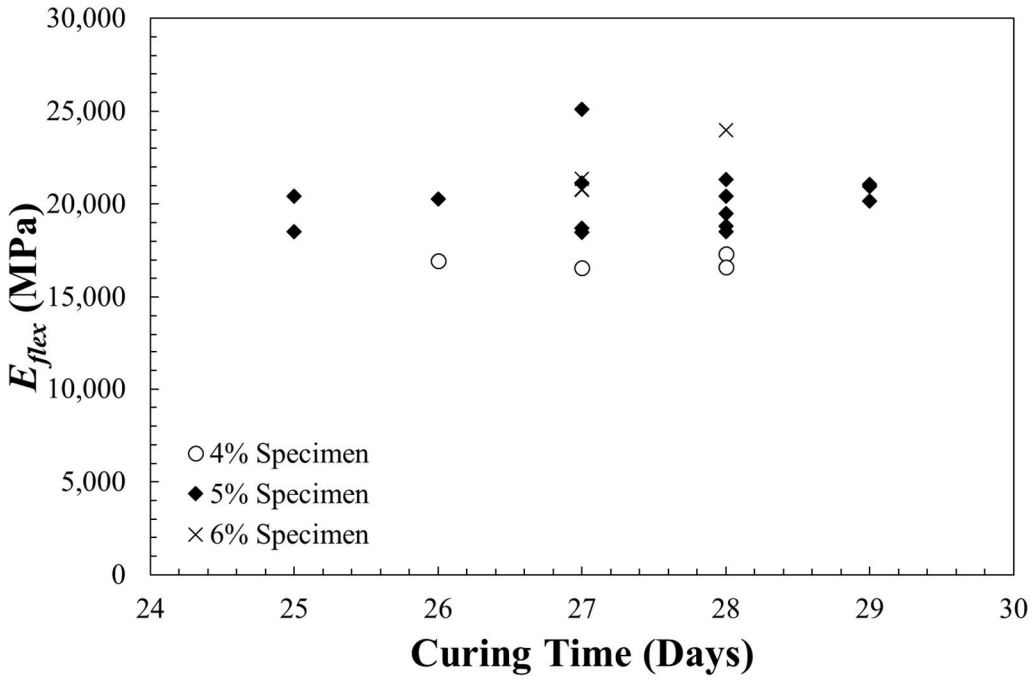

Figure 4.4: Relationship between cyclic flexural modulus and curing time

Table 4.2 summarises the average cyclic flexural moduli determined from the four-point bending test results. Similar to the characteristics of UCS, the cyclic flexural modulus of CTB increased with respect to the rise in the specimen's cement content. The cyclic flexural modulus of the 5% specimen, measured using strain-controlled testing conditions, was slightly smaller than the value obtained from the stress-controlled test. The difference may due to two main reasons; (1) that there were differences between the magnitude of applied stress and applied strain achieved during

the stress-controlled and strain-controlled tests, and (2) that the fluctuated tensile strain was unavoidably occurred during the strain-controlled test. It has been proven in previous literature that the cyclic flexural modulus is influenced by the magnitude of applied tensile strain (or stress) during testing (Austroads, 2011, 2014a). Austroads (2014a) reported that an increase in strain of 1 ($\mu\varepsilon$) then led to a reduction in cyclic flexural modulus which was approximately equal to 40 MPa. Apart from the effects of applied tensile strain (or stress) seen during the test, high fluctuations in targeted tensile strain observed during the strain-controlled test may be another rationale for explaining the variation in the cyclic flexural modulus. The variations in cyclic flexural modulus and tensile strain measured during stress-controlled and strain-controlled tests are illustrated in Figures 4.5a and b, respectively. It can be clearly seen from Figure 4.5 that the cyclic flexural modulus measured from the stress-controlled test was more consistent than the values obtained from the strain-controlled test. The fluctuation in cyclic flexural modulus observed from the strain-controlled test also affected the fatigue test results in this research. A detailed analysis related to the inconsistent results obtained from the strain-controlled test is provided in Chapter 5.

Table 4.2: Average cyclic flexural modulus of CTB specimens

Cement Content (%)	No. of Specimens	Average E_{flex} (MPa)	E_s (MPa)	SD (MPa)	COV (%)
Stress-Controlled Test					
4	4	16,864	22,800	362	2.14
5	15	20,231	25,000	1,710	8.45
6	4	21,738	24,600	1,531	7.04
Strain-Controlled Test					
5	6	19,320	25,000	1,603	8.30

E_s = Secant flexural modulus from flexural strength test, and calculated at 30% of FS
SD = Standard deviation
COV = Coefficient of variation

Besides presenting the cyclic flexural modulus of CTB, Table 4.2 also summarises the secant flexural moduli (E_s) determined from the flexural strength test in this research. The values of the secant modulus of CTB were generally higher than the cyclic flexural modulus. However, it should be highlighted that the secant moduli of CTB specimens were computed from only one specimen for each percentage of cement content.

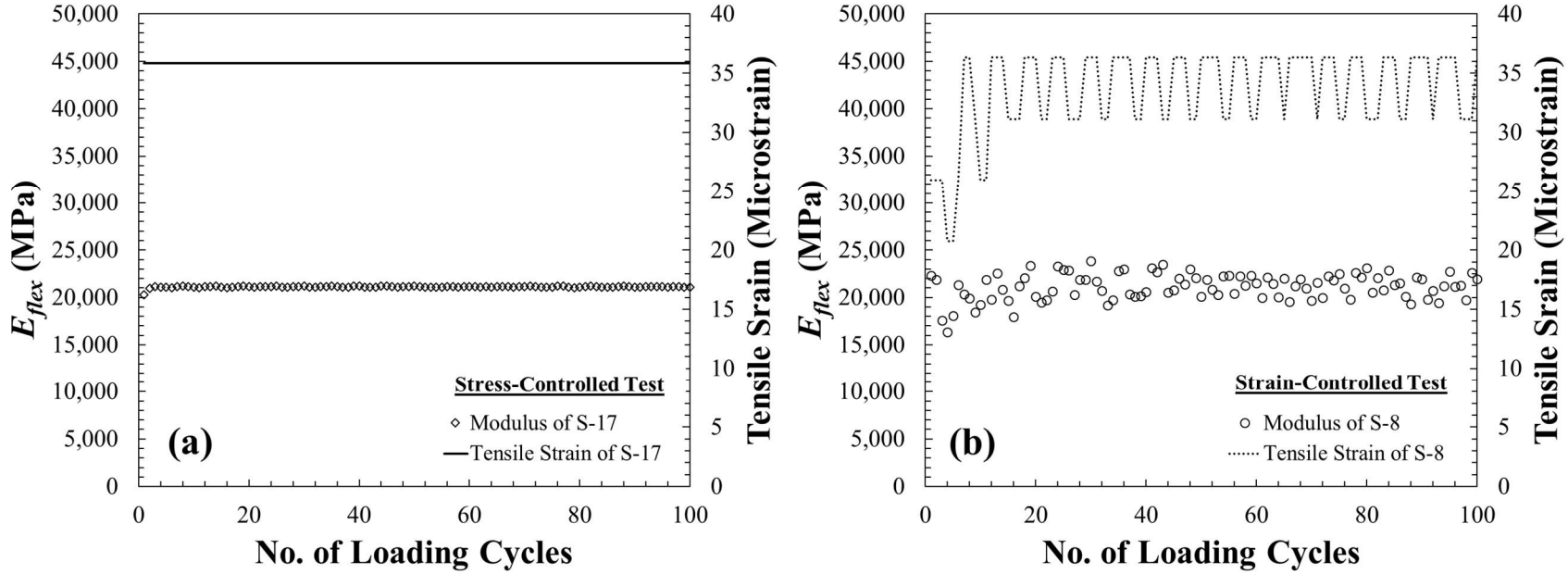

Figure 4.5: The variations in cyclic flexural modulus and tensile strain during (a) stress-controlled test, and (b) strain-controlled test

As mentioned earlier, the fatigue tests in this research were continued after the cyclic flexural modulus measurements were completed. Therefore, the cyclic flexural moduli obtained during the fatigue test was also characterised in this section. It should be emphasised that the fatigue tests in this research were performed using a loading frequency of 2 Hz instead of 1 Hz as employed in the cyclic flexural modulus measurement. Figure 4.6a shows the relationship line between the applied stress ratio and the cyclic flexural modulus measured during the fatigue test, while the relationship line between the average tensile strain and the cyclic flexural modulus is presented in Figure 4.6b. The average tensile strain and cyclic flexural modulus in Figure 4.6 are the average values obtained from cycle number 51 to 100 of the fatigue test. Similar to the findings of Austroads (2014a), Figure 4.6b shows that the increase in average tensile strain by 1 $\mu\varepsilon$ led to a reduction in the cyclic flexural modulus by approximately 100 MPa.

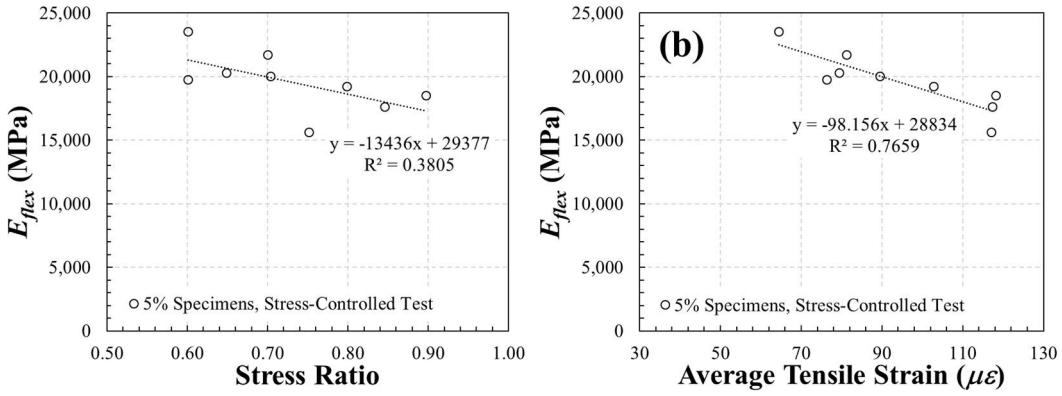

Figure 4.6: (a) Relationship between stress ratio and cyclic flexural modulus, and (b) relationship between average tensile strain and cyclic flexural modulus measured during fatigue test

4.6 Dynamic modulus of bound CTB determined from AMPT

4.6.1 Methodology

The Asphalt Mixture Performance Tester (AMPT) was developed in accordance with the Superior Performing Asphalt Pavement (Superpave^{TM}) system (Bonaquist, Christensen, & Stump, 2008) for the purpose of evaluating the performance of Hot

Mix Asphalt (HMA). The machine was the outcome of Project 9-19 and 9-29 conducted by the National Cooperative Highway Research Program (NCHRP) (Bonaquist et al., 2008). In the projects, the dynamic modulus, flow number and flow time are the three most important parameters recommended in representing the performance of HMA (Diaz & Archilla, 2013). According to the Superpave^{TM} system, flow number and flow time indicate the respective rutting and creep performance of HMA, while the dynamic modulus is usually applied in the analysis of pavement response. Figure 4.7 illustrates the major components of AMPT which comprise: conditioning chamber, dynamic actuator, controller, and data acquisition system. Throughout the test, both the testing temperature and the confining pressure are controlled inside an environmental conditioning chamber. The AMPT testing temperature can be assigned to the specimen(s), using a range of 4 °C to 60 °C, which is precise to a degree of ± 0.5 °C. With regard to confinement conditions, the pressure in the conditioning chamber can be increased up to 450 kPa. A loaded cell is installed in the middle of three vertical-columns, surrounded by an acrylic frame, where the applied sinusoidal load generated from the actuator in the conditioning chamber is measured. Three LVDTs located in between the columns are assigned to measure the axial displacements of the test specimen. Two aluminum loading platens are placed on the top and bottom of the specimen. In order to ensure uniform loading on the specimen, a steel ball is placed on top of the loading platen. Teflon sheeting, or greased double latex, is placed in-between the specimen faces and the loading platen in order to reduce friction.

In mechanistic-empirical pavement design, the primary parameter of interest for asphalt pavement design is the dynamic modulus (|E*|) which is measured at different frequencies and temperatures (NCHRP, 2004). The dynamic modulus is the modulus of a visco-elastic material subjected to applied loads in the form of a sinusoidal loading function. The dynamic modulus can be determined directly from laboratory testing. Alternatively, predictive models can be used to determine the dynamic modulus without testing, using the fundamental properties of HMA as a basis (Robbins, 2009). The sinusoidal stress produced from one-dimensional cyclic loading can be represented by Eq. 4.5.

$$\sigma^* = \sigma_0 e^{i\omega t} \tag{4.5}$$

Accordingly, the strain produced by sinusoidal stress is illustrated by Eq. 4.6.

$$\varepsilon^* = \varepsilon_0 e^{i(\omega t - \phi)} \tag{4.6}$$

in which, σ_0 is the stress amplitude, ε_0 is the strain amplitude, ω is the angular frequency, t is time and ϕ is the phase angle. The phase angle is a phase lag, or phase difference, between sinusoidal stress and strain wave forms. For an elastic material, the phase angle is equal to 0°, while a viscous material has a phase angle of 90°. |E*| can be defined as the absolute value of a complex modulus. Therefore, the calculation for |E*| can be written as shown in Eq. 4.7.

$$|E^*| = \left|\frac{\sigma^*}{\varepsilon^*}\right| = \left|(\sigma_0/\varepsilon_0)e^{i\phi}\right| = E_{AMPT} \tag{4.7}$$

in which, E_{AMPT} represents the dynamic modulus of CTB measured by AMPT in this research. The dynamic modulus of a visco-elastic material is greatly reliant on loading rates and temperatures (Kim, 2009), along with its particular position within the pavement structure (Robbins, 2009). For a visco-elastic material such as asphalt concrete, |E*| at a constant loading rate can vary greatly from a few hundred to ten thousand MPa in the AMPT at high temperatures (40 °C), and low temperatures (4 °C), respectively. Similarly, the |E*| of asphalt concrete at a constant temperature can double when the loading rate is increased from 0.1 Hz to 10 Hz.

AASHTO TP62 (AASHTO, 2007a) replaced by AASHTO T342 (AASHTO, 2011a) was adopted as the dynamic modulus testing standard for HMA. According to the standard, at least two replicate specimens at five temperatures and six loading rates are required for the dynamic modulus test to be completed. This makes the tests both time-consuming and expensive. Dougan, Stephens, Mahoney, and Hansen (2003) recommended reducing the testing time, if AASHTO TP62 (AASHTO, 2007a) were to be employed as a routine test standard by highway agencies. Li and Williams (2012) also suggest shortening the testing time. Specifically, they recommend reducing the number of testing temperatures and loading rates. In their research, the relationship curve between the dynamic modulus and the loading rate, or *"Master Curve"* used in a mechanistic-empirical design framework is constructed quite adequately using only

three testing temperatures (4.4 °C, 21.1 °C and 37.8 °C) and six frequencies (25 Hz, 10 Hz, 5 Hz, 1 Hz, 0.5 Hz and 0.1 Hz), plus one additional frequency (0.01 Hz) at 37.8 °C. The loading rates recommended by AASHTO PP61 (AASHTO, 2010) were later further reduced to three frequencies (10Hz, 1Hz, 0.1 Hz), plus an additional 0.01 Hz for the highest testing temperature. The number of testing temperatures recommended by AASHTO PP61 (AASHTO, 2010) was kept to three. However, the degrees of temperature were changed to 4 °C, 20 °C and 35 °C (or 40 °C and 45 °C depending on the grade of asphalt). Besides AASHTO TP62 (AASHTO, 2007a) and AASHTO PP61 (AASHTO, 2010), AASHTO TP79 (AASHTO, 2011b) was developed as a standard test for dynamic modulus measurement using the AMPT. Accordingly, based on the solid and comprehensive platform of testing procedures to detect and evaluate the dynamic responses of a material under AMTP examination, the responses in this research of CTB material under cyclic loading were characterized based on AASHTO TP79 (AASHTO, 2011b).

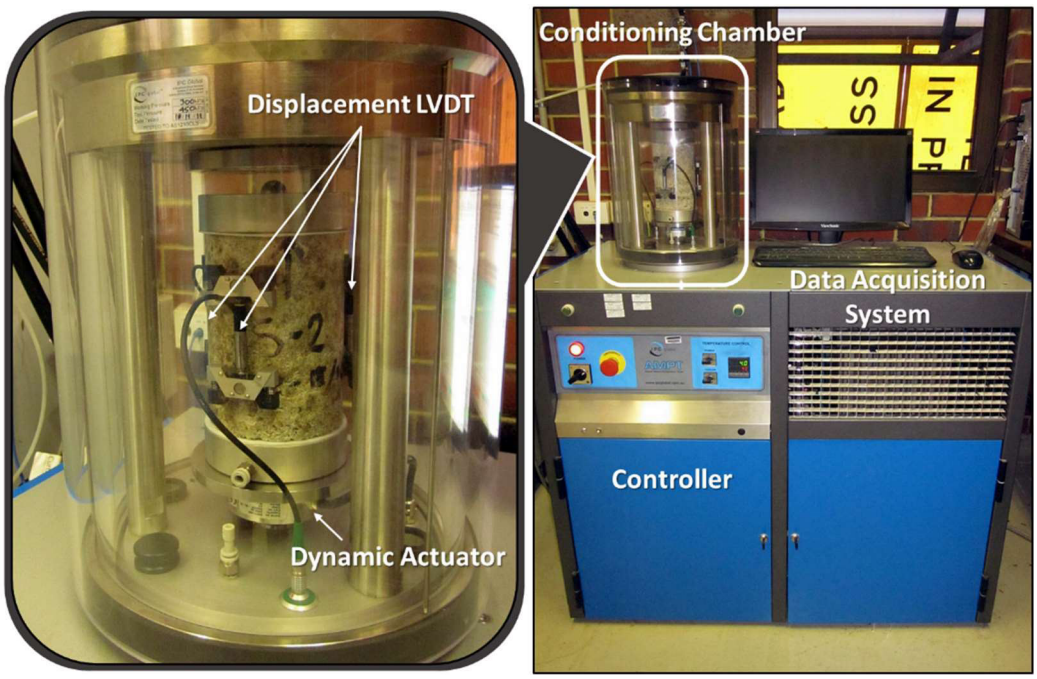

Figure 4.7: Asphalt Mixture Performance Tester (AMPT)

It should be noted that the notation "E_{AMPT}" used in this research, refers to defining the ratios between sinusoidal stresses and strains of CTB specimens measured by AMPT (calculated based on Eq. 4.7). This dynamic modulus differs from the elastic modulus in that the elastic modulus of a material refers to the ratios between axial stresses and

strains, with these ratios being measured from statically-monotonic compression (or tension) tests. The dynamic modulus also differs from the resilient modulus of a material by its definition, since the resilient modulus refers to the ratios of applied cyclic stresses and recoverable strains. Therefore, the resilient modulus was recommended as the design parameter for granular materials (unbound materials) and lightly stabilised materials (Wen et al., 2014). However, the main aim of this research is examining the dynamic response of bound material. Accordingly, the available testing protocol for asphalt material was used to investigate the dynamic responses of CTB in this research. Moreover, the AMPT has the capability of investigating the influence of varying temperatures and loading rates on the dynamic modulus of CTB materials. In order to investigate the effects of the cement content percentages and curing periods on the E_{AMPT} values of CTB materials, the test specimens for the dynamic modulus tests were prepared using three different cement content percentages and three different curing periods.

4.6.2 Testing

After the specimens had been cured for the specified periods, they were cut to the required height and soaked in water for four hours in the same manner as the specimens for the UCS test (Standard Australia, 2008b). Prior to the test, it is a requirement that the water from the soaked specimen be drained out for a minimum of 15 minutes. The gauge points were then glued to the specimen and prepared for LVDT installation, as shown in Figure 4.7. Epoxy adhesive usually requires at least 30 minutes to set firmly; therefore, the specimens were wrapped in plastic film in order to prevent moisture loss. This process was conducted to ensure that the moisture content of all specimens was the same as that of the specimens produced for the UCS test.

For all of the dynamic modulus tests conducted in this research, the testing process began by placing the specimen in a conditioning chamber at the specified temperature, and allowing the specimen to equilibrate overnight. The curing time depends on the degree of the testing temperature. As recommended by AASHTO T342 (AASHTO, 2011a), the minimum equilibrium times for testing at 4 °C, 21 °C and 37 °C are: overnight, three, and two hours respectively. According to the standard requirements, the first testing temperature is the lowest (4 °C) in a specific temperature range (4 °C,

21 °C and 37 °C). Therefore, the specimens were put in the conditioning chamber the night before testing. The following morning, the dynamic modulus tests were initiated at the highest loading rate, and the tests were then automatically generated until the measurement taken at the lowest loading rate was completed. The loading rates used for the dynamic modulus tests in this research were 20 Hz, 10 Hz, 1 Hz and 0.1 Hz for testing at 4 °C and 20 °C. A load of 0.01 Hz was added for the tests taken at 40 °C. At the commencement of the test, a small seating load was automatically applied to the specimen. The specimen was then cyclically compressed with a sinusoidal loading function but without confining pressure. It should be noted that the dynamic modulus tests were stress-controlled tests, and the magnitude of the applied load at a specified strain level was determined based on the process of trial and error. This specified strain level was an average value of the strain measured from three LVDTs attached to the specimen. Thus the magnitude of sinusoidal compressive loads was automatically adjusted by the machine to maintain the specified strain level throughout the test. At each test temperature, the dynamic modulus values were measured continuously from the highest loading rate, and terminated after the measurement at the lowest loading rate was completed. At every test frequency, ten cycles of the preconditioning process are required prior to the dynamic modulus measurements. After the preconditioning process, another ten cycles of sinusoidal compressive loads were instantly applied and the dynamic moduli were averaged from this last set of loadings. At the end of the test, the specimen was automatically unloaded after completing the measurements at the lowest loading rate. The next testing temperature was then applied and the specimen was allowed to equilibrate again for a specified curing time. This process was repeated until the dynamic modulus value at the highest temperature and lowest frequency (40 °C and 0.01 Hz) was achieved. The conditioning chamber was kept closed until all the testing processes were completed.

In order to examine the effects of various parameters on the dynamic modulus of CTB, the testing was divided into two stages. The first stage was designed to investigate the effects of dynamic strain levels on the dynamic moduli of CTB. A suitable strain range for testing CTB could then be determined. The influence of cement content, curing time, changes in temperature and loading rates were examined in the second stage of testing.

Stage one: Measurement at different levels of strain

In order to investigate the influences of strain levels on the dynamic modulus values of CTB, the test was firstly conducted based on AASHTO TP79 (AASHTO, 2011b) with various strain level inputs. According to AASHTO T342 (AASHTO, 2011a), during the dynamic modulus test, the test specimen should be cyclically loaded within a varying dynamic strain range of between 50 $\mu\varepsilon$ and 150 $\mu\varepsilon$. The values recommended by the NCHRP Project 9-29 for the dynamic strain range in the AMPT test are 75 - 125 $\mu\varepsilon$ (Bonaquist et al., 2008). However, the AASHTO standards and testing guidelines were developed as a template for the asphalt concrete performance test, and the strain range recommended by AASHTO may not be compatible with the unique test performed on the CTB specimens used in this research. This is due to the fact that these CTB specimens were found to be stiffer than general asphalt concrete, and the load would have exceeded the actuator limit if the AASHTO dynamic strain range used for asphalt concrete was applied in this case. Therefore, the trial and error process for determining a suitable strain range for CTB material was necessary in the early stages of testing. Accordingly, the tests at this stage were subdivided further into: (1) tests on the same specimen using increases in dynamic strain input, and (2) testing on different specimens with same cement content and curing duration, but using different strain levels during testing. Details of the testing scheme for both sub-stages are shown in Figure 4.8.

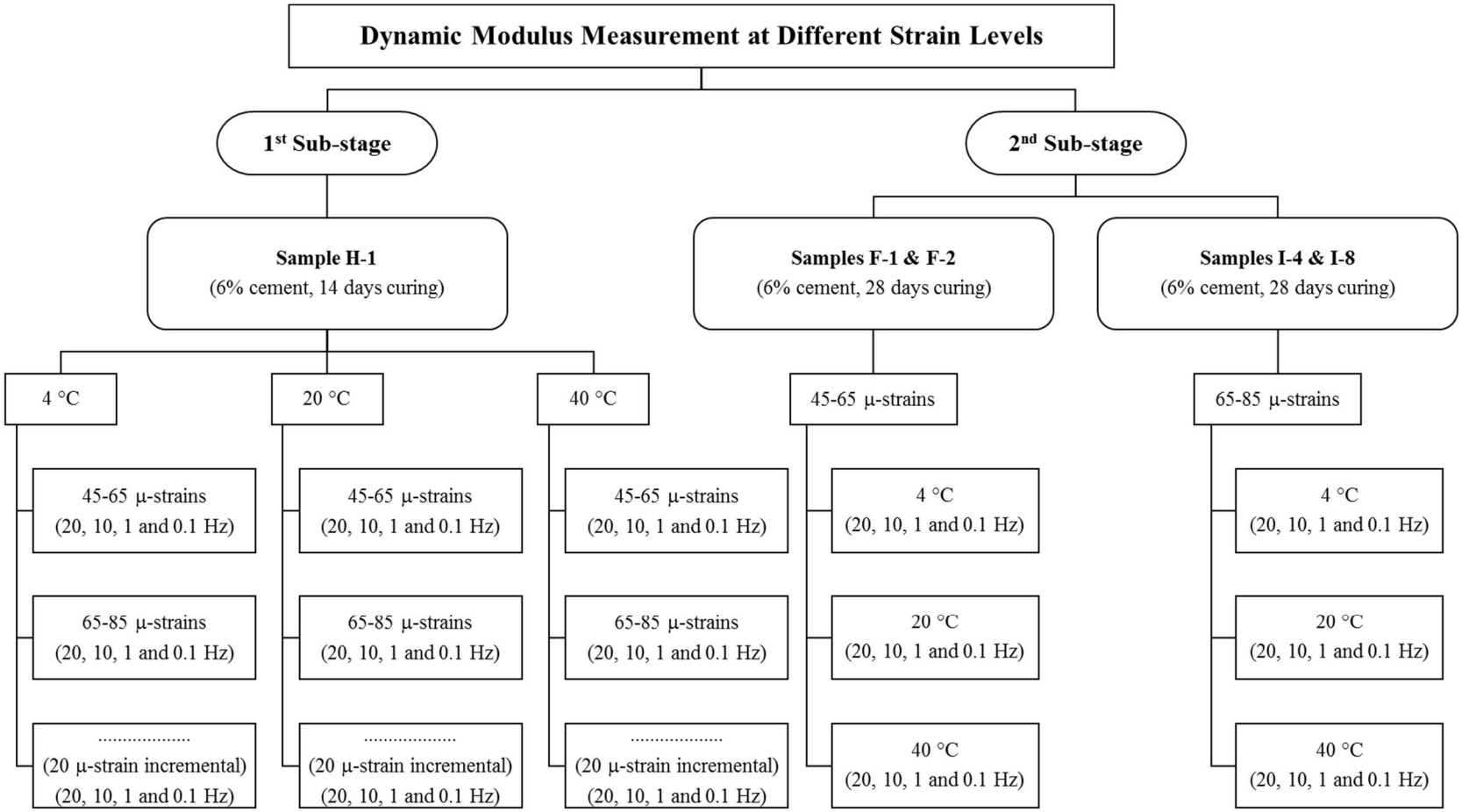

Figure 4.8: Testing scheme for stage one

In order to characterise the effects of strain levels, the first trial test was performed on specimen H-1. At each test temperature, the test strain ranges were increased in 20 $\mu\varepsilon$ increments, starting at 45 - 65 $\mu\varepsilon$. The loading rates used in this sub-stage were 20 Hz, 10 Hz, 1 Hz and 0.1 Hz. The specimen H-1 was placed in a conditioning chamber overnight at 4 °C before the 45 - 65 $\mu\varepsilon$ test was conducted at loading rates equal to 20 Hz, 10 Hz, 1 Hz and 0.1 Hz. Once the dynamic modulus was achieved at 0.1 Hz, the same series of loading rates were tested again at 65 - 85 $\mu\varepsilon$, while the temperature was maintained at 4 °C. This process was repeated at 20 $\mu\varepsilon$ increment intervals until the AMPT machine reached its limit. When the dynamic strain range could not be increased any further, the same testing process was repeated again at 20 °C and 40 °C. At the end of this sub-stage, an appropriate range of dynamic strain levels for testing CTB specimens could be determined and designed as the testing strain range for use in this research.

The second sub-stage was performed on four different specimens, namely F-1, F-2, I-4 and I-8. All four specimens were CTB with 6% cement content and 28-days curing time. In this sub-stage test, the specimens were tested at 4 °C, 20 °C and 40 °C, with loading frequencies equal to 20 Hz, 10 Hz, 1 Hz, 0.1 Hz and 0.01 Hz. The dynamic strain range for test specimens F-1 and F-2 was 45 - 65 $\mu\varepsilon$, while 65 - 85 $\mu\varepsilon$ were used for specimens I-4 and I-8. Finally, the effects of the dynamic strain range were characterized based on the test results from this stage.

Stage two: Influences of cement content, curing time, temperature and loading rates on the dynamic modulus

The objectives of this testing stage were to evaluate the effects of cement content, curing time, temperature and loading rate on the dynamic modulus of CTB specimens. In this testing stage, the dynamic modulus measurements were taken at 4 °C, 20 °C and 40 °C with a loading rate equal to 20 Hz, 10 Hz, 1 Hz, 0.1 Hz and 0.01 Hz. Specimens I-1, I-2, I-4, I-5, I-7 and I-8 were tested at 65 - 85 $\mu\varepsilon$, while 45 - 65 $\mu\varepsilon$ were used for specimens G-1, G-2, H-1, H-2, F-1 and F-2. Figure 4.9 outlines the testing parameters, with the test results and analysis detailed in the following section.

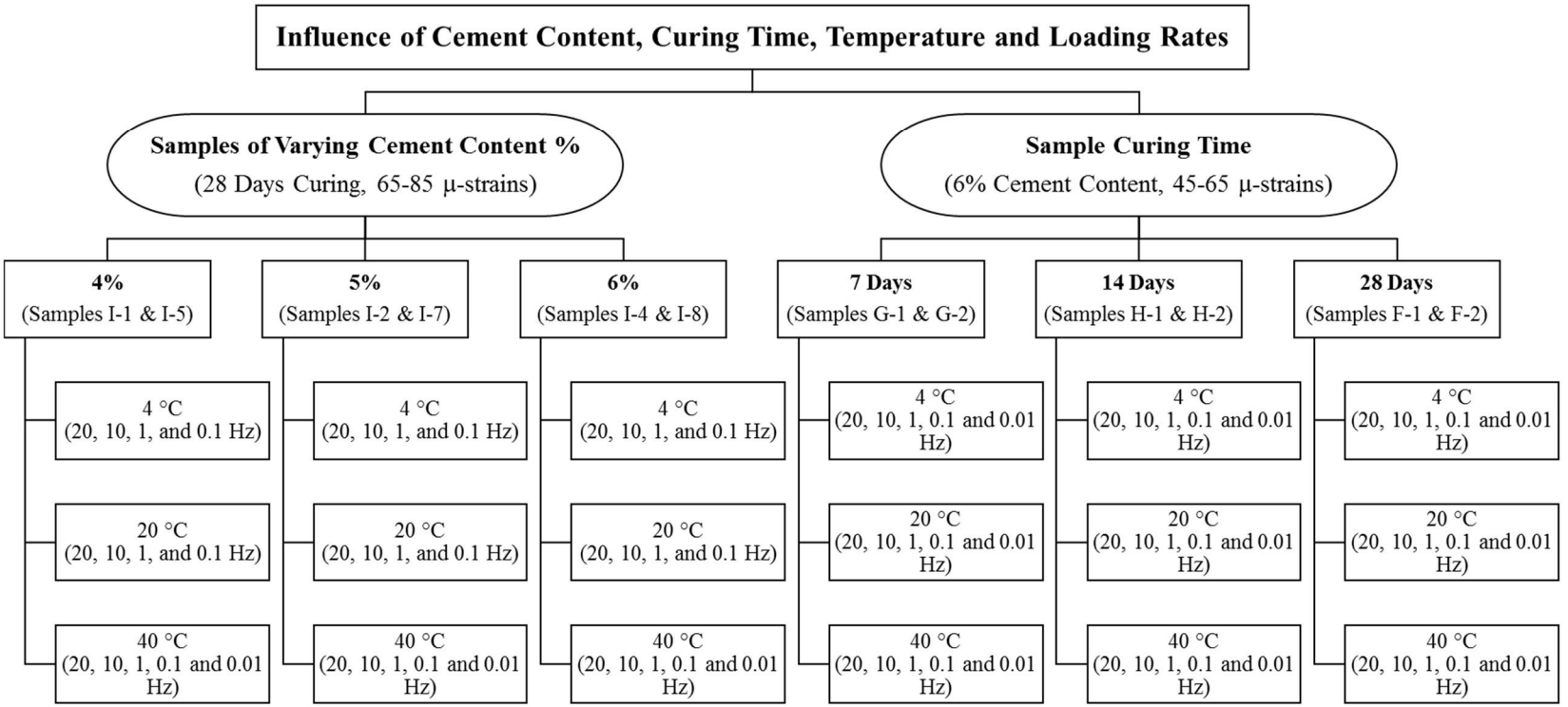

Figure 4.9: Testing scheme for stage two

4.6.3 Test results

The test results of the dynamic modulus measurement in this research are summarised in Tables 4.3 and 4.4. Table 4.3 provides the specimen information, phase angles and data quality statistics measured during the tests, while the dynamic moduli of CTB specimens are summarised in Table 4.4. Table 4.3 also presents the Coefficient of Variation (COV) in percentages, for every pair of tests shown in Table 4.4. Generally, the COV can be calculated from the standard deviation divided by the mean or average value. For example, the COV of a 7-day specimen is the standard deviation of the dynamic modulus calculated from specimens G-1 and G-2 divided by the average value. After the COV of all temperatures and loading frequencies was calculated, the minimum and maximum values were summarised, as presented in Table 4.3. In this research, the COV represents the measurement variations in each pair of specimens; thus the test with the highest COV has the greatest variation. Table 4.3 indicates that the dynamic modulus of CTB specimens measured from the AMPT can have a COV varying from 0% to 20%. AASHTO TP79 (AASHTO, 2011b) recommends a value of 9.7% when two asphalt concrete specimens are tested using AMPT. *"The load standard error"* and *"deformation standard error"* in Table 4.3 are defined as the standard error of the measured load and deformation waveforms respectively; compared with the ideal waveforms. The average difference among the amplitude of the measured deformation represented by the percentage of the mean value is defined as *"deformation uniformity"*. Similarly, the average difference among the measured phase angles, in degrees, is expressed as *"phase uniformity"*. The information in Table 4.3 clearly shows that only the load standard error and deformation standard error in specimen F-2 are higher than the specified values recommended by AASHTO TP79 (AASHTO, 2011b). It should be highlighted that the high percentages of standard error were only observed when testing at 20 Hz, and this was not found when testing other specimens with same cement content and curing time as F-2. This may be the reason that AASHTO PP61 (AASHTO, 2010) suggests a value of 10 Hz as the highest loading rate when testing using AMPT.

Table 4.3: Specimen details, phase angle, Coefficient of Variation (COV) of the mean dynamic modulus, and data quality statistics

Specimen No.	Curing Time (Days)	Dynamic Strain Range ($\mu\varepsilon$)	Cement (%)	Phase Angle (Degree)	Coefficient of Variation (COV)[1] (%)	Load Standard Error[2] (%)	Deformation Standard Error[3] (%)	Deformation Uniformity[4] (%)	Phase Uniformity[5] (Degree)
Curing time									
G-1	7	45-65	6	2.97-3.88	0.50-3.50	0.20-5.40	1.60-5.10	22.80-27.60	0.50-1.60
G-2	7	45-65	6	3.28-3.85		0.20-5.00	1.40-4.30	22.20-25.20	0.60-1.00
H-1	14	45-65	6	2.38-5.21	10.57-16.59	0.20-6.00	1.60-4.80	14.00-17.50	0.10-1.50
H-2	14	45-65	6	3.50-3.92		0.20-5.60	1.60-4.50	8.70-11.40	0.10-0.30
F-1	28	45-65	6	2.68-3.38	0.13-2.25	0.20-5.50	1.60-5.50	9.30-12.30	0.20-0.90
F-2	28	45-65	6	1.63-3.94		0.20-12.80[6]	2.10-14.20[6]	17.70-21.70	0.40-0.70
Cement content									
I-4	28	65-85	6	1.72-2.81	9.11-13.66	0.20-4.70	1.60-5.80	22.20-28.20	0.70-1.30
I-8	28	65-85	6	2.18-3.96		0.20-4.90	1.90-8.40	26.90-28.30	0.20-1.40
I-2	28	65-85	5	3.68-4.44	16.61-19.49	0.20-3.00	3.40-5.40	20.50-29.60	1.10-1.60
I-7	28	65-85	5	2.42-4.06		0.20-7.40	2.00-7.60	21.80-27.40	0.50-1.10
I-1	28	65-85	4	4.52-5.20	8.12-10.81	0.20-3.10	2.70-4.50	26.20-29.50	0.70-1.50
I-5	28	65-85	4	2.97-4.71		0.30-5.10	2.20-8.90	10.50-17.50	0.10-1.20

Note: Requirements for data quality statistics specified by AASHTO TP79 (AASHTO, 2011b) are listed as follows:

1. COV is approximately 9.2% for dynamic modulus test using two specimens,
2. Load standard error should not exceed 10%,
3. Deformation standard error should not exceed 10%,
4. Deformation uniformity should not exceed 30%, and
5. Phase uniformity should not exceed 3 degrees
6. The values higher than standard requirements were observed at 20 Hz loading rate only

Table 4.4: Dynamic modulus of CTB measured from AMPT

Specimen No.	Dynamic Strain Range	Dynamic modulus - E_{AMPT} (MPa)												
		4 °C				20 °C				40 °C				
	($\mu\varepsilon$)	20 Hz	10 Hz	1 Hz	0.1 Hz	20 Hz	10 Hz	1 Hz	0.1 Hz	20 Hz	10 Hz	1 Hz	0.1 Hz	0.01 Hz
Curing Time														
G-1	45-65	18,947	18,519	18,239	18,036	18,237	18,002	17,732	17,418	18,117	17,711	17,231	17,004	17,079
G-2	45-65	20,224	19,864	19,401	18,956	19,218	18,862	18,353	17,938	18,303	17,969	17,480	17,207	17,251
	Average	**19,586**	**19,192**	**18,820**	**18,496**	**18,728**	**18,432**	**18,043**	**17,678**	**18,210**	**17,840**	**17,356**	**17,106**	**17,165**
H-1	85-105	14,176	13,672	13,358	13,057	13,415	12,907	12,521	12,148	12,593	12,223	11,910	11,700	N.A.[1]
	65-85	14,924	14,662	14,301	13,936	13,675	13,395	12,976	12,607	13,125	12,866	12,494	12,195	N.A.[1]
	45-65	15,363	15,301	14,833	14,575	13,467	13,339	12,922	12,587	12,924	12,831	12,349	12,159	12,317
H-2	45-65	19,520	19,202	18,624	18,078	18,654	18,316	17,747	17,374	18,047	17,690	17,263	16,940	16,828
	Average[2]	**17,442**	**17,252**	**16,729**	**16,327**	**16,061**	**15,828**	**15,335**	**14,981**	**15,486**	**15,261**	**14,806**	**14,550**	**14,573**
F-1	45-65	24,630	24,353	23,823	23,187	23,479	23,229	22,635	22,164	23,146	22,806	22,034	21,422	21,095
F-2	45-65	25,181	24,726	24,444	24,037	24,284	23,800	23,231	22,737	23,913	22,745	22,135	21,644	21,559
	Average	**24,906**	**24,545**	**24,134**	**23,612**	**23,882**	**23,515**	**22,933**	**22,451**	**23,530**	**22,776**	**22,085**	**21,533**	**21,327**
Cement Content														
I-4	65-85	26,346	26,354	25,964	25,697	26,290	26,188	25,792	25,312	25,316	25,042	24,307	23,620	23,254
I-8	65-85	21,372	21,952	20,691	19,765	21,204	20,548	19,781	19,229	20,256	20,083	19,453	18,886	18,542
	Average	**23,859**	**24,153**	**23,328**	**22,731**	**23,747**	**23,368**	**22,787**	**22,271**	**22,786**	**22,563**	**21,880**	**21,253**	**20,898**
I-2	65-85	N.A.[1]	16,335	15,459	15,103	N.A.[1]	15,206	14,593	14,396	N.A.[1]	14,437	13,569	13,261	13,327
I-7	65-85	23,752	23,043	21,978	21,121	21,576	21,331	20,763	20,245	20,975	20,727	20,140	19,560	19,274
	Average	**-**	**19,689**	**18,719**	**18,112**	**-**	**18,269**	**17,678**	**17,321**	**-**	**17,582**	**16,855**	**16,411**	**16,301**
I-1	65-85	N.A.[1]	15,503	14,432	14,056	N.A.[1]	14,688	13,953	13,739	N.A.[1]	14,504	13,880	13,764	13,981
I-5	65-85	18,455	18,262	17,812	17,463	17,635	17,517	17,254	16,716	17,221	17,069	16,635	16,288	16,144
	Average	**-**	**16,883**	**16,122**	**15,760**	**-**	**16,103**	**15,604**	**15,228**	**-**	**15,787**	**15,258**	**15,026**	**15,063**

Note:
1. Not Available (no measurement)
2. Average from specimens H-1 and H-2 for the dynamic strain range, equal to 45 - 65 $\mu\varepsilon$ only

As detailed earlier, the first stage of testing was performed in order to: (1) determine a suitable dynamic strain range for the testing of the CTB material, and (2) characterise the influences of dynamic strain range on the dynamic modulus values. Figure 4.10 shows the applied load from the machine actuator versus time curves during the dynamic modulus measurement of specimen H-1. The testing at 4 °C and 20 Hz and the testing at 4 °C and 0.1 Hz with different dynamic strain levels is presented in Figures 4.10a and b, respectively. It can be clearly observed that the magnitude of peak sinusoidal load increases dramatically with respect to the dynamic strain input levels.

However, this magnitude reduces when the loading rate is slowed. On the other hand, the magnitude of peak sinusoidal load is slightly influenced by the changes in testing temperature, as shown in Figures 4.10c and d, where the measurements were performed at a fixed range of dynamic strain level and loading rate. Furthermore, Figure 4.10a shows that the actuator almost reaches its capacity (14,490 N) when testing at 85 - 105 $\mu\varepsilon$ and the input dynamic strain rate should not be increased further. The stress produced at 85 - 105 $\mu\varepsilon$ is approximately 16% of the UCS (specimen H-1). However, it seems that testing with a different dynamic strain range has no significant effect on the dynamic modulus properties of a CTB test specimen. This finding can be confirmed by the test results summarised in Table 4.4. It can be seen that the dynamic moduli of specimen H-1 at different dynamic strain levels differ by only 1% to 2%. Testing was also conducted on four different specimens with the same cement content and curing time (specimens F-1, F-2, I-4 and I-8) in the second sub-stage of test. Although these four specimens were tested at different dynamic strain ranges (different peak loads), it seems that the differences in average dynamic moduli from both sets of tests was less than 4%. These changes that occurred in the dynamic modulus when using different dynamic strain ranges may have been caused either by specimen variations or measurement errors. Based on the test results, a dynamic strain range of between 45 and 85 $\mu\varepsilon$ was selected as the testing strain range for use this research.

According to Table 4.4, the dynamic moduli measured at the same loading rate varied from 5% to 10% when the testing temperature was increased from 4 °C to 40 °C. This behaviour was also observed when the CTB specimens were tested at different loading rates but constant temperatures. In this case, the increases in the dynamic modulus were only approximately 5% when the loading rates were increased. It can be concluded that the dynamic modulus of the CTB specimen is slightly influenced by loading rates and temperatures, based on the test range used in this research. This finding is also supported by load and time curves as shown in Figure 4.10c and d, where loaded waveforms varied slightly when testing temperatures were changed. This may be caused by the elastic behaviour of the testing materials. Cement-stabilised pavement base course is elastic, evidenced by the phase angles measured from the AMPT, which were generally close to zero (Table 4.3).

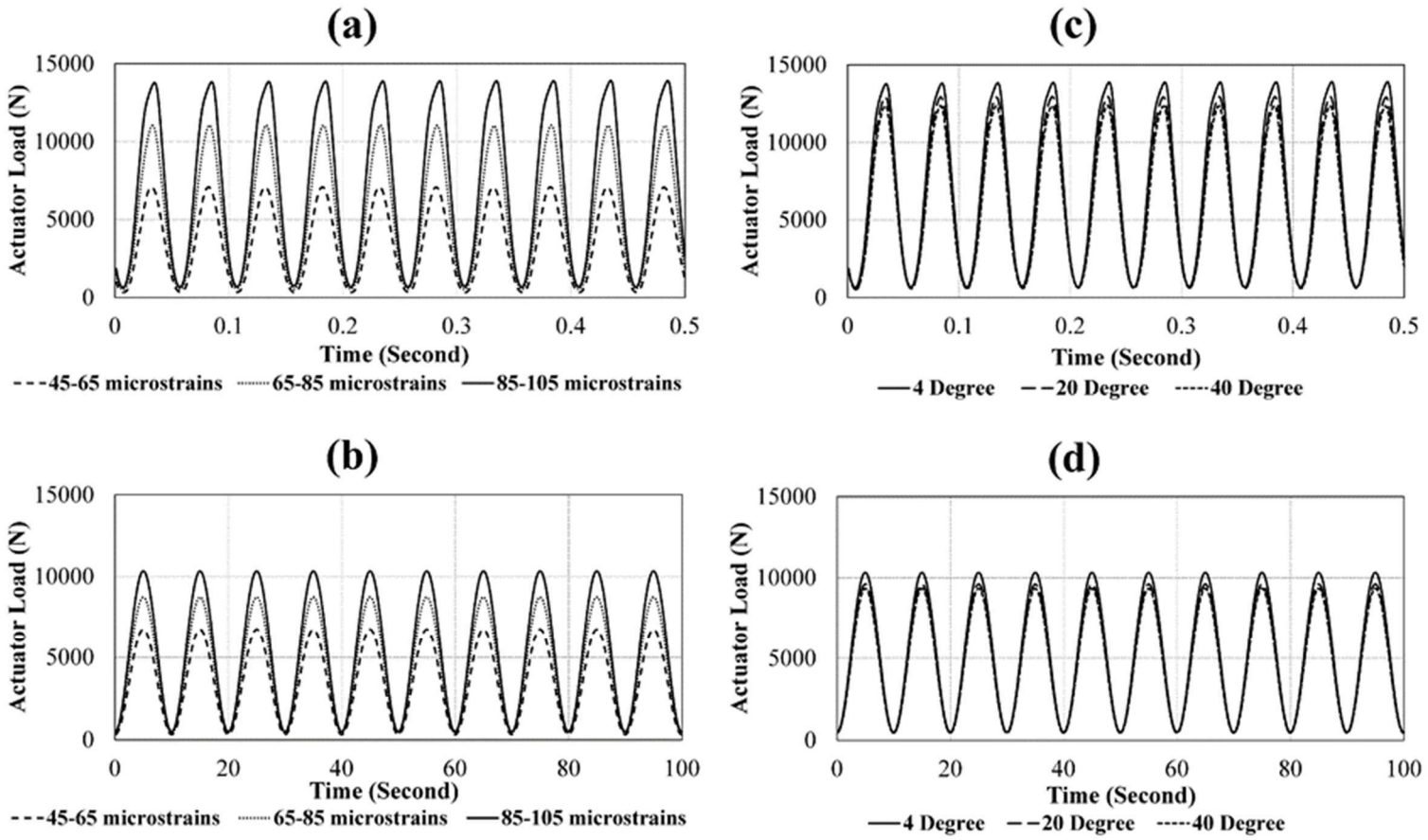

Figure 4.10: Load and time curve from dynamic modulus test of specimen H-1, measured at (a) 4 °C and 20 Hz, (b) 4 °C and 0.01 Hz, (c) 85 - 105 $\mu\varepsilon$ and 20 Hz, and (d) 85 - 105 $\mu\varepsilon$ and 0.01 Hz

The influences of curing time on the dynamic modulus properties of CTB material can also be observed in Table 4.4. It can be seen that the average dynamic moduli after 7 days curing (G-1 and G-2) can increase by up to 16%, if the specimens continue to cure to the 28-day (F-1 and F-2) mark. However, there is no difference in the average values of the dynamic modulus between specimens of 7 days curing and 14 days curing (H-1 and H-2). This behaviour can also be observed in Figure 4.1, where the UCS of a 14-day specimen increased by only 0.96 MPa from the UCS value of the 7-day specimen. However, differences in the amount of cement content added to the CTB do lead to significant changes in the average of the dynamic modulus. As shown in Table 4.4, the average dynamic moduli (I-1, I-2, I-4, I-5, I-7 and I-8) can increase by approximately 17%, up to 46%, when respective amounts of 1% and 2% cement are added to the CTB specimens. Accordingly, it can be concluded that cement content and curing time have significant effects on the dynamic modulus of CTB material.

4.7 Discussion

Figures 4.1 and 4.2 clearly indicate that the response of CTB specimens tested under static and dynamic strain rates are different. This leads to concerns regarding the employment of parameters derived from the static loading regime in road pavement design, as road pavements are normally subjected to the dynamic loading conditions of moving vehicles. The dynamic responses of CTB material were further investigated in this research by performing the cyclic bending tests and cyclic compression tests. The cyclic flexural modulus (E_{flex}) measured based on Austroads's testing protocol (Austroads, 2014a) represents the dynamic response of CTB under cyclic bending force. However, it should be emphasised that the cyclic flexural moduli measured from the four-point bending test may inaccurately represent the material response due to: (1) various uncertainty factors inevitably associated with the four-point bending test, and (2) the E_{flex} values being generally calculated based on ideal elastic assumptions (such as those illustrated by Eqs. 4.3 and 4.4). This is rarely encountered in practice.

To design pavement structures with a CTB layer, the material responses in terms of maximum tensile stress and strain are needed, as displayed in Figure 2.7. Accordingly, the elastic modulus of CTB is generally required if linear-elastic assumptions are

employed in numerical calculations or finite element analysis. It should be highlighted that the elastic modulus and flexural modulus defined within this research are practically different. Due to the effects of shear stress induced during the four-point bending tests (Huurman & Pronk, 2012; Timoshenko & Young, 1968), an accurate method for determining the elastic modulus from the four-point bending test is not yet available (Iyer, 2005). Consequently, the dynamic responses of CTB under monotonic loading condition were investigated in this research. The dynamic modulus (E_{AMPT}) was obtained by directly applying the cyclic-compressive load onto the cylindrical specimen. More importantly, the dynamic response of CTB was examined using the cyclic strain ranges possibly occurring in the field. Therefore, the dynamic modulus is believed to provide a more accurate response of CTB tested under dynamic loads than that obtained from the cyclic flexural modulus.

Correlations between the strength of CTB in term of UCS, static moduli estimated from the monotonic-compression test, and the dynamic moduli determined from the AMPT (E_{AMPT}) are provided in Figure 4.11. It should be emphasised that all test specimens are classified as stabilised material (cement content greater than 3%) based on Austroads (2006b). Figure 4.11 shows that the 28-day static modulus of CTB is approximately 1.5 times higher than the 7-day static modulus, but about 10 to 15 times lower than the dynamic modulus of the same aged specimens measured by the AMPT. It should be highlighted that the moduli reported in Figure 4.11 are the values obtained from laboratory investigations; the design moduli, or field moduli, are usually smaller than those measured in the laboratory (Austroads, 2014a). Accordingly, Figure 4.11 was produced to compare the CTB responses examined using ordinary UCS tests with the results from the AMPT test.

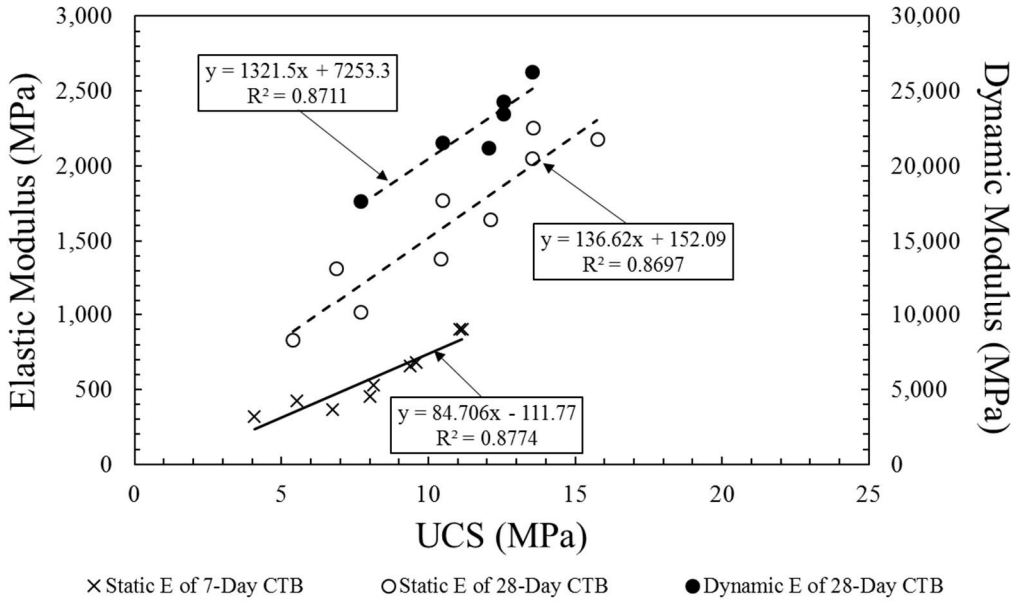

Figure 4.11: Relationship between UCSs, static moduli, and dynamic moduli (E_{AMPT}) of CTB

Figure 4.12 shows the cyclic flexural modulus (E_{flex}) development with respect to the changes in flexural strength (FS) of 28-day CTB specimens. The relationship equation between the cyclic flexural modulus and flexural strength is also provided in Figure 4.12. A comparison between the E_{AMPT} and E_{flex} of specimens with 4%, 5%, and 6% cement content is illustrated in Figure 4.13. The values of E_{flex} in Figure 4.13 are the average values of cyclic flexural modulus summarised in Table 4.2. To compare with E_{flex} values, the E_{AMPT} values measured at 20 °C and 1 Hz were used to plot Figure 4.13. However, the measurements of E_{AMPT} were performed under strain-controlled tests with sinusoidal loading waveform, while E_{flex} values in Figure 4.13 were obtained by stress-controlled tests with haversine loading waveform. It can be seen from Figure 4.13 that the differences between E_{flex} and E_{AMPT} are approximately equal to 1,000 MPa to 3,000 MPa.

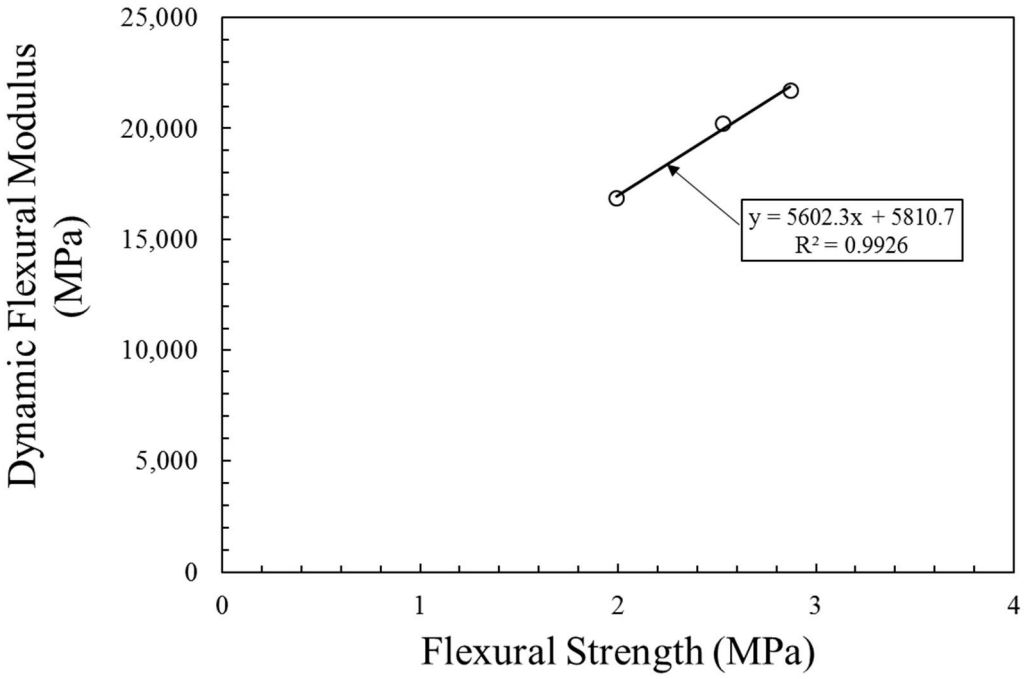

Figure 4.12: Relationship between *FS* and E_{flex} of 28-day CTB

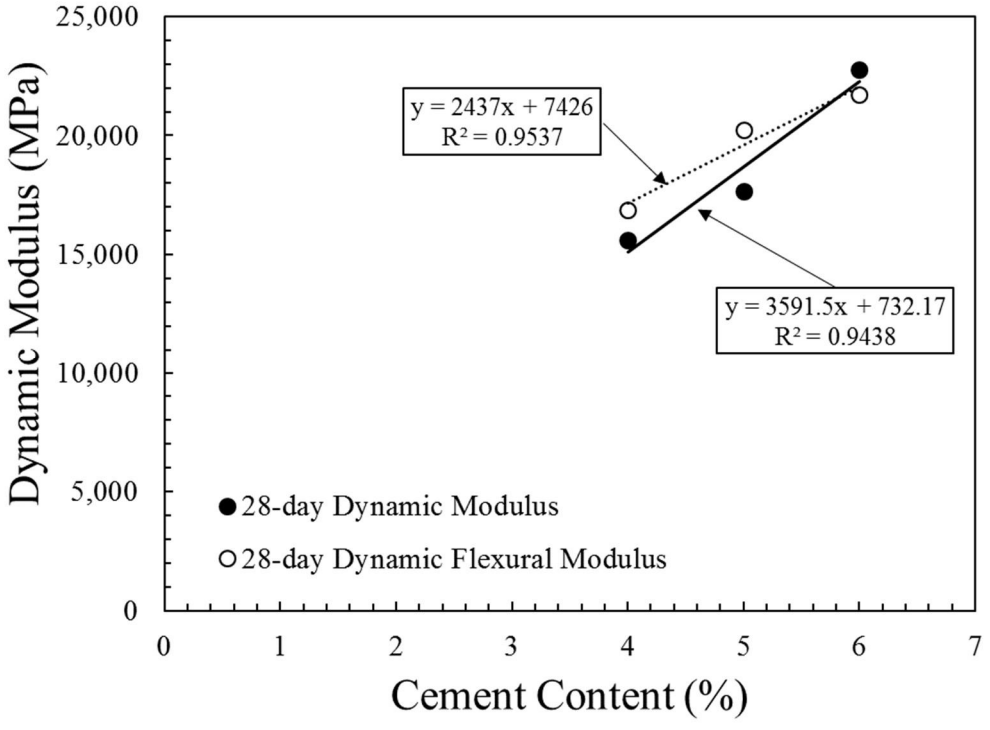

Figure 4.13: Comparison between E_{AMPT} and E_{flex} of 28-day CTB

The significant difference in modulus values between the dynamic and elastic moduli may possibly be attributed to two main causes. Firstly, strain levels used in modulus calculations are different. The dynamic modulus of a CTB material is approximately equal to the initial tangent modulus while the elastic modulus is the chord modulus at a higher strain level (Kolias & Williams, 1980). Secondly, the strength and elastic properties of CTB material are loading rate dependent, as demonstrated by the test results in this chapter and in previous literature (Watstein, 1953; O. Xiao et al., 2008). An increase in the loading rate on a test specimen leads to an increase in the strength and modulus of a material. The cyclic flexural moduli determined from the four-point bending test are roughly equal to the dynamic moduli. Although, the flexural test yields modulus values very close to the AMPT test, the test usually requires the utmost attention and care during specimen preparation and testing. Moreover, the flexural modulus from the four-point tests gives only the estimated values, since the shear stress effect is neglected in the calculations. For this reason, the dynamic modulus measured from the AMPT seems to be the most suitable parameter for pavement response analysis at this stage.

4.8 Summary and recommendations

A comprehensive testing program was developed in this chapter to investigate the dynamic responses of CTB under different loading conditions. Brief details of the investigations are repeated below where they relate to the conclusions which are also outlined.

- Under monotonic-compression tests with dynamic and static loading strain rates, test results reveal that the responses of CTB test specimens under different rates of loading are explicitly different. The damage evolution through the damage parameters can be successfully used to capture the different behaviour of CTB under the different loading regimes of static and dynamic.

- The dynamic response of CTB was firstly investigated using the four-point bending test results. The 28-day cyclic flexural modulus of CTB (E_{flex}) is

dependent on cement content and applied tensile strain (or stress) magnitude. An increase in cement content led to an increase in the cyclic flexural modulus. On the other hand, the rise in applied tensile strain (or stress) caused a reduction in the E_{flex} value. According to the four-point bending test setup used in this research, the stress-controlled test seems to provide more consistent results than the strain-controlled test.

- To design pavement structures based on a linear-elastic assumption, the elastic modulus is generally applied as the design input parameter. In addition, this input parameter should adequately explain the material response under dynamic loading conditions. However, the cyclic flexural modulus determined from the four-point bending test is restricted by two limitations: (1) the inevitable factors associated with the four-point bending test generally lead to uncertain results, (2) the precise value of the elastic modulus is rarely accurately determined from the four-point bending test due to the effects of shear stress. Consequently, the dynamic response of CTB under cyclic-compressive loads was further examined with the AMPT used in this research.

- The dynamic response of CTB was then investigated using the asphalt testing platform (AASHTO, 2011b). Initially, a suitable dynamic strain range for testing CTB specimens was determined and assigned as the dynamic strain range to be used. Apart from identifying a suitable dynamic strain range, the influences of dynamic strain on dynamic response were also examined at this stage. The testing results revealed that a CTB cylindrical specimen behaves in the manner of an elastic material when tested at 45 - 105 $\mu\varepsilon$. This is due to the fact that the dynamic modulus is not influenced by changes in the dynamic strain range nor the magnitude of the cyclic load.

- In the second stage, the effects of cement content, curing time, temperature and loading rate were investigated. Testing results show that the dynamic modulus of CTB is significantly influenced by cement content and curing time. The dynamic modulus can increase by 17%, up to 46%, if an additional 1% and 2% cement respectively, is added to the CTB material. Moreover, the 28-day

specimens have dynamic moduli which are higher than the 7-day specimens by approximately 16%. However, changes in temperature and loading frequency have only a slight effect on the dynamic modulus values of the CTB material.

- The different moduli measured within this research were compared and discussed. In accordance with other research, the dynamic modulus of CTB material is higher than the elastic modulus measured from the monotonic-compression test. Therefore, the pavement response analysis, using the elastic modulus measured from the monotonic-compression test, may result in higher stress or strain values than would actually occur in reality. It should be emphasised that the dynamic moduli in this research were measured by directly applying a cyclic load to the sample; while other researchers have used the ultrasonic pulse velocity or vibration resonance method.

- The cyclic flexural modulus determined from the four-point bending test seems to be very close to the dynamic modulus measured in this research. However, specimen preparation for flexural tests is cumbersome and this may lead to inaccurate testing results. Accordingly, employing the dynamic modulus in pavement response analysis is the preferred option due to it being obtained from a simple test, along with the fact that a similar in-service loading regime is applied during measurement.

Recommendations based on the comparison between the strength of CTB in terms of UCS and the static moduli estimated from the monotonic-compression test and the dynamic moduli determined from the AMPT are illustrated below.

- A concern of using design parameters derived from the static loading tests could be raised due to the difference in the intrinsic behaviour of CTB under static and dynamic loading conditions, based on the test results in this research. In real road pavement conditions, all pavement materials are under the dynamic (cyclic) loading condition of moving vehicles, but almost all current design parameters rely on static loading tests.

- Relationship equations between the static modulus from the UCS tests and the dynamic modulus directly measured under applied cyclic loading have been formulated. In addition, the relationship equation between flexural strength and the cyclic flexural modulus was also developed.

CHAPTER 5

FATIGUE CHARACTERISTICS OF BOUND CTB

5.1 Introduction and background

Bound Cement-Treated Base (CTB) inherently exhibits fatigue deterioration under repeated (cyclic) loads due to its inflexible response under such loads. Therefore, in the long-term performance of CTB pavement, avoidance of fatigue failure in the CTB layer should be specified as one of the design criteria. Based on the current pavement structural design viewpoint, a stabilised base layer (i.e., CTB) is subjected to a wheel load on a pavement surface, causing development of tensile stress at the bottom and compressive stress at the top of the stabilised base layer. Such tensile stress is more critical to the performance of a CTB-layer structure, and generally is considered to be a CTB pavement design criterion (Austroads, 2010b; NCHRP, 2004). The tensile strength of a CTB layer can be determined practically using various test methods (Wen et al., 2014), for example, direct tensile tests (ASTM, 2008), indirect tensile tests (or splitting tests) (ASTM, 2011b), and flexural tests (Austroads, 2010b, 2014a). However, all conventional tensile strength tests are under static loading conditions that cannot capture real pavement material behaviour, particularly fatigue, under vehicle loads. Consequently, those tensile strength tests would not be suitable to determine a rational design parameter for a mechanistically structural CTB pavement design. Reliable design parameters for CTB road pavement should be derived from fatigue tests under a cyclic loading regime to simulate the real fatigue characteristics of a CTB pavement layer under traffic loading conditions. However, a fundamental assessment of fatigue characteristics of CTB under real loading conditions is almost unobtainable due to the need for sophisticated laboratory facilities capable of applying cyclic loads with a certain frequency that are compatible with CTB material characteristics.

Fatigue four-point bending tests under cyclic loading conditions have been employed to assess the fatigue characteristics of Asphalt Concrete (AC) since the late 1950's (Pell, McCarthy, & Gardner, 1961). Currently, four-point bending tests using prismatic beams are popularly used to measure the flexural modulus, and evaluate the fatigue

characteristics of AC (AASHTO, 2007b; ASTM, 2010a; Austroads, 2006a; BS, 2004a). The four-point bending tests are used to simulate a wheel-loading interaction with an AC layer in pavement. Theoretically, the cyclic load (i.e., traffic load) is applied in the mid-part of a test beam toward two inner clamps during the test. Based on the loading configuration of the four-point bending test, the uniform strain distribution corresponding to the test beam length is believed to take place in this mid-span area. Therefore, the maximum tensile stress occurs in the outer beam surface at this mid-section of the bottom of the beam (i.e., from the haversine loading waveform) and the bottom and the top of the test beam (i.e, from the sinusoidal loading waveform). It could be stated that the four-point bending test apparatus is acceptable, and it is widely used in advanced pavement laboratories. Therefore, it could be a good facility platform for a fatigue examination of CTB. Recent research into the characteristics of cement-stabilised materials, based on the four-point bending test platform, can be found in limited sources based on the literature review. Some of the literature reported the fatigue behaviour of prismatic beam specimens moulded from cement-stabilised recycled concrete aggregate blended with recycled crushed brick and fine recycled glass, respectively (Arulrajah, Disfani, Haghighi, Mohammadinia, & Horpibulsuk, 2015; Disfani, Arulrajah, Haghighi, Mohammadinia, & Horpibulsuk, 2014). Other literature, such as Paul and Gnanendran (2016) focused on the static and dynamic modulus of granular based materials stabilised by cement-fly-ash binder. However, the prismatic beam specimens had dimensions which were 100 mm thick, 100 mm wide, and 400 mm long, and a binder content of only 3% was employed in their studies.

CTB has been widely used in pavement structures in many countries, such as the US, China, South Africa, and South Korea (Cho, Lee, & Ryu, 2006). However, limitations of using CTB for roads in some countries, including Australia, remain. For Western Australia in particular, CTB is only permitted for use in constructing road working platforms, not for use in the main structural layers of road pavements (Y. S. Yeo, 2011). It must then be overlaid with an unbound granular material. Thickness reduction of an unbound granular layer when using CTB as the foundation is not permitted, to prevent the tendency towards cracking. These limitations are specified by the Main Roads authority of Western Australia (MRWA, 2010). The short-term and long-term cracking of CTB in pavement cannot effectively be solved theoretically due to a lack

in the fundamental understanding of CTB behaviour under traffic loading conditions. Practical experience in road pavement construction since CTB has been introduced has shown that fatigue cracking is one of the major distress modes in CTB pavements; it results from CTB modulus degradation under repetitive loads from traffic. Cracks from fatigue failure generally originate at the bottom of a CTB layer and propagate to the asphalt pavement surface (George, 2002).

Based on the standard four-point bending tests of AC, fatigue failure is generally specified to take place at a number of (cyclic) loading cycles that reduces the flexural modulus of a material to 50% of initial modulus (Austroads, 2006a). The fatigue relationship can be drawn from the correlation between fatigue life and applied stress or strain conditions. The experimental data for fatigue life against tensile strains/stresses induced in test samples can be obtained via a number of fatigue tests conducted at different magnitudes of applied strains or stresses. Fatigue tests can be carried out in two modes, "*strain-controlled*" and "*stress-controlled*" modes, depending on testing protocols, to simulate real conditions in pavement. In the strain-controlled test, strain is maintained by reducing the applied load during the test (constant strain test). For the stress-controlled test, the stress is kept constant and strain is increased (constant stress test). The simplest form of the fatigue relationship is shown in Eq. 5.1 (Chummuneerat, Jitsangiam, Nikraz, & Patel, 2013).

$$N = \left(\frac{k_1}{\varepsilon_t}\right)^{k_2} or \left(\frac{k_3}{\sigma_t}\right)^{k_4} \tag{5.1}$$

in which N is the fatigue life or loading cycle to failure, ε_t is the tensile strain at the bottom of the specimen, σ_t is the applied tensile stress, and k_1 - k_4 are regression parameters.

The fatigue relationship of CTB is introduced for the structural analysis and design of flexible pavements. For mechanistic road pavement design, the tensile strain at the bottom of the CTB layer is converted to a number of standard axle load repetitions and compared with the designed number of standard axle repetitions. Eq. 5.2 is an example of the fatigue relationship for pavement design (Austroads, 2014b). If pavement thicknesses are well designed and strains in pavement caused by cyclic loadings are

low enough, accordingly, fatigue cracking is not a problem (Soliman, Zeiada, Kaloush, & Mamlouk, 2012).

$$N = RF\left(\frac{\left(113000/E^{0.804}\right)+191}{\mu\varepsilon_t}\right)^{12} \quad (5.2)$$

in which, N is the allowable number of standard axle load repetitions, $\mu\varepsilon_t$ is the tensile micro-strain at the bottom of the CTB layer, E is the cemented material modulus (MPa), and RF is the reliability factor for the fatigue life of cemented materials.

To characterise the fatigue behaviour of CTB, a fatigue examination of CTB following the four-point bending tests protocol of AC (Austroads, 2006a) was performed in the first investigation stage. The main objective of employing the AC testing protocol in the first stage is to maximise the application of the fatigue testing facility developed for AC material. It is well known that fatigue characteristics of AC are necessary for road pavement design, hence the extensive development by many researchers of the fatigue test for AC. The fatigue behaviour of CTB was then examined in accordance with testing protocols developed, based on the standard of test for concrete materials (Austroads, 2014a) in the second stage. The effects of cement content, testing mode (stress-controlled or strain-controlled), loading frequency, and loading configuration (haversine or sinusoidal) were investigated through the fatigue results obtained from the tests in both investigation stages. The details of the materials, experimental works, and results are explained in the following sections.

5.2 Materials and methods

Fatigue characteristics of CTB specimens with varying cement contents of 3%, 5%, 7.5%, and 10% were investigated in the first stage. A cement content of 3% was selected based on the minimum requirement of cement-stabilised materials (Austroads, 2006b). A cement content of 10% was chosen as the upper boundary as this is the highest cement content recommended for economical use in road construction (NAASRA, 1970). In support of a limitation on the percentage, the test results in Chapter 3 demonstrated that the CTB specimens moulded using WA crushed

rock developed minimal strength improvement when the cement content of the specimen exceeded approximately 7% (see Figure 3.7).

The four-point bending test for AC in accordance with Austroads (2006a) was adapted for testing on CTB specimens with the two loading waveforms, sinusoidal and haversine, along with two loading modes of stress-controlled and strain-controlled conditions. The sinusoidal loading waveform was employed in this research as it is recommended by BS (2004a) and AASHTO (2007b) for the four-point bending test on AC. On the other hand, Austroads (2006a) proposed using a haversine loading waveform for determining the fatigue life of AC from the four-point bending test. It should be highlighted that the aforementioned test standards (AASHTO, 2007b; BS, 2004a) and guidelines (Austroads, 2006a) suggest measuring the fatigue life of AC under strain-controlled and displacement-controlled conditions, respectively.

In the second stage of the fatigue investigation, CTB specimens with a cement content of 4%, 5%, and 6% were tested in accordance with the test protocol developed by Austroads (Austroads, 2014a). It should be emphasised that this test protocol was developed to examine the fatigue characteristics of cement-stabilised materials for road pavement design. According to Austroads (2014a), the haversine loading waveform under stress-controlled or strain-controlled mode is recommended for fatigue investigation of CTB materials. The details on specimen preparation and testing procedure are illustrated in the following sections.

5.2.1 Materials

CTB specimens were prepared by blending standard Crushed Rock Base (CRB) with General Purpose (GP) Portland cement (Standard Australia, 2010) at the Optimum Moisture Content (OMC) derived from a modified compaction test (ASTM, 2012b). CRB material conforming to MRWA specifications (MRWA, 2012) were collected from a local quarry in Western Australia (WA). In addition, the employed CRB was geologically classified as Granite/Diorite (intrusive igneous rock). The geotechnical properties and Particle Size Distribution (PSD) of the selected CRB are presented in Table 3.1 and Figure 3.1, respectively. Figure 3.5 presents the moisture-density relationship of CTB (3% to 10% cement by mass of dry CRB) determined in this

research. Based on Figure 3.5, cement content has little influence on the Maximum Dry Density (MDD) and OMC of CTB. Accordingly, OMC and MDD equal to 6.20% and 2.29 g/cm^3, respectively, were employed in the specimen preparation for the four-point bending tests.

5.2.2 Specimen preparation

The specimens for the four-point bending test were prepared in accordance with the procedures provided in Section 3.3.2. Accordingly, specimens with dimensions 50 mm thick, 63.5 mm wide, and 400 mm long (Austroads, 2006a) were employed in the first stage of the fatigue investigation. In the second stage, specimens with dimension 100 mm thick, 100 mm wide, and 400 mm long were used in the fatigue investigation, based on the recommendation by Austroads (2014a).

5.2.3 Test methodology

In this research, the fatigue behaviour of CTB was characterised by employing the test protocol for AC material (Austroads, 2006a) in the first stage, followed by the test protocol for stabilised material (Austroads, 2014a) in the second stage. The test methodology employed during both stages of the investigation is summarised in this section. Figure 5.1 illustrates the two sub-stages of test methodology required in the first stage of the fatigue investigation. According to Austroads (2006a), beam specimens with dimension 50 mm thick, 63.5 mm wide, and 400 mm long (50×63.5×400 mm^3) were recommended for the fatigue test. In Sub-stage 1, the effects of loading waveforms and applied strain levels were investigated. In addition, a suitable strain level for fatigue life measurements of CTB was determined according to the test results obtained in Sub-stage 1. In Sub-stage 2, a suitable strain level obtained from Sub-stage 1 was then applied to four-point bending tests to investigate the effects of cement content on a CTB specimen. The four-point bending tests under stress-controlled mode were also examined in Sub-stage 2.

Beam specimens with dimension 100 mm thick, 100 mm wide, and 400 mm long (100×100×400 mm^3) were employed in the second stage of the fatigue investigation. The fatigue tests in this stage were performed according to Austroads (2014a). Figure 5.2 presents the test methodology employed in the second stage. The effects of the

testing mode (stress-controlled and strain-controlled), and the applied stress and strain level were investigated in Sub-stage 1. In the first sub-stage, only the specimens with 5% cement content were employed for the fatigue tests. The specimens for fatigue test in the second stage were cured for approximately 28 days. Every specimen was tested under the haversine loading waveform with a loading frequency of 2 Hz (Austroads, 2014a). The loading frequency was then changed to 4 Hz, and 10 Hz in Sub-stage 2. Accordingly, the influences of loading frequency on the fatigue life of CTB were examined in the second sub-stage. Finally, the effects of cement content were investigated in Sub-stage 3.

This research seeks to examine the fatigue characteristics of CTB using four-point bending tests. The purpose is to overcome a shortcoming in suitable facilities for fatigue assessment of CTB, and gain a better understanding of the fatigue characteristics of CTB under cyclic loading conditions. The fatigue testing program was developed to investigate the effects of the most relevant factors which may affect the fatigue characteristics of CTB materials. The relevant factors include testing mode, loading waveform, loading frequency, cement content, and applied stress and strain level. According to the test methodology presented earlier, recommendations on the fatigue testing standard development are provided later in this chapter.

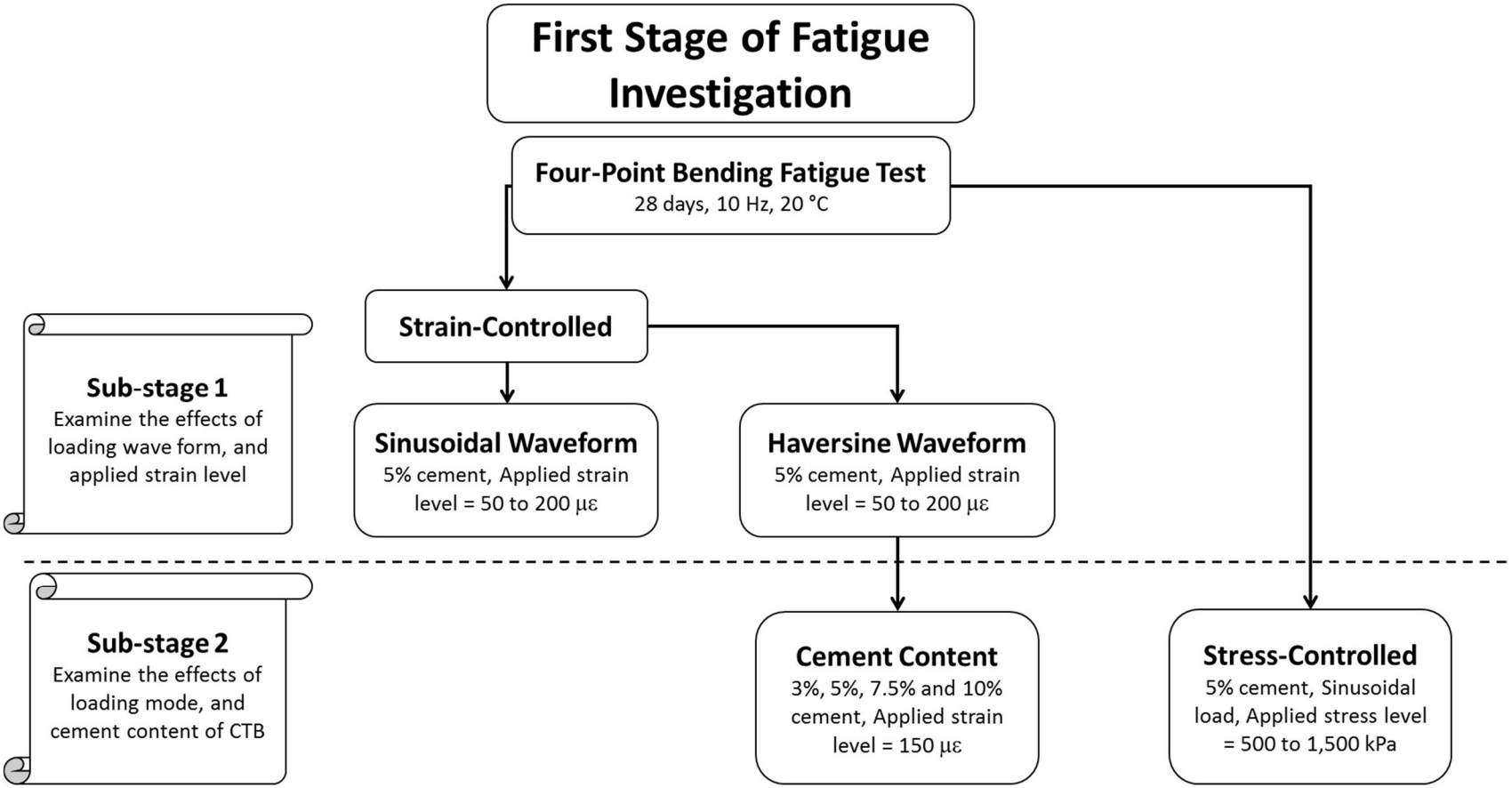

Figure 5.1: Test methodology in the first stage of fatigue investigation

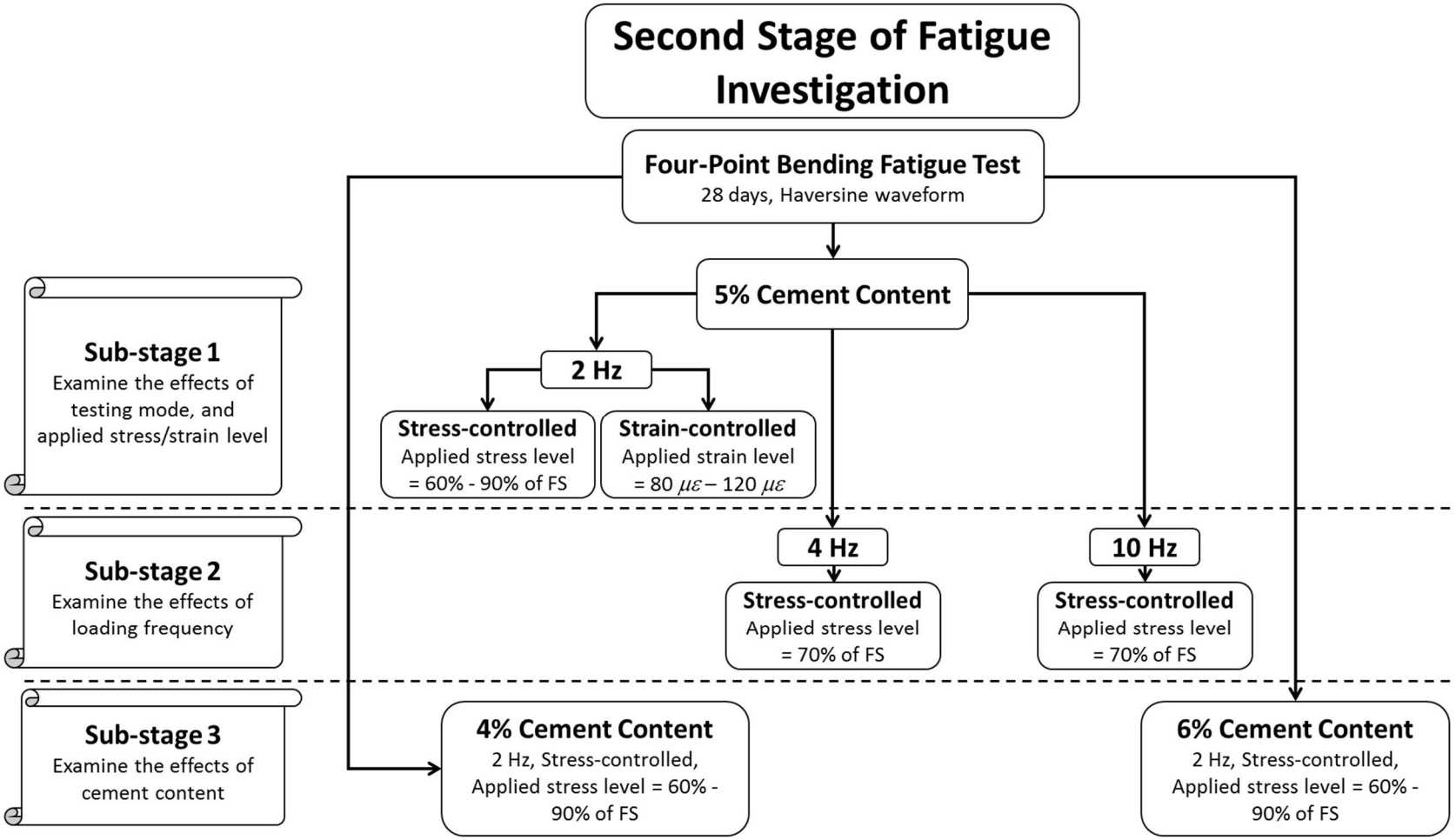

Figure 5.2: Test methodology in the second stage of fatigue investigation

5.2.4 Four-point bending fatigue test of CTB

Fatigue test Stage 1

Figure 5.3 illustrates a European (EN) standard tester equipped with a four-point bending jig, manufactured by IPC Global. The tester consists of three major components: the test chamber, the Control and Data Acquisition System (CDAS), and the four-point bending jig (Figure 5.3a). The major test control system is a real-time computer control and flexible data acquisition system, called the Integrated Multi-Axis Control System (IMACS), which helps to improve data resolution and reduce data noise. Throughout the test process, the testing temperature is controlled inside the test chamber (Figure 5.3b). A temperature can be assigned to the specimens in the range of 0 °C to 60 °C with a temperature stability of ±0.2 °C. Inside the test chamber, the four-point bending jig is located at the middle of the loading frame (Figure 5.3a). Suitable heights and widths of the test specimens are either 50×50 mm^2, 50×63.5 mm^2, or 70×70 mm^2 (height × width). The test specimen is restrained by four clamps, with two outside clamps as beam supports and two points of loading applied via the two central clamps, as shown in Figure 5.3a. The spacing between each clamp is 118.5 mm. During the tests, a cyclic load is continually applied to the prismatic test specimen in the form of a haversine or sinusoidal waveform. Test conditions for the constant applied stress or strain on test specimens are generally in either the stress-controlled or strain-controlled mode. The load actuator is connected to both central clamps at the bottom of the four-point bending jig. The frequency range of the load actuator is 0.01 to 60 Hz. During cyclic loading, beam deflection is measured at the mid-span of the top fibre of a test specimen by a Linear Variable Differential Transformer (LVDT). The stroke of the LVDT is limited to ±0.50 mm with a resolution of ±0.25 μm and an accuracy of ±1 μm (Austroads, 2006a). Consequently, the maximum tensile stress ($\sigma_{t,max}$) and the maximum tensile strain ($\varepsilon_{t,max}$) at mid-span of the top of a test beam can be calculated from Eqs. 4.3 and 4.4, respectively. Finally, the cyclic flexural maximum of the prismatic beam can be estimated by dividing the maximum tensile stress by the maximum tensile strain ($\sigma_{t,max}/\varepsilon_{t,max}$). The limitations of the applied dynamic load and actuator stroke are ±4.4 kN and ±5.0 mm, respectively. Based on Eq. 4.3, this maximum applied load of 4.4 kN is equivalent to 9,850 kPa of the maximum tensile stress, when a 63.5 mm-width and 50.0 mm-height prismatic beam

is tested under the haversine waveform. The resolution of the applied dynamic load is ±2.2 N with an accuracy of ±20 N (Austroads, 2006a).

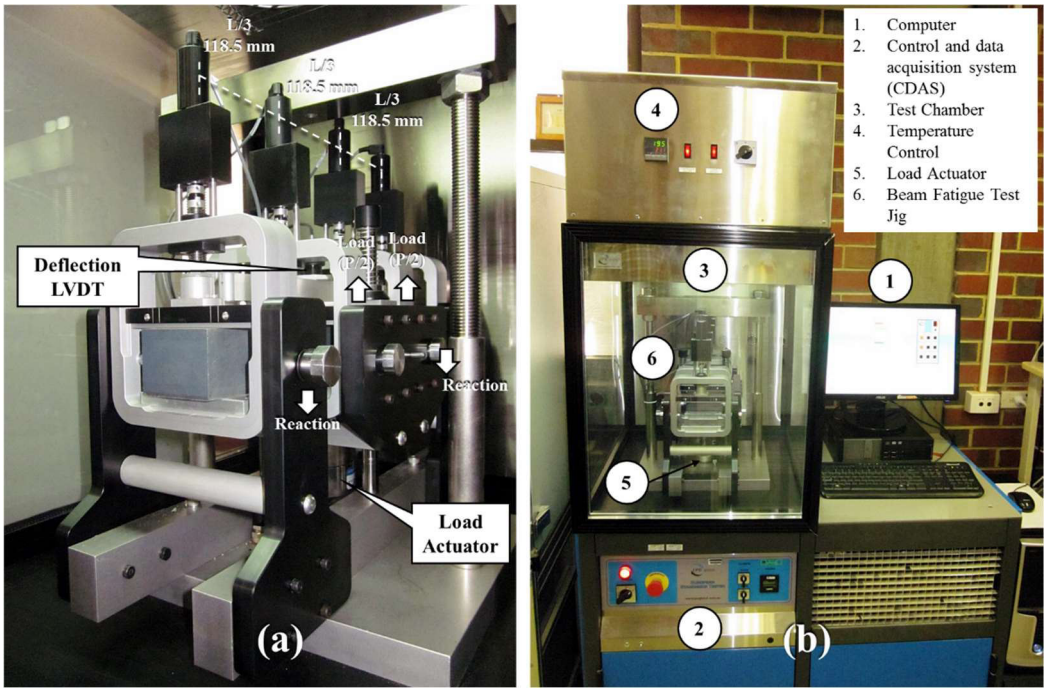

Figure 5.3: Four-point bending test apparatus: (a) the four-point bending jig, and (b) EN standard tester equipped with four-point bending jig

Austroads (2006a) recommends measuring the fatigue life of the AC by applying a haversine cyclic load with a frequency of 10 Hz to the specimens. In this research, a loading frequency of 10 Hz was also used in the four-point bending tests of the CTB material. It should be noted that in a real situation, applied loading frequencies for an AC layer and a CTB layer may not be the same, as the loading time decreases with depth in a pavement. However, with no strong proof of the right frequency magnitude in a CTB layer at this stage, using the applied loading frequency of 10 Hz in this research relies on the hypothesis that a CTB layer is conventionally overlaid by a relatively thin AC layer within the same pavement structure. Therefore, they would be eventually subjected to almost the same loading frequency in an underlying CTB layer. During the AC tests, the applied tensile strain at the top of the beam is generally specified to be equal to a constant 400 $\mu\varepsilon$ under the strain-controlled mode. However, the applied tensile strains in this research were varied to suit the inherent properties of the CTB test specimens. The test temperature in the chamber is kept constant at 20 °C

throughout the test. The reduction in the cyclic flexural modulus is monitored and terminated when either the cyclic flexural modulus is reduced to 50% of the initial value or one million loading cycles is completed (approximately 28 hours).

Fatigue test stage 2

The second stage of the fatigue investigation was conducted based on Austroads (2014a) using the hydraulic universal testing machine illustrated in Figure 4.3. The peak stress applied during the stress-controlled test was varied between 60% and 90% of the Flexural Strength (*FS*). For the strain-controlled test, the maximum strain magnitude employed during the fatigue test was varied from 80 $\mu\varepsilon$ to 120 $\mu\varepsilon$. The loading frequency recommended by Austroads (2014a) is 2 Hz. Therefore, the loading duration applied in the standard fatigue test in the second stage was 250 ms with a rest period of 250 ms. However, loading durations of 250 ms and 100 ms, without a rest period, were employed in the fatigue tests with loading frequencies of 4 Hz and 10 Hz, respectively. In the first stage of the fatigue investigation, the fatigue tests were terminated when the cyclic flexural modulus reduced to 50% of the initial value or when one million cycles loading was completed. However, fatigue tests with a loading frequency of 2 Hz require approximately one week to complete one million cycles of cyclic loading. Due to the time constraints in this research, the maximum number of loading cycles in the second stage was assigned at 200,000 cycles (approximately 28 hours). This termination condition was designed based on the test results from the first stage. A detailed analysis around choosing the termination condition at 200,000 cycles is provided later in the results section.

5.3 Fatigue testing results

5.3.1 Fatigue life measurement from Stage 1

Sub-stage 1: The effects of loading waveform and applied strain levels

In Sub-stage 1, 5% cement specimens were tested under the strain-controlled (constant strain) mode. The two main loading waveforms of the repeated sinusoidal and haversine load were applied separately to the CTB specimens, without a rest period, until the specimens failed from fatigue damage (a reduction in cyclic flexural modulus

reaches one-half of the initial value) or one million cycles of cyclic loading was completed. Figure 5.4 shows the results of the four-point bending tests under the haversine load at different applied strain levels, while Figure 5.5 presents the results of the four-point bending test under the sinusoidal load at different applied strain levels.

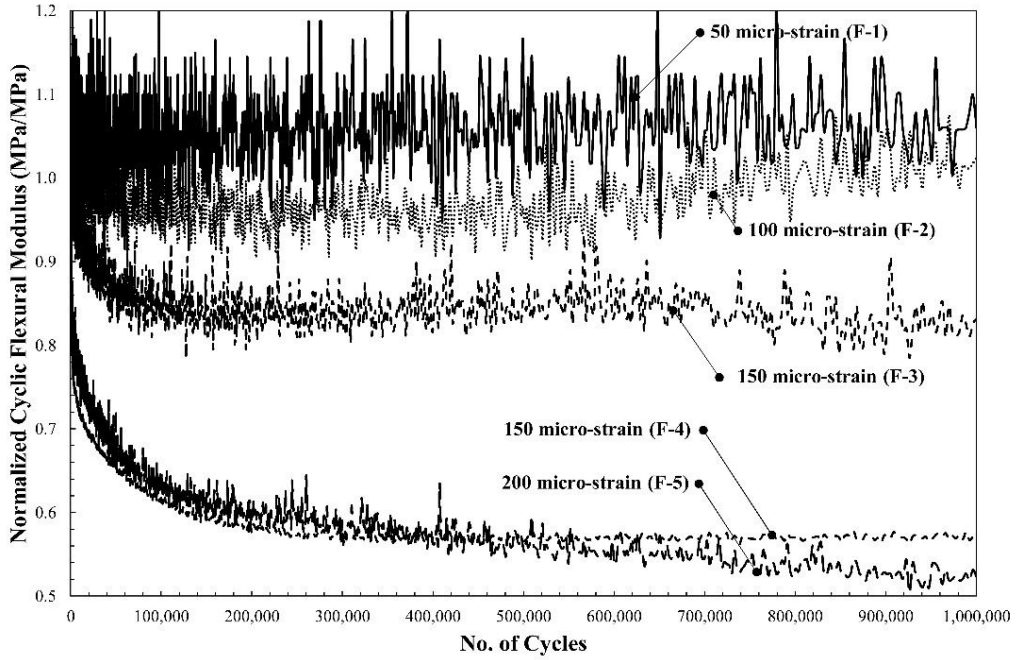

Figure 5.4: Strain-controlled four-point bending test results of 5% cement specimens under haversine load and different strain levels (Stage 1)

Table 5.1 provides information on the four-point bending test parameters and test results in the first stage. Note that specimens F-1, F-2, F-3, F-5, F-15, F-16, F-17, and F-18 were prepared and tested prior to the other specimens (1st batch).

Table 5.1: Four-point bending test parameters and test results of Stage 1

Specimen ID	Cement Content (%)	Specimen Dimension (mm)		Test Controlled Mode/Applied Loading Waveform	Applied Stress/Strain Level	Cyclic Flexural Modulus (MPa)		No. of Tested Cycle (Cycles)
		Width	Depth			Initial[a]	Final[b]	
Sub-stage 1: Haversine loading waveform under strain-controlled test								
F-1	5	63.95	49.72	Strain/Haversine	50 με	20,500	21,966	1,000,000
F-2	5	58.30	49.30	Strain/Haversine	100 με	20,407	20,733	1,000,000
F-3	5	62.10	49.00	Strain/Haversine	150 με	14,721	12,155	1,000,000
F-4	5	63.34	49.41	Strain/Haversine	150 με	8,244	4,698	1,000,000
F-5	5	63.40	45.40	Strain/Haversine	200 με	22,510	11,797	1,000,000
Sub-stage 1: Sinusoidal loading waveform under strain-controlled test								
F-6	5	62.52	48.78	Strain/Sinusoidal	75 με	9,982	8,716	1,000,000
F-7	5	62.25	48.47	Strain/Sinusoidal	100 με	12,308	10,934	1,000,000
F-8	5	62.66	49.68	Strain/Sinusoidal	150 με	9,737	4,970	1,000,000
F-9	5	61.67	48.62	Strain/Sinusoidal	175 με	11,097	5,547	18,889
F-10	5	61.21	47.13	Strain/Sinusoidal	200 με	7,818	3,909	3,941
Sub-stage 2: Sinusoidal loading waveform under stress-controlled test								
F-11	5	61.87	49.93	Stress/Sinusoidal	800 kPa	9,573	9,724	1,000,000
F-12	5	62.62	49.33	Stress/Sinusoidal	1,000 kPa	14,882	14,913	1,000,000
F-13	5	62.62	49.69	Stress/Sinusoidal	1,000 kPa	13,916	12,028	1,000,000
F-14	5	62.32	49.02	Stress/Sinusoidal	1,500 kPa	13,690	5,574	350
Sub-stage 1 and 2: Haversine loading waveform under strain-controlled test								
F-15	3	63.60	50.10	Strain/Haversine	50 με	12,579	13,504	1,000,000
F-16	3	64.60	48.90	Strain/Haversine	100 με	9,617	8,051	1,000,000
F-17	3	63.20	49.60	Strain/Haversine	150 με	5,687	4,668	1,000,000
F-18	3	62.90	50.20	Strain/Haversine	200 με	1,985	1,740	1,000,000
Sub-stage 2: Haversine loading waveform under strain-controlled test								
F-19	7.5	62.77	50.04	Strain/Haversine	150 με	9,949	4,968	1,000,000[c]
F-20	7.5	62.80	49.36	Strain/Haversine	150 με	7,492	4,927	1,000,000
F-21	7.5	63.33	49.51	Strain/Haversine	150 με	10,339	5,167	1,000,000[d]
F-22	10	62.59	49.84	Strain/Haversine	150 με	15,075	11,434	1,000,000
F-23	10	61.76	49.88	Strain/Haversine	150 με	13,224	7,369	1,000,000
F-24	10	61.94	49.13	Strain/Haversine	150 με	13,349	11,492	1,000,000

a = Cyclic flexural modulus averaged from the loading cycle number 50 to 100

b = Cyclic flexural modulus measured at the last loading cycle

c = Number of cycles to 50% of the initial value was 49,660

d = Number of cycles to 50% of the initial value was 82,856

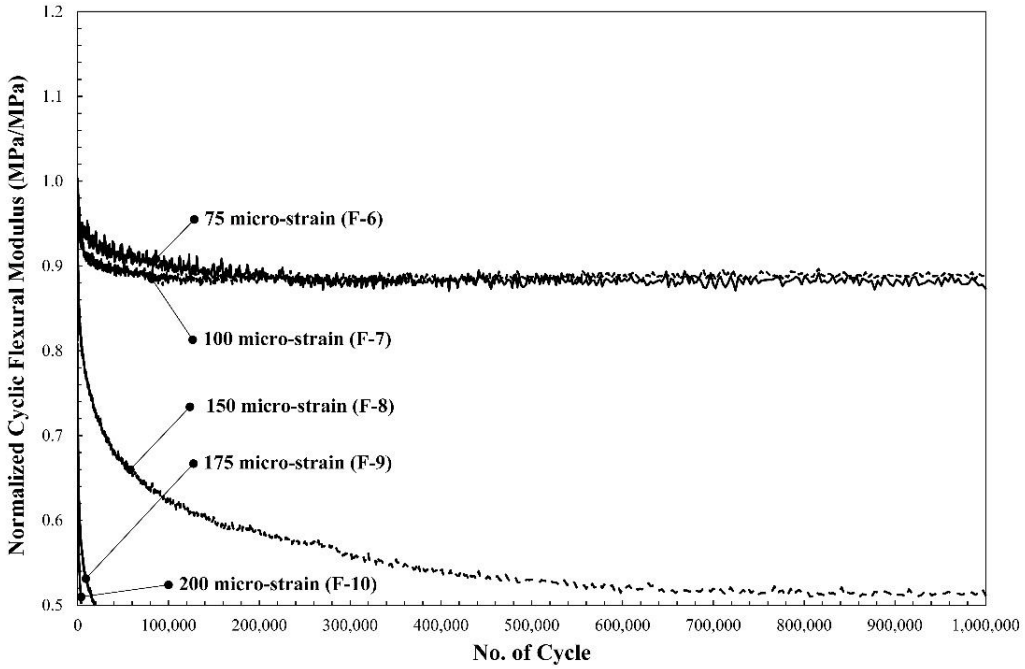

Figure 5.5: Strain-controlled four-point bending test results of 5% cement specimens under sinusoidal load and different strain levels (Stage 1)

In Figures 5.4 and 5.5, the normalised cyclic flexural modulus is defined as the ratio between the cyclic flexural modulus measured at a specified loading cycle and the initial cyclic flexural modulus. According to AG:PT/T233 (Austroads, 2006a), the test specimen is considered as a failed specimen with fatigue damage if the cyclic flexural modulus is reduced by one-half of the initial value. Therefore, the maximum and minimum values of normalised cyclic flexural modulus are 1.0 and 0.5, respectively. The fatigue test results revealed that the CTB specimens show fatigue characteristics (i.e., more cyclic flexural modulus reduction with more loading cycles) when they are tested by sinusoidal and haversine loads under the strain-controlled mode. Furthermore, Figures 5.4 and 5.5 show that the fatigue behaviour, represented by the fatigue curves from the tests, of the CTB specimens is significantly influenced by the applied strain level. Different fatigue curves corresponding to different applied strain levels can be observed. Table 5.1 shows that the final cyclic flexural modulus values of specimens F-1, F-2, F-6, and F-7 are reduced by less than 15% of the initial value. Moreover, the cyclic flexural modulus values of these specimens were not dropped further after the cyclic load was applied by 150,000 to 200,000 cycles. Therefore, it should be highlighted that from the results of this particular research, the CTB

specimens subjected to applied strain levels less than or equal to 100 $\mu\varepsilon$ are likely to have minor damage induced by repeated sinusoidal and haversine loads. In contrast, the cyclic flexural modulus of specimens F-4, F-5, F-8, F-9, and F-10 were markedly influenced by the cyclic load. In the case of the cyclic load with an applied strain level of 150 $\mu\varepsilon$ (specimens F-4 and F-8), the cyclic flexural modulus values of the specimens under such a condition were reduced by approximately 50% of their initial values at the one millionth cycle. For strain levels greater than or equal to 175 $\mu\varepsilon$, the cyclic flexural moduli of the test specimens were dropped by one-half of the initial value within the early cycles of loading. According to the test results at this stage, repeated sinusoidal and haversine loads with a strain level greater than 150 $\mu\varepsilon$ created significant fatigue damage to the CTB specimens. However, this does not conform with specimens F-3 and F-5, where the results of the cyclic load with applied constant strain levels equal to 150 $\mu\varepsilon$ (F-3) and 200 $\mu\varepsilon$ (F-5) led to a reduction in the cyclic flexural modulus by less than 50%. Based on the information illustrated in Table 5.1, the high initial cyclic flexural modulus of specimens F-3 and F-5 may be the cause of a slight reduction in the cyclic flexural modulus. A similar finding is encountered in the four-point bending test of specimens with higher cement content (F-22, F-23, and F-24).

Some levels of stress or strain that are repeatedly applied under cyclic conditions to pavement materials, for an assigned number of loading cycles, and cause no bottom-up fatigue damage can be defined as "*the fatigue endurance limit*" (Prowell et al., 2010). The concept of the fatigue endurance limit was formally proposed for metal by Wohler in 1870 (Witczak, Mamlouk, Souliman, & Zeiada, 2013). It was later applied to the perpetual pavement design concept for flexural pavement in the early 2000's (Portillo, 2008). Witczak et al. (2013) defined the concept of the perpetual pavement as a designed and built pavement that could last longer than the designed lifetime of road structure, without requirements in major rehabilitation and reconstruction. Additional literature and basic knowledge on the perpetual pavement design can be found in Portillo (2008) and Witczak et al. (2013). For concrete pavement, Huang (2004) stated that fatigue damage in concrete pavement can be disregarded if the applied stress levels from vehicles are maintained at 45% of flexural strength of concrete and lower. The aforementioned concrete pavement is a conventional road

structure paved by concrete. Figure 5.6 shows the relationship between applied strain levels and fatigue life (i.e., at a 50% reduction of the cyclic flexural modulus compared to the initial value) of the CTB specimens in the first stage of fatigue investigation. Figure 5.6 indicates that the CTB specimens with 5% cement content did not fail from cyclic loading with an applied strain level of 150 $\mu\varepsilon$ under less than one million cycles. According to Austroads (2014a), the number of load repetitions throughout the design life of road pavement with a CTB layer can be calculated from Eq. 5.3.

$$N = RF\left[\frac{SFxk}{\mu\varepsilon_t}\right]^{12} = RF(SF)^{12}\left[\frac{k}{\mu\varepsilon_t}\right]^{12} \tag{5.3}$$

in which, N is the design number of load repetitions in the field, RF is the reliability factor (equal to 1 for project reliability equal to 95%), $\mu\varepsilon_t$ is the load-induced tensile strain at the base of the CTB layer (micro-strain), SF is the laboratory-to-field shift factor, and k is the fatigue constant obtained from four-point bending test data. Based on Austroads (2014a), the presumptive value of 1.8 is recommended for SF. Consequently, the design number of load repetitions in the field can be determined by multiplying the number of load repetitions acquired from the four-point bending tests by 1,150 (or 1.8^{12}). This means that one million cycles of the cyclic load from the four-point bending tests are equivalent to $1.15\text{x}10^9$ load repetitions in the field. If traffic estimation assumptions and procedures in Appendix H of Austroads (2010b) are applied to this research, $1.15\text{x}10^9$ cycles is approximately equal to the number of load repetitions in an 80-year period on the road structure. It should be noted that the number of load repetitions calculated earlier is based on Annual Averaged Daily Traffic (AADT) and a Cumulative Growth Factor (CGF) equal to 5,350 vehicles per year, and 4% were presumed in the calculation, respectively. Therefore, a CTB layer with 5% cement in the field, under cyclic load-induced tensile strain equal to 150 $\mu\varepsilon$ and less, may succumb to fatigue failure after up to 80 years based on given conditions. However, this conclusion was established from a limited number of test results. The four-point bending tests in this investigation stage only revealed the existence of a fatigue endurance limit; further verification is required for an endurance limit determination of the CTB material in road pavement design.

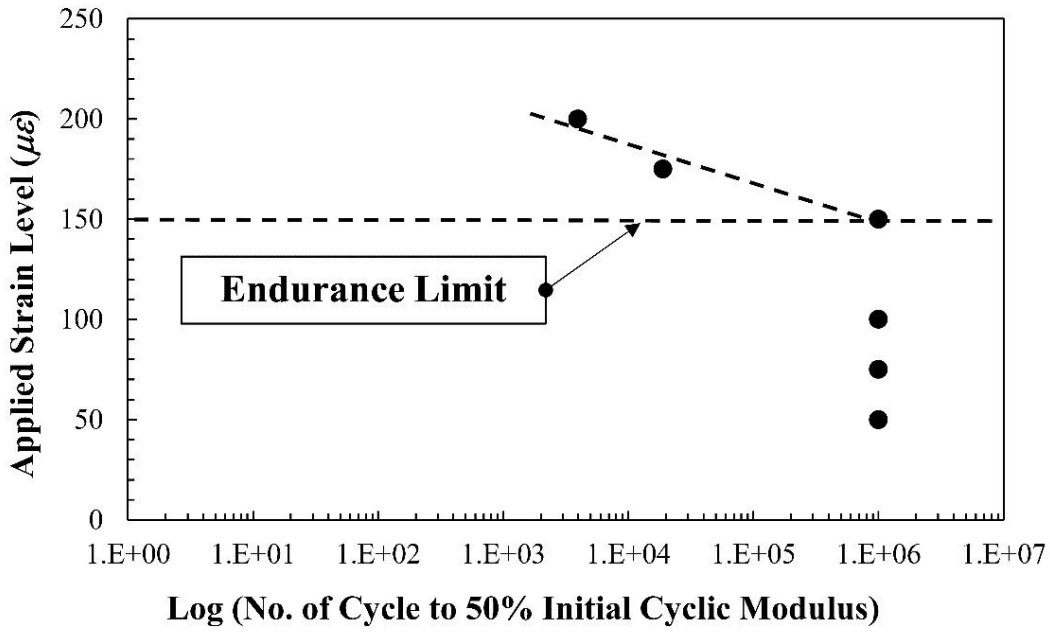

Figure 5.6: Proposed fatigue endurance limit of 5% cement specimens (Stage 1)

The four-point bending tests of 3% cement specimens under different applied strain levels were also performed in this investigation stage (see Table 5.1). These included specimens F-15, F-16, F-17, and F-18. However, high variations in the initial cyclic flexural modulus were observed, which may influence the fatigue life measurement in the four-point bending test. Inconsistency in the cyclic initial flexural modulus of these specimens with the same cement content indicates that the specimen preparation process has relevant effects on four-point bending test results, especially with specimens with relatively low cement content. Cracks would occur (i.e., more likely for relatively low cement content specimens) during specimen preparation. The process of cutting and handling would be the main reason for considerable fluctuations in the initial cyclic flexural modulus. Consequently, the process of alternative specimen preparation for CTB with low cement content should be developed to manipulate the inconsistency in material properties.

Sub-stage 2: Four-point bending test under stress-controlled mode

Eight CTB test specimens were examined in this sub-stage under a sinusoidal loading waveform and stress-controlled mode. However, only four tests were successful. The other half of the specimens failed mostly in the very early stages of the test. This could be explained by the fact that CTB is too brittle or fragile to withstand test condition

under the stress-controlled mode. Relatively low excessive stress levels may cause immediate damage to the prismatic beam specimens. Accordingly, only the details of completed tests are given in this section (Table 5.1 and Figure 5.7). It should be emphasised that the relevant properties of CTB measured from the four-point bending test are typically uncertain (Austroads, 2014b; Walker & Bloem, 1957). Furthermore, determining the appropriate applied stress level for the four-point bending test under the stress-controlled mode by means of the trial-and-error approach is difficult and almost impossible. In contrast, an appropriate applied strain level was potentially determined from the test results in the previous section with the strain-controlled mode. In addition, Austroads (2014b) suggests employing the strain-based equation for the fatigue life estimation of road pavement with a CTB layer for two main reasons. Firstly, the strain-based equation is fitted with the four-point bending test results better than the stress-based equation. Secondly, fatigue data from full-scale tests by the accelerated loading facility (ALF) are more appropriately explained by the strain-based equation. Moreover, the strain-controlled test was recommended for fatigue life estimation of all asphalt pavement types (Prowell et al., 2010).

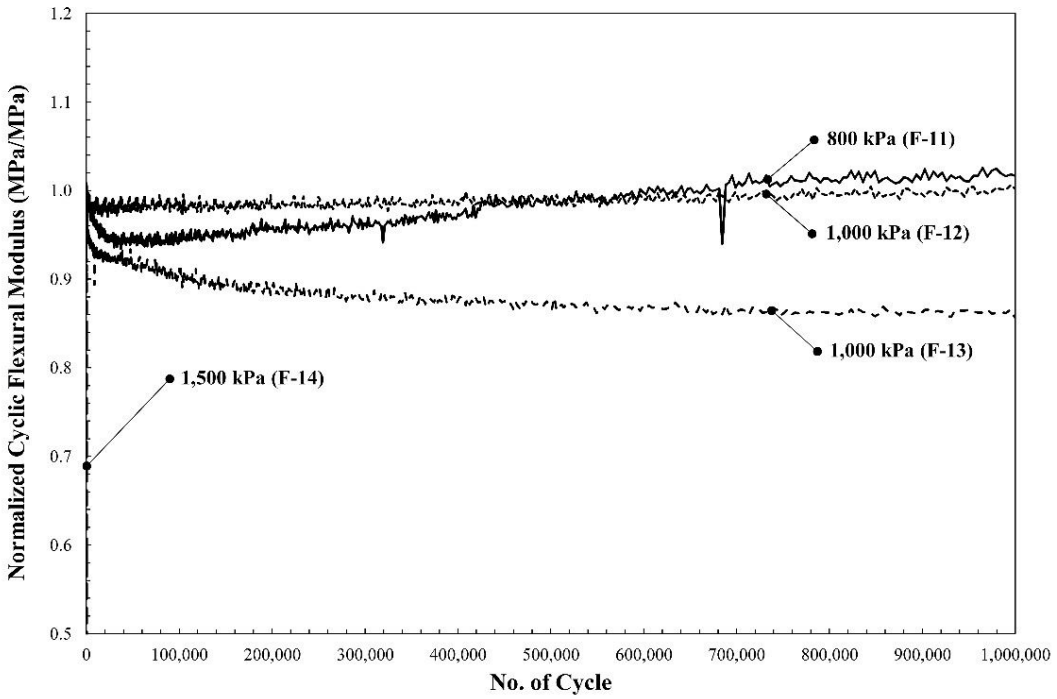

Figure 5.7: Stress-controlled four-point bending test results of 5% cement specimens under sinusoidal load and different stress levels (Stage 1)

Based on the test results shown in Figure 5.7, applied sinusoidal load with stress levels equal to 800 kPa, 1,000 kPa, and 1,500 kPa are equivalent to 52%, 65%, and 98% of the CTB flexural strength (see Table 5.1). The maximum tensile strains of a test beam at the top and the bottom for applied stresses of 800 kPa, 1,000 kPa, and 1,500 kPa were approximately equal to 75 $\mu\varepsilon$, 80 $\mu\varepsilon$, and 100 $\mu\varepsilon$, respectively. According to the four-point bending test guidelines (Austroads, 2014a), applied force within the range of 60% to 90% of the ultimate load (*FS*) is recommended for the fatigue life measurement of CTB. The guidelines recommend that a loading range that is equivalent to applied strain levels varying from 50 $\mu\varepsilon$ to 120 $\mu\varepsilon$ should be employed in the fatigue testing of CTB materials. However, this strain range created only minor damage to the CTB specimens in the first stage of the investigation (see Figures 5.4 and 5.5). This is because the specimen size, test configuration, and load configuration recommended by Austroads (2014a) are different from those for the four-point bending test conducted in this stage. Therefore, the four-point bending tests in accordance with Austroads (2014a) were performed in the second stage of this research. Results from the first stage revealed that an appropriate stress level for the four-point bending test under the stress-controlled mode cannot be correlated with any applied strain levels in the strain-controlled tests.

Sub-stage 2: The effects of cement content on fatigue characteristics of CTB specimens

In the second sub-stage, the effects of the cement content on the fatigue characteristics of the CTB specimens were examined. Test results from the previous sections indicated that a cyclic load with an applied strain level of 150 $\mu\varepsilon$ reduces the cyclic flexural modulus of the CTB specimens by one-half of the initial value within one million cycles of the applied cyclic load (see Figures. 5.4 and 5.5). Therefore, a haversine load with a strain level of 150 $\mu\varepsilon$ was applied to all tests in this sub-stage. Figure 5.8 shows the results of the strain-controlled four-point bending test of CTB specimens with varying cement content. It should be emphasised that the cyclic flexural moduli of CTB specimens measured in this sub-stage were allowed to reduce to more than one-half of the initial value to investigate the completed modulus-reduction curves. Therefore, the four-point bending tests at this sub-stage were terminated at one million cycles without considering the modulus reduction criteria at 50% of the initial value. Besides the uncertainty of the four-point bending test results,

it can be seen clearly from Figure 5.8 that cement content affects the fatigue characteristics of CTB specimens. The 10% cement specimens showed a lesser tendency to fail by cyclic load compared to the specimens with 5% and 7.5% cement content. In this sub-stage, specimens with differing cement content were tested under the same strain level (150 $\mu\varepsilon$), and in the strain-controlled condition. This means that specimens with higher cement content (higher strength) were subjected to a lower initial stress ratio (ratio between applied peak stress and flexural strength) compared to the specimens with lower cement content or lower strength. Similar to concrete material, an applied lower initial stress ratio in the beam fatigue test leads to a longer fatigue life in a test specimen than the fatigue life of a specimen subjected to higher initial stress ratio (Destrebecq, 2010). It also indicates that based on the test conditions of this research, a specimen with a higher initial cyclic flexural modulus has a higher fatigue failure resistance than that of a specimen with a lower initial cyclic flexural modulus. This finding also supports the hypothesis established in the first sub-stage of this investigation. Consequently, a suitable applied strain level for the four-point bending test should be increased with respect to the level of the initial cyclic flexural modulus and cement content of the test specimens.

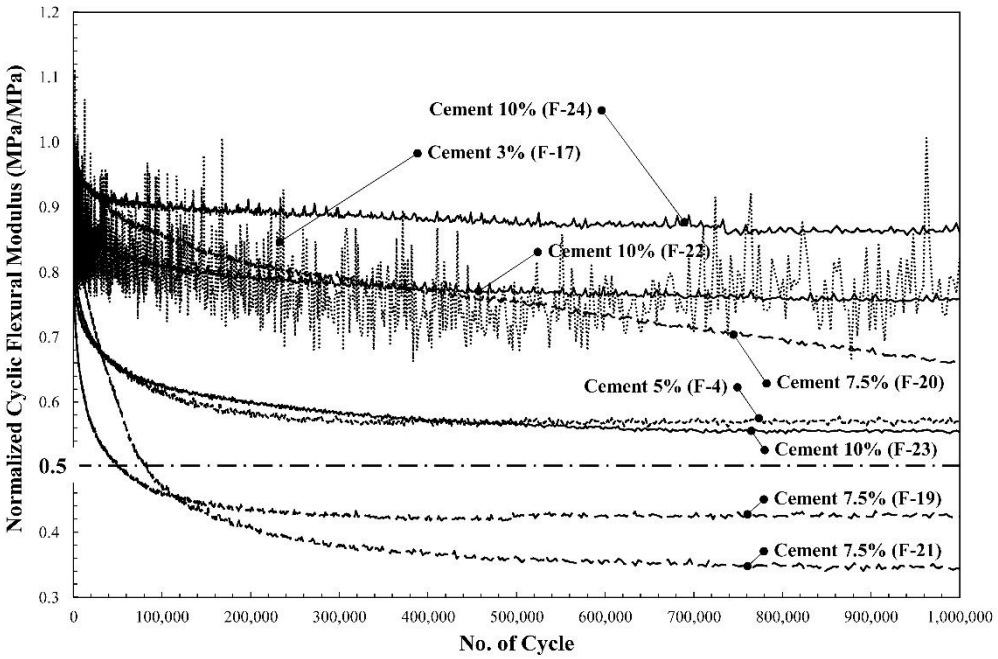

Figure 5.8: Strain-controlled four-point bending test results of CTB specimens under haversine load with strain level equal to 150 $\mu\varepsilon$ (Stage 1)

5.3.2 Fatigue life measurement from Stage 2

The fatigue behaviour of CTB in the second stage was investigated based on Austroads (2014a). The influences of testing mode, applied strain level, applied stress level, and cement content were examined again at this stage. These repeated investigations were performed to explore the effects of testing and loading configurations, which differed between the test set-up performed in the first stage and second stage. The fatigue test results obtained from the second stage are summarised in this section as follows.

Sub-stage 1: The effects of applied stress level under stress-controlled mode

Similar to the first stage, the CTB specimens with 5% cement content were examined in the first sub-stage of the investigation. The CTB specimens were tested using a 2-Hz haversine load until they failed from the applied cyclic loads. Various applied stress levels, varying from 60% to 90% of *FS*, were applied to the specimens during the stress-controlled tests. The fatigue test results obtained from the stress-controlled four-point bending test of 5% cement specimens are presented in Figure 5.9. Table 5.2 summarises the test parameters and test results in the second stage of this research.

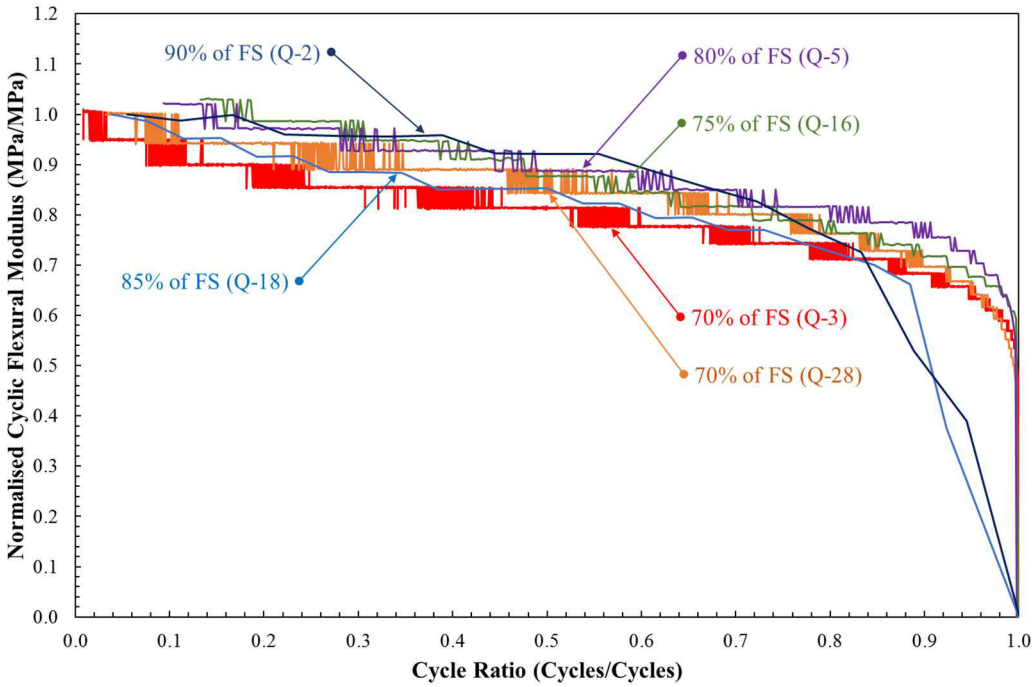

Figure 5.9: Stress-controlled four-point bending test results of 5% cement specimens under haversine load and different stress levels (Stage 2)

Table 5.2: Four-point bending test parameters and test results of Stage 2

Specimen ID	Cement Content (%)	Curing Duration (Days)	Testing Frequency (Hz)	Test Controlled Mode	Applied Stress/Strain Level	Equivalent Initial Stress/Strain[a] (kPa/με)	Applied Stress Ratio[b]	Initial Cyclic Flexural Modulus[c] (MPa)	Final Cyclic Flexural Modulus (MPa)	No. of Tested Cycle (Cycles)
Sub-stage 1: Effects of testing mode, applied stress, and applied strain level										
Q-1*	5	27	2	Stress	1,520 kPa	65 με	0.60	23,546	23,185	84,792
Q-2	5	28	2	Stress	2,270 kPa	118 με	0.90	18,507	N.A.	18
Q-3	5	26	2	Stress	1,780 kPa	90 με	0.70	20,054	N.A.	6,016
Q-4*	5	28	2	Stress	1,520 kPa	76 με	0.60	19,776	19,626	165,805
Q-5	5	25	2	Stress	2,020 kPa	103 με	0.80	19,240	N.A.	532
Q-16	5	27	2	Stress	1,900 kPa	117 με	0.75	15,623	N.A.	377
Q-17*	5	27	2	Stress	1,640 kPa	79 με	0.65	20,313	13,369	92,632
Q-18	5	28	2	Stress	2,140 kPa	117 με	0.85	17,652	N.A.	26
Q-28	5	28	2	Stress	1,770 kPa	81 με	0.70	21,735	N.A.	1,551
Q-6	5	26	2	Strain	98 με	2,050 kPa	0.81	21,434	18,527	22,647
Q-7	5	29	2	Strain	128 με	2,390 kPa	0.95	21,030	5,126	441
Q-8	5	26	2	Strain	99 με	1,900 kPa	0.75	21,284	26,234	301
Q-11	5	29	2	Strain	82 με	1,400 kPa	0.55	19,357	11,000	70,331
Q-12	5	27	2	Strain	114 με	1,840 kPa	0.73	17,344	14,376	165,131
Q-13	5	29	2	Strain	123 με	1,520 kPa	0.60	19,023	9,752	144,271
Sub-stage 2: Effects of loading frequency										
Q-9	5	29	4	Stress	1,780 kPa	77 με	0.70	22,990	N.A.	132,023
Q-10	5	27	10	Stress	1,780 kPa	90 με	0.70	19,732	N.A.	93,011
Q-14*	5	29	4	Stress	1,780 kPa	83 με	0.70	21,494	19,125	20,541
Q-15	5	29	4	Stress	1,780 kPa	87 με	0.70	20,467	N.A.	8,321
Sub-stage 3: Effects of cement content										
Q-20	4	28	2	Stress	1,490 kPa	89 με	0.75	16,320	N.A.	1,486
Q-21	4	27	2	Stress	1,290 kPa	83 με	0.65	15,357	N.A.	1,001
Q-22*	4	26	2	Stress	1,090 kPa	57 με	0.55	19,037	14,082	195,597
Q-23	4	28	2	Stress	1,690 kPa	N.A.	0.85	N.A.	N.A.	10
Q-24	6	27	2	Stress	2,140 kPa	118 με	0.75	19,208	N.A.	32
Q-25	6	27	2	Stress	2,350 kPa	134 με	0.82	17,544	N.A.	17
Q-26	6	27	2	Stress	1,860 kPa	89 με	0.65	20,495	N.A.	17,879
Q-27	6	28	2	Stress	2,000 kPa	81 με	0.70	24,593	N.A.	19,899

a = Stress or strain values averaged from the cycle number 50 to number 100

b = Applied stress or equivalent initial stress divided by flexural strength

c = Cyclic flexural modulus averaged from the cycle number 50 to number 100

N.A. = Not available

In Figure 5.9, the changes in normalised cyclic flexural moduli of test specimens were plotted against the cycle ratio in the x-axis. The cycle ratio is defined as the ratio between the number of current loading cycles and the number of final loading cycles. The cycle ratio was chosen instead of the number of loading cycles for analysis purposes, due to the CTB specimens tested at this stage being broken at different loading cycles. Therefore, the comparison between fatigue development lines obtained from different specimens could be explicitly achieved by plotting the changes in specimen's modulus against the cycle ratio. Specimen numbers Q-1, Q-4, and Q-17 were excluded from the plot in Figure 5.9. This is because the aforementioned specimens did not fail within 200,000 cycles of applied cyclic loads. At this second stage, the number of loading cycles equivalent to 200,000 cycles was chosen as the termination criteria based on the test results from the first stage of the fatigue investigation. Figure 5.8 indicates that the cyclic flexural moduli of test specimens were not reduced further after 200,000 cycles of applied cyclic loads. It can be observed from Table 5.2 that the modulus of specimens Q-1 and Q-4 reduced by less than 2% of their initial values at the end of the four-point bending test. Similarly, the cyclic flexural modulus of specimen Q-17 at the end of the test dropped by approximately 34% of the initial value. It means that the normalised cyclic flexural moduli of these three specimens remained unchanged after a certain number of cyclic loads were applied to the test specimens. On the other hand, the cyclic flexural modulus of specimens Q-2, Q-3, Q-5, Q-16, Q-18, and Q-28 reduced to 50% to 60% of their initial values before the specimens were completely broken by the applied cyclic loads.

Figure 5.10 illustrates the relationship between the applied stress ratio and the number of loading cycles to failure acquired from the fatigue tests at this stage. The applied stress ratio is the ratio between the maximum tensile stress and the flexural strength (see Table 3.5). It can be seen from Figure 5.10 that an increase in the applied stress ratio usually led to a reduction in the number of loading cycles to failure. It also means that the fatigue life of the specimens subjected to a low stress ratio is usually higher than the fatigue life of specimens tested with a high stress ratio. However, the test results indicate that fatigue failure was unobserved from the specimens tested with an applied stress ratio lower than 0.65 (within 200,000 cycles of cyclic loading). A stress ratio higher than 0.60 was recommended in various literature as a suitable level of

applied stress for the fatigue life determination of CTB (Austroads, 2014a; Shahid, 1997). Accordingly, the applied stress levels of 60% to 65% of *FS* may be considered as the endurance limit of 5% cement specimens tested in this second stage. However, this limit requires further verification in the future with additional fatigue test results.

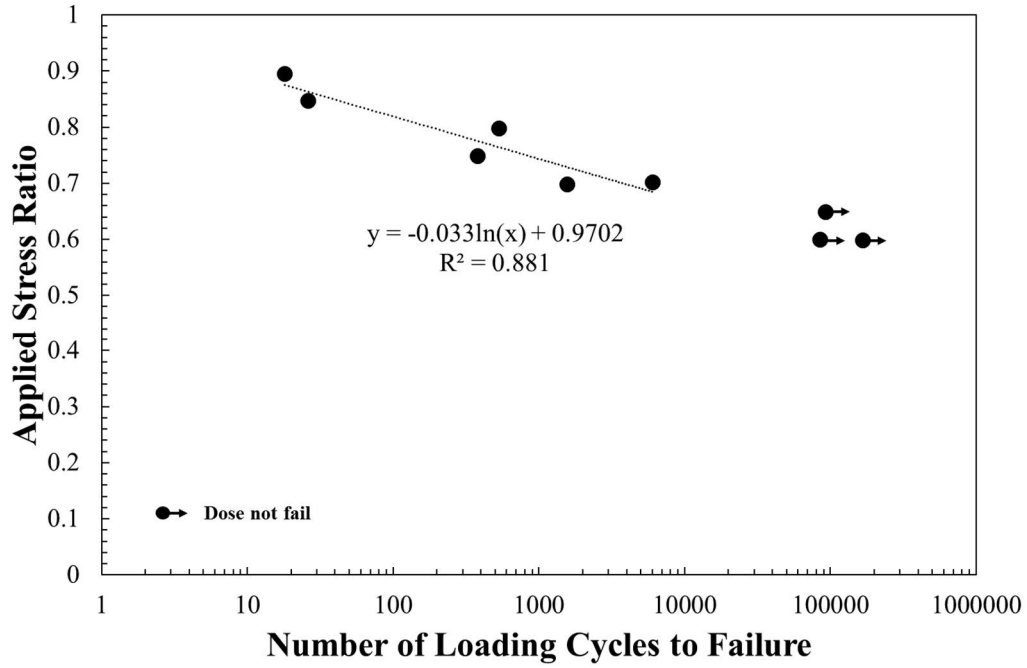

Figure 5.10: Relationship between applied stress ratio and number of loading cycle to failure of 5% cement specimens (Stage 2)

Sub-stage 1: Four-point bending test under strain-controlled mode

An applied tensile strain level varying between 80 $\mu\varepsilon$ and 130 $\mu\varepsilon$ was employed in the strain-controlled fatigue test at this second stage. This applied strain level is equivalent to an applied stress ratio varying from 0.55 to 0.95. Figure 5.11 displays the strain-controlled fatigue test results of CTB specimens with 5% cement content. It can be seen from the figure that the cyclic flexural modulus of specimens Q-11 and Q-13 reduced by approximately 50% of their initial values in the early stage of testing, while the cyclic flexural modulus of specimens Q-7 dropped by 75% of the initial value. On the other hand, specimens Q-6 and Q-12 seem to be secured from failure by the cyclic loads. This is because the cyclic flexural modulus of specimens Q-6 and Q-12 was reduced by only 10% of the initial value. It should be highlighted that the CTB's modulus reduction shown in Figure 5.11 behaved similarly according to the results

obtained from the strain-controlled fatigue tests at the first stage (see Figure 5.4). Unlike the fatigue results obtained from the stress-controlled tests, an explicit fatigue failure could not be observed from the strain-controlled fatigue tests performed in this stage. This is because the applied displacement of the loading actuator (see Figure 4.3) was maintained throughout the strain-controlled test, when the cyclic flexural moduli of test specimens reached their minimum values. However, a correlation between the applied strain level and the number of loading cycles to failure, such as shown in Figures 5.6 and 5.10, could not be established from the strain-controlled fatigue test results. Verification of the fatigue test results obtained from the strain-controlled test is presented in Figure 5.12.

Figure 5.12 demonstrates that the loading actuator maintained the levels of applied stress during the stress-controlled tests better than the levels of applied strain during the strain-controlled tests. Therefore, the target applied stresses shown in Figure 5.12a were consistently controlled by the testing machine throughout the fatigue test. On the contrary, the applied strain levels aimed for in the strain-controlled fatigue tests fluctuated greatly (see Figure 5.12b). Accordingly, variations in the fatigue test result were generated during the strain-controlled fatigue tests at this stage. Fluctuations in targeted strain during the strain-controlled test were also observed during the cyclic flexural modulus measurement (see Chapter 4). Consequently, only the stress-controlled fatigue test was employed in Sub-stage 2 and 3 of the second stage in this research.

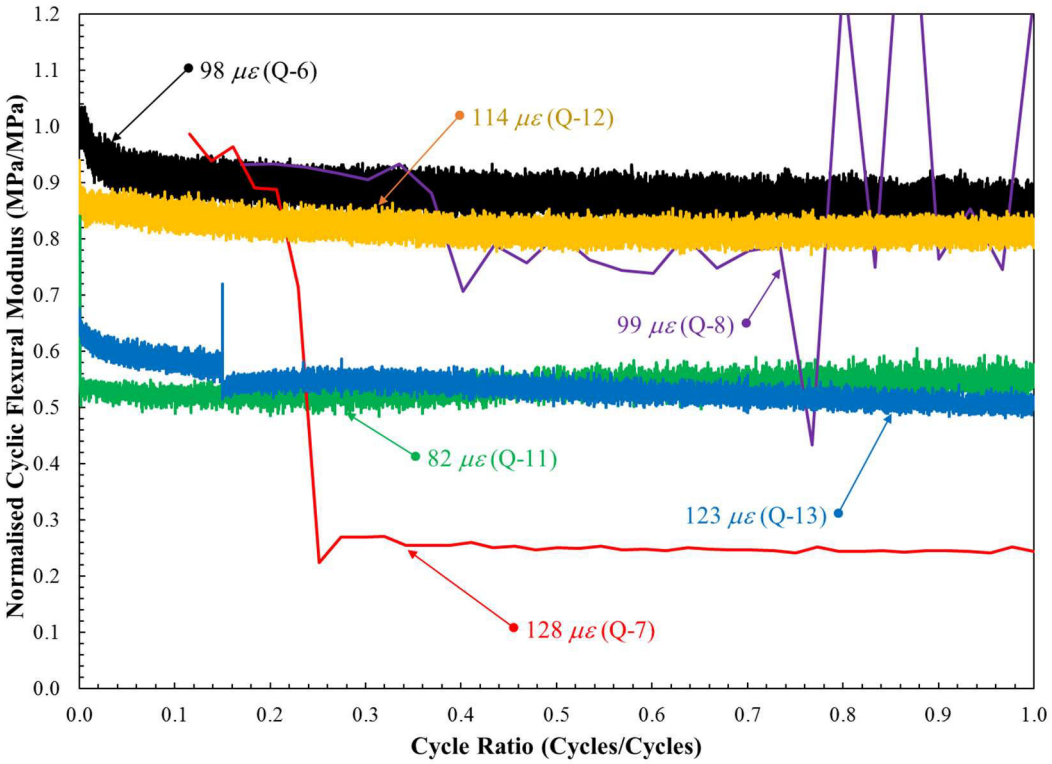

Figure 5.11: Strain-controlled four-point bending test results of 5% cement specimens under haversine load and different strain levels (Stage 2)

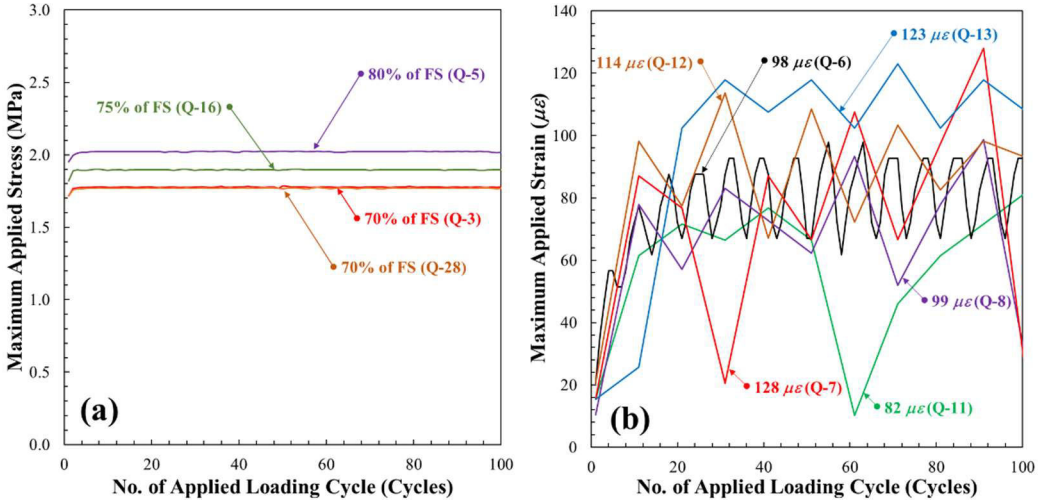

Figure 5.12: Test results from the first-hundred cycles of applied load under (a) stress-controlled mode, and (b) strain-controlled mode (Stage 2)

Sub-stage 2: The effects of loading frequency

The stress-controlled fatigue tests with two additional loading frequencies were employed in Sub-stage 2. The main aim of this sub-stage was to investigate the effects of loading frequency on the fatigue characteristics of CTB. Four additional specimens with 5% cement content were employed in this sub-stage, as detailed in Table 5.2. With concrete material, the effects of loading frequency on the fatigue response have been examined by various researchers for more than a decade (ACI Committee 215, 1974; Destrebecq, 2010; Sparks & Menzies, 1973; B. Zhang, Phillips, & Wu, 1996). B. Zhang et al. (1996) determined the frequency influence coefficient (C_f) and implemented it in the well-known fatigue life prediction equation for concrete material, which is Aas-Jakobsen's formula. The fatigue life prediction equation developed by B. Zhang et al. (1996) is illustrated in Eq. 5.4.

$$\frac{S_{max}}{FS} = C_f[1 - (1 - R)\beta logN] \tag{5.4}$$

in which, R is the ratio between minimum and maximum stress ($\sigma_{min}/\sigma_{max}$), β is the material parameter (0.0685 for concrete material), and N is the fatigue life or number of loading cycles to failure. The value of C_f can be estimated from Eq. 5.5.

$$C_f = ab^{-logf} + c \tag{5.5}$$

in which, a, b, and c are material parameters, and f is the loading frequency in Hz. According to Austroads (2014a), the input parameters for CTB fatigue life prediction are recommended to be used to estimate fatigue life ranging from between 10^4 cycles and 10^5 cycles. Based on the test results shown in Figure 5.10, an expected fatigue life varying from 10^4 cycles to 10^5 cycles was observed from the CTB specimens tested under the applied stress ratio varying from 0.65 to 0.70. Therefore, an applied stress ratio equal to 0.70 was employed for every fatigue test in this sub-stage. Figure 5.13 demonstrates the relationship between applied loading frequency and number of loading cycles to failure of 5% cement specimens. The 5% cement specimens tested in Sub-stage 1 with a loading frequency of 2 Hz (specimens Q-3 and Q-28) were also included in Figure 5.13 to produce the regression line. Figure 5.13 shows that the fatigue life of CTB tends to increase with the rise in the applied loading frequency. In

short summary, the results obtained from this research indicate that the applied loading frequency influences the fatigue life of CTB materials.

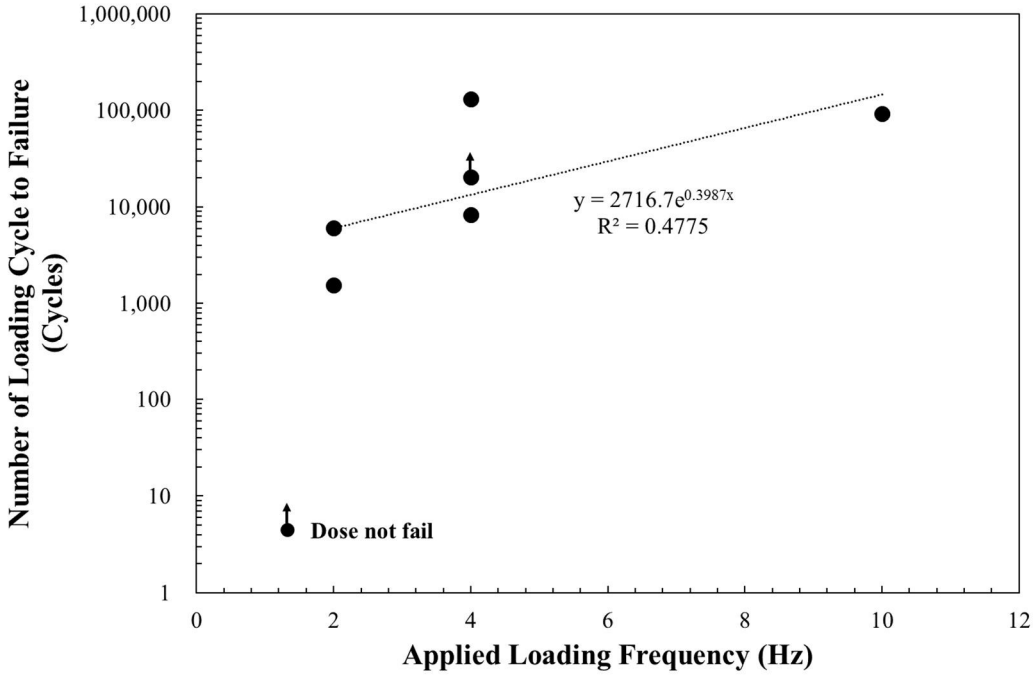

Figure 5.13: Relationship between loading frequency and number of cycles to failure of 5% cement specimens (Stage 2)

Sub-stage 3: The effects of cement content

In the third sub-stage, the effects of cement content on the fatigue characteristics of CTB were examined using additional results from the stress-controlled fatigue tests. Four specimens with 4% cement content and four specimens with 6% cement content were subjected to 2-Hz haversine loads during the fatigue tests. The test parameters and fatigue test results of this sub-stage are also summarised in Table 5.2. The test results in Chapter 3 indicate that the flexural strength of CTB specimens increased with respect to the cement content (see Table 3.5). To compare the fatigue life of CTB specimens with different cement content, the applied cyclic stress was normalised by the value of *FS* and plotted against the number of loading cycles to failure, as shown in Figure 5.14. This normalised value is defined as the applied stress ratio in this research. The fatigue life of CTB determined in Sub-stages 1 and 3 are included in Figure 5.14. It can be seen from Figure 5.14 that the applied stress ratio was reasonably correlated with the number of loading cycles to failure (R^2 = 0.7). The endurance limit

of 4% cement specimens (0.50) seem to be lower than the limit of 5% cement specimens (0.65). However, it can be seen from Figure 5.14 that a minimum applied stress ratio equivalent to 0.65 is needed in order to obtain reasonable values for CTB's fatigue life from the four-point bending test.

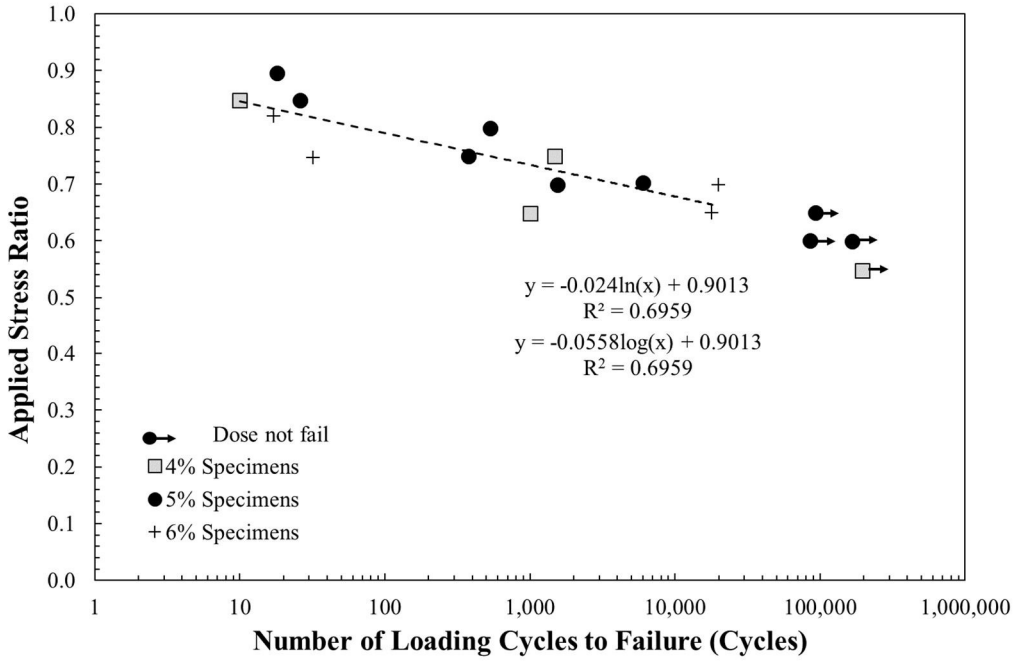

Figure 5.14: Relationship between applied stress ratio and number of loading cycles to failure of 4%, 5%, and 6% cement specimens (Stage 2)

Fatigue life estimation equations

According to Aas-Jacobsen's formula illustrated in Eq. 5.4, the relationship curve between applied stress ratio and the value of $(1-R)log$ is illustrated in Figure 5.15. In this research, the minimum applied stress (σ_{min}) was maintained at 100 kPa for every stress-controlled fatigue test. Therefore, the values of R were varied between 0.05 and 0.07. By assuming the value of C_f as equivalent to one, the value of β determined by the regression analysis was 0.0932. The β value determined in this research was considerably higher than the value recommended for concrete material. However, additional fatigue test results are required for confirmation of the β value estimated in this research.

The test results from this research were also used to calibrate the fatigue life estimation equations recommended by various road pavement design guidelines. Table 5.3 shows the calibration results using the fatigue life of 4%, 5%, and 6% cement specimens tested according to Austroads (2014a). In the US, Wen et al. (2014) recommended the value of $k_2 = 0.85$ and $k_3 = 0.03$ to be employed for the fatigue life prediction of cement stabilised gravel with 5% cement content. It should be emphasised that the four-point bending test was also used to characterise the fatigue behaviour of cement stabilised material in a study by Wen et al. (2014). The recommended values of k_2 and k_3 are very close to the values determined from the fatigue test results in this research. For the Australian fatigue life prediction equation, the exponent number (e) of 12 is recommended by Austroads (Austroads, 2010b, 2014a). However, an exponent number equal to six was determined by calibrating the fatigue life estimation equation with the test results from this research.

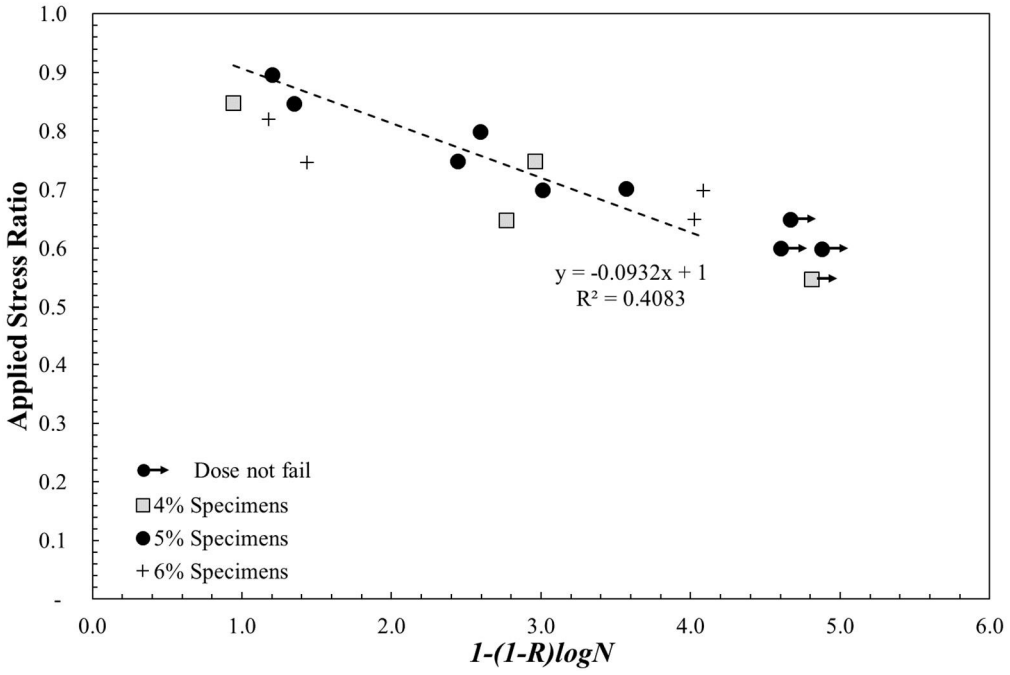

Figure 5.15: Relationship between applied stress ratio and $(1 - R)logN$ for estimating the β value

5.3.3 Discussion of fatigue test results

In this section, the fatigue behaviours of the CTB materials characterised in this research were compared. Although the fatigue behaviour of CTB in both stages was examined from the four-point bending test results, the test configurations employed in both stages were different. Firstly, the specimens used in the tests in the first stage were smaller than the specimens employed in the tests at second stage. Secondly, the distances between each loading span (L/3 in Figures 5.3 and 2.4) applied in the first and second stage were 118.5 mm and 100 mm, respectively. Thirdly, the loading frequency used in the first stage was 10 Hz, while the loading frequency of 2 Hz was applied in the second stage. It should be highlighted that the test specimens in the first stage were subjected to continuous cyclic loads, but a loading pulse with a rest period was employed in the fatigue tests at the second stage. Finally, the locations of applied cyclic bending force in the first and second stage were at the bottom and top of the beam specimen, respectively. However, the deflection measurements of test specimens in both stages were carried out at the beam top using a single LVDT. The following is the comparison between the results obtained from the fatigue tests in both stages.

Table 5.3: Fatigue life prediction equation and calibration results

Country	Fatigue prediction equation	Input parameters	Reference
France	$\log N = \frac{1}{\beta}\left[\frac{\sigma_t}{FS} - 1\right]$	σ_t = Critical tensile stress FS = Flexural strength $\boldsymbol{\beta}$ **= -0.09** **(R^2 = 0.7)**	LCPC (1997)
United States	$\text{Ln}\, N = k_1\left(\frac{k_2 - \left({}^{\sigma_t}/_{FS}\right)}{k_3}\right)$	σ_t = Critical tensile stress FS = Flexural strength k_1 = Field calibration factors = 1 $\boldsymbol{k_2}$ **= 0.90** $\boldsymbol{k_3}$ **= 0.02** **(R^2 = 0.7)**	Wen et al. (2014)
Australia	$N = RF\left[\frac{{}^{113000}/_{E_{Flex}^{0.804}} + 191}{\varepsilon_t}\right]^e$	ε_t = Critical tensile strain E_{Flex} = Flexural modulus RF = Reliability factor $\boldsymbol{e}$ **= 9** **(R^2 = 0.7)**	Austroads (2010b)

- The strain-controlled test results were satisfactorily obtained from the first stage of fatigue investigation in this research, while the strain-controlled tests in the second stage showed an inconsistent relationship between the applied strain level and the fatigue life of CTB. On the other hand, reasonable fatigue results were obtained from the stress-controlled tests in the second stage. This variation may be caused by the difference in specimen dimension employed in the tests of both investigation stages. Specimens with a thickness of 50 mm were used in the first stage of investigation, while the fatigue tests in the second stage were conducted using 100 mm thick specimens. The findings from this research may well support the design assumptions recommended in the previous literature, namely that: *the strain-controlled test mode is more suitable in representing the loading regime for relatively thin pavements, while an appropriate loading condition for thick pavements can be found from the stress-controlled tests* (Prowell et al., 2010; Rao Tangella, Craus, Deacon, & Monismith, 1990; Tayebali, Deacon, Coplantz, Harvey, & Monismith, 1994). This means that strain-controlled test may be effectively used to examine the fatigue behaviour of 50-mm thick specimens in this research, and the stress-controlled test is suitable for characterising the fatigue response of 100 mm thick specimens. However, an additional analysis and comprehensive testing program are required for the verification of aforementioned assumption. Detailed analysis of the loading mode selection for the asphalt road pavement design can be found in Rao Tangella et al. (1990).

- Figure 5.3 presents CTB's modulus reduction measured from the strain-controlled fatigue test in the first stage. It can be seen from the figure that the CTB's moduli usually reached constant values after one hundred thousand to two hundred thousand cycles of cyclic load were applied. The moduli of most specimens seem to be constant after two hundred thousand cycles of applied load. A constant applied strain magnitude equal to 150 $\mu\varepsilon$ was equivalent to an applied stress ratio of 0.79 for the 5% cement specimen. In the second stage of the fatigue investigation, the controlled-stress test was continued for up to approximately 200,000 cycles (approximately 28 hours), if the test specimens did not fail from the applied cyclic load. However, most of the specimens were broken by the cyclic loads, when the applied stress ratios were greater than

0.65 (see Figure 5.14). The moduli of failed specimens in the second stage usually reduced to 50% to 60% of their initial values prior to failure (see Figure 5.9). This finding supports the fatigue failure assumption applied in the first stage, where the reduction in specimen's modulus to 50% of the initial value was used as the termination criteria for the strain-controlled fatigue test.

- Figure 5.16 compares the fatigue results obtained from the tests in the first stage and second stage with variations in applied strain level. In the figure, the "*equivalent applied strain level"* (averaged values from cycle number 51 to 100) represents the applied strain level employed during the stress-controlled fatigue tests in the second stage (see Table 5.2). It should be emphasised that only the specimens with 5% cement content and cured for approximately 28 days were used in the comparison. The test results obtained from the application of both haversine and sinusoidal loading waveforms in the first stage were used to produce Figure 5.16. Figure 5.16 shows that a higher applied strain level is normally required to fail the small-sized beams within one million cycles of applied load. The comparison curves shown in Figure 5.16 indicate the sign of size effects.

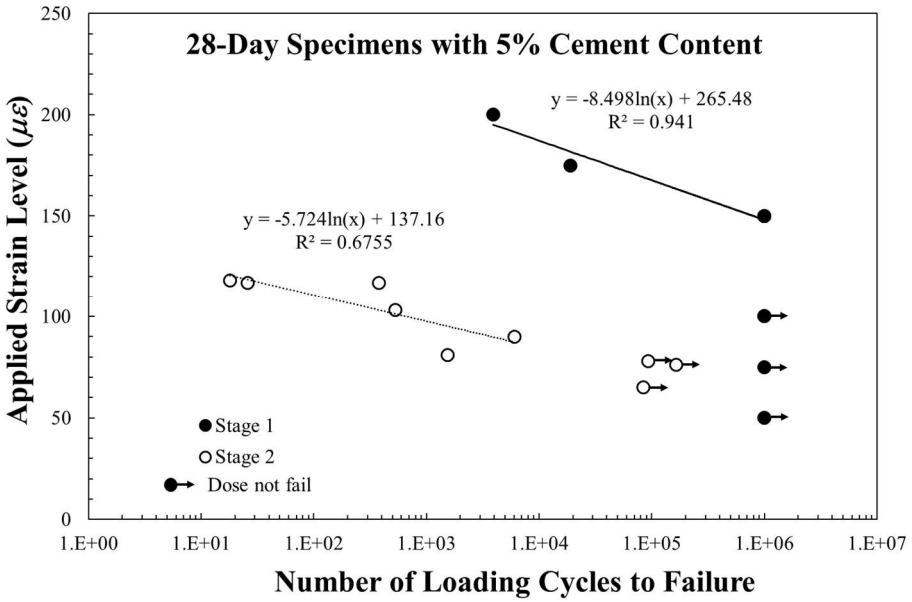

Figure 5.16: Comparison between the fatigue results of 5% cement specimens obtained from the tests in the first and second stages with various applied strain levels

- The relationship between the applied stress ratio and the fatigue life of CTB material obtained from the tests in the first stage and second stage is demonstrated in Figure 5.17. The applied stress ratios of the strain-controlled fatigue tests in the first stage were calculated by dividing the "*average maximum tensile stress"* measured during the tests by the flexural strength (see Table 3.4). Similar to the equivalent initial stress displayed in Table 5.2, average maximum tensile stresses were calculated from the values measured at cycle number 51 to 100 of the applied cyclic loads. It can be seen from Figure 5.17 that the relationship curve between the applied stress ratio and the fatigue life obtained from the tests in both stages can be formed using a regression line with an acceptable R-Squared value ($R^2 = 0.8$). However, additional test results of the 50 mm thick specimens are recommended for the verification of the aforementioned relationship curve. According to Figure 5.17, the size of the test specimen seems to have a minor effect on the fatigue life of CTB, if the applied stress ratio was employed in the analysis.

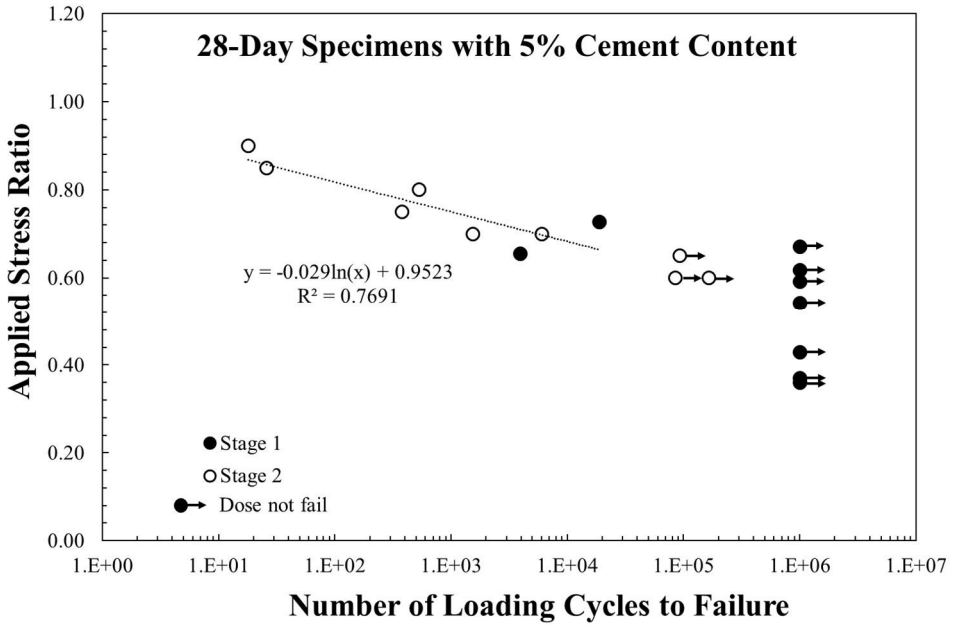

Figure 5.17: Comparison between the fatigue results of 5% cement specimens obtained from the tests in the first and second stages with various applied stress ratios

- Similar to Figure 5.17, the results in Figure 5.18 are derived from all specimens which failed during the fatigue tests in the first stage (modulus was reduced to 50% of the initial value) and second stage (broken) of the investigation. It can be concluded at this stage that the fatigue life of CTB material can be successfully predicted with the applied stress ratio, regardless of the effects of the cement content or the flexural strength, and size of the specimen.

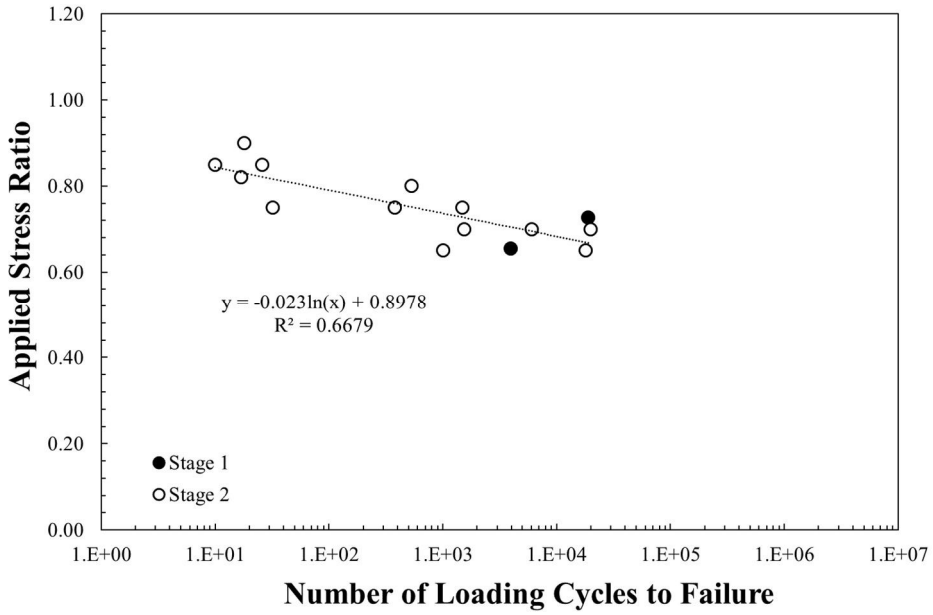

Figure 5.18: Comparison between the fatigue life of CTB specimens obtained from the tests in the first and second stages with various applied stress ratios

5.4 Conclusions

The fatigue characteristics of CTB material were investigated using two stages of the cyclic four-point bending test in this research. In the first stage of the investigation, prismatic beam specimens with dimensions of 50×63.5×400 mm^3 were prepared to achieve at least 95% of MDD using a roller compactor. The cement content varied from 3% to 10% and water equivalent to OMC was used for moulding the specimens in this stage. After cutting and trimming, the specimens were cured at 25 °C for 28 days. During the four-point bending tests, the cyclic load with a constant loading frequency of 10 Hz was applied to test specimens at 20 °C in the temperature-controlled chamber throughout the tests in the first stage. Specimens with dimensions of 100×100×400 mm^3 were employed in the second stage of the fatigue investigation.

These specimens were manually compacted to achieve at least 95% of MDD in a steel mould. In the second stage, specimens were prepared from standard crushed rock, 4% to 6% of cement content, and water at OMC. Similar to the first stage, the specimens were cured in a moist environment for approximately 28 days prior to the fatigue tests. Unlike the first stage of the investigation, a loading pulse of 250 ms was applied to the test specimens in the second stage with a rest period of 250 ms (2 Hz). Important key findings discovered from both stages of the fatigue investigation are as follows.

- The effects of sinusoidal and haversine loading waveforms on the fatigue characteristics of CTB specimens were examined in the first stage of the fatigue investigation. For the strain-controlled tests, CTB specimens exhibited fatigue responses under both sinusoidal loads and haversine loads. However, the fatigue characteristics of the CTB specimens were greatly influenced by the applied strain level. The greater the applied strain level, the shorter the fatigue life of the CTB specimen.

- The effects of the applied stress level or applied stress ratio were investigated in the second stage. The rise in the applied stress ratio led to a reduction in the fatigue life of CTB specimens. In addition, the influences of loading frequency were examined in the second stage. The test results showed that the fatigue life of CTB specimens depended on the applied loading frequency.

- Cement content affects the fatigue characteristics of CTB specimens in this research. Test results in the first stage show that under the same applied strain level, specimens with a higher cement content and initial cyclic flexural modulus have more fatigue failure resistance compared to those of specimens with lower cement content and initial modulus. Similarly, the fatigue life of CTB material obtained from stress-controlled tests in the second stage was also influenced by the cement content. However, the relationship between the fatigue life of CTB specimens and the applied stress ratio seems to be unaffected by the cement content. Accordingly, the relationship curve between the applied stress ratio and the fatigue life of specimens with differing cement content can be developed as shown in Figure 5.14.

- The specimen's size also affects the fatigue life of CTB specimens. Figure 5.16 shows that the 50 mm thick beams tended to have a longer fatigue life than the 100-mm thick beams, when the same magnitude of strain level was applied to the test specimens. However, the specimen's size effects can be ignored if the applied stress ratio is used to estimate the fatigue life of CTB specimens (see Figure 5.17).

- The results obtained from the four-point bending test in both stages reveal the existence of *"the fatigue endurance limit"*. After one million cycles of cyclic loading in the first stage, the cyclic flexural moduli of such specimens under applied strain levels less than 150 $\mu\varepsilon$ were reduced by only approximately 15% of their initial values. In contrast, applied strain levels greater than 150 $\mu\varepsilon$ resulted in rapid and significant reductions of the cyclic flexural moduli to 50% of the initial values within the early cycles of the cyclic load. Therefore, a fatigue endurance limit of 5% cement specimens should be the applied strain level located under 150 $\mu\varepsilon$. In the second stage, the stress-controlled fatigue test of 5% cement specimens indicated the applied stress level equal to 65% of *FS* as the fatigue endurance limit. The specimens subjected to a cyclic load greater than 0.65*FS* usually failed within two hundred thousand cycles of the applied cyclic load.

- The stress-controlled tests in the second stage demonstrated that the cyclic flexural modulus of the test specimens was normally reduced to 50% to 60% of the initial values before the specimens were completely broken by the cyclic loads. This finding supports the hypothesis of fatigue failure employed in the first stage of the investigation in this research. For the strain-controlled test in the first stage, the specimens were assumed to fail from the cyclic loading if the specimen's modulus was reduced to 50% of the initial value.

- The prismatic beam specimens with dimensions of 50×63.5×400 mm^3, prepared based on the particular conditions in the first stage of investigation, were sensitive to the applied stress levels in stress-controlled test conditions. A

small increase in an applied stress level may lead to an abrupt failure of test specimens. On the other hand, inconsistent fatigue test results were obtained from the strain-controlled tests in the second stage of the investigation. It should be emphasised that specimens with dimensions of 100×100×400 mm^3 were employed in the second stage. Nevertheless, test results from both stages in this research adequately describe the fatigue characteristics of CTB specimens. Previous literature recommended that the strain-controlled test is suitable for demonstrating the fatigue response of thin pavements. On the other hand, the loading regime on thick pavements is appropriately represented by the tests under stress-controlled mode.

5.5 Recommendations for fatigue testing protocol development

The test results in this chapter show that the fatigue characteristics of CTB material were adequately explained by the testing protocols developed for AC material (Austroads, 2006a) and stabilised road base material (Austroads, 2014a). The key findings of this research were previously summarised in the conclusion section. Based on the findings, important recommendations for fatigue testing standards development are as follows.

- At this stage, the cyclic four-point bending test is the appropriate testing platform for characterising the fatigue response of CTB materials. The same facility used for examining the fatigue behaviour of AC material can be employed as fatigue investigation tools for CTB materials. It is recommended by Austroads (2014b) that at least 10 fatigue results will be required for the development of fatigue life prediction equation.

- The strain-controlled test is suitable for simulating the loading spectrum induced by traffic loads for relatively thin pavement. On the other hand, the loading regime applied to a thick pavement layer is effectively generated by the stress-controlled test.

- According to the test results in the first stage, the loading waveform had insignificant effects on the fatigue response of CTB. However, the test results

in the second stage illustrate the effects of loading frequency on the fatigue life of CTB material. Therefore, it is recommended the real loading spectrum (loading waveform and frequency) expected in the field be applied in the fatigue test of CTB material. The loading regime generated by traffic loads can be predicted using traffic data collected from real road construction sites or adjacent road sites. Consequently, the effects of loading waveform and loading frequency on the fatigue characteristics of CTB can be minimised.

- A suitable applied stress level for the fatigue test varies between 60% to 90% of flexural strength. An applied stress level less than 60% of *FS* is the endurance limit of CTB material tested in this research. The appropriate applied strain level for the fatigue test varies and is influenced by the specimen's size. The smaller the size of the test beam, the greater the applied strain level required for the fatigue test.

- The test results from the second stage indicate that the existence of the fatigue failure assumption based on the reduced value of the specimen's modulus. The reduction in modulus to 50% of the initial value has been used as the termination criteria in the strain-controlled test in the first stage. This assumption was confirmed by the test results from the second stage, where the moduli of test specimens under the stress-controlled test reduced to 50% to 60% of the initial values prior to the failure.

- The fatigue life of CTB is successfully characterised by the applied stress ratio, regardless of the effects of cement content, flexural strength, and size of the specimen. Therefore, the fatigue test on CTB should be performed based on different levels of applied stress ratio (0.60 to 0.90).

- An alternative preparation method should be developed for small sized specimens with relatively low cement content. This is because the initial cyclic flexural modulus of 50 mm thick specimens with 3% cement content fluctuated consistently. The variation of the initial cyclic flexural modulus was caused by the processes of specimen cutting, trimming, and handling.

CHAPTER 6

DAMAGE EVOLUTION OF BOUND CTB UNDER CYCLIC LOADING

6.1 Introduction and background

In Chapter 5, the behaviour of CTB material under cyclic loading was characterised using the results from four-point bending tests. The modulus reduction of CTB specimens, when the number of loading cycles increased, represented the degradation of material due to fatigue damage. For the strain-controlled fatigue test, the amplitude of applied load or stress reduced with an increase in the number of loading cycles. However, the amplitude of beam deflection or strain *increased* with an increase in the number of loading cycles during the stress-controlled fatigue test. Despite this, the material damage in both stress-controlled and strain-controlled fatigue tests was reasonably represented by the reduction in the modulus of the test specimens. Section 2.5 briefly explains the background of Continuum Damage Mechanics (CDM) theory. Based on the CDM framework, a damage variable is used to describe material damage or degradation. The damage variable usually varies from zero for the intact state to one for the failure state. Accordingly, the fatigue life of materials can be forecast based on the rate of damage per loading cycle, based on the CDM framework. The rate of material damage per loading cycle can be estimated by using an analytical approach (see example in Eq. 2.18). However, most of the recent research has focused on the damage to materials tested in the laboratory (Alliche, 2004; Aramoon, 2014; Artamendi & Khalid, 2005; Bennett, 1980; Daniel & Bisirri, 2005; Destrebecq, 2010; Disfani, Arulrajah, Haghighi, Mohammadinia, & Horpibulsuk, 2014; Ghuzlan & Carpenter, 2006; Gnanendran & Paul, 2016; Gnanendran & Piratheepan, 2010). Research on damage to field CTB materials can be found in a limited range of literature (Busch, Thogersen, & Henrichsen, 2006; De Vos, 2007; R. Yeo, 2012).

For road pavement design, a shift factor is usually used to correlate the service life of road pavement structure to the fatigue life of AC material measured in the laboratory (Witczak, Mamlouk, Souliman, & Zeiada, 2013). Austroads (2014b) and Wen et al. (2014) developed shift factors for CTB materials to be implemented in road pavement

design guidelines. Consequently, the service life of road pavement can be predicted by multiplying a single shift factor by the laboratory-measured fatigue life of the pavement. Guo (2007) developed a reliability-based fatigue life estimation framework for AC road pavements. Base on Guo's work, the fatigue life of AC road pavement can be predicted by employing a set of bias factors in the calculations. These bias factors were developed to consider the effects coming from various sources of uncertainty, i.e. temperature, loading speed (frequency), traffic wandering, moisture and loading ratio. It should be the case that a more rigorous fatigue life would be obtained from the reliability-based approach compared to the result estimated by multiplying the laboratory-measured fatigue life by a single shift factor.

Busch (2008) developed a fatigue life estimation approach for road pavement with CTB layers based on the CDM framework. Accelerated Loading Facility (ALF) test results were used to calibrate the proposed approach in his study. Busch (2008) showed that the fatigue life of CTB layers was reasonably estimated from the proposed approach without the application of a shift factor (Busch, 2008; Busch et al., 2006). However, the proposed approach was developed from specific categories of CTB materials and as such may not properly predict the fatigue life of other CTB materials (e.g. different parent materials, different cement content). In the US, NCHRP (2004) proposed a model for estimating the damaged moduli of CTB layers degraded during the service-life or roads. Later, Wen et al. (2014) modified the model to provide more accurate results of the estimated moduli based on the level of damage. However, the calibration approach and application details of the proposed model were unavailable in the guidelines. This may be the reason that the proposed model was not completely implemented in the design software (MEPDG software) released by AASHTO (Saxena, Tompkins, Khazonovich, & Balbo, 2010).

The CDM framework has been popularly employed to capture the deterioration behaviour of Asphalt Concrete (AC), concrete, and cement-treated road based by many researchers. However, the recently developed models were mostly calibrated using either laboratory test results or field test results. This chapter, therefore, focuses on characterising the damage development or damage evolution of the CTB materials induced by cyclic loads in the laboratory and by wheel loads in the field tests. The damage evolution of CTB layers in the pavement structure was then related to the

damage behaviour of specimens tested in the laboratory. Accordingly, laboratory test results may then be used to best explain the damage evolution of CTB layers in the field, where such information may not be always available.

6.2 Damage behaviour of CTB materials under cyclic loading

6.2.1 Damage variable definition

A damage variable can be defined based on the changes in the engineering properties of materials when they are subjected to external forces. A damage variable is defined based on the reduction in the material modulus, with respect to the increase in the number of loading cycles, as illustrated by Eq. 6.1 (Thiele, Petryna, & Rogge, 2016).

$$D = \frac{E_0 - E_D}{E_0} \tag{6.1}$$

in which D is the damage variable at the current loading cycle, E_0 is the initial secant modulus, and E_D is the secant modulus at the current loading cycle (see Figure 6.1).

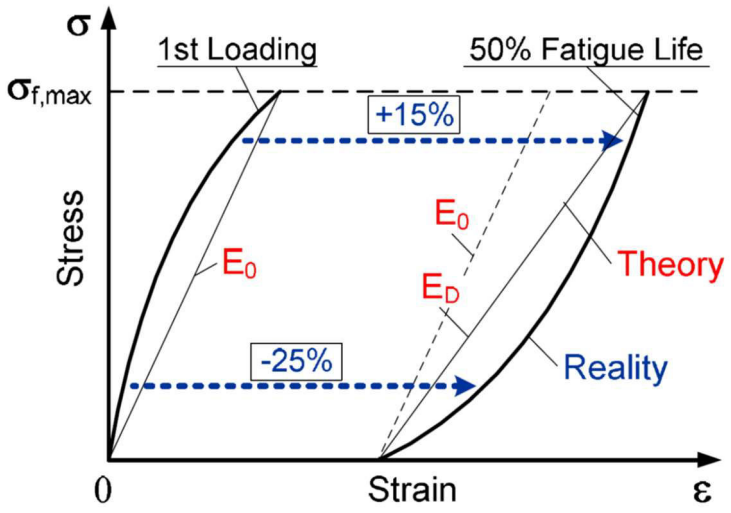

Figure 6.1: Impact of fatigue damage on stress-strain relationship (Thiele et al., 2016)

Thiele et al. (2016) also stated that the stress-strain relationship of concrete-like material under cyclic loading is strongly influenced by the applied stress level at the

current loading cycle (see Figure 6.1). Therefore, the modulus of materials can be determined using Eq. 6.2.

$$E_D(\sigma) = E_o(1 - D(\sigma)) \tag{6.2}$$

The damage variable is defined based on the changes in applied stress level, as presented in Eq. 6.3 (Rogge & Thiele, 2012).

$$D = \frac{\sigma_o - \sigma_{eff}}{\sigma_o} \tag{6.3}$$

in which, σ_{eff} is the stress at a certain load level in the damaged element, and σ_o is the fictitious or theoretical stress in the undamaged element under the same strain. On the other hand, Vega, Bhatti, and Nixon (1995) defined the damage variable of concrete materials based on the increase in strain, as seen in Eq. 6.4.

$$D = \frac{\varepsilon_D - \varepsilon_o}{\varepsilon_{ult} - \varepsilon_o} \tag{6.4}$$

in which, ε_D is the maximum tensile strain at the current loading cycle, ε_o is the maximum tensile strain at the first loading cycle, and ε_{ult} is the maximum tensile strain at failure. It can be seen from Eq. 6.4 that the damage variable of material can be calculated when the value of ε_{ult} is provided.

As mentioned earlier, the damage variable generally varies from zero for the undamaged state to one for the completely damaged state. It also means that the damage variable theoretically reaches the maximum value when the material fails from fatigue damage. Therefore, to assign the failure state to materials (D = 1), the fatigue failure assumption is necessary. Gnanendran and Paul (2016) reviewed the fatigue failure assumption of CTB materials from various theories. The most widely employed fatigue failure assumption for CTB materials is the 50% modulus reduction method. However, the aforementioned method is not suitable for lightly stabilised materials due to the brittle response of such materials (Gnanendran & Paul, 2016). Therefore, Gnanendran and Paul (2016) suggested defining the fatigue life of lightly stabilised materials using the dissipated energy approach.

Dissipated energy is defined as the energy dissipating from damage or deterioration to the material (Grzybowski & Meyer, 1993). It can be calculated from the area under a hysteresis loop of a loading and unloading curve (Aramoon, 2014). The changes in cumulative dissipated energy have also been used to calculate the damage variable of CTB material (Gnanendran & Paul, 2016) and concrete (Aramoon, 2014; Grzybowski & Meyer, 1993; Paskova & Meyer, 1997). However, the calculation process for cumulative dissipated energy is cumbersome and requires a completed hysteresis loop of load-displacement relationship. For AC material, the dissipated energy per loading cycle can be determined by Eq. 6.5 (Ghuzlan & Carpenter, 2006; Gnanendran & Paul, 2016; Rowe, 1993).

$$W = \pi\sigma\varepsilon \sin\phi \tag{6.5}$$

in which, W is the dissipated energy per loading cycle, σ and ε is the stress and strain at the current loading cycle, respectively, and ϕ is the phase angle. It should be emphasised that the dissipated energy equation of Eq. 6.5 was developed for viscoelastic materials such as AC material (Rowe, 1993). Accordingly, the Dissipated Energy Ratio (*DER*) can be calculated by Eq. 6.6 (Gnanendran & Piratheepan, 2010; Khalid, 2000; Rowe, 1993).

$$DER = \frac{W_o}{\left(W/N_i\right)} \tag{6.6}$$

in which, W_o is the initial dissipated energy, W is the dissipated energy at the n^{th} loading cycle, and N_i is the number of loading cycles. Rowe (1993) determined the loading cycle where the first crack appears in AC materials from the relationship curves between the *DER* and the number of applied loading cycles. If the *DER*s calculated by Eq. 6.6 are plotted against the number of loading cycles in the x-axis, the position of the first crack is defined as the peak *DER* in a stress-controlled fatigue test. On the other hand, the sharply deviated point of *DER* from the linear line is assigned as the position of the first crack in a strain-controlled fatigue test (Rowe, 1993). Accordingly, Eq. 6.6 can be further modified for the cases of stress-controlled fatigue tests and strain-controlled fatigue tests, as shown in Eq. 6.7a and 6.7b, respectively (Rowe, 1993).

$$R_\sigma = N_i E_D \tag{6.7a}$$

$$R_\varepsilon = \frac{N_i}{E_D} \tag{6.7b}$$

in which, R_σ and R_ε are the equivalent ratios for the stress-controlled fatigue test and strain-controlled fatigue test, respectively. The concept of *DER* was successfully applied to determine the position at the first crack or fatigue life of AC material. Daniel and Bisirri (2005) applied the *DER* concept for predicting the fatigue life of concrete pavement. The fatigue life prediction model for concrete pavement developed by Daniel and Bisirri (2005) was compared with the other prediction models, as shown in Figure 6.2.

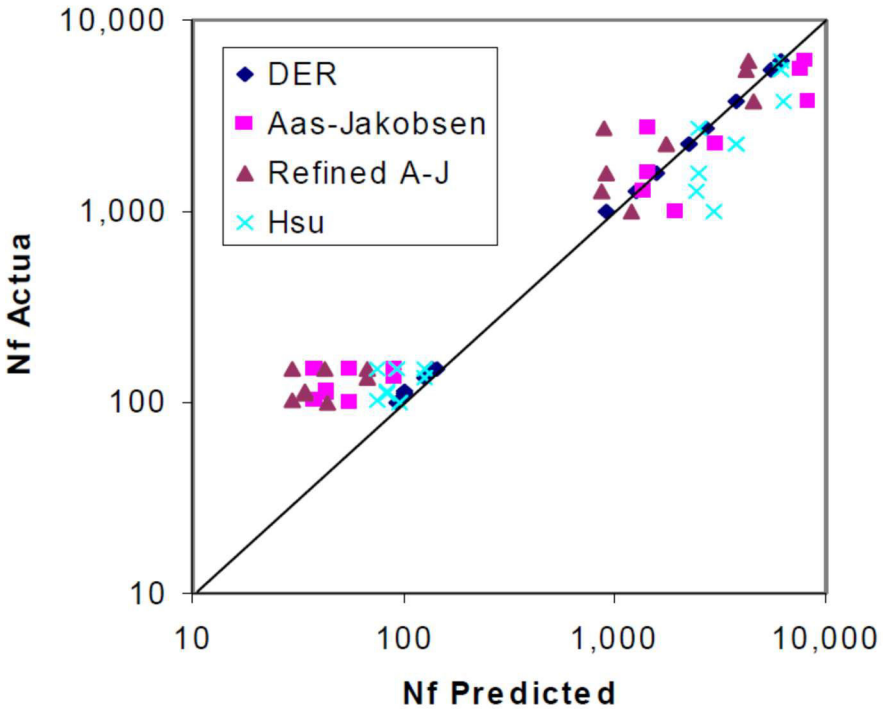

Figure 6.2: Predicted fatigue life versus actual fatigue life of Portland cement concrete (Daniel & Bisirri, 2005)

Aramoon (2014) examined the fatigue behaviour of reinforced concrete beams, based on the dissipated energy approach. The fatigue life of plain concrete and reinforced concrete beams was initially determined from the four-point bending test results. According to Aramoon (2014), the dissipated energy per loading cycle can be calculated by Eq. 6.8.

$$W = \sum_{i=1}^{n} \frac{(P_i + P_{i+1})}{2} (D_{i+1} - D_i) \quad (6.8)$$

in which, i is the load (P) or deflection (D) increment, P_i, P_{i+1}, D_i, and D_{i+1} are defined as in Figure 6.3. It can be seen from Figure 6.3 that to calculate the dissipated energy per loading cycle, the loads and deflections (or stresses and strains) at various increments on the hysteresis loop are required. However, limited stress and strain information was obtained from the four-point bending tests. For example, the stresses and strains obtained from the tests in this research included maximum and minimum stress, maximum and minimum strain, and the chord modulus of each loading cycle, as illustrated by Figure 6.4. Therefore, the dissipated energy per loading cycle for the stress-controlled fatigue test in this research can be estimated based on Eq. 6.9.

$$W = \frac{(\sigma_{max} - \sigma_{min})}{2} \left(\varepsilon_{min,n+1} - \varepsilon_{min,n}\right) + \sigma_{min}\left(\varepsilon_{min,n+1} - \varepsilon_{min,n}\right) \quad (6.9)$$

in which, the definition of all parameters in Eq. 6.9 is provided in Figure 6.4.

It can be seen from Eq. 6.9 that, the term $\sigma_{min}\left(\varepsilon_{min,n+1} - \varepsilon_{min,n}\right)$ is equal to zero, if σ_{min} = 0. The dissipated energy estimated by Eq. 6.9 was verified by the fatigue test results of a small-sized beam (50×63.5×400 mm^3) as shown in Figure 6.5. The test results of 5% CTB specimens were used in this section. The 28-day specimen was tested using 10-Hz of sinusoidal loading waveform to 500,000 cycles. An amplitude of tensile strain equivalent to 150 $\mu\varepsilon$ was maintained during the test (strain-controlled test). The details of the small-sized beam fatigue tests can be found in Section 5.2.

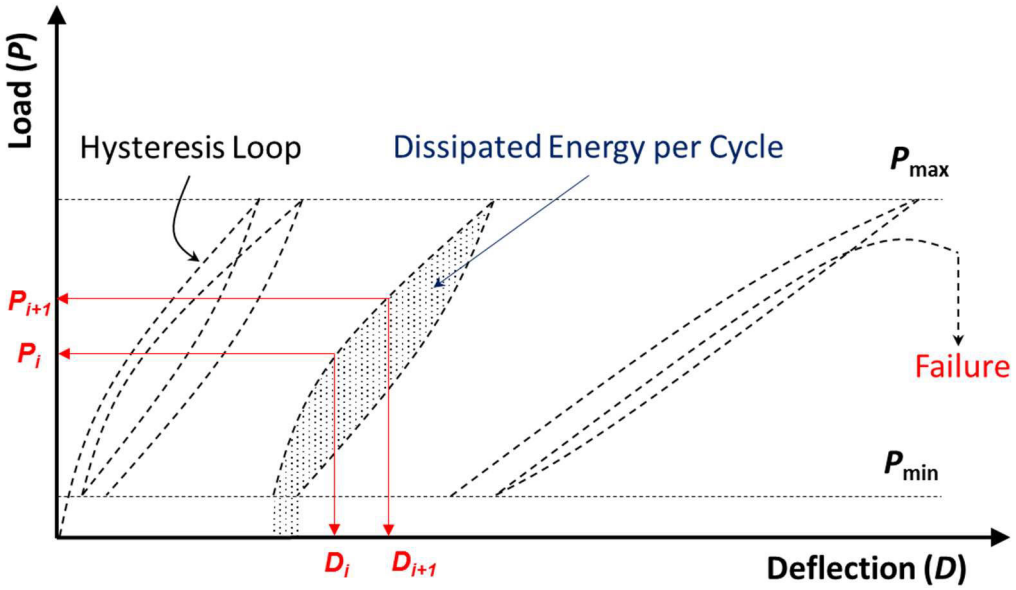

Figure 6.3: Load versus deflection curves from stress-controlled four-point bending test (modified from Aramoon (2014))

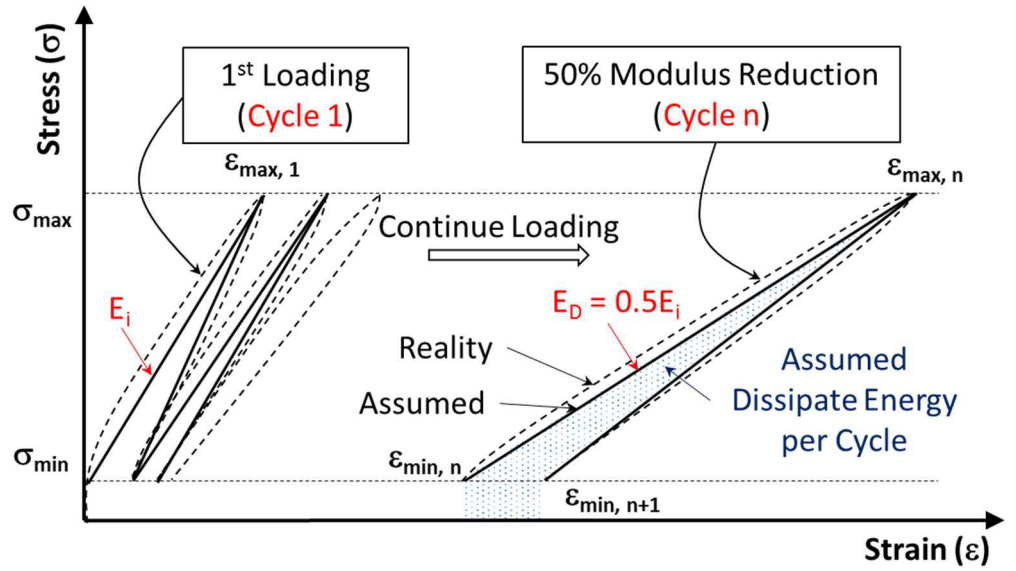

Figure 6.4: Definition of all parameters for Eq. 6.9

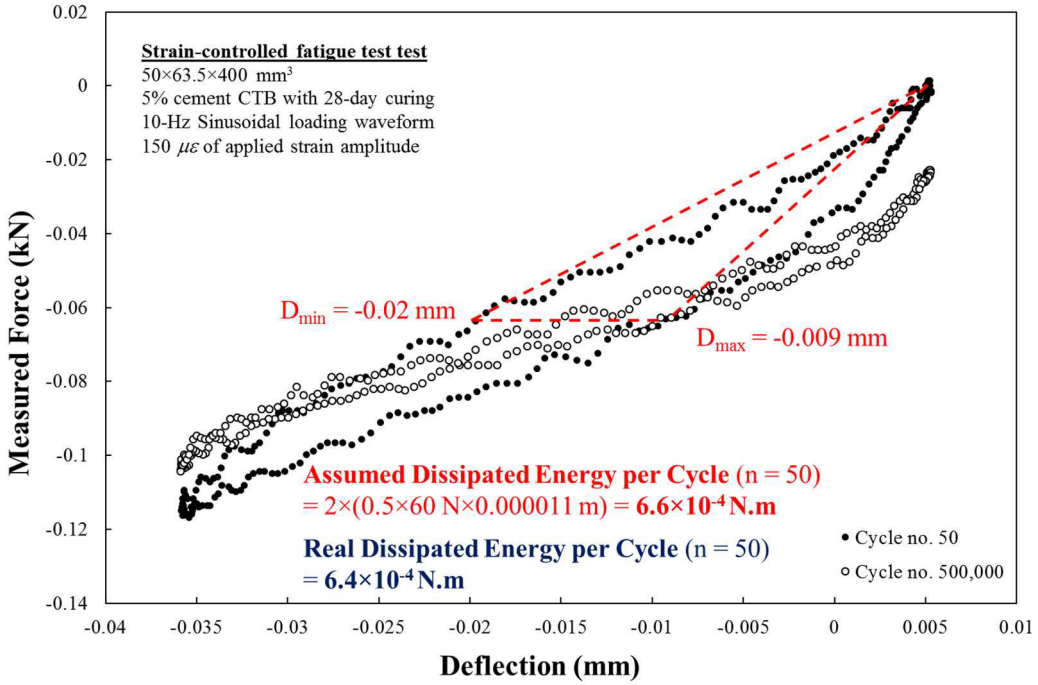

Figure 6.5: Load-deflection hysteresis loops obtained from strain-controlled fatigue test in this research

During the test of the beam specimen referred to, the load and displacement increments at 50th and 500,000th cycles were collected, as shown in Figure 6.5. Accordingly, the dissipated energy per loading cycle at cycle number 50 calculated based on Eq. 6.8 was 6.4×10^{-4} N.m. On the other hand, the dissipated energy per loading cycle estimated by a similar concept demonstrated in Eq. 6.9 was 6.6×10^{-4} N.m. Therefore, it can be concluded that in this research, Eq. 6.9 can be reasonably used to estimate the dissipated energy per loading cycle of CTB material.

6.2.2 Damage evolution of CTB specimens tested in the laboratory

Fatigue life estimated from the 50% modulus reduction approach seems to be the most widely used method for CTB materials (Gnanendran & Paul, 2016). On the other hand, the fatigue life estimation model developed based on the dissipated energy approach provides the best fit with actual data (Daniel & Bisirri, 2005). Therefore, both approaches were initially employed for assigning the fatigue life of CTB materials in this research.

Table 6.1 summarises the determined fatigue life of CTB specimens based on a 50% modulus reduction and the dissipated energy approach. The number of cycles determined at first crack (Rowe, 1993) based on the dissipated energy approach was considered as the fatigue life of CTB specimens in this research. Examples of the relationship between *DER*s and the number of loading cycles (N_i) are presented in Figures 6.6 and 6.7 for the stress-controlled and strain-controlled fatigue tests, respectively. Figures 6.6 and 6.7 illustrate that the fatigue life of CTB specimens (N_f) calculated from the dissipated energy approach is usually lower than those determined by the 50% modulus reduction approach. This is because the number of loading cycles at failure defined by the dissipated energy approach represents the crack initiation point (Rowe, 1993).

Table 6.1: Fatigue life of CTB specimens defined based on different approaches

Specimen	**Applied stress ratio**	**50% modulus reduction**		**Dissipated energy ratio**	
		N_f **(Cycles)**	ε_{ult} $(\mu\varepsilon)$	N_f **(Cycles)**	ε_{ult} $(\mu\varepsilon)$
4% cement content specimens					
S-21	0.65	994	170	878	108
S-20	0.75	1,480	184	1,296	128
5% cement content specimens					
S-3	0.70	6,006	182	5,569	150
S-28	0.70	1,543	163	1,392	132
S-16	0.75	373	195	337	164
S-5	0.80	530	191	482	154
S-18	0.85	23	214	22	184
S-2	0.90	15	224	15	224
6% cement content specimens					
S-26	0.65	17,633	185	16,642	144
S-27	0.70	19,878	188	18,873	122
S-24	0.75	30	211	27	191
S-25	0.85	17	N.A.	N.A.	N.A.

N_f = Number of cycles at fatigue failure.
ε_{ult} = Ultimate strain at fatigue failure.
N.A. = Not available due to limited data.

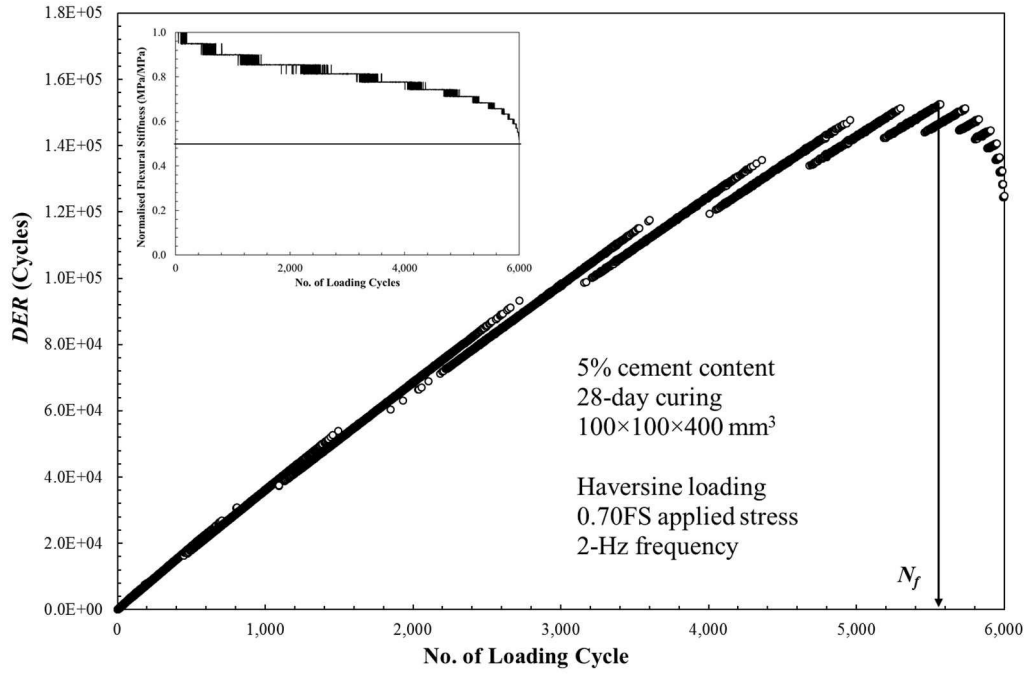

Figure 6.6: Relationship between equivalent ratio and number of loading cycles from stress-controlled test

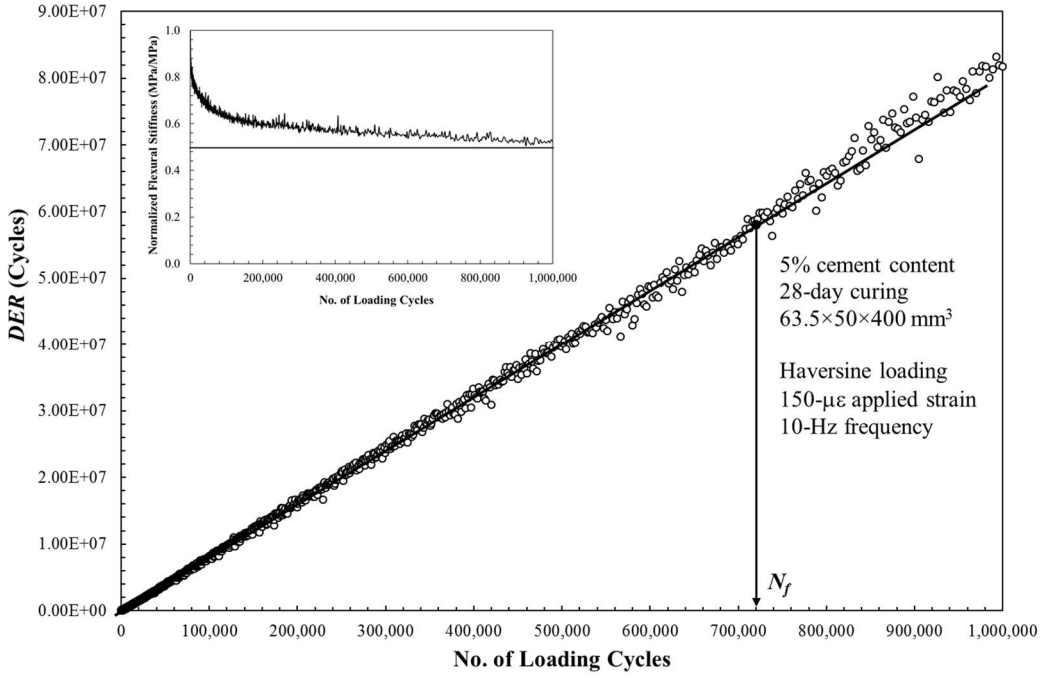

Figure 6.7: Relationship between equivalent ratio and number of loading cycles from strain-controlled test

The ultimate strain, as seen in Table 6.1 can be correlated with the breaking strain measured from flexural strength tests (see Chapter 3) by constant parameters, as shown in Eq. 6.10.

$$\varepsilon_{ult} = k \times \varepsilon_b \tag{6.10}$$

in which, ε_b is the breaking strain or strain at a stress equal to 95% of flexural strength (R. Yeo, 2012), and k is the constant parameter.

Table 6.2: Constant parameter for ultimate strain estimation

Cement content	**No. of specimens**	**Breaking strain ($\mu\varepsilon$)**	***k***							
			50% modulus reduction				**Dissipated energy ratio**			
			Max	**Min**	**μ**	**σ**	**Max**	**Min**	**μ**	**σ**
4%	2	103	1.79	1.65	1.72	0.10	1.24	1.05	1.15	0.14
5%	6	127	1.54	1.28	1.42	0.10	1.37	0.88	1.16	0.20
6%	3	148	1.29	1.25	1.27	0.02	1.01	0.69	0.89	0.18

At this stage, the damage variable can be calculated based on the fatigue life determined by two different approaches. The dissipated energy approach seems to provide the most suitable measure of damage compared to other approaches (Grzybowski & Meyer, 1993). The damage variable estimated based on the dissipated energy approach can be calculated by Eq. 6.11.

$$D = \frac{\sum_{i=1}^{n+1} W_i}{\sum_{i=1}^{N_f} W_i} \tag{6.11}$$

in which, W_i is the dissipated energy at any loading cycle (i). Eq. 6.11 demonstrates that the damage variable is the ratio between cumulative dissipated energy at any loading cycle and total cumulative dissipated energy at failure. Accordingly, the cumulative dissipated energy of the specimens tested by the stress-controlled fatigue test can be simplified, as illustrated in Eq. 6.12.

$$\sum_{i=1}^{n+1} W_i = \frac{1}{2}\Delta\sigma\left[\left(\varepsilon_{min,2} - \varepsilon_{min,1}\right) + \left(\varepsilon_{min,3} - \varepsilon_{min,2}\right) + \cdots + \left(\varepsilon_{min,n+1} - \varepsilon_{min,n}\right)\right] = \frac{1}{2}\Delta\sigma\left[\left(\varepsilon_{min,n+1} - \varepsilon_{min,1}\right)\right] \quad (6.12)$$

If one incorporates Eq. 6.12 into Eq. 6.11, the damage variable of the CTB specimens tested by the stress-controlled fatigue test can be calculated based on the strain development as shown in Eq. 6.13.

$$D = \frac{\frac{1}{2}\Delta\sigma\left[\left(\varepsilon_{min,n+1} - \varepsilon_{min,1}\right)\right]}{\frac{1}{2}\Delta\sigma\left[\left(\varepsilon_{min,N_f} - \varepsilon_{min,1}\right)\right]} = \frac{\left[\left(\varepsilon_{min,n+1} - \varepsilon_{min,1}\right)\right]}{\left[\left(\varepsilon_{min,N_f} - \varepsilon_{min,1}\right)\right]} \quad (6.13)$$

It can be seen from Eq. 6.13 that the change in the minimum strain of each loading cycle, ($\varepsilon_{min,n+1}$ - $\varepsilon_{min,n}$), is equivalent to the (minimum) permanent strain progressively induced by the cyclic load. If the changes in minimum strain per loading cycle were assumed to be approximately equal to the average permanent strains per loading cycle, Eq. 6.13 can therefore be rewritten, as shown by Eq. 6.14.

$$D = \frac{\left[\left(\varepsilon_{min,n+1} - \varepsilon_{min,1}\right)\right]}{\left[\left(\varepsilon_{min,N_f} - \varepsilon_{min,1}\right)\right]} = \frac{\varepsilon_D - \varepsilon_o}{\varepsilon_{ult} - \varepsilon_o} \quad (6.14)$$

From Eq. 6.14, it can be concluded that the damage variable calculated from the dissipated energy approach (Eq. 6.11) is approximately equivalent to the damage variable estimated in Eq. 6.4.

Figure 6.8 shows the damage evolution of 5% specimens calculated based on Eq. 6.4. The ultimate tensile strains obtained from the 50% modulus reduction and dissipated energy approach (see Table 6.1) were employed in the damage variable calculations. It can be seen from Figure 6.8 that the damage evolution of CTB specimens calculated using the ultimate strain obtained from the dissipated energy approach agreed with the damage evolution line developed from Palmgren-Miner's law.

The development of damage with respect to the increase in the number of loading cycles is a very useful assessment tool for pavement engineers. It means that the performance of existing road pavement can be monitored throughout its service life using damage evolution curves, as shown in Figure 6.8. Vega et al. (1995) developed

the damage evolution prediction equation for concrete in tension. In their analysis, the increase in maximum tensile strain induced by the cyclic load was employed as an independent parameter (see Eq. 6.4). The maximum and minimum cyclic stress, and number of loading cycles were chosen as the input parameters, as illustrated in Eq. 6.15 (Vega et al., 1995).

$$D(\varepsilon) = \alpha_1 \sigma_{r,max}^2 + \alpha_2 \sigma_{r,max} \sigma_{r,min} + \alpha_3 (\sigma_{r,max} - \sigma_{r,min}) \tag{6.15}$$

in which, $\sigma_{r,max}$ is the maximum applied stress amplitude divided by the flexural strength (σ_{max}/FS), $\sigma_{r,min}$ is the minimum applied stress amplitude divided by the flexural strength (σ_{min}/FS), and α_1, α_2, and α_3 are regression parameters as the function of loading cycles (Figure 6.9). Therefore, Eq. 6.15 can be rewritten as shown in Eq. 6.16.

$$D(\varepsilon) = f(\sigma_{max}, \sigma_{min}, FS, N) \tag{6.16}$$

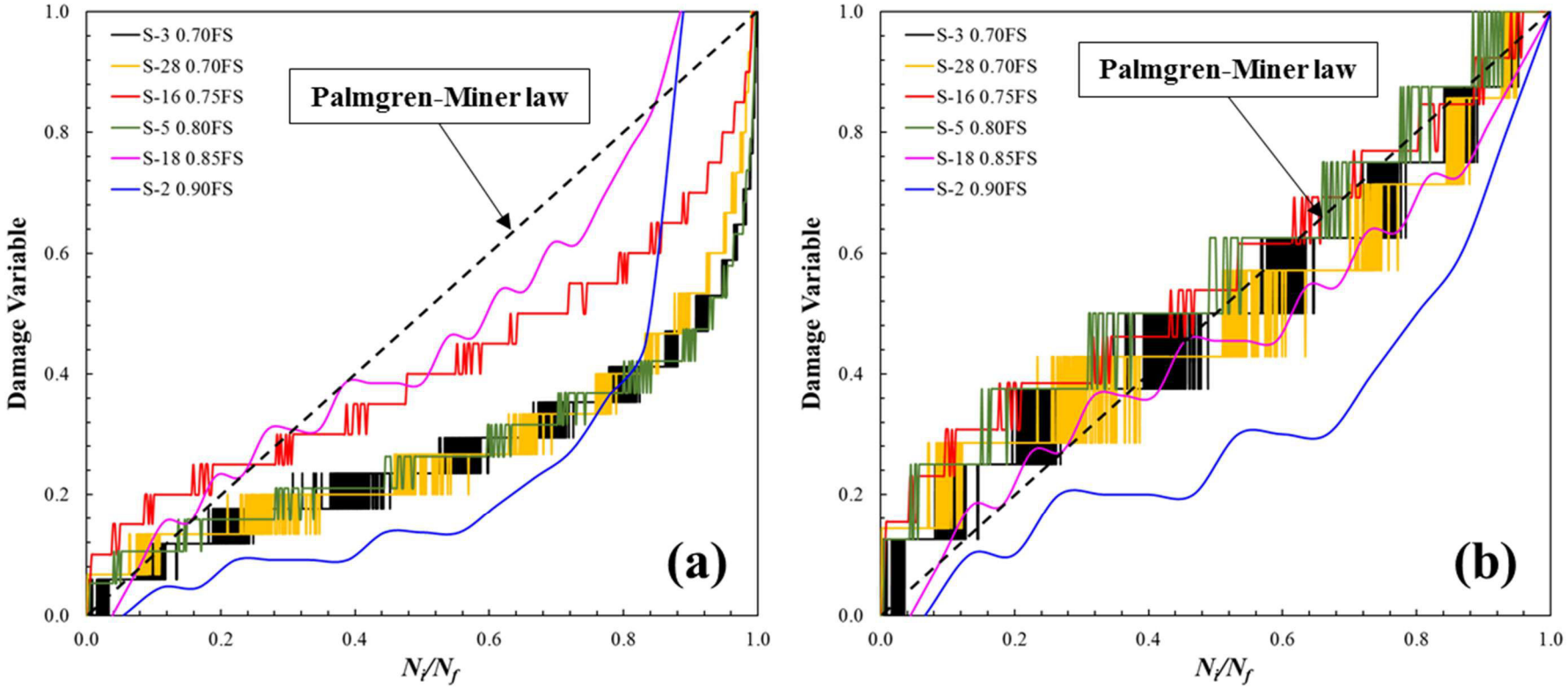

Figure 6.8: Damage variable of 5% specimens calculated based on ultimate strain obtained from (a) 50% modulus reduction approach, and (b) dissipated energy approach

$N_r = N/N_f$	α_1	α_2	α_3
0.025	0.182	0.110	0.085
0.050	0.371	−0.084	0.020
0.100	0.191	0.280	0.225
0.150	−0.028	0.631	0.437
0.200	−0.053	0.698	0.479
0.300	−0.161	0.891	0.627
0.400	−0.525	1.260	0.978
0.500	−0.694	1.500	1.170
0.600	−0.666	1.490	1.200
0.700	−0.680	1.550	1.260
0.800	−0.762	1.690	1.380
0.850	−0.756	1.690	1.410
0.950	−0.810	1.770	1.590
0.975	−1.080	2.120	1.900

Figure 6.9: Regression parameters for damage variable calculation (Vega et al., 1995)

Based on Eq. 6.15 and Figure 6.9, the damage evolution of concrete in tension can be created as shown in Figure 6.10.

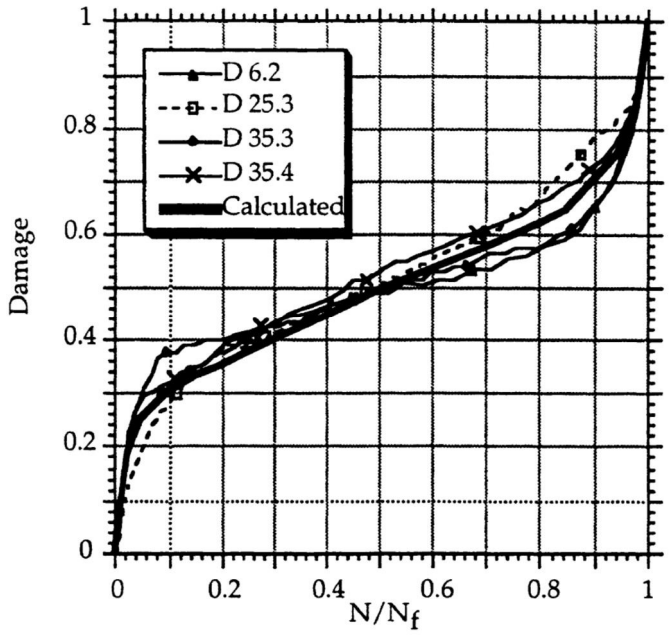

Figure 6.10: Comparison between tested and predicted (calculated) damage evolution of concrete (Vega et al., 1995)

The damage evolution curves shown in Figure 6.10 acted similarly to the damage evolution curves of CTB specimens tested in this research (see Figure 6.8). Moreover,

a similar trend of damage evolution curves can also be observed in the works of Grzybowski and Meyer (1993). Accordingly, the logit function (inverse of the sigmoidal logistic function) was used to develop a prediction equation for damage evolution of CTB specimens in this research. Eq. 6.17 shows the general form of the damage evolution prediction equation developed based on the logit function.

$$D(\varepsilon) = \theta_1 Log\left(\frac{(N_i/N_f)^{\theta_2}}{(1-(N_i/N_f)^{\theta_3})}\right) \tag{6.17}$$

in which, θ_1, θ_2, and θ_3 are regression parameters. Figure 6.11 shows the comparison example between damage variables calculated from the experimental data and values estimated from the prediction equation.

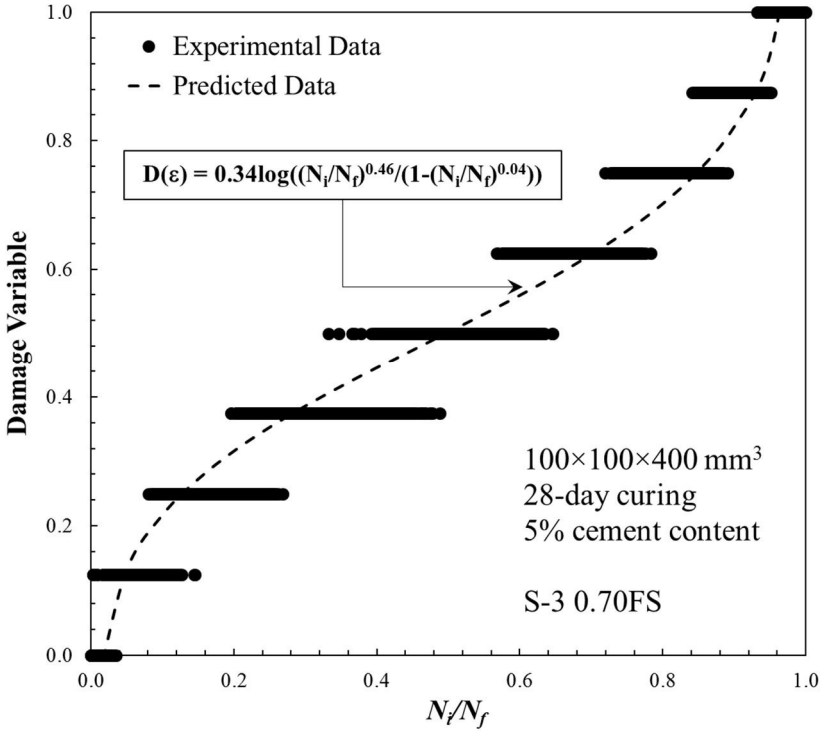

Figure 6.11: Damage variables calculated from the experimental data and values estimated from the prediction equation

Table 6.3 provides the regression parameters for damage variable estimation. The estimated damage to all beam specimens of the size 100×100×400 mm^3 is illustrated by Figures 6.12, 6.13, and 6.14.

Table 6.3: Regression parameters for damage variable estimation

Specimen	σ/FS	θ_1	θ_2	θ_3	*Standard Error*
4% cement content specimens					
S-21	0.65	0.269	0.460	0.007	0.049
S-20	0.75	0.249	0.753	0.006	0.049
5% cement content specimens					
S-3	0.70	0.343	0.459	0.037	0.058
S-28	0.70	0.374	0.233	0.065	0.060
S-16	0.75	0.309	0.569	0.015	0.052
S-5	0.80	0.327	0.559	0.018	0.059
S-18	0.85	0.356	0.623	0.053	0.026
S-2	0.90	0.572	0.002	0.652	0.037
6% cement content specimens					
S-26	0.65	0.342	0.187	0.049	0.042
S-27	0.70	0.138	2.373	0.000	0.044
S-24	0.75	0.436	0.291	0.123	0.094

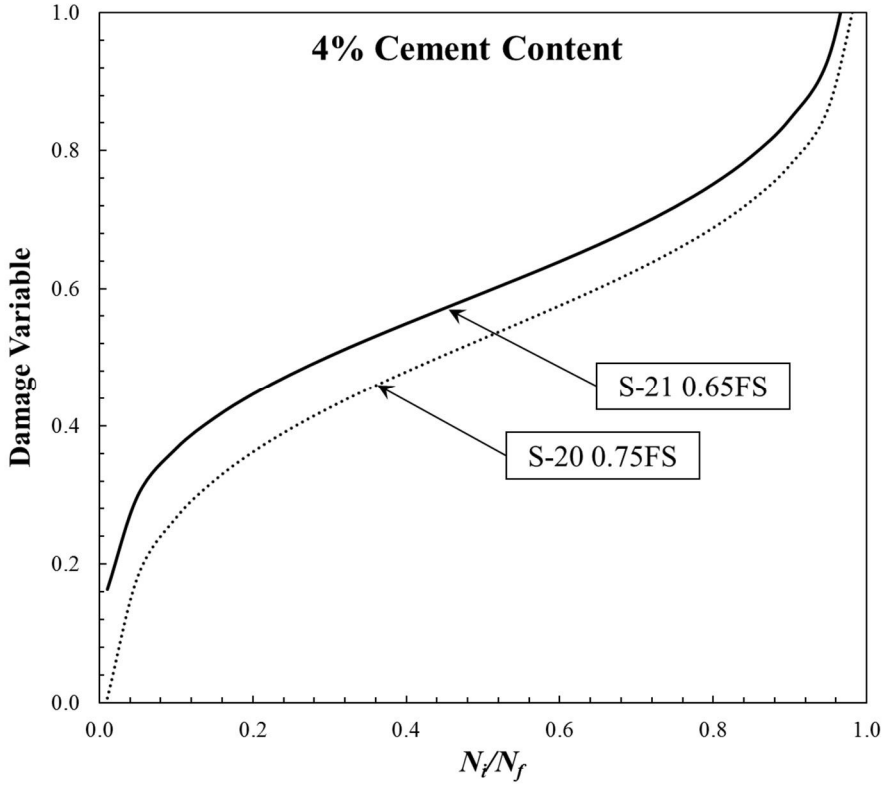

Figure 6.12: Damage evolution of 4% specimens

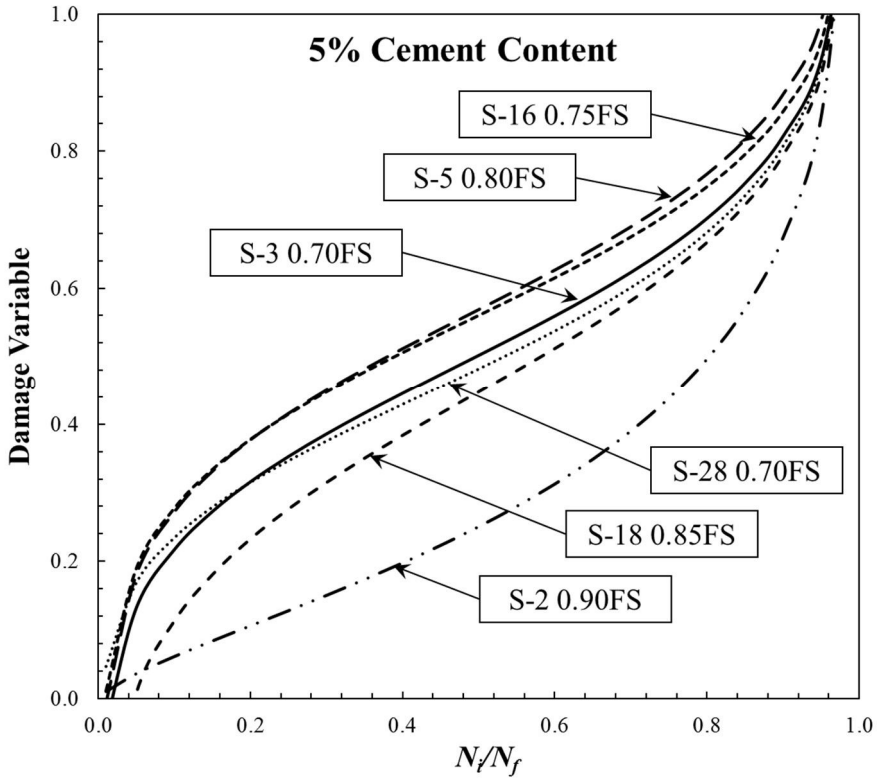

Figure 6.13: Damage evolution of 5% specimens

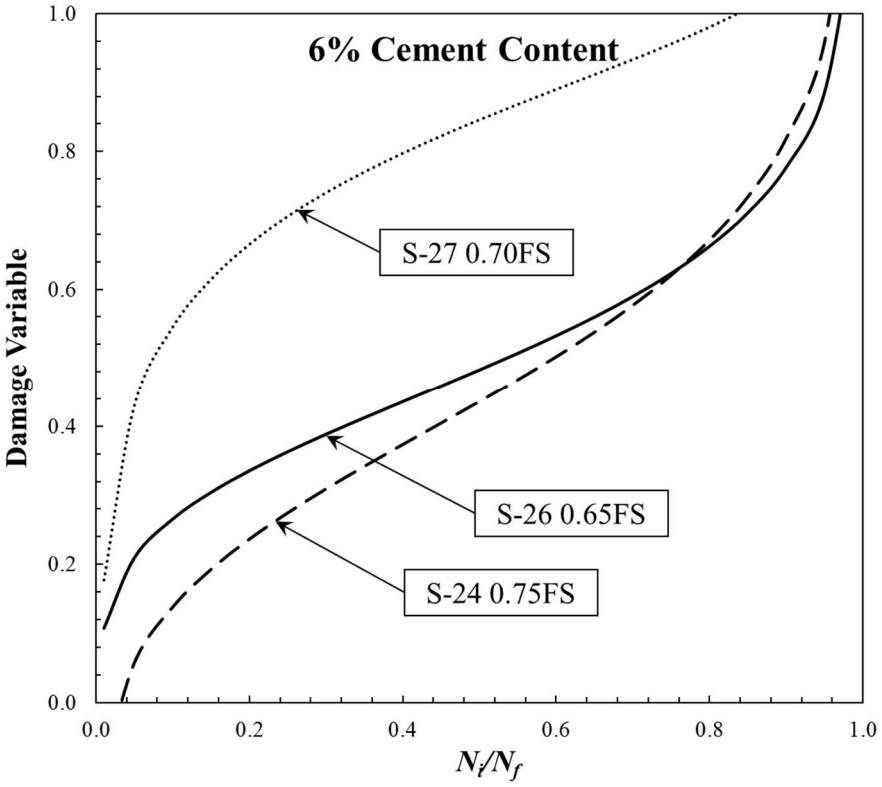

Figure 6.14: Damage evolution of 6% specimens

It can be seen in Figures 6.12 to 6.14 that the damage evolution curves were not significantly influenced by the cement content of the CTB specimens. Nevertheless, the increase in the applied stress ratio greatly affected the damage behaviour of CTB specimens. Based on the fatigue test results in Chapter 5, an applied stress ratio equal to 0.60*FS* was presumed as the endurance limit of CTB specimens tested in this research. It is understood that the damage variable of CTB specimens subjected to a stress ratio lower than the endurance limit would never reach one. This is because fatigue failure did not occur within the specified range of testing cycles. Accordingly, the specimens subjected to a stress ratio lower than the endurance limit (0.60*FS*) were not considered in this analysis. Based on the damage evolution curves illustrated in Figures 6.12 to 6.14, the damage behaviour of CTB can be further categorised, based on the applied stress ratio, into two more groups. The first group is made up of the specimens tested under stress ratios varying between 0.60*FS* and 0.85*FS*. In this group, the damage variable increased dramatically from the starting point until the cycle ratio approached 0.2. The rate of damage can be calculated by using Eq. 6.17 and the parameters shown in Table 6.3, if the fatigue life (N_f) of the CTB specimen is available (see Table 6.1). With the first group, the damage variable stably increased within cycle ratios ranging from 0.2 to 0.8. The rate of damage then rose again until the specimens completely failed from the cyclic load. The damage evolution curves of specimens in this group agreed well with the test results by Vega et al. (1995). It should be emphasised that the damage of specimens subjected to a lower applied stress ratio developed faster than the specimens subjected to a higher stress ratio at the beginning of the tests (cycle ratios varied from 0 to 0.2).

On the other hand, Figure 6.13 shows that the damage evolution curve of specimens tested by 0.90*FS* was different to that of the other specimens. The damage variables at the lower cycle ratio (0 – 0.1) were lower than the first group, but the rate of damage accelerated when the cycle ratio was greater than 0.8. Therefore, the damage behaviour of specimens subjected to an applied stress ratio greater than 0.85*FS* should be categorised as a new group. The damage behaviour of specimens categorised in this second group evolved similarly to the damage behaviour of specimens tested by a monotonic compressive load, as demonstrated in Section 4.4.

6.2.3 Damage variable of CTB layers calculated from the ALF test results

To calculate the damage variable of CTB layers in a pavement structure, the value of the ultimate strain (ε_{ult}) must be known. This value can be estimated based on flexural strength test results, as demonstrated in Eq. 6.10. However, test results from R. Yeo (2012) show that the breaking strain and flexural strength of CTB materials depends on age (curing time) and the relative density of specimens. Moreover, the effects of initial micro-cracks induced by shrinkage seem to be the source of the difference between the breaking strains measured from the field specimens and the laboratory-prepared specimens. Table 6.4 summarises the results of the flexural strength test performed by R. Yeo (2012). Based on R. Yeo (2012), two different types of CTB materials were considered. The first CTB material was Hornfels crushed rock treated with 3% GP cement (Hornfels CTB). The second type of CTB material was siltstone quartzite quarry rubber mixed with 4% GP cement (Siltstone CTB).

Table 6.4: Results summary of the flexural strength test performed by R. Yeo (2012)

Parent Materials	**Flexural Strength (Curing Time) (MPa (Days))**		**Breaking Strain (Curing Time) ($\mu\varepsilon$ (Days))**	
	Laboratory	**Field**	**Laboratory**	**Field**
Hornfels	1.00 (28)	0.97 (29)	95 (28)	103 (29)
	1.26 (576)	0.61 (95)	188 (576)	487 (95)
Siltstone	1.12 (32)	1.32 (34)	178 (32)	159 (34)
	1.03 (616)	1.89 (1025)	451 (616)	197 (1025)

Table 6.5 illustrates the fatigue test results and ultimate strain at 50% modulus reduction provided by R. Yeo (2012). The flexural strengths measured from laboratory-prepared specimens (see Table 6.5) were used to estimate the stress ratio (σ/FS) shown in Table 6.5. Similarly, the breaking strains presented in Table 6.4 were correlated with the ultimate strain in Table 6.5 to obtain the *k*-parameter illustrated by Eq. 6.10. The maximum applied cyclic stress was assumed to be constant throughout the stress-controlled fatigue test. Accordingly, the ultimate strains in Table 6.5 were calculated based on Eq. 6.18.

$$\varepsilon_{ult} = \frac{\sigma_{t,max}}{E_{50\%}} \times 10^6 \tag{6.18}$$

in which, $\sigma_{t,max}$ is the maximum applied cyclic tensile stress (MPa), $E_{50\%}$ is the modulus equivalent to 50% initial flexural modulus (MPa), and ε_{ult} is the ultimate strain at fatigue failure ($\mu\varepsilon$). Based on Table 6.5, the mean values of the *k*-parameter are equal to 1.04 and 0.75 for Hornfels CTB and Siltstone CTB respectively. These values are lower than the *k*-parameters obtained from the test results in this research (see Table 6.2).

Table 6.5: Test results summary of fatigue test performed by R. Yeo (2012)

Specimens	Curing Time (Days)	Stress Ratio [a]	Initial Flexural Modulus [b] (MPa)	Initial Applied Strain [c] ( )	No. of Cycle to 50% Modulus Reduction	Ultimate Strain [d] ( )
Hornfels CTB						
BL 6	28	0.61	15,100	40	N.A.	N.A.
BL 3	28	0.62	14,820	42	64,441	83.81
A05-427	28	0.73	16,380	45	33,381	89.01
A05-424	28	0.71	15,300	46	N.A.	N.A.
BL 2	28	0.72	15,340	47	13,291	92.68
BL 5	28	0.70	13,830	51	1,081	93.61
A05-423	28	0.85	16,560	52	10,991	101.81
BL 4	28	0.64	12,410	52	3,061	103.14
A05-426	28	0.83	15,260	54	17,031	108.39
A05-425	28	0.87	15,380	56	2,871	112.48
BL 1	28	0.80	13,100	61	241	122.14
Siltstone CTB						
A05 429-2	32	0.48	11,707	47	N.A.	N.A.
PH 3b	28	0.34	6,724	57	289,121	113.33
A05 431-2	38	0.63	12,210	58	N.A.	N.A.
A05 429-1	30	0.63	11,719	60	N.A.	N.A.
PH 1	28	0.61	10,895	63	N.A.	N.A.
A05 428	28	0.63	10,980	64	150,797	128.23
PH 3a	28	0.47	8,065	65	411	129.45
PH 2a	28	0.56	8,415	74	4,071	148.54
A05 430-2	37	0.70	9,550	83	496	164.61
PH 2b	28	0.59	6,810	98	461	192.95

a Stress ratio = σ/FS
b Mean modulus over the first 50 loading cycles (R. Yeo, 2012)
c Mean tensile strain over the first 50 loading cycles (R. Yeo, 2012)
d Estimated using Eq. 6.12

The ALF test results reported by R. Yeo (2012) are illustrated in Figures 6.15 and 6.16 for Hornfels CTB and Siltstone CTB, respectively. It should be emphasised that the relationship lines between the modulus reduction ratio and the number of ALF loading cycles were reproduced using Eq. 6.19 (R. Yeo, 2012).

$$\frac{E_D}{E_i} = m \times Ln(N_{ALF}) + a \tag{6.19}$$

in which, N_{ALF} is the number of ALF loading cycles (×1,000 cycles), and m and a are the regression parameters, summarised in Table 6.6.

Table 6.6: Regression parameters for the relationship lines between modulus reduction and number of ALF load cycles (Austroads, 2008b; R. Yeo, 2012)

Parent Material	ALF Half-Axle Load (kN)	Equivalent Stress Ratio**	*m*	*a*	R^2	*n*	E_i (MPa)	No. of Cycle to 50% E_i
Hornfels	40	0.66	-0.077	0.944	0.85	14	11,900	313
	60	0.68	-0.093	0.746	0.95	21	6,100	14
	80	1.18	-0.097	0.666	0.93	22	11,000	6
Average*							**12,000**	
Siltstone	40	0.80	-0.049	0.856	0.84	13	12,800	-
	50	0.94	-0.057	0.830	0.86	7	10,500	322
	60	0.96	-0.061	0.748	0.93	18	11,300	58
	80	1.13	-0.070	0.649	0.94	11	11,500	8
Average*							**11,000**	

n = Number of data points

E_i = Initial modulus of CTB layers

Average* = Values determined by R. Yeo (2012)

Stress Ratio** = Equivalent tensile stresses divided by laboratory-measured *FS* at 95-97 days

The modulus reduction curves of the CTB layers measured during the ALF tests behaved differently from those obtained from the four-point bending tests. Figure 5.9 illustrates that the normalised cyclic flexural modulus (E_D/E_i) curves developed from the laboratory test results can be divided into three different phases, as detailed in Austroads (2010a) (see Figure 2.10). Similar to Theyse, De Beer, and Rust (2014), three phases of E_D/E_i curves were also observed in ALF test results (see Figure 2.9).

However, the E_D/E_i curves in the third phase of the ALF test behaved in a different way to the curves developed from the laboratory test results. The equivalent granular phase was observed from the ALF test results where the modulus of the CTB layers reduced to the minimum value and remained constant. On the contrary, the modulus of CTB specimens in the third phase reduced dramatically until they were broken by the cyclic loads. The variation between fatigue response observed from the laboratory tests and ALF tests may be caused by various factors. The first important factor is the difference in the support conditions between two tests. The CTB specimens were supported by two steel rollers at the base of specimens with a distance of 300 mm, while the CTB layers were fully supported by the subbase layers in the field. Loading conditions and configurations should be considered as another important factor. In the laboratory, the specimens were tested using a constant load magnitude and frequency. Cyclic loads were continuously applied on top of the CTB specimens with two steel rollers located at a distance of 100 mm. This is unlike the field conditions where pavement structures were loaded by using a moving wheel. The CTB layer in the pavement structure was usually overlaid with an AC layer, which means the moving wheel was indirectly applied on the top of the CTB layer through the AC layer. The other factors which may contribute to variation include degree of compaction, compaction method, moisture, curing time, and environmental factors.

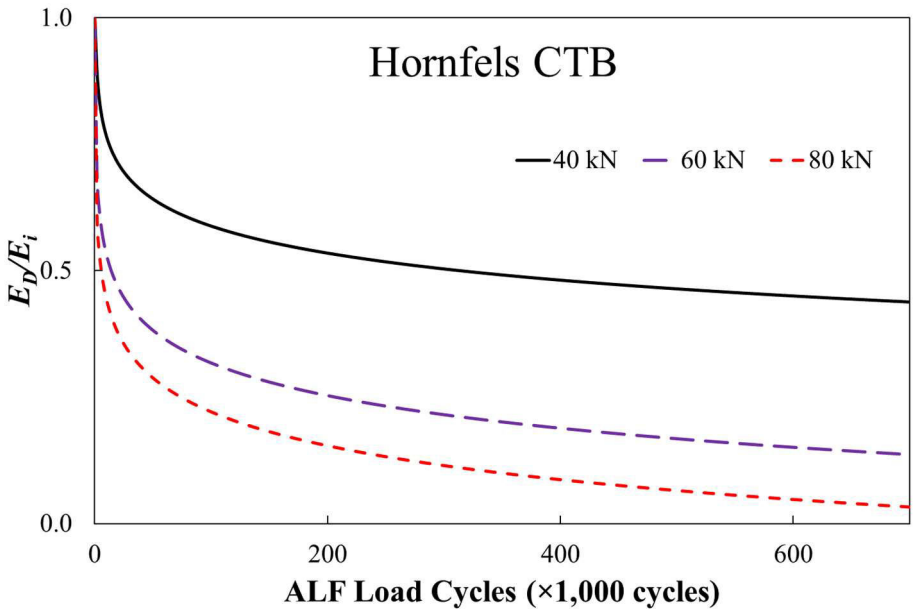

Figure 6.15: Reduction in modulus of Hornfels CTB layer with ALF loading cycles (modified from R. Yeo (2012))

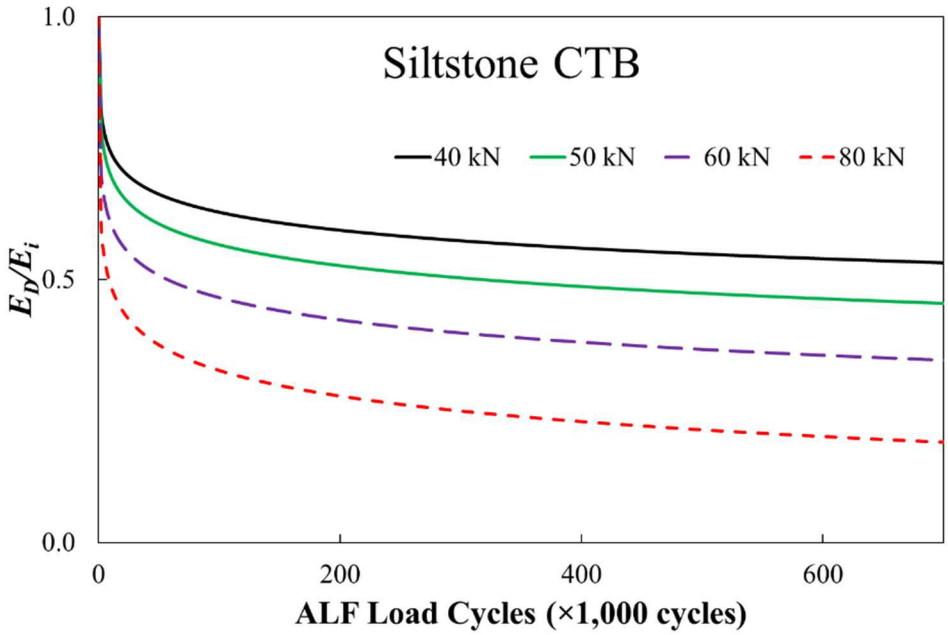

Figure 6.16: Reduction in modulus of Siltstone CTB layer with ALF loading cycles (modified from R. Yeo (2012))

From the ALF tests performed by R. Yeo (2012), the damage variables of the ALF test were calculated based on Eq. 6.20.

$$D(\varepsilon) = \frac{\sigma_{ALF}/E_D - \sigma_{ALF}/E_i}{\varepsilon_{ult} - \sigma_{ALF}/E_i} \tag{6.20}$$

in which, σ_{ALF} is the constant stress applied during the ALF test, E_D is the modulus of CTB layers measured at current ALF loading cycles, and E_i is the initial modulus of the CTB layers. The back-calculated initial moduli used for damage variable calculation can be found in R. Yeo (2012). The mean moduli equal to 12,000 MPa for Hornfels CTB and 11,000 MPa for Siltstone CTB were reported by the author.

Figures 6.17 and 6.18 illustrate the damage evolution of Hornfels CTB layers and Siltstone CTB layers, respectively.

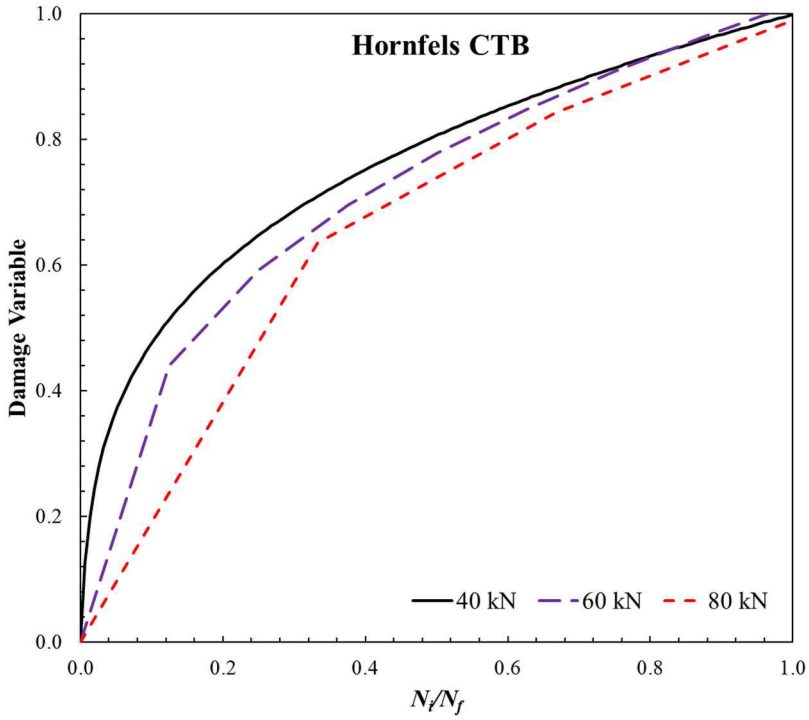

Figure 6.17: Damage evolution of Hornfels CTB calculated based on the ultimate strain defined by 50% modulus reduction approach

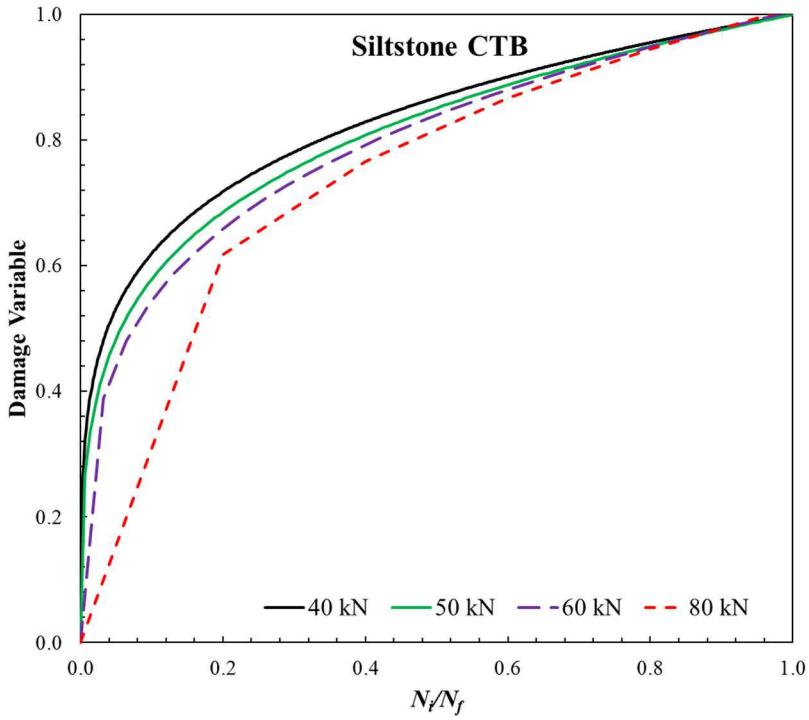

Figure 6.18: Damage evolution of Siltstone CTB calculated based on the ultimate strain defined by 50% modulus reduction approach

The dissipated energy approach was also employed in this section to determine the fatigue life of CTB layers tested by the ALF. However, the failure cycle cannot be assigned from the *DER*-N_i curve such as the example shown in Figure 6.6. Figure 6.19 illustrates that the peak value of *DER* was unable to be defined from the ALF test results. This is because the failure of the CTB layer tested by the ALF was not sudden as was the failure of the CTB specimens tested in laboratory. Moreover, it should be highlighted that the inputs for damage calculation in the ALF tests were estimated from Eq. 6.19. Therefore, the failure cycle of CTB layers may be difficult to determine from the dissipated energy approach, since the relationship curve strongly depends on the empirical equation (Eq. 6.19). It also obscures the fact that the changes in cyclic flexural modulus in the field and during the ALF test are caused by either changes in stress, changes in strain, or a combination of both. Unlike the results from the laboratory test, the applied stress or strain is perfectly controlled using the testing facilities in the laboratory. Accordingly, the magnitude of applied stress or strain can be precisely maintained during the tests. The fatigue life of CTB layers tested by the ALF was then initially defined based on the 50% modulus reduction approach. The same fatigue failure assumption was also employed by De Vos (2007) and R. Yeo (2012).

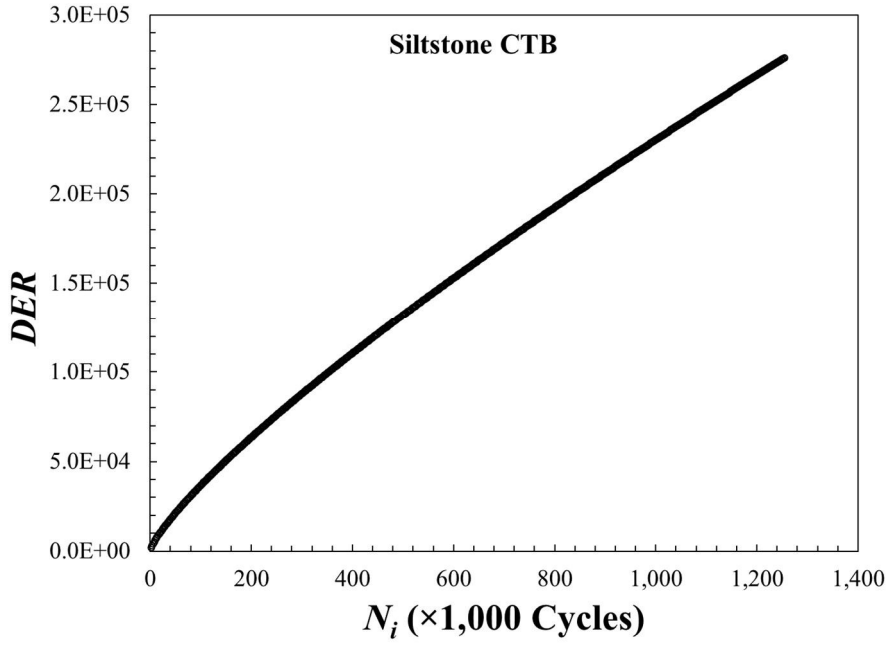

Figure 6.19: Relationship between *DER* and number of loading cycles from the ALF test with 40-kN load on the Hornfels CTB layer

In Mozambique, De Vos (2007) performed the ALF test on a pavement structure with a cement stabilised sand base layer. After the pavement structures were loaded using a certain number of loading cycles, transverse cracks were usually generated by the ALF load prior to longitudinal cracks. The transverse cracks propagated from the bottom of the CTB layer and could be seen on the asphalt surface. If the ALF loads were continually applied to the pavement structures, longitudinal cracks began to form through the junction of two adjacent transverse cracks. Accordingly, the modulus reduction rate of CTB layers in the longitudinal direction was more dramatic than the reduction rate in the transverse direction. Moreover, the modulus in the bottom zone of the CTB layer was reduced more severely than the modulus in the top and middle zones of the CTB layer. After the longitudinal cracks had propagated from the bottom of the CTB layer up to approximately two-thirds of the layer depth, a shear plane then developed through the connection of the longitudinal cracks in the horizontal direction. At this stage, the CTB blocks were finally formed. In excavating the pavement section, where the modulus of the CTB layer was reduced to 50% of the initial value, the investigation produced all the failure modes explained above. The application of a wheel load on the pavement structures after block formation broke the blocks down further to a smaller size. At this final stage, the CTB material may be deemed equivalent to the "*granular equivalent phase*" described by Theyse et al. (2014). Therefore, the "*effective fatigue life phase*" may be defined as the period of loading from the beginning of the ALF test to the cycle at failure (50% modulus reduction) (De Vos, 2007).

6.2.4 Comparison between damage evolution calculated from laboratory tests and ALF tests

In this section, the damage behaviour of CTB specimens tested in the laboratory and CTB layers tested by the ALF were compared. It is understood that the field pavement tested by the accelerated pavement testing facility (or ALF in this research) provided more reliable results than those achieved from the laboratory tests. However, field tests using ALF are more costly and difficult. This can be logically explained by the relationship chart illustrated in Figure 6.20 (Hugo, McCullough, & Van der Walt, 1991). Accordingly, it would be of great advantage to pavement engineers if fatigue behaviour in field pavement could be reasonably explained by laboratory test results.

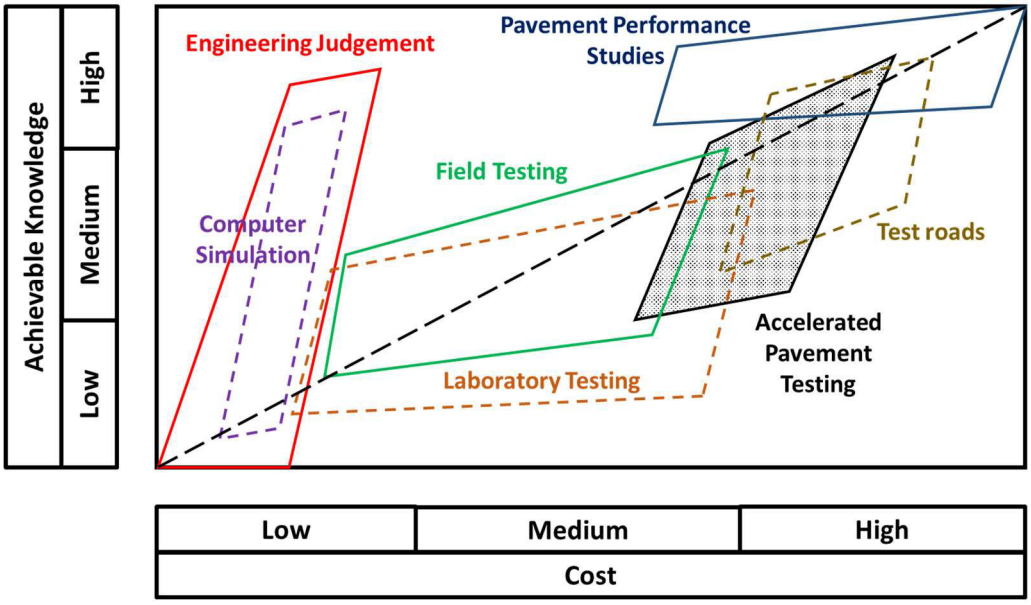

Figure 6.20: Relationship between financial investment and achievable knowledge (Hugo et al., 1991)

Figure 6.21 demonstrates the damage evolution examples calculated from the four-point bending test results and the ALF test results. The damage evolution estimated from laboratory test results was produced from specimens tested by cyclic loads ranging from 0.60*FS* to 0.85*FS*. It can be seen from Figure 6.21 that at low cycle ratios ($N/N_f = 0 – 0.20$), the damage variables calculated from the ALF test results increased more rapidly than those calculated from the four-point bending test results. In the zone of low cycle ratios, the damage variables in the ALF test rose to 0.40 – 0.70, while the damage variables of the four-point bending test results increased to approximately 0.25 - 0.45. The damage variables calculated from the four-point bending test results rose steadily to approximately 0.80 when the cycle ratios were increased from 0.20 to 0.90. Similarly, the damage variables of the ALF test results increased with a constant rate of 0.95 at the cycle ratio of 0.90. Figure 6.21b shows that the CTB layers consistently deteriorated at a constant rate until the material's moduli reduced to 50% of its initial value ($D = 1$) at $N/N_f = 1$. However, for the cycle ratios ranging from 0.90 – 1, the damage rate of the CTB specimens accelerated again until the specimens failed from the cyclic loads.

The different behaviour of CTB materials at a high cycle ratio ($N/N_f = 0.90 – 1$) was greatly affected by the supporting conditions and loading conditions as mentioned

earlier. Accordingly, the failure scheme developed in the CTB layers was different to that which was observed in the CTB specimens.

It can be seen from Figure 6.21 that the pre-cracked phase of the CTB layer in the field test may be comparable to the flaw initiation phase of the CTB specimens. The damage variables calculated from the CTB specimens and CTB layers dramatically rose within this initial phase as shown in Figures 6.21a and b, respectively. Similarly, the damage variables of CTB specimens and CTB layers steadily increased in the second phase as explained earlier. Therefore, the effective fatigue life phase of the CTB layers was assumed to be equivalent to the micro-crack development phase of CTB specimens. The damage rate of the CTB specimens increased again in the failure phase until the specimens were broken by the cyclic load. On the other hand, the damage rate of CTB layers stayed at the same rate as the effective fatigue life phase in the equivalent granular phase (not shown in Figure 6.21b). The damage behaviour of CTB layers in the equivalent granular phase can be observed in Figure 2.9. Consequently, the damage evolution curves of CTB specimens should be adjusted to match the results of the ALF tests. The fatigue failure of CTB specimens can be assumed to be located at the end of the micro-crack development phase or at the beginning of the macro-crack development phase (see Figure 6.21a).

Figure 6.22a shows the modified damage evolution curves of CTB specimens by defining the end of the micro-crack development phase as the fatigue life. The damage evolution curves shown in Figure 6.22a then fitted with the power model as illustrated in Figure 6.22b. Eq. 6.21 represents the power model used in this research.

$$D(\varepsilon) = \theta_4 \left({}^{N_i}\!/\!_{N_f} \right)^{\theta_5} \tag{6.21}$$

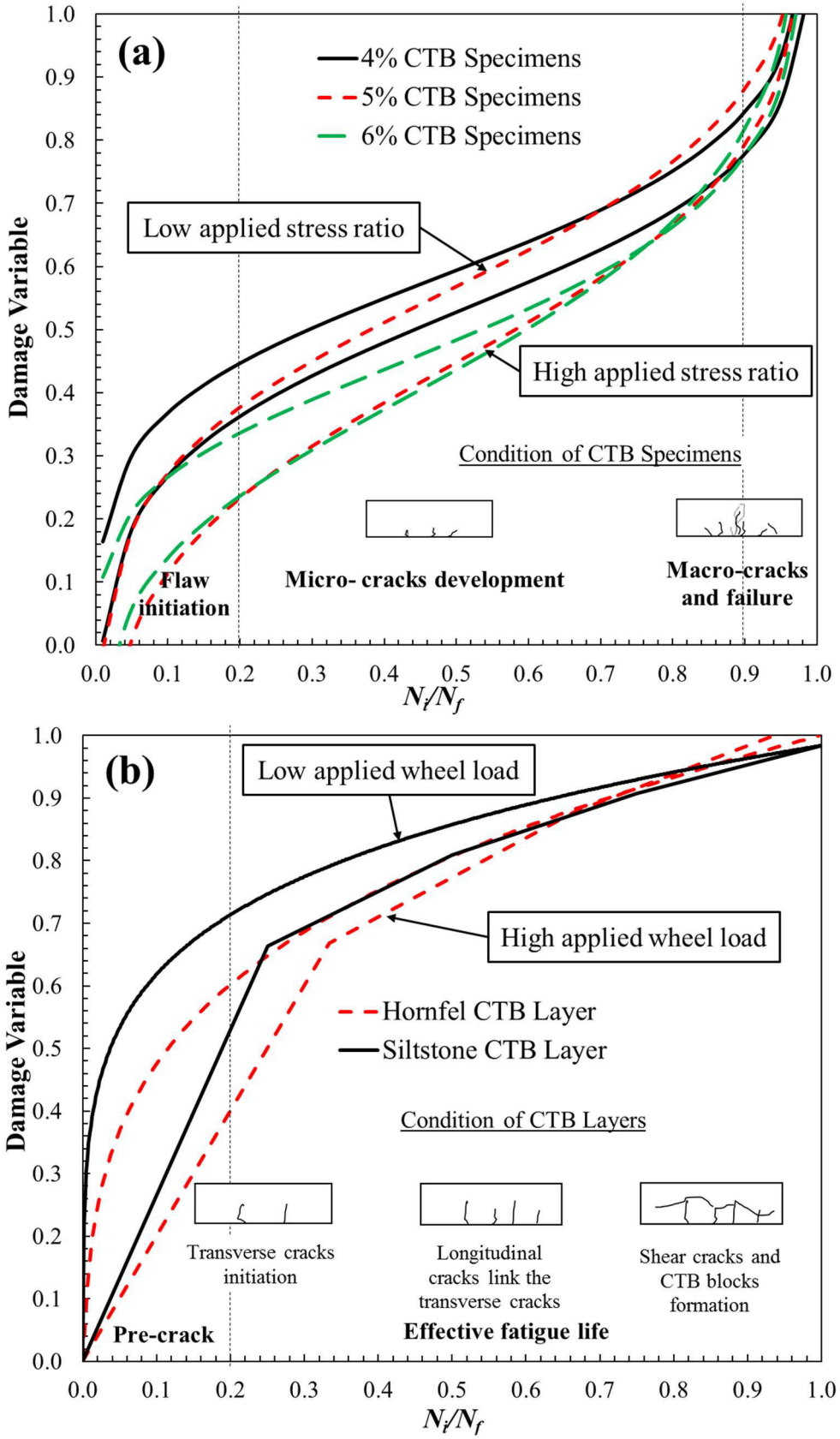

Figure 6.21: Damage evolution curves calculated from (a) cyclic four-point bending test results, and (b) ALF test results

In which, θ_4, and θ_5 are the regression parameters. At the maximum cycle ratio (N/N_f = 1), the damage of all specimens reached one. Therefore, the parameter θ_4 of all specimens is equal to one. This means that the damage variables of CTB specimens depend on the θ_5-parameter only. Table 6.7 summarises the regression parameters for the modified damage evolution curves. At the end of the micro-crack development phase, the moduli of all beam specimens reduce to approximately 66% of initial values, as illustrated by Table 6.8. Therefore, the termination criteria for CTB layers from the ALF test was assigned at the cycle where the modulus of CTB layers was equivalent to 66% of the initial modulus. The amended damage evolution curves of cement-treated Hornfels and Siltstone are presented in Figure 6.23.

Table 6.7: Regression parameters for the modified damage variable calculation

Specimen	σ/FS	θ_5	*Standard Error*
4% cement content specimens			
S-21	0.65	0.345	0.067
S-20	0.75	0.491	0.056
5% cement content specimens			
S-3	0.70	0.559	0.068
S-28	0.70	0.500	0.086
S-16	0.75	0.603	0.052
S-5	0.80	0.660	0.082
S-18	0.85	0.719	0.058
6% cement content specimens			
S-26	0.65	0.453	0.070
S-24	0.75	0.611	0.068

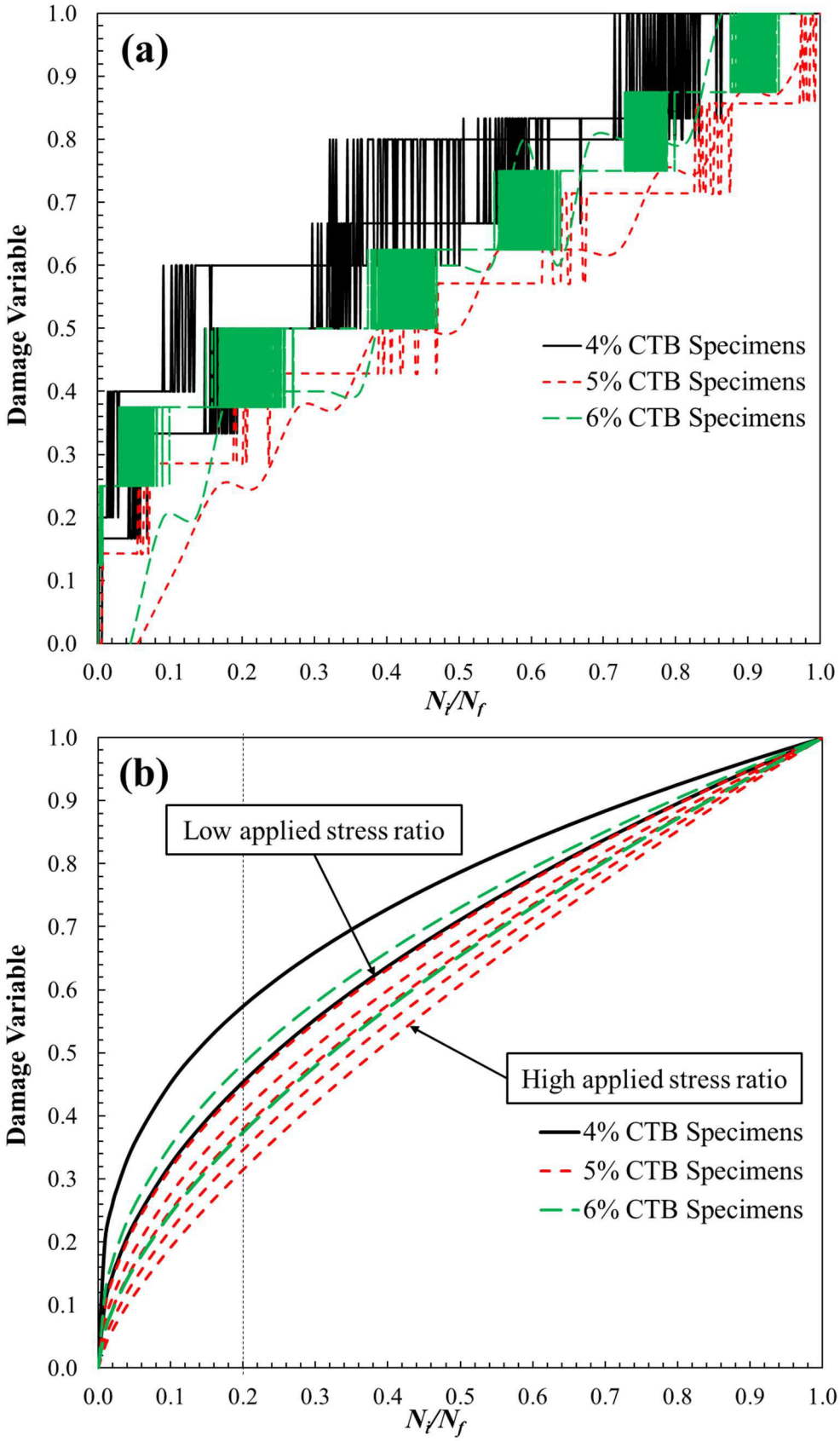

Figure 6.22: (a) Modified damage evolution calculated from cyclic four-point bending test results, and (b) Damage evolution trends fitted with power model

Table 6.8: Moduli of CTB specimens at failure defined by different approaches

Specimen	σ/FS	E_i (MPa)	Moduli at Different Fatigue Failure Assumptions			
			Dissipated Energy Ratio		Modified Dissipated Energy Ratio	
			MPa	% of E_i	MPa	% of E_i
4% cement content specimens						
S-21	0.65	17,200	11,000	64%	11,500	67%
S-20	0.75	18,000	11,600	64%	12,100	67%
5% cement content specimens						
S-3	0.70	20,300	12,700	63%	13,300	66%
S-28	0.70	23,100	14,800	64%	15,600	68%
S-16	0.75	18,700	11,600	62%	11,900	64%
S-5	0.80	21,600	14,100	65%	14,700	68%
S-18	0.85	17,700	10,400	59%	11,200	63%
6% cement content specimens						
S-26	0.65	21,800	13,000	59%	13,900	64%
S-24	0.75	19,200	12,400	65%	12,900	67%
Average Percentage				**63%**		**66%**

The comparisons between the modified damage evolution calculated from four-point bending test results and the damage evolution calculated from the ALF test results are illustrated by Figure 6.23. It can be seen from Figure 6.23 that the modified damage variables calculated from the four-point bending test results are comparable to the damage variables determined from the ALF test results. Pavement engineers may now benefit if the damage behaviour of the CTB layer in a pavement structure can be predicted from laboratory test results (see Figure 6.20). The findings in this research demonstrate that the damage behaviour of field CTB was reasonably described by the cyclic four-point bending test results. These findings are summarised as follows:

- The damage behaviour of CTB specimens in the first phase of the cyclic four-point bending test was similar to that of the CTB layers tested by the ALF in the field. The first phase of damage development represented by the cyclic ratio ranged between 0 and 0.2 in this research. Within this first phase, the damage variable of CTB specimens and CTB layers increased to more than 50% of the fatigue life for the lower strength materials and lower applied stress ratios, as illustrated by Figure 6.23.

- In the second phase of damage development, the damage variables of CTB specimens and CTB layers steadily increased to the failure stage. At failure, the damage variables of CTB materials and cycle ratio are equal to one.

- The CTB specimens and CTB layers behaved similarly under different loading levels. Within the first phase of damage evolution, the higher loading levels created less damage on the CTB specimens and CTB layers compared to those tested under lower loading levels. The damage created by higher loading levels then accelerated within the final phase of damage evolution. It can be concluded from Figure 6.23 that the damage rate produced by the higher applied loading levels was more consistent than the rate of damage created by lower applied loading levels.

- Cement equivalent to 3% and 4% of dry weight was used to treat the Hornfels base course and Siltstone base course, respectively (R. Yeo, 2012). Therefore, the damage in the 4% specimens developed the closest similarity to the damage to the cement-treated Siltstone layers from the ALF test. It should be noted that the 28-day Flexural Strength (*FS*) of 4% specimens measured in this research was 1.99 MPa (see Table 3.5), while 1.26 MPa was reported as the 95-day *FS* for cement-treated Siltstone by R. Yeo (2012). Moreover, the applied stress ratios of 4% specimens in this research were equal to 0.65 to 0.75. On the other hand, higher applied stress ratios (see Table 6.6) were employed during the ALF test of CTB layers.

- The CTB specimens and CTB layers with lower initial modulus seemed to incur damage faster during the flaw initiation and pre-cracked phase. Accordingly, the 4% specimens (E_i = 16,800 MPa) had the highest damage rate of the other specimens (E_i = 20,000 MPa) within the flaw initiation phase. Similarly, the damage variables of cement-treated Siltstone layers (E_i = 11,000 MPa) were higher than the damage variable of cement-treated Hornfels layers (E_i = 12,000 MPa) within the pre-cracked phase.

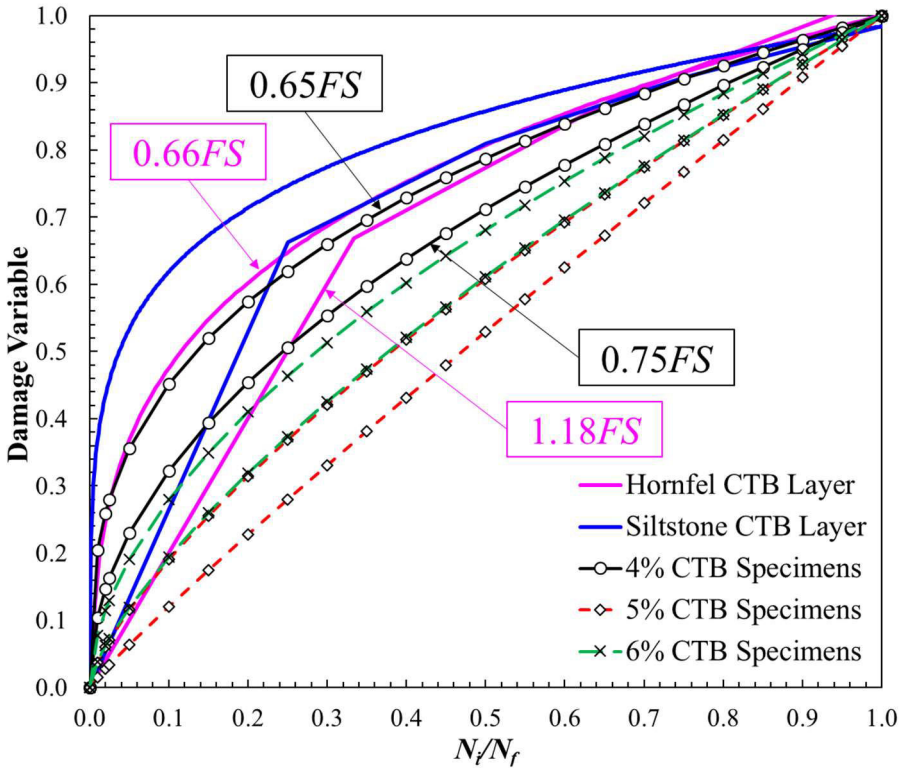

Figure 6.23: Comparison between modified damage evolution calculated from four-point bending test results and ALF test results

6.3 Estimation of field fatigue life based on damage evolution obtained from laboratory test results

In the previous section, the damage evolution of CTB specimens and CTB layers was characterised based on the CDM framework. The comparison between damage evolution calculated from four-point bending test results and field ALF test results indicated that the damage behaviour of CTB layers in the field could be logically described by the four-point bending test results. To do this, the damage evolution of laboratory test results was modified to match with the ALF test results. The end of the micro-crack development phase, or the beginning of the macro-crack development phase was assumed to be the point of fatigue failure for CTB specimens (see Figure 6.21a). At the failure point of the CTB specimens specified in this research, the moduli of specimens reduced to 66% of the initial values (see Table 6.8). Accordingly, the fatigue life of CTB layers was defined at the loading cycle where the moduli of CTB layers was equal to 66% of the initial modulus.

It can be seen from Figure 6.23 that the damage to CTB layers can be estimated based on four-point bending test results, if the damage rate is available. On the other hand, Eq. 6.21 can be used to predict the damage variable with respect to the increase in the number of loading cycles in terms of cycle ratio (N/N_f). The fatigue life of CTB layers may then possibly be estimated from the damage evolution of CTB specimens by employing the following steps:

1. Estimate the fatigue life of CTB specimens (N_f) from any fatigue life estimation model based on the applied stress level expected in the field. For example, Figure 6.24 may be used to obtain the N_f values, if the same CTB material was used to construct the pavement structures. The curve shown in Figure 6.24 is different from Figure 5.14, since fatigue failure was assigned at the number of cycles where the modulus of CTB materials was equal to 66% of initial values. However, the fatigue prediction equation produced in Figure 6.24 did not differ greatly from the predictions obtained from Figure 5.14.

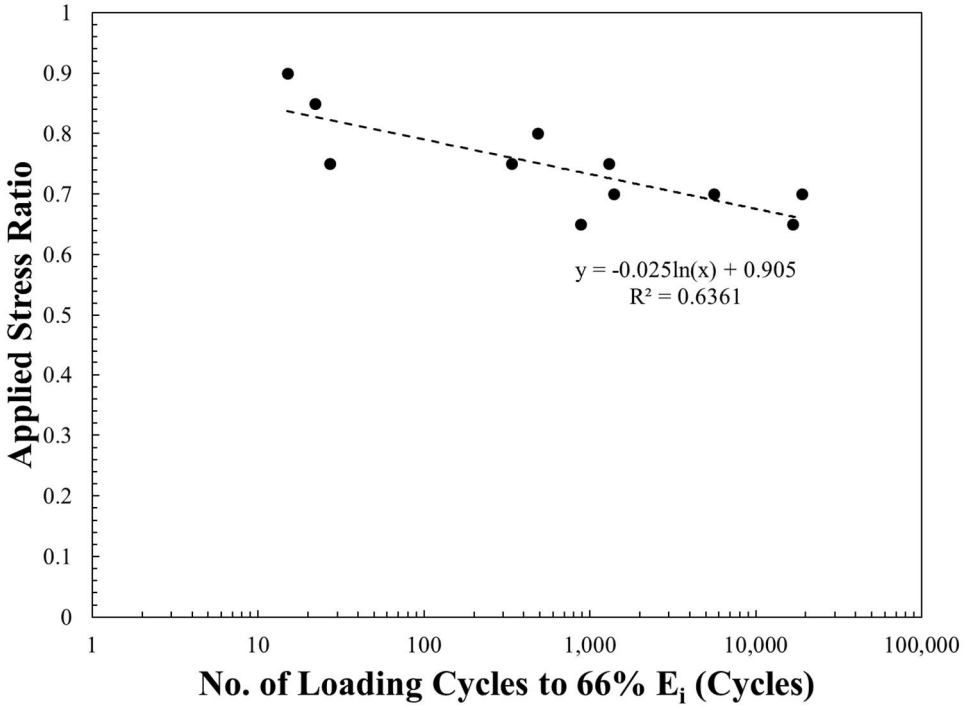

Figure 6.24: Number of applied loading cycles to 66% E_i versus applied stress ratio

2. Assume the fatigue life of CTB layers in the field is equal to the fatigue life of CTB specimens at the equivalent applied stress ratio. Based on the analysis

results in this research, assume the CTB materials reach failure from the cyclic load or traffic load when the modulus of CTB materials reduces to 66% of the initial modulus.

3. Determine the damage evolution curves of CTB specimens based on Eq. 6.21 and the regression parameters provided in Table 6.7. The regression parameter, θ_5, shown in Table 6.7 were also plotted against the applied stress ratios as shown in Figure 6.25.

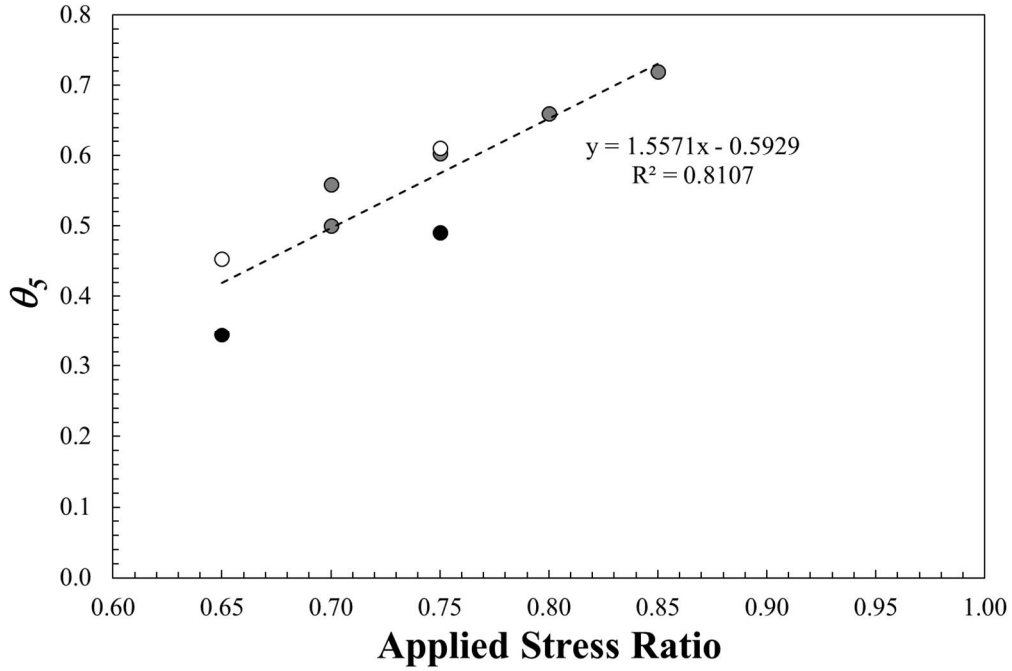

Figure 6.25: Regression parameter (θ_5) versus applied stress ratio

4. At this stage, assume the damage evolution of CTB layers in the pavement structure to be the same as that of the CTB specimens tested in the laboratory. However, the fatigue life of CTB layers should be recalculated based on the real rate of damage induced by traffic loads in the field.

5. Based on the fatigue estimation approach proposed in this research, only the rate of damage in the early stages of traffic loading is required in the recalculation process. This is because the damage evolution trend of CTB layers in the pavement structure is assumed to be equivalent to the CTB specimens tested in the laboratory. The recalculated fatigue life of CTB layers can then be determined by Eq. 6.22.

$$D(\varepsilon_A) - D(\varepsilon_o) = \frac{\varepsilon_A - \varepsilon_o}{\varepsilon_{ult} - \varepsilon_o} - 0 = \left(N_A / N_f\right)^{\theta_5} - 0 \qquad (6.22)$$

in which, ε_A is the tensile strain at the bottom of the CTB layer measured at any time after the road pavement is open for service, ε_o is the initial tensile strain of the CTB layers, ε_{ult} is the tensile strain determined by dividing the applied tensile stress by $E = 0.66E_i$, and N_A is the number of Standard Axle Repetitions (*SAR*) determined from the real pavement site. On the other hand, the rate of damage may be estimated based on a numerical approach or an analytical approach. Therefore, the recalculated N_f is the only unknown variable in Eq. 6.22.

Table 6.9 illustrates the fatigue life of a CTB layer estimated by the proposed approach developed in this research. It can be seen from Table 6.9 that the estimated N_f of cement-treated Hornfels layer was reasonably close to the fatigue life of the CTB layer measured during the ALF tests. However, the estimated N_f of cement-treated Siltstone were largely different from the measured N_f. It should be emphasised that the estimation of ALF fatigue life was performed using the damage evolution of cement-treated granite (parent material employed in this research). Therefore, the accuracy of the prediction model would be improved if the damage evolution curve is developed based on the same parent materials.

The fatigue life estimation approach developed in this research is summarised in the diagram shown in Figure 6.26.

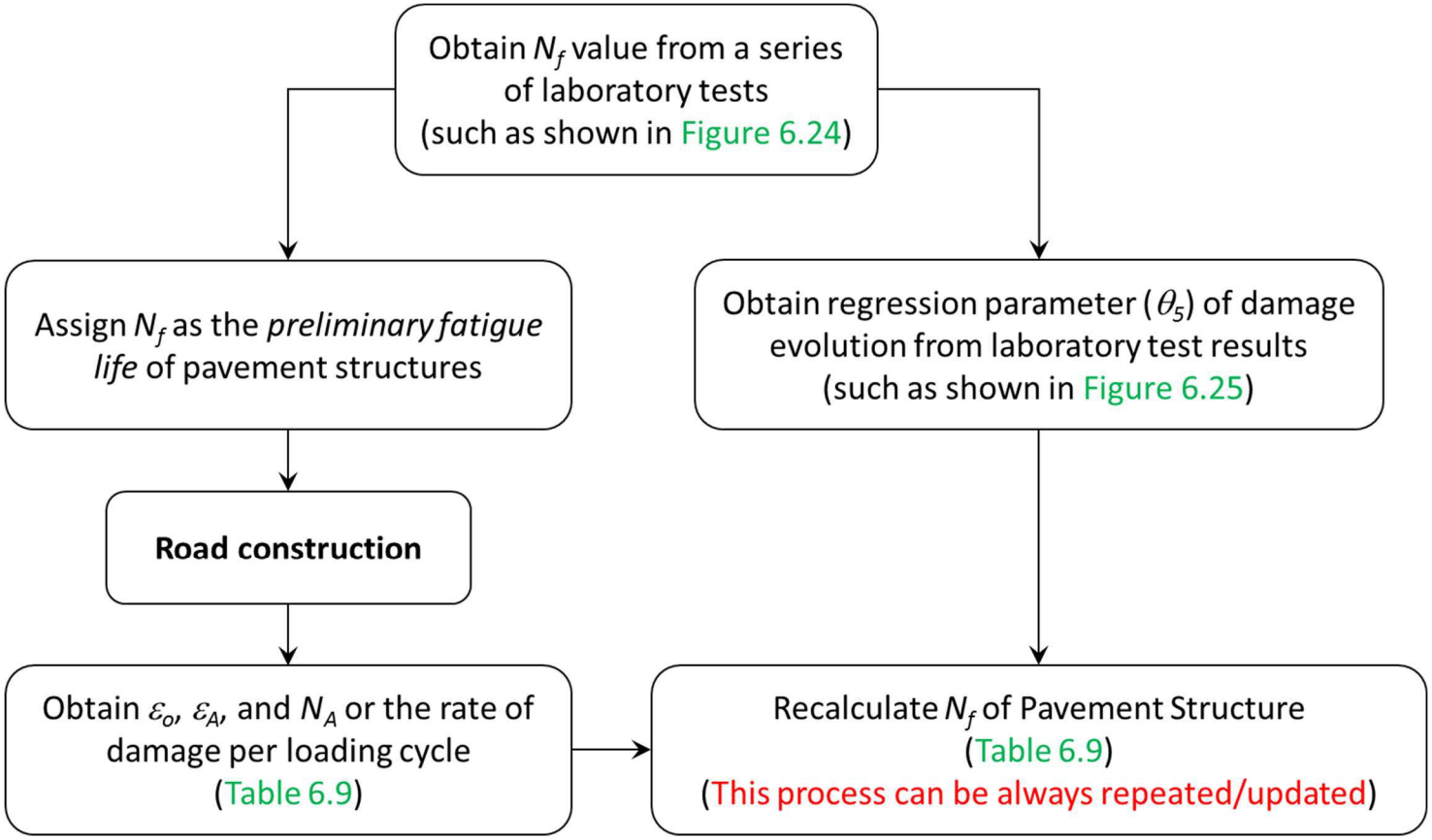

Figure 6.26: Fatigue life estimation procedure for the cement-treated base layer in the road pavement structure

Table 6.9: Fatigue life of CTB layers predicted using the approach developed in this research

Applied Stress Ratio	N_f of CTB Specimen* (Cycles)	θ_5 (see Figure 7.25)	ε_o ($\mu\varepsilon$)	ε_{ult} ($\mu\varepsilon$)	ε_A ($\mu\varepsilon$)	N_A (Cycles)	**Estimated N_f (Cycles)**	**Measured N_f* (Cycles)**
Hornfels CTB Layers								
0.66	17,500	0.736	70	106	79	2,000	**53,317**	**52,000**
0.68	80	0.742	140	212	205	2,000	**2,473**	**4,000**
1.18	100	0.881	135	254	225	2,000	**2,492**	**3,000**
Siltstone CTB Layers								
0.80	368,000	0.775	70	106	85	2,000	**7,504**	**N.A.**
0.94	39,000	0.814	100	152	126	2,000	**4,296**	**52,000**
0.96	53,900	0.819	95	144	135	2,000	**2,523**	**12,000**
1.13	21,400	0.867	110	199	183	2,000	**2,373**	**4,000**
*	Values estimated from prediction equations developed by R. Yeo (2012)							
N.A.	Not Available (The modulus of CTB layer did not reduced to 50% initial value during the ALF test)							

6.4 Conclusion and recommendations

The fatigue damage in concrete, asphalt concrete, and cement-treated materials induced by cyclic loads has been successfully characterised based on the CDM framework by many researchers. However, previous work has focused on the damage behaviour in either laboratory-prepared specimens or CTB layers in pavement structures. The damage evolution of the CTB materials developed from the laboratory test results and ALF test results were compared in this research. Accordingly, the damage characteristics of CTB layers in the field can be reasonably forecast by the damage evolution of CTB specimens tested in the laboratory. Important key findings discovered from the analysis in this chapter are as follows.

- The 50% modulus reduction approach and dissipated energy approach were used to define the fatigue life of CTB materials in this research. The number of cycles at the specimen modulus equivalent to 50% initial values was chosen as the fatigue life based on the 50% modulus reduction approach. For the dissipated energy approach, the peak point from the relationship curve between *DER* and N_i was designed as the fatigue life of CTB specimens tested by the stress-controlled fatigue test. However, the fatigue life determined based on the dissipated energy ratio approach was always lower than that obtained using the 50% modulus reduction approach. This is because the fatigue life of materials determined from the dissipated energy approach represents the crack initiation point.

- The damage evolution curves of CTB specimens developed from the dissipated energy approach aligned reasonably with the damage evolution of specimens tested by other researchers. Moreover, the damage variables calculated based on the dissipated energy approach developed closely along the lines of the damage variable determined from Palmgren-Miner's law. However, the dissipated energy per loading cycle of the CTB specimens in this research was estimated based on Eq. 6.9. It is recommended that the exact values of dissipated energy should be used for determining the fatigue life of CTB materials. This requires complete information on the load and displacement on each hysteresis loop, as illustrated in Figures 6.3 and 6.5.

- In the primary stage, the evolution curves of CTB specimens developed based on the dissipated energy approach was compared to the damage evolution curves of CTB layers calculated based on the 50% modulus reduction approach. The damage evolution curves developed from the CTB materials tested in the laboratory and tested in the field can be divided into three phases. The material deterioration accelerated at the first phase until the cycle ratio reached approximately 0.2. The material damage in the second phase then developed steadily until the cycle ratio approached 0.8. In the third phase, the damage to CTB specimens accelerated again until the specimens failed from the cyclic loads. On the other hand, the damage to CTB layers developed steadily when the materials were degraded into the smaller blocks.

- The comparison between damage evolution curves in the primary stage revealed that the damage evolution of CTB layers in the field can be reasonably forecast by the damage evolution of CTB specimens tested in the laboratory. Therefore, the loading cycle at the end of the micro-crack development phase (or at the beginning of the macro-crack development phase) was assigned as the failure point of CTB specimens. At this failure point, the moduli of beam specimens were reduced to 66% their initial values. Accordingly, the fatigue life of CTB layers was reassigned at the loading cycle where the moduli of CTB layers were equal to 66% of their initial values (see Figure 6.23).

- The fatigue life estimation framework for CTB layers in the field was then developed based on the damage characteristics of CTB specimens tested in the laboratory. The significant points of the developed framework are listed as follows:
  (1) The damage characteristics in CTB specimens tested in the laboratory can be used to explain material deterioration in the field under real traffic loads,
  (2) unlike the other fatigue life prediction models, the applied stress, initial strain, and material modulus were required as the inputs for estimating the fatigue life of CTB layers in the fields, and

(3) the damage levels of CTB layers can be progressively monitored and forecast using damage evolution curves. In addition, the fatigue life of CTB layers can always be updated or recalculated based on current traffic loads.

CHAPTER 7

CONCLUSIONS AND RECOMMENDATIONS

7.1 Conclusions

A comprehensive study of cement-treated materials for road pavement basecourse was conducted in this research. The mechanical characteristics and performance of CTB were examined by both conventional and sophisticated tests in order to fill the gaps in knowledge and understand the material responses under operating conditions. This research aimed to develop a practical design criteria and an effective mechanistic-empirical design framework for cement-treated materials for road pavement basecourse. Therefore, a modified mix design framework for CTB was proposed to incorporate the effects of uncertainty that may be encountered during construction. For the mechanistic-empirical road pavement design approach, the design pavement section significantly depended on the material responses and the design parameters of road construction materials, e.g., the material modulus. However, the existing literature showed uncertainty around recent design parameters for cement-treated materials for road pavement basecourse. Accordingly, the appropriate design parameters representing the intrinsic responses of material under traffic loading conditions was defined, based on the test results in this research.

The service lifetime of a road pavement structure with a CTB layer is generally estimated from the fatigue distress model of CTB materials. This research developed a fatigue damage evolution model of CTB which characterised the performance of a road pavement structure throughout its service lifetime. In addition, the deterioration of in-situ CTB can now be forecast, based on the damage evolution of laboratory CTB, using the proposed fatigue damage evolution model.

7.1.1 Characteristics of CRB and CTB

The major findings of this research are presented below.

1. The UCS of CRB and CTB is influenced by the compacted moisture content, compacted dry density, and the degree of compaction. The maximum UCS of CTB was obtained by moulding the test specimen, using moisture content equal to OMC. However, the UCS of CRB reduced with an increase in compacted moisture content. The UCS development of CTB can be divided into three zones with respect to the amount of cement binder. The analysis results from this research revealed that the appropriate cement content for CTB should stay within the soil-cement interaction zone. Moreover, the gradation and fines content of parent material also affected the strength performance of CTB. The investigation in this research revealed that the CRB, which contained fewer amounts of particles less than 75 μm (particle passing through #200 sieve) provided a higher UCS of CTB.

2. An extended investigation into CTB's shrinkage behaviour according to the study by Chummuneerat (2014) was performed in this research. The analysis results show that the shrinkage behaviour of CTB was greatly influenced by the gradation and fines content of the parent material, and the delayed compaction time. For the parent material used in this research, the drying shrinkage of CTB increased with respect to the rise in the amount of fine particles (finer than 75 μm). Similarly, the drying shrinkage of CTB specimens compacted after mixing with cement for 2 – 3 hours were 1.6 – 2 times greater than those of CTB specimens compacted immediately after mixing with cement.

7.1.2 Modified mix design framework for CTB

3. It is possible to predict the UCS of CTB from the water-cement ratio and curing times. However, the UCS of CTB specimens prepared with moisture content less than OMC cannot be reliably estimated. This may be caused by the material grain interlocking of CTB compacted on the dry-side of OMC.

4. A modified mix design concept of CTB based upon the relationship of strength and effective water-cement ratio was suggested. The advantage of this modified mix design concept is that the amount of water and/or cement can be instantly adjusted in-situ to achieve the design strength value. On the other hand, the *actual* strength of field CTB can also be determined from the design curve without the requirement of additional tests. Accordingly, the UCS of 7-day and 28-day CTB can be estimated from the following equations:

$$q_{u,7\ days}(MPa) = 1.9171/(\frac{W_{eff}}{c})^{0.88}$$

$$q_{u,28\ days}(MPa) = 2.2635/(\frac{W_{eff}}{c})^{0.92}$$

7.1.3 Design parameters for mechanistic-empirical road pavement design approach

5. In this research, the rates of compressive loading equivalent to the static and dynamic loading rates recommended by Bischoff and Perry (1991) were employed during the conventional UCS tests. The rate of loading significantly influenced the performance of CTB. The UCS and elastic modulus (chord modulus) of CTB determined by the dynamic loading tests were usually higher than those calculated from the static loading tests. Since CTB is usually subjected to dynamic loading conditions induced by traffic in the field, static parameters should not be used for road pavement structural design.

6. Traffic loading conditions were simulated by the cyclic loading test in this research to examine the responses of field CTB. The investigation was performed using the cyclic four-point bending test and the AMPT. Accordingly, the dynamic flexural modulus and (uniaxial) dynamic modulus were obtained from the cyclic four-point bending test and the AMPT, respectively. The cyclic flexural modulus determined from the four-point bending test seemed to be very close to the dynamic modulus measured by the AMPT. However, specimen preparation for flexural tests is cumbersome and this may lead to inaccurate testing results. Accordingly, the dynamic modulus

measured by the AMPT should be employed as a design parameter in the mechanistic-empirical design of road pavement.

7. The dynamic modulus of CTB is significantly affected by the cement content and the curing duration of the test specimens. However, the loading frequency and temperature contributed minor effects to the changes in dynamic modulus. Moreover, the CTB behaved in the manner of an elastic material, since the dynamic modulus was not influenced by the changes in dynamic strain range or magnitude of the cyclic load. It should be emphasised that the dynamic modulus in this research was determined by the direct application of the cyclic load, while the indirect approach (ultrasonic pulse velocity or vibration resonance method) has been used in other research.

7.1.4 Fatigue behaviour of CTB and the proposed fatigue damage evolution model

8. Two cyclic four-point bending test platforms were employed to examine the fatigue damage behaviour of cement-treated material in this research. The stress-controlled fatigue tests demonstrated that the cyclic flexural modulus of the test specimens was normally reduced to 50% to 60% of the initial values before the specimens were completely broken by the cyclic loads.

9. The fatigue life of CTB specimens determined by the cyclic four-point bending test greatly depended on the applied stress level, the applied strain level, and the loading frequency. The fatigue life of CTB significantly reduced when the applied stress/strain level was increased. On the contrary, the loading waveform (haversine and sinusoidal) had insignificant effects on the fatigue response of CTB specimens.

10. The cement content, testing mode (stress-controlled or strain-controlled), and size of the specimens also influenced the fatigue life of CTB, determined by the cyclic four-point bending tests. However, the effects of these factors can be normalised in term of applied stress ratio, e.g. the ratio between stress level and flexural strength. Therefore, the relationship curves between the fatigue life of CTB and the applied stress ratio can be developed regardless of the effects of

cement content (Figure 6.14), or the effects of the testing mode and the size of the test specimen (Figure 6.17).

11. The results obtained from the four-point bending test in this research revealed the existence of *"the fatigue endurance limit"*. For the strain-controlled fatigue test of beam specimen sizes 50×63.5×400 mm^3, the fatigue endurance limit of a 5% cement specimen was the applied strain level under 150 $\mu\varepsilon$. The stress-controlled fatigue test of 5% cement specimens, with the dimensions of 100×100×400 mm^3, indicated an applied stress level equal to 65% of *FS* as the fatigue endurance limit. The specimens subjected to a cyclic load greater than 0.65*FS* usually failed within two hundred thousand cycles of the applied cyclic load.

12. To develop the fatigue damage evolution model, the fatigue life of CTB was redefined, based on a 50% modulus reduction approach, and a dissipated energy approach. The damage evolution curves of CTB specimens developed from the dissipated energy approach agreed reasonably well with the damage evolution of specimens tested in other literature and with Palmgren-Miner's law.

13. The damage evolution characteristics of laboratory CTB and field CTB were compared in this research. The damage evolution curves of laboratory CTB and field CTB can be divided into three phases. The first phase started from the cycle ratio equal to zero and ended at a cycle ratio approximately equal to 0.2. The damage to laboratory CTB and field CTB rose dramatically within the first phase. The damage to laboratory CTB and field CTB then developed steadily in the second phase, until the cycle ratio approached 0.8. In the third phase, the damage to laboratory CTB accelerated again until the specimens failed from the cyclic loads. On the other hand, the damage to field CTB developed steadily when the materials were degraded into smaller blocks in the third phase.

14. To develop the fatigue damage evolution model for CTB materials, the damage evolution curves of laboratory CTB were matched with the damage evolution

curves of field CTB. These comparisons led to the process of redefining the fatigue failure assumption. The loading cycle at the end of the micro-crack development phase was assigned as the failure point of laboratory CTB. At this failure point, the moduli of beam specimens were reduced to 66% of their initial values. Accordingly, the fatigue life of field CTB was reassigned at the loading cycle where the moduli of field CTB were equal to 66% of their initial values.

15. The fatigue life estimation framework for field CTB was developed based on the damage characteristics of laboratory CTB tested in this research. The significant points of the developed framework are listed as follows:

    (1) The damage characteristics of laboratory CTB can be used to explain material deterioration in the field under real traffic loads,

    (2) unlike the other fatigue life prediction models, the applied stress, initial strain, and material modulus were required as inputs for estimating the fatigue life of field CTB, and

    (3) the damage levels of field CTB can be progressively monitored and forecast using damage evolution curves. In addition, the fatigue life of CTB layers can always be updated or recalculated based on current traffic loads.

7.2 Recommendations for further work

1. The modified mix design framework for CTB materials was developed to incorporate the influences of mix proportion variation, which may emerge at construction sites. Yet the uncertainty caused by different compaction methods, delayed compaction time, and unforeseen factors have not been considered in the proposed mix design framework. These factors may be taken into accounted using a reliability based analysis approach. Further research is needed to characterise the aforementioned factors.

2. The modified mix design framework developed at this stage only accounted for the strength performance aspect. The durability performance of CTB should be implemented into the mix design framework through extended research.

3. The fatigue life of CTB materials determined by the cyclic four-point bending tests is generally uncertain due to the nature of the specimen preparation process, handling, and testing. It is recommended that the fatigue testing platform of CTB be verified by a conventional cyclic loading test, such as the uniaxial cyclic tension test, in future work.

4. The dissipated energy per loading cycle in this research was calculated based on the developed estimation equation. This is because the information obtained from the existing testing platforms was inadequate for the actual dissipated energy calculation. Therefore, the fatigue testing platform should be developed to gather enough information, i.e., load-displacement data on each hysteresis loop, during the fatigue tests.

5. The proposed fatigue evolution model was verified by the field results obtained from the other research. Even though the fatigue evolution of field CTB was reasonably explained by the damage evolution model developed from the laboratory test results in this research, the parent materials and mix proportion employed in other research were different. Therefore, it is recommended that the proposed model be verified in future work. The same CTB used for developing the fatigue evolution model in the laboratory should be tested by the ALF to obtain the damage characteristics of field CTB. In summary, the model could be further developed and implemented into mechanistic-empirical road pavement design guidelines.

REFERENCES

AASHTO. (2007a). *Standard method of test for determining dynamic modulus of Hot-Mix Asphalt concrete mixtures* (AASHTO TP62). Washington, D.C.: American Association of State and Highway Transportation Officials.

AASHTO. (2007b). *Standard method of test for determining the fatigue life of compacted Hot Mix Asphalt (HMA) subjected to repeated flexural bending* (AASHTO T321). Washington, D.C.: American Association of State and Highway Transportation Officials.

AASHTO. (2008). *Mechanistic-empirical pavement design guide: A manual of practice* (Interim Edition). Washington, D.C.: American Association of State Highway and Transportation Officials.

AASHTO. (2010). *Standard practice for developing dynamic modulus master curves for Hot Mix Asphalt (HMA) using the Asphalt Mixture Performance Tester (AMPT)* (AASHTO PP61). Washington, D.C.: American Association of State and Highway Transportation Officials.

AASHTO. (2011a). *Standard method of test for determining dynamic modulus of Hot-Mix Asphalt concrete mixtures* (AASHTO T342). Washington, D.C.: American Association of State and Highway Transportation Officials.

AASHTO. (2011b). *Standard method of test for determining the dynamic modulus and flow number for Hot Mix Asphalt (HMA) using the Asphalt Mixture Performance Tester (AMPT)* (AASHTO TP79). Washington, D.C.: American Association of State and Highway Transportation Officials.

AASHTO. (2015). *Mechanistic-empirical pavement design guide: A manual of practice* (2nd Edition). Washington, D.C.: American Association of State Highway and Transportation Officials.

ACI Committee 215. (1974). *Considerations for design of concrete structures subjected to fatigue loading* (ACI 215R-74). Farmington Hills, MI: American Concrete Institute.

Adaska, W. S., & Luhr, D. R. (2004). *Control of reflective cracking in cement stabilized pavements*. Paper presented at the 5th International RILEM Conference, Limoges, France.

Aderibigbe, D. A., Akeju, T. A. I., & Orangun, C. O. (1985). Optimal water/cement ratios and strength characteristics of some local clay soils stabilized with cement. *Materials and Structures 18*(2), 103-108. doi:10.1007/BF02473376.

Alliche, A. (2004). Damage model for fatigue loading of concrete. *International Journal of Fatigue 26*(9), 915-921. doi:10.1016/j.ijfatigue.2004.02.006.

Ameen, P., & Szymanski, M. (2006). *Fatigue in plain concrete - Phenomenon and methods of analysis.* (M.Eng.), Chalmers University of Technology, Goteborg, Sweden.

American Concrete Institute. (2005). *Specifications for structural concrete ACI 301-05* (SP-15). Farmington Hills, MI.: American Concrete Institute.

Aramoon, A. (2014). *Flexural fatigue behaviour of fiber-reinforced concrete based on dissipated energy modeling.* (Ph.D.), University of Maryland, College Park, MD.

Arellano, D., & Thompson, M. R. (1998). *Stabilized base properties (strength, modulus, fatigue) for mechanistic-based airport pavement design* (Final Report, COE Report No. 4). Illinois: Center of Excellence for Airport Pavement Research.

Arora, U., Kumar, M., & Dhoopad, S. (2015). Variation of workability of fresh concrete. *Transactions on Engineering and Sciences, 3*(4), 131-140.

Artamendi, I., & Khalid, H. (2005). Characterization of fatigue damage for paving asphaltic materials*. *Fatigue & Fracture of Engineering Materials & Structures, 28*(12), 1113-1118. doi:10.1111/j.1460-2695.2005.00949.x.

Arulrajah, A., Disfani, M. M., Haghighi, H., Mohammadinia, A., & Horpibulsuk, S. (2015). Modulus of rupture evaluation of cement stabilized recycled glass/recycled concrete aggregate blends. *Construction and Building Materials, 84*, 146-155. doi:10.1016/j.conbuildmat.2015.03.048.

ASTM. (2000). *Standard test methods for compressive strength of molded soil-cement cylinders* (ASTM D1633). West Conshohocken, PA.: ASTM International.

ASTM. (2007a). *Standard practice for making and curing soil-cement compression and flexure test specimens in the laboratory* (ASTM D1632). West Conshohocken, PA.: ASTM International.

ASTM. (2007b). *Standard test method for particle-size analysis of soils* (ASTM D422). West Conshohocken, PA.: ASTM International.

ASTM. (2008). *Standard test method for direct tensile strength of intact rock core specimens* (ASTM D2936). West Conshohocken, PA.: ASTM International

ASTM. (2010a). *Standard test method for determining fatigue failure of compacted asphalt concrete subjected to repeated flexural bending* (ASTM D7460). West Conshohocken, PA.: ASTM International.

ASTM. (2010b). *Standard test method for static modulus of elasticity and Poison's ratio of concrete in compression* (ASTM C469). West Conshohocken, PA.: ASTM International.

ASTM. (2011a). *Standard practice for classification of soils for engineering purposes (unified soil classification system)* (ASTM D2487). West Conshohocken, PA.: ASTM International.

ASTM. (2011b). *Standard test method for splitting tensile strength of cylindrical concrete specimens* (ASTM C496). West Conshohocken, PA.: ASTM International.

ASTM. (2011c). *Standard test methods for moisture-density (unit weight) relations of soil-cement mixtures* (ASTM D558). West Conshohocken, PA.: ASTM International.

ASTM. (2012a). *Standard test methods for flexural strength of soil-cement using simple beam with third-point loading* (ASTM D1635). West Conshohocken, PA.: ASTM International.

ASTM. (2012b). *Standard test methods for laboratory compaction characteristics of soil using modified effort (56,000 ft-lbf/ft^3 (2,700 kN-m/m^3))* (ASTM D1557). West Conshohocken, PA.: ASTM International.

ASTM. (2013). *Standard test method for obtaining and testing drilled cores and sawed beams of concrete* (ASTM C42). West Conshohocken, PA.: ASTM International.

ASTM. (2015a). *Standard test methods for freezing and thawing compacted soil-cement mixtures* (ASTM D560). West Conshohocken, PA.: ASTM International.

ASTM. (2015b). *Standard test methods for wetting and drying compacted soil-cement mixtures* (ASTM D559). West Conshohocken, PA.: ASTM International.

Austroads. (2005). *Sample preparation - Compaction of asphalt slabs suitable for characterisation* (AG:PT/T220). Sydney, NSW: Austroads.

Austroads. (2006a). *Fatigue life of compacted bituminous mixes subjected to repeated flexural bending* (AG:PT/T233). Sydney, NSW: Austroads.

Austroads. (2006b). *Guide to pavement technology part 4D: Stabilised materials* (AGPT04D-06). Sydney, NSW: Austroads.

Austroads. (2008a). *The development and evaluation of protocols for the laboratory characterisation of cemented materials* (AP-T101-08). Sydney, NSW: Austroads.

Austroads. (2008b). *Fatigue performance of cemented materials under accelerated loading – Influence of vertical loading on the performance of unbound and cemented materials* (AP-T102-08). Sydney, NSW: Austroads.

Austroads. (2010a). *Cost-effective structural treatments for rural highways: cemented materials* (AP-T168-10). Sydney, NSW: Austroads.

Austroads. (2010b). *Guide to pavement technology part 2: Pavement structural design* (AGPT04A-08). Sydney, NSW: Austroads.

Austroads. (2011). *A laboratory study of the influenced of multiple axle loads on the performance of a cement treated material: interim report* (AP-T185-11). Sydney, NSW: Austroads.

Austroads. (2013a). *Prediction of flexural strength and breaking strain of cemented materials: Laboratory study* (AP-T251-13). Sydney, NSW: Austroads.

Austroads. (2013b). *Review of definition of modified granular materials and bound materials* (AP-R434-13). Sydney, NSW: Austroads.

Austroads. (2014a). *Cemented materials characterisation: Final report* (AP-R462-14). Sydney, NSW: Austroads.

Austroads. (2014b). *Framework for the revision of Austroads design procedures for pavements containing cemented materials* (AP-R463-14). Sydney, NSW: Austroads.

Baran, E., & Aubrey, S. R. (1987). *Preliminary report on pavement thickness design curves for Queensland conditions based on elastic layer methods* (RP531). Brisbane, QLD: Materials Branch, Department of Main Roads.

Bennett, E. W. (1980). Fatigue of plain concrete in compression under varying sequences of two-level programme loading. *International Journal of Fatigue 2*(4), 171-175. doi:10.1016/0142-1123(80)90045-6.

Bischoff, P. H., & Perry, S. H. (1991). Compressive behaviour of concrete at high strain rates. *Materials and Structures 24*(6), 425-450.

Bonaquist, R. F., Christensen, D. W., & Stump, W. (2008). *Simple performance tester for superpave mix design: First-article development and evaluation* (NCHRP Report No. 513). Washington, D.C.: National Cooperative Highway Research Program.

Brown, S. F. (1979). Design of pavements with lean concrete bases. *Transportation Research Record, 725*, 51-58.

BS. (1983). *Testing concrete - Part 121: Method of determination of static modulus of elasticity in compression* (BS 1881-121). European Committee for Standardization.

BS. (1986). *Testing concrete - Part 203: Recommendations for measurement of velocity of ultrasonic pulses in concrete* (BS 1881-203). European Committee for Standardization.

BS. (2004a). *Bituminous mixtures - Test methods for hot mix asphalt - Part 24: Resistance to fatigue* (BS EN 12697-24). European Committee for Standardization.

BS. (2004b). *Hydraulically bound mixtures - Specification - Part 1: Cement bound granular mixtures* (BS EN 14227-1). European Committee for Standardization.

Busch, C. (2008). *Incremental-recursive modeling of performance for cement bound base layers.* Paper presented at the Proceedings of the 3rd International Conference on Accelerated Pavement Testing, Madrid, Spain.

Busch, C., Thogersen, F., & Henrichsen, A. (2006). Development and validation mechanistic recursive-incremental deterioration model for cement-stabilized base courses. *Transportation Research Record, 1974*, 128-137.

Chakrabarti, S., & Kodikara, J. (2005). Shrinkage behaviour of crushed basaltic rock and residual clay mixture stabilised with cementitious binders. *International Journal of Pavement Engineering 6*(1), 27-37.

Chehub, G. S. (2002). *Characterisitic of asphalt concrete in tension using a viscoelastoplastic model.* (Ph.D.), North Carolina State University, Raleigh.

Cho, Y. H., Lee, K. W., & Ryu, S. W. (2006). Development of cement-treated base material for reducing shrinkage cracks. *Journal of the Transportation Research Board, 1952*, 134-143.

Chummuneerat, S. (2014). *Performance, evaluation, and enhancement of hydrated cement treated crushed rock base (HCTCRB) as a road base material for Western Australian roads.* (Ph.D.), Curtin University, Bentley, WA.

Chummuneerat, S., Jitsangiam, P., Nikraz, H., & Patel, R. (2013). *Fatigue characteristics of cement treated base for Western Australian roads.* Paper presented at the 2nd International Conference on Engineering and Applied Sciences, Tokyo, Japan.

Cook, D. J., & Chindaprasirt, P. (1980). Influence of loading history upon the compressive properties of concrete. *Magazine of Concrete Research, 32*(111), 89-100.

Corte, J. F., & Goux, M. T. (1996). Design of pavement structures: The France technical guide. *Transportation Research Record, 1539*, 116-124.

Craig, R. F. (2004). *Craig's soil mechanics* (7th ed.). New York: Taylor & Francis Group.

Croney, D., & Croney, P. (1998). *The design and performance of road pavement* (3rd ed.). UK: McGraw-Hill.

Daniel, J. S., & Bisirri, W. M. (2005). *Characterizing fatigue in pavement materials using a dissipated energy parameter*. Paper presented at the Geo-Frontiers Congress 2005, Austin, Texas.

Davis, K. A., Warr, L. S., Burns, S. E., & Hoppe, E. J. (2007). Physical and chemical behavior of four cement-treated aggregates. *Journal of Materials in Civil Engineering 19*(10), 891-897. doi:10.1061/(ASCE)0899-1561(2007)19:10(891).

De Beer, M. (1990). *Aspects of the design and behaviour of road structures incorporating lightly cementitious layer.* (Ph.D.), University of Pretoria, Pretoria, South Africa.

De Vos, E. R. (2007). *Performance characterization of cement treated sand base material of Mozambique.* (M.Sc.), University of Stellenbosch, Stellenbosch, South Africa.

Department of the Army; the Navy and the Air Force. (1994). *Soil stabilization of pavements* (Army TM 5-822-14, Air Force AFJMAN 32-1019). Wasington, D.C., USA: Headquaters Department of the Army, the Navy and the Air Force.

Destrebecq, J. F. (2010). Cyclic and dynamic loading fatigue of structural concrete. In J. M. Torrenti, G. Pijaudier-Cabot, & J. M. Reynouard (Eds.), *Mechanical behavior of concrete* (pp. 185-224). London, UK.: ISTE Ltd.

Diaz, L. G., & Archilla, A. R. (2013). From testing to design: An easy way use and interpret the results from the Asphalt Mixture Performance Tester (AMPT). *International Journal of Pavement Research and Technology, 6*(5), 527-538.

Disfani, M. M., Arulrajah, A., Haghighi, H., Mohammadinia, A., & Horpibulsuk, S. (2014). Flexural beam fatigue strength evaluation of crushed brick as a supplementary material in cement stabilized recycled concrete aggregates. *Construction and Building Materials, 68*, 667-676. doi:10.1016/j.conbuildmat.2014.07.007.

Dougan, C., Stephens, J., Mahoney, J., & Hansen, G. (2003). *E* - dynamic modulus test protocal - problems and solutions* (CT-SPR-0003084-F03-3). Washington, D.C.: Connecticut Department of Transportation and Federal Highway Administration.

George, K. P. (1990). Characterization and structural design of cement-treated base. *Transportation Research Record, 1288*, 78-87.

George, K. P. (2002). *Minimizing cracking in cement-treated materials for improved performance* (Research and Development Bulletin RD123). Skokie, Illinois: Portland Cement Association.

Ghuzlan, K. A., & Carpenter, S. H. (2006). Fatigue damage analysis in asphalt concrete mixtures using the dissipated energy approach. *Canadian Journal of Civil Engineering 33*(7), 890-901. doi:10.1139/l06-032.

Gnanendran, C., & Paul, D. K. (2016). Fatigue characterization of lightly cementitiously stabilized granular base materials using flexural testing. *Journal of Materials in Civil Engineering 28*(9), 04016086. doi:10.1061/(ASCE)MT.1943-5533.0001598.

Gnanendran, C., & Piratheepan, J. (2010). Determination of fatigue life of a granular base material lightly stabilized with slag lime from indirect diametral tensile testing. *Journal of Transportation Engineering, 136*(8), 736-745. doi:10.1061/(ASCE)TE.1943-5436.0000138.

Golterman, P., Johansen, V., & Palbfl, L. (1997). Packing of aggregates: an alternative tool to determine the optimal aggregate mix. *ACI Materials Journal 94*(5), 435-443.

Grzybowski, M., & Meyer, C. (1993). Damage accumulation in concrete with and without fiber reinforcement. *ACI Materials Journal 90*(6), 594-604.

Guo, R. (2007). *Predicting in-service fatigue life of flexible pavements based on accelerated pavement testing.* (Ph.D.), The University of Texas at Austin, Austin, Texas.

Highways Agency. (2006). *Design manual for roads and bridges (DMRB), Vol. 7: Pavement design and maintenance* (Section 2, Part 3, HD 26/06: Pavement design). London, UK.: Department for Transport.

Highways Agency. (2009). *Manual of contract documents for highway works: Volume 1 specification for highway works* (Series 800 road pavement - (11/04) unbound, cement and other hydraulically bound mixture). London, UK.: Department for Transport.

Horpibulsuk, S., Katkan, W., Sirilerdwattana, W., & Rachan, R. (2006). Strength development in cement stabilized low plasticity and coarse grained soils: Laboratory and field study. *Soils and Foundations, 46*(3), 351-366.

Horpibulsuk, S., Miura, N., & Nagaraj, T. S. (2003). Assessment of strength development in cement-admixed high water content clays with Abrams' law as a basis. *Geotechnique, 53*(4), 439-444.

Huang, Y. H. (2004). *Pavement analysis and design* (2nd ed.). Upper Saddle River, N.J.: Pearson Education, INC.

Hugo, F., McCullough, B. F., & Van der Walt, B. (1991). Full-scale accelerated pavement testing for the Texas state department of highway and public trasportation. *Transportation Research Record, 1293*, 52-60.

Huurman, M., & Pronk, A. C. (2012). *A detailed FEM simulation of a 4-point bending test device.* Paper presented at the Proceeding of the 3rd Conference on Four-Point Bending, CA, USA.

Iyer, H. (2005). *The effects of shear deformation in rectangular and wide flange sections.* (M.Sc.), Virginia Polytechnic Institute and State University, Blacksburg, Virginia.

Jameson, G. W., Dash, D. M., Tharan, Y., & Vertessy, N. J. (1995). *Performance of deep-lift in situ pavement recycle under accerelated loading: the Cooma ALF trial, 1994* (APRG Report No. 11). Vermont South, VIC.: Australian Road Research Board.

Jameson, G. W., Sharp, K. G., & Yeo, R. (1992). *Cement-treattted crushed rock pavement fatigue under accerelated loading: the mulgrave (Victoria) ALF trial* (Research report ARR 229). Vermont South, VIC.: Australian Road Research Board.

Jitsangiam, P., & Nikraz, H. (2009). Mechanical behaviours of hydrated cement treated crushed rock base as a road base material in Western Australia. *International Journal of Pavement Engineering 10*(1), 39-47. doi:10.1080/10298430802342682.

Khalid, H. A. (2000). A comparison between bending and diametral fatigue tests for bituminous materials. *Materials and Structures 33*(7), 457-465. doi:10.1007/bf02480666.

Kim, Y. R. (2009). *Modeling of asphalt concrete*. NY: ASCE Press, McGraw-Hill.

Kim, Y. R., & Little, D. N. (1990). One-dimensional constitutive model for asphalt concrete under cyclic loading. *Journal of Engineering Mechanics, 116*(4), 751-772.

Kohgo, Y., Nakaho, M., & Miyaki, T. (1993). Theoretical aspects of constitutive modeling for unsaturated soils. *Soils and Foundations, 33*(4), 49-63.

Kolias, S., & Williams, R. I. T. (1978). *Cement bound road materials: strength and elastic properties measured in the laboratory* (SR 344). Crowthorne, UK.: Transport and Road Research Laboratory.

Kolias, S., & Williams, R. I. T. (1980). Relationships between the static and the dynamic moduli of elasticity in cement stabilized materials. *Materials and Structures 13*(74), 99-107.

LCPC. (1997). *French design manual for pavement structures*. Paris, France: Laboratoire Central des Ponts et Chaussees.

Lee, P. K. K., Kwan, A. K. H., & Zheng, W. (2013). Tensile strength and elastic modulus of typical concrete made in Hong Kong. *HKIE Transactions, 7*(2), 35-40.

Leroueil, S., & Hight, D. W. (2013). Compacted soils: From physics to hydraulic and mechanical behaviour. In B. Caicedo, C. Murillo, H. Laureano, J. E. Colmenares, & I. R. Berdugo (Eds.), *Advances in unsaturated soils* (pp. 41-59). Broken Sound Parkway, N.W.: CRC Press.

Li, X., & Williams, C. (2012). A practical dynamic modulus testing protocal. *Journal of Testing and Evaluation 40*(1), 1-7.

Little, D. N., Scullion, T., Kota, P. B. V. S., & Bhuiyan, J. (1995). *Guidelines for mixture design and thickness design for stabilised bases and subgrades* (Final Report No. FHWA/TX-95/1287-3F). Texas: Texas Transportation Institute.

Litwinowicz, A. (1986). *Characterisation of cement stabilised crushed rock pavement materials.* (M.Eng.), University of Queensland, Brisbane, QLD.

Mai, S. H., Le-Corre, F., Foret, G., & Nedjar, B. (2012). A continuum damage modeling of quasi-static fatigue strength of plain concrete. *International Journal of Fatigue 37*, 79-85. doi:10.1016/j.ijfatigue.2011.10.006.

Mandal, T., Tinjum, J. M., Gokce, A., & Edil, T. (2016). Protocol for testing flexural strength, flexural modulus, and fatigue failure of cementitiously stabilized materials using third-point flexural beam tests. *Geotechnical Testing Journal 39*(1), 91-105.

Marukami, S. (2012). *Continuum damage mechanics*. Tokyo: Springer, Morikita Publishing Cp. Ltd.

Mbaraga, A. N., Jenkins, K. J., & Van De Ven, M. (2014). Influence of beam geometry and aggregate size on the flexural strength and elastic moduli of cement-stabilized materials. *Journal of Transportation Research Board, 2401*, 22-29. doi:10.3141/2401-03.

Medeiros, A., Zhang, X., Ruiz, G., Yu, R. C., & Velasco, M. d. S. L. (2015). Effect of the loading frequency on the compressive fatigue behavior of plain and fiber reinforced concrete. *International Journal of Fatigue 70*, 342-350. doi:10.1016/j.ijfatigue.2014.08.005.

Mindess, S., & Young, J. (1981). *Concrete*. Englewood Cliffs, N.J.: Prentice-Hall.

Moffatt, M. A., Jameson, G. W., & Young, W. (2012). *A laboratory study of the influence of multiple axel loads on the fatigue performance of a cementd material.* Paper presented at the 3rd Conference on Four-point bending, University of California, Davis, USA.

Mohammadinia, A., Arulrajah, A., Sanjayen, J., Disfani, M. M., Bo, M. W., & Darmawan, S. (2015). Laboratory evaluation of the use of cement-treated construction and demolition materials in pavement base and subbase applications. *Journal of Materials in Civil Engineering 27*(6), 04014186. doi:10.1061/(ASCE)MT.1943-5533.0001148.

MRWA. (2010). *Engineering road note 9* (TRIM 05/5236). Perth, WA: MAIN ROADS Western Australia.

MRWA. (2012). *Specification 501-Pavements*. Perth, WA: MAIN ROADS Western Australia.

NAASRA. (1970). *Guide to stabilization in roadworks, including metric addendum*. Syndney, NSW: National Association of Australian State Road Authorities.

NAASRA. (1987). *Pavement design: A guide to the structural design of road pavement*. Milsons Point, NSW: National Association of Australia State Road Authorities.

NCHRP. (2004). *Guide for mechanistic-empirical design of new and rehabilitated pavement structures* (Final Report, Project No. 1-37A). Washington, D.C.: National Cooperative Highway Research Program.

Neville, A. M. (1998). *Properties of concrete* (4th ed.): Addison Wesley Longman Limited.

Neville, A. M. (2006). *Concrete: Neville's insights and issues*. Heron Quay, London: Thomas Telford Ltd.

Newman, K. (1959). The effect of water absorption by aggregates on the water/cement ratio of concrete. *Magazine of Concrete Research, 11*(33), 135-142.

Otte, E., Salvage, P. F., & Monismith, C. L. (1982). Structural design of cemented pavement. *Transportation Engineering Journal of ASCE, 108*(TE4), 428-446.

Paskova, T., & Meyer, C. (1997). Low-cycle fatigue of plain and fiber-reinforced concrete. *ACI Materials Journal 94*(4), 273-285.

Paul, D. K., & Gnanendran, C. T. (2016). Characterization of lightly stabilized granular base materials using monotonic and cyclic load flexural testing.

Journal of Materials in Civil Engineering 28(1), 04015074. doi:10.1061/(ASCE)MT.1943-5533.0001302.

PCA. (1956). *Soil-cement laboratory handbook*. Chicago, Illinois: Portland Cement Association.

PCA. (1992). *Soil-cement laboratory handbook*. Chicago, Illinois: Portland Cement Association.

Pell, P. S., McCarthy, P. F., & Gardner, R. R. (1961). Fatigue of bitumen and bituminous mixes. *International Journal of Mechanical Sciences 3*(4), 247-248.

Planas, J., Guinea, G. V., & Elices, M. (1992). *Softening curves for concrete and structural response*. Paper presented at the Proceeding of the 2nd International Conference on Fracture and Damage of Concrete and Rock, Vienna, Austria.

Poon, C. S., Shui, Z. H., Lam, L., Fok, H., & Kou, S. C. (2004). Influence of moisture states of natural and recycled aggregates on the slump and compressive strength of concrete. *Cement and Concrete Research 34*(1), 31-36. doi:10.1016/S0008-8846(03)00186-8.

Portillo, M. G. (2008). *Measured and theoretical response of perpetual pavement structures.* (M.Sc.), University of Texas at Arlington, Arlington, TX.

Powell, W. D., Potter, J. F., Mayhew, H. C., & Nunn, M. E. (1984). *The structural design of bituminous roads* (TRRL Laboratory Report 1132). Berkshire, UK.: Transport and Road Research Laboratory.

Prowell, B. D., Brown, E. R., Anderson, R. M., Daniel, J. S., Swamy, A. K., Quintus, H. V., . . . Maghsoodloo, S. (2010). *Validating the fatigue endurance limit for hot mix asphalt* (NCHRP Report No. 646). Washington, D.C., USA: National Cooperative Highway Research Program.

Raad, L. (1981). A mechanistic model for strength and fatigue of cement-treated soils. *Geotechnical Testing Journal 4*(3), 104-110.

Rao Tangella, S. C. S., Craus, J., Deacon, J. A., & Monismith, C. L. (1990). *Summary report on fatigue response of asphalt mixtures* (SHRP A-003-A). Washington, D.C.: Strategic Highway Research Program, National Research Council.

Reinhardt, H., Cornelissen, H., & Hordijk, D. (1986). Tensile tests and failure analysis of concrete. *Journal of Structural Engineering, 112*(11), 2462-2477. doi:10.1061/(ASCE)0733-9445(1986)112:11(2462).

Robbins, M. M. (2009). *An investigation into dynamic modulus of hot-mix asphalt and its contributing factors.* (M.Sc.), Auburn University, Alabama.

Rogge, A., & Thiele, M. (2012). *Damage evolution in concrete under high compressive cyclics loadings.* Paper presented at the Proceedings of the 3rd International Symposium on Life-Cycle Civil Engineering, HofBurg Palace, Vienna.

Rowe, G. M. (1993). Performance of asphalt mixtures in the trapezoidal fatigue test. *Proceedings of the Association of Asphalt Paving Technologists, 62*, 344-384.

Sánchez-Leal, F. J. (2007). Gradation chart for asphalt mixes: Development. *Journal of Materials in Civil Engineering 19*(2), 185-197. doi:10.1061/(ASCE)0899-1561(2007)19:2(185).

SANRAL. (2013). *South African pavement engineering manual*. Republic of South Africa: An Initiative of the South African National Roads Agency Ltd.

Saxena, P., Tompkins, D., Khazonovich, L., & Balbo, J. T. (2010). Evaluation of characterization and performance modeling of cementitiously stabilized layers in the mechanistic-empirical pavement design guide. *Journal of Transportation Research Board, 2186*, 111-119. doi:10.3141/2186-12.

Shah, S. P. (1984). Predictions of cumulative damage for concrete and reinforced concrete. *Matériaux et Construction, 17*(1), 65-68. doi:10.1007/BF02474059.

Shahid, M. A. (1997). *Improved cement bound base design for flexible composite pavements.* (Ph.D.), University of Nottingham, Nottingham, UK.

Soliman, M. I., Zeiada, W. A., Kaloush, K. E., & Mamlouk, M. S. (2012). Assessment of different flexure fatigue failure analysis methods to estimate the number of cycles to failure of asphalt mixtures. In J. Pais & J. Harvey (Eds.), *Four Point Bending* (pp. 27-34). London, UK.: CRC Press.

Sparks, P. R., & Menzies, J. B. (1973). The effect of rate of loading upon the static and fatigue strengths of plain concrete in compression. *Magazine of Concrete Research, 25*(83), 73-80.

Standard Australia. (1992). *Determination of drying shrinkage of concrete for samples prepared in the field or in the laboratory* (AS 1012.13). Sydney, NSW: Standard Australia.

Standard Australia. (2000a). *Methods of testing concrete - Method 11: Determination of the modulus of rupture* (AS 1012.11). Sydney, NSW: Standards Australia.

Standard Australia. (2000b). *Particle density and water absorption of coarse aggregate - Weighing-in-water method* (AS 1141.6.1). Sydney, NSW: Standard Australia.

Standard Australia. (2000c). *Particle density and water absorption of fine aggregate* (AS 1141.5). Sydney, NSW: Standard Australia.

Standard Australia. (2008a). *Methods for preparation and testing of stabilized materials, Method 2.2: Sampling - preparation of stabilized pavement materials* (AS 5101.2.2). Sydney, NSW: Standards Australia.

Standard Australia. (2008b). *Methods for preparation and testing of stabilized materials, Method 4: Unconfined compressive strength of compacted materials* (AS 5101.4). Sydney, NSW: Standards Australia.

Standard Australia. (2010). *General purpose and blended cements* (AS 3972). Sydney, NSW: Standards Australia.

Su, Z. (2012). *Durability performance of cementitiously stabilized layers.* (M.Sc.), University of Wisconsin-Madison, WI.

Sukontasukkul, P., Nimityongsakul, P., & Mindess, S. (2004). Effect of loading rate on damage of concrete. *Cement and Concrete Research 34*(11), 2127-2134.

Tayebali, A. A., Deacon, J. A., Coplantz, J. S., Harvey, J. T., & Monismith, C. L. (1994). *Fatigue response of asphalt-aggregate mixes: Part I test method selection* (SHRP A-404). Washington, D.C.: Strategic Highway Research Program, National Research Council.

Theyse, H. L. (2008). *The classical South African mechanistic-empirical design method* (Flexible Pavement Design Course). Pretoria, South Africa: Pavement Modelling Corporation.

Theyse, H. L., De Beer, M., & Rust, F. C. (2014). Overview of the South Africa mechanistic pavement design method. *Journal of the Transportation Research Board, 1539*, 6-17. doi:10.3141/1539-02.

Thiele, M., Petryna, Y., & Rogge, A. (2016). *Experimental investigation of damage evolution in concrete under high-cycle fatigue*. Paper presented at the 9th International Conference on Fracture Mechanics of Concrete and Concrete Structures, University of California, Berkeley.

Thompson, I. (2001). *Use of steel fibres to reinforce cement bound roadbase.* (Ph.D.), University of Nottingham, Nottingham, UK.

Timoshenko, S., & Young, D. H. (1968). *Elements of strength of materials* (5th ed.). Princeton, N.J.: Van Nostrand Company, INC.

van-Blerk, P. G., & Scullion, T. (1995). *Evaluation of stabilized base durability using a modified South Africa wheel tracking devise* (Research Report No. TX-96/2919-1). Texas: Texas Transportation Institute, The Texas A&M University System College Station.

Vega, I. M., Bhatti, M. A., & Nixon, W. A. (1995). A non-linear fatigue damage model for concrete in tension. *International Journal of Damage Mechanics 4*(4), 362-379.

Walker, S., & Bloem, D. L. (1957). *Studies of fleural strength of concrete - Part 3: Effects of variations in testing procedures*. Paper presented at the ASTM Proceedings, Philadelphia.

Wang, J. (2013). *Characterization and modeling of shrinkage cracking of cementitiously stabilized layers in pavement.* (Ph.D.), Washington State University, Pullman, Washington.

Watstein, D. (1953). Effect of straining rate on the compressive strength and elastic properties of concrete. *Journal of the American Concrete Institute, 49*(4), 729-744.

Wen, H., Muhunthan, B., Wang, J., Li, X., Edil, T., & Tinjum, J. M. (2014). *Characterization of cementitiously stabilized layers for use in pavement design and analysis* (NCHRP Report No. 789). Washington, D.C.: National Cooperative Highway Research Program.

Wen, H., & Ramme, B. (2008). *A performance evaluation of asphalt pavement with recycled pavement materials treated by self cementing fly ash and field verification using M-E design guide: A case study*. Paper presented at the 2008 ASCE Pavement Conference, Bellevue, WA.

Williams, R. I. T. (1986). *Cement-treated pavement: Materials, design and construction*. London: Elsevier Applied Science Publisher, LTD.

Witczak, M., Mamlouk, M., Souliman, M., & Zeiada, W. (2013). *Validating an endurance limit for HMA pavements: Laboratory experiment and algorithm development* (NCHRP 9-44A Final Report). Washington, D.C.: National Cooperative Highway Research Program.

Xiao, O., Li, H., & Lin, G. (2008). Dynamic behaviour and constitutive model of concrete at different strain rates. *Magazine of Concrete Research, 60*(4), 271-278.

Xiao, S., Li, H., & Monteiro, P. J. M. (2011). Influence of strain rates and loading histories on the compressive damage behaviour of concrete. *Magazine of Concrete Research, 63*(12), 915-926.

Xiao, Y., Tutumluer, E., Qian, Y., & Siekmeier, J. A. (2012). Gradation effects influencing mechanical properties of aggregate base-granular subbase materials in Minnesota. *Journal of the Transportation Research Board, 2267*, 14-26.

Xuan, D. (2012). *Cement treated recycled crushed concrete and masonry aggregates for pavements.* (Ph.D.), Delft University of Technology, Delft, the Netherlands.

Yeo, R. (2012). *The performance of cemented pavement materials under heavy axle loading.* (Ph.D.), Monash University, NSW, Australia.

Yeo, Y. S. (2011). *Characterisation and classification of cement treated crushed rock basecourse for Western Australian roads.* (Ph.D.), Curtin University, Western Australia, Australia.

Yoon, S., & Abu-Farsakh, M. (2009). Laboratory investigation on the strength characteristics of cement-sand as base material. *KSCE Journal of Civil Engineering, 13*(1), 15-22. doi:10.1007/s12205-009-0015-x.

Zhang, B., Phillips, D. V., & Wu, K. (1996). Effects of loading frequency and stress reversal on fatigue life of plain concrete. *Magazine of Concrete Research, 48*(177), 361-375. doi:10.1680/macr.1996.48.177.361.

Zhang, W., & Cai, Y. (2010). *Continuum damage mechanics and numerical applications*. Zhejiang University Press, Hangzhou: Springer.

Zhang, Z., & Tao, M. (2008). Durability of cement stabilized low plasticity soils. *Journal of Geotechnical and Geoenvironmental Engineering, 134*(2), 203-213. doi:10.1061/(ASCE)1090-0241(2008)134:2(203).

APPENDIX :

BEAM FATIGUE TEST RESULTS

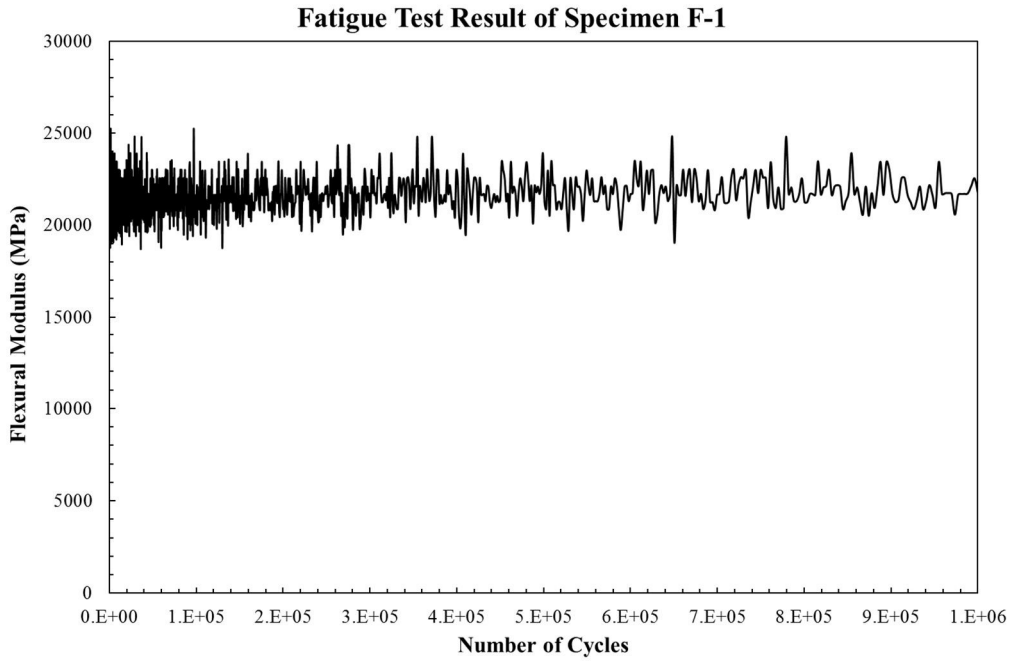
Fatigue Test Result of Specimen F-1
Flexural Modulus (MPa)
30000
25000
20000
15000
10000
5000
0
0.E+00
1.E+05
2.E+05
3.E+05
4.E+05
5.E+05
6.E+05
7.E+05
8.E+05
9.E+05
1.E+06
Number of Cycles

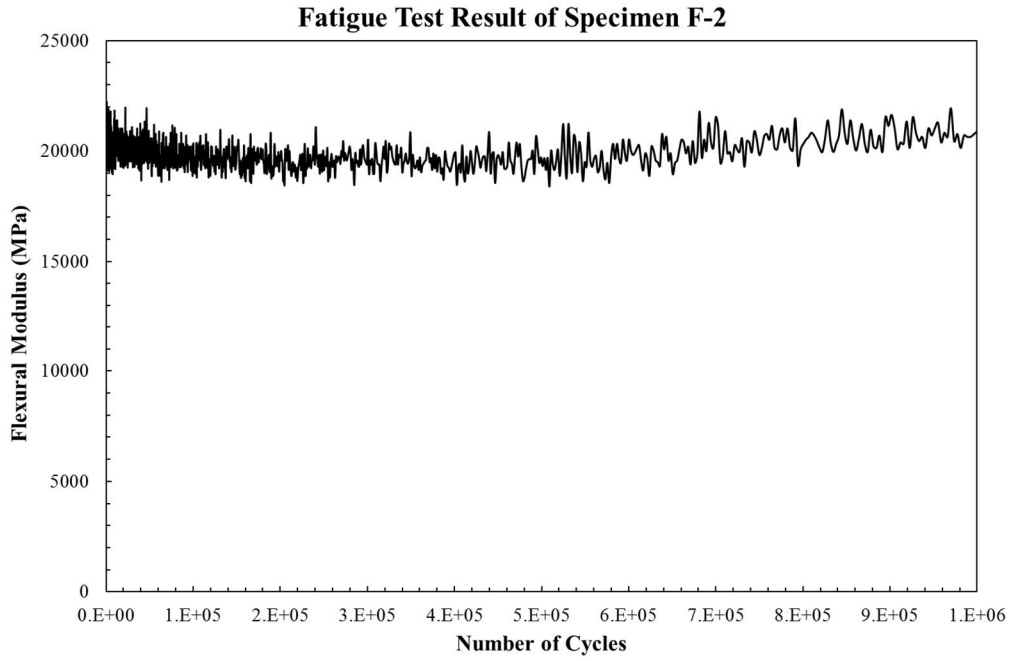
Fatigue Test Result of Specimen F-2
Flexural Modulus (MPa)
25000
20000
15000
10000
5000
0
0.E+00
1.E+05
2.E+05
3.E+05
4.E+05
5.E+05
6.E+05
7.E+05
8.E+05
9.E+05
1.E+06
Number of Cycles

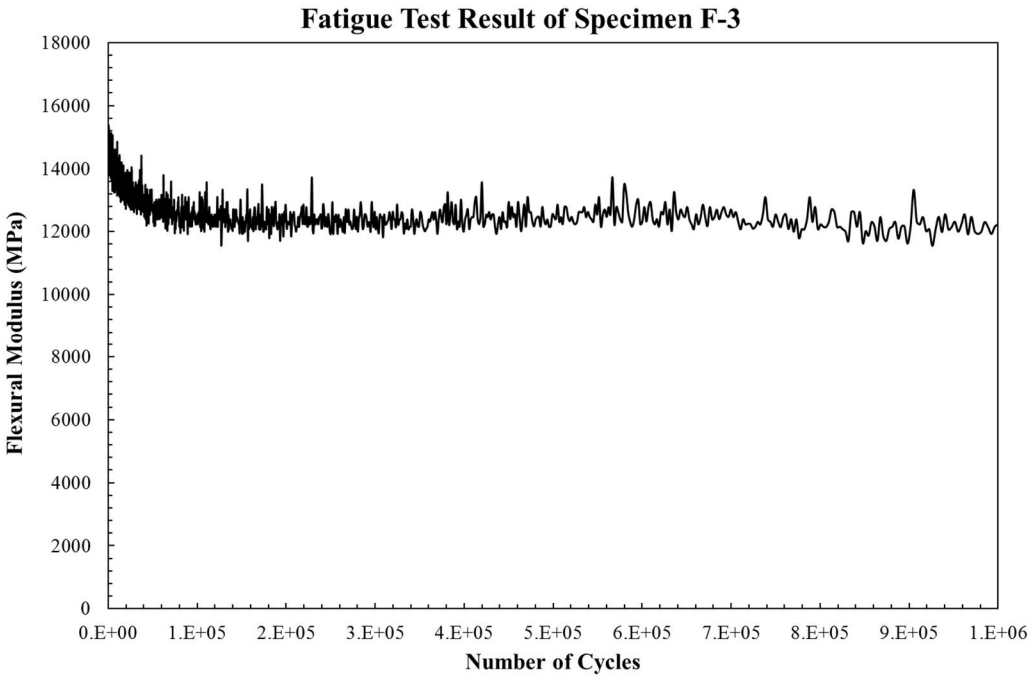
Fatigue Test Result of Specimen F-3
Flexural Modulus (MPa)
18000
16000
14000
12000
10000
8000
6000
4000
2000
0
0.E+00
1.E+05
2.E+05
3.E+05
4.E+05
5.E+05
6.E+05
7.E+05
8.E+05
9.E+05
1.E+06
Number of Cycles

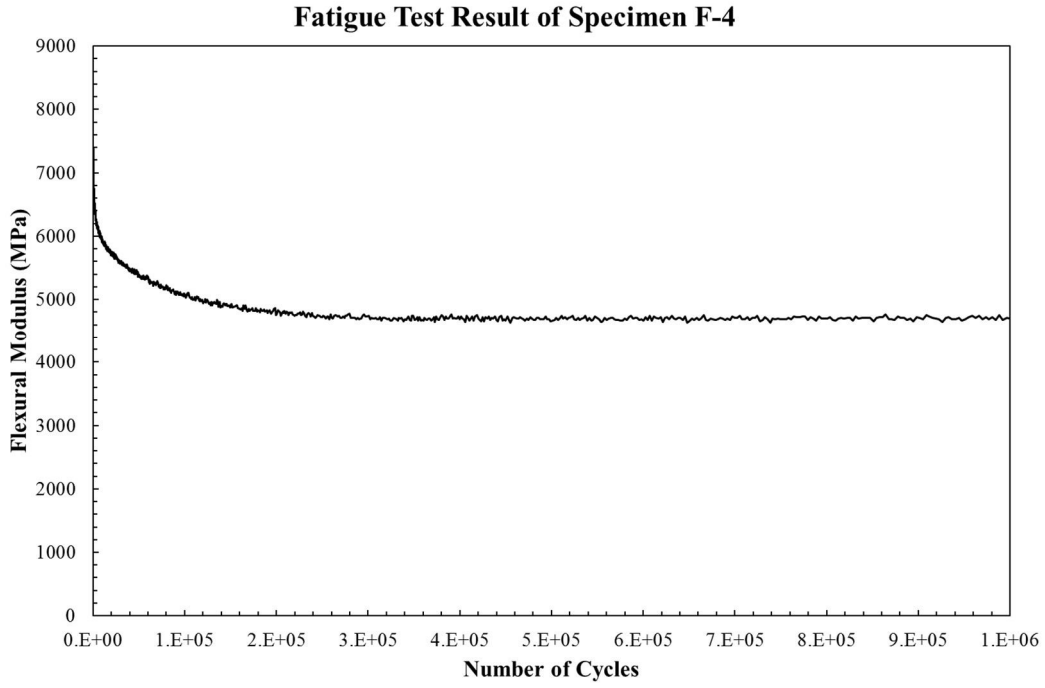
Fatigue Test Result of Specimen F-4
Flexural Modulus (MPa)
9000
8000
7000
6000
5000
4000
3000
2000
1000
0
0.E+00
1.E+05
2.E+05
3.E+05
4.E+05
5.E+05
6.E+05
7.E+05
8.E+05
9.E+05
1.E+06
Number of Cycles

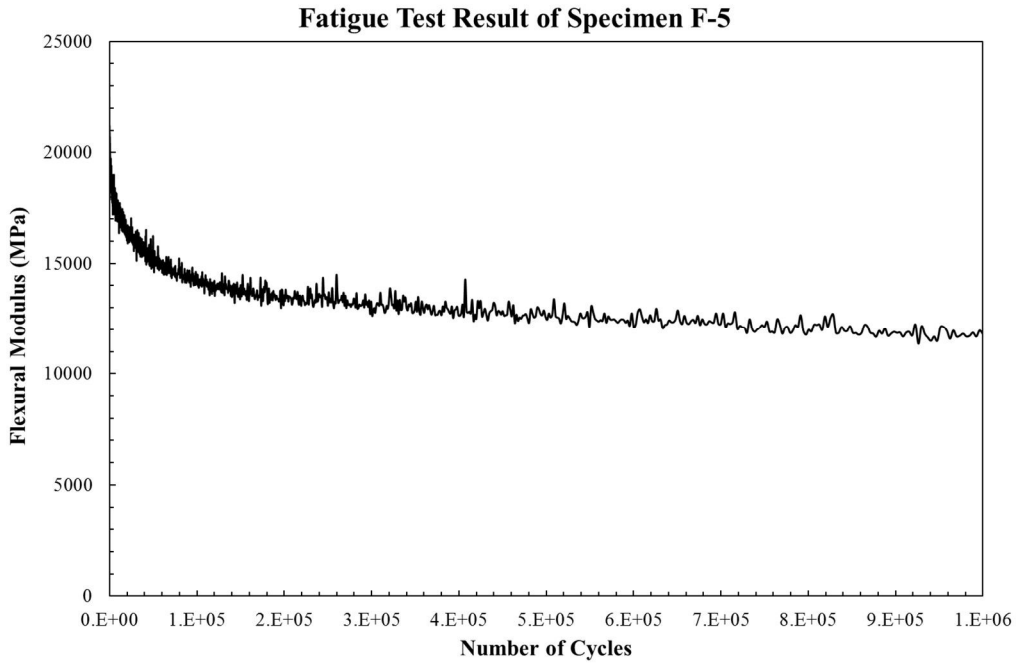
Fatigue Test Result of Specimen F-5
Flexural Modulus (MPa)
25000
20000
15000
10000
5000
0
0.E+00
1.E+05
2.E+05
3.E+05
4.E+05
5.E+05
6.E+05
7.E+05
8.E+05
9.E+05
1.E+06
Number of Cycles

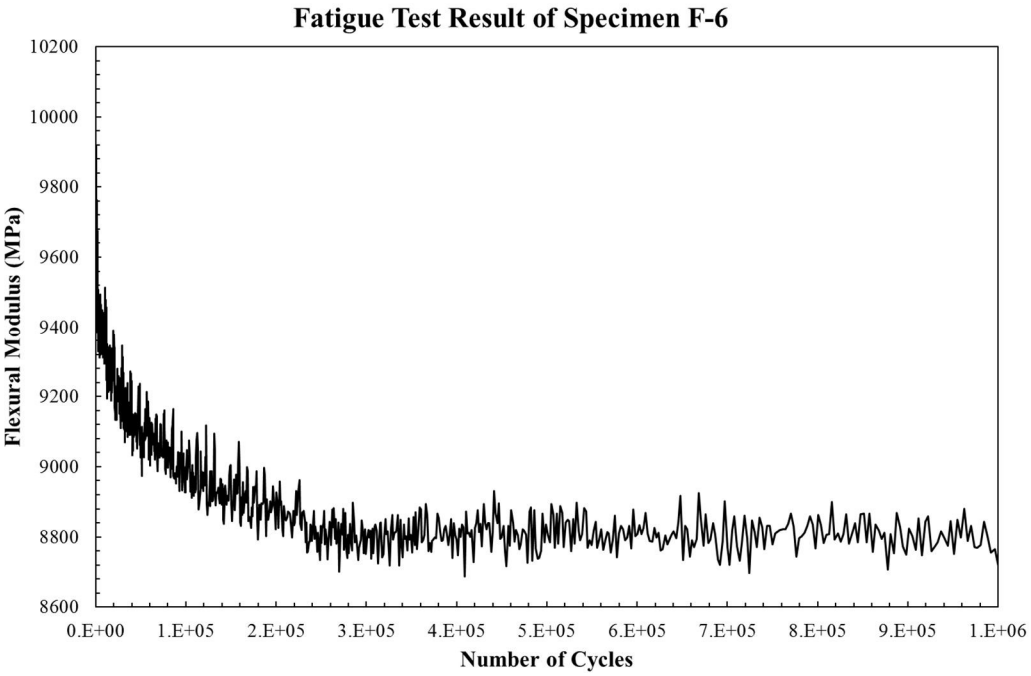
Fatigue Test Result of Specimen F-6
Flexural Modulus (MPa)
10200
10000
9800
9600
9400
9200
9000
8800
8600
0.E+00
1.E+05
2.E+05
3.E+05
4.E+05
5.E+05
6.E+05
7.E+05
8.E+05
9.E+05
1.E+06
Number of Cycles

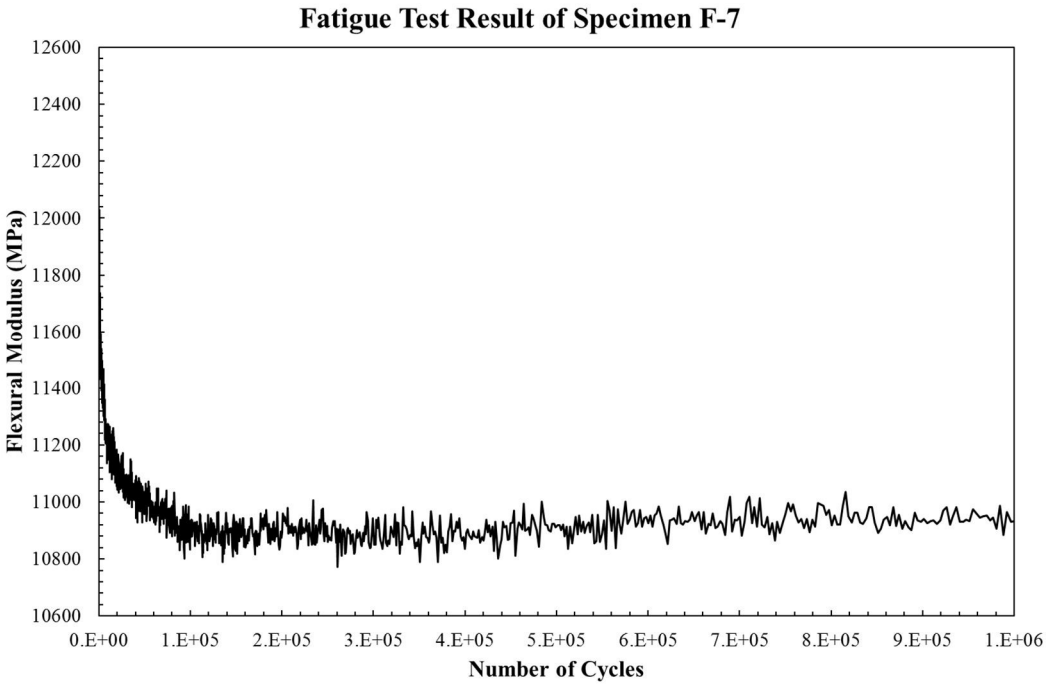
Fatigue Test Result of Specimen F-7
Flexural Modulus (MPa)
12600
12400
12200
12000
11800
11600
11400
11200
11000
10800
10600
0.E+00
1.E+05
2.E+05
3.E+05
4.E+05
5.E+05
6.E+05
7.E+05
8.E+05
9.E+05
1.E+06
Number of Cycles

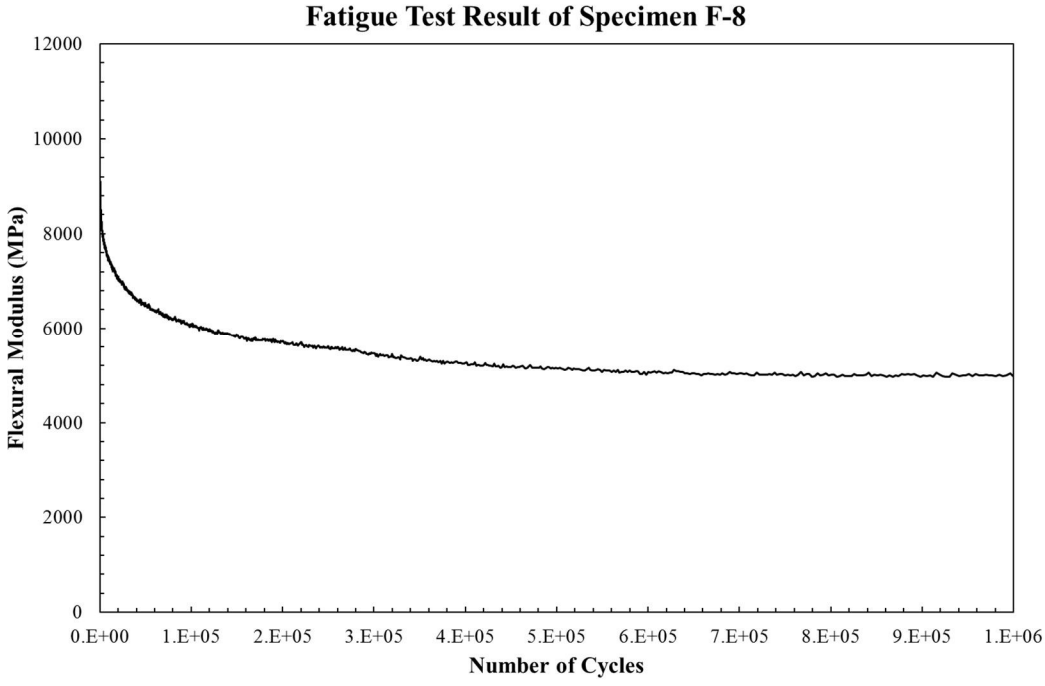
Fatigue Test Result of Specimen F-8
Flexural Modulus (MPa)
12000
10000
8000
6000
4000
2000
0
0.E+00
1.E+05
2.E+05
3.E+05
4.E+05
5.E+05
6.E+05
7.E+05
8.E+05
9.E+05
1.E+06
Number of Cycles

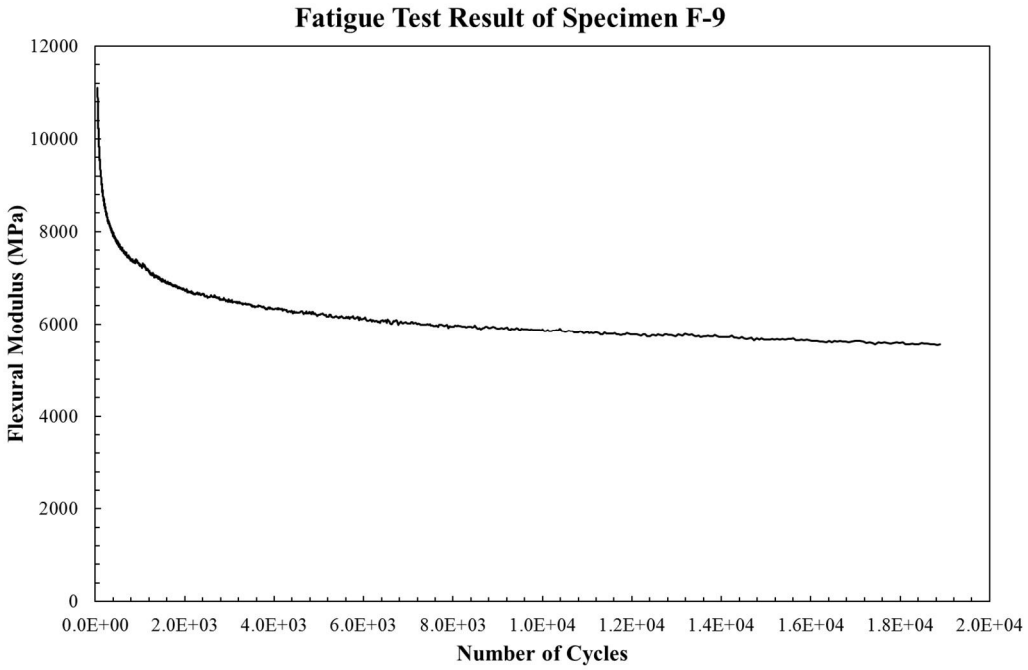
Fatigue Test Result of Specimen F-9
Flexural Modulus (MPa)
12000
10000
8000
6000
4000
2000
0
0.0E+00
2.0E+03
4.0E+03
6.0E+03
8.0E+03
1.0E+04
1.2E+04
1.4E+04
1.6E+04
1.8E+04
2.0E+04
Number of Cycles

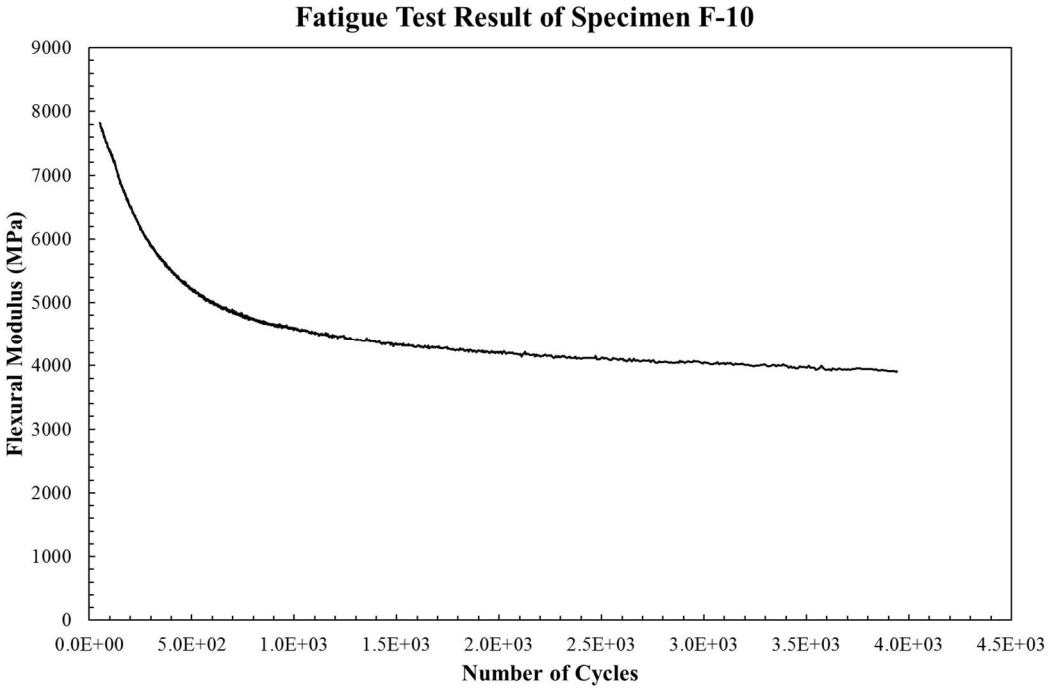
Fatigue Test Result of Specimen F-10
Flexural Modulus (MPa)
9000
8000
7000
6000
5000
4000
3000
2000
1000
0
0.0E+00
5.0E+02
1.0E+03
1.5E+03
2.0E+03
2.5E+03
3.0E+03
3.5E+03
4.0E+03
4.5E+03
Number of Cycles

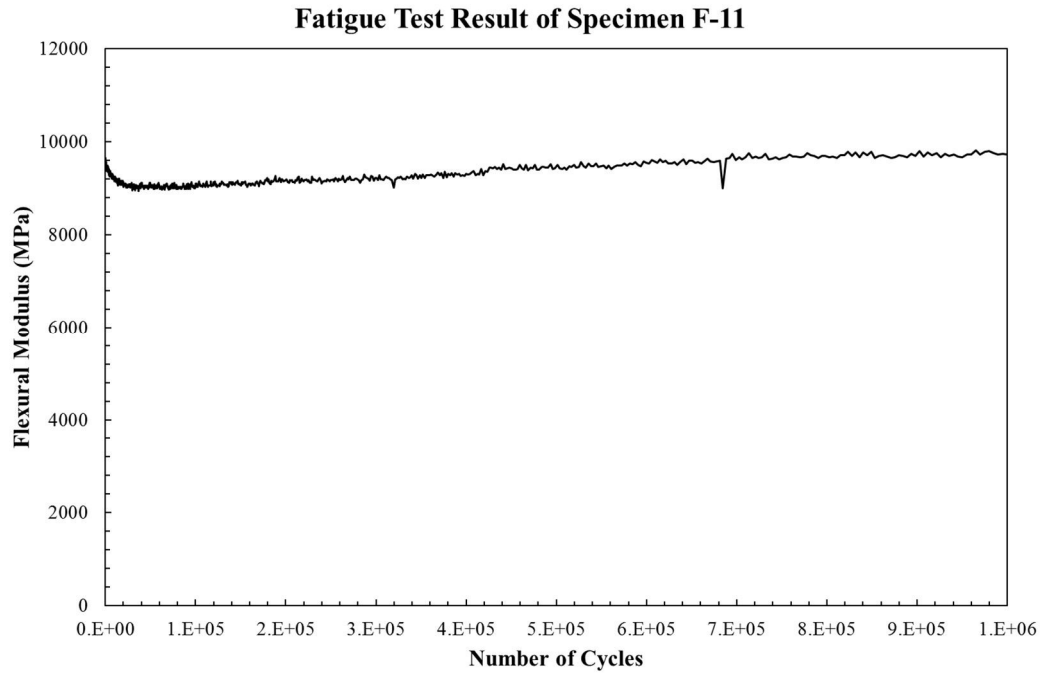
Fatigue Test Result of Specimen F-11
Flexural Modulus (MPa)
12000
10000
8000
6000
4000
2000
0
0.E+00
1.E+05
2.E+05
3.E+05
4.E+05
5.E+05
6.E+05
7.E+05
8.E+05
9.E+05
1.E+06
Number of Cycles

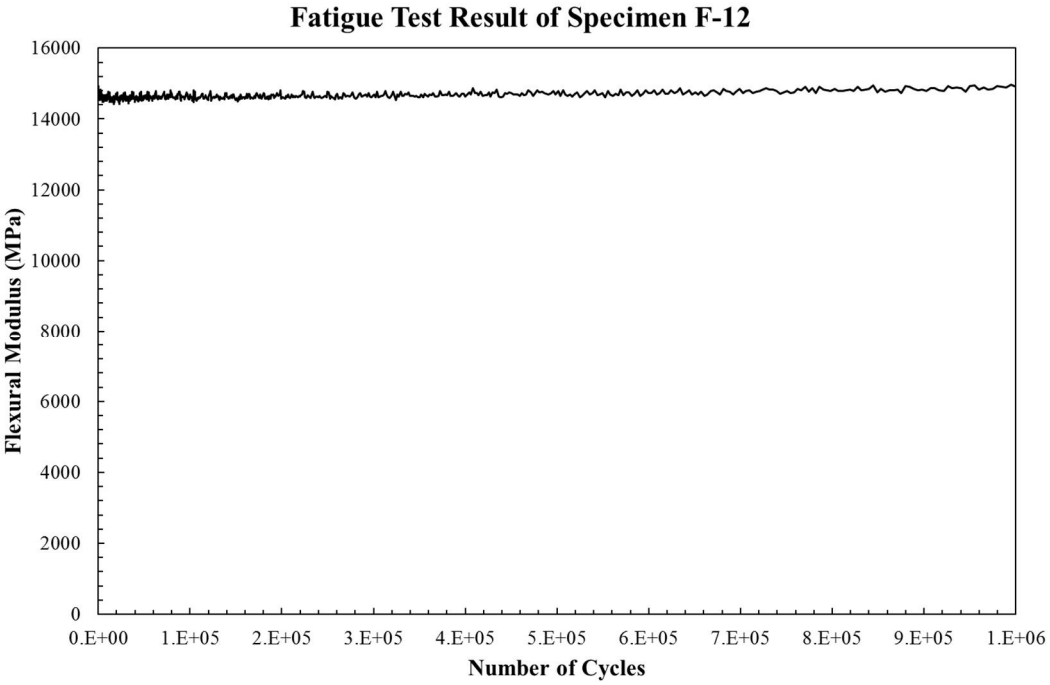
Fatigue Test Result of Specimen F-12
Flexural Modulus (MPa)
16000
14000
12000
10000
8000
6000
4000
2000
0
0.E+00
1.E+05
2.E+05
3.E+05
4.E+05
5.E+05
6.E+05
7.E+05
8.E+05
9.E+05
1.E+06
Number of Cycles

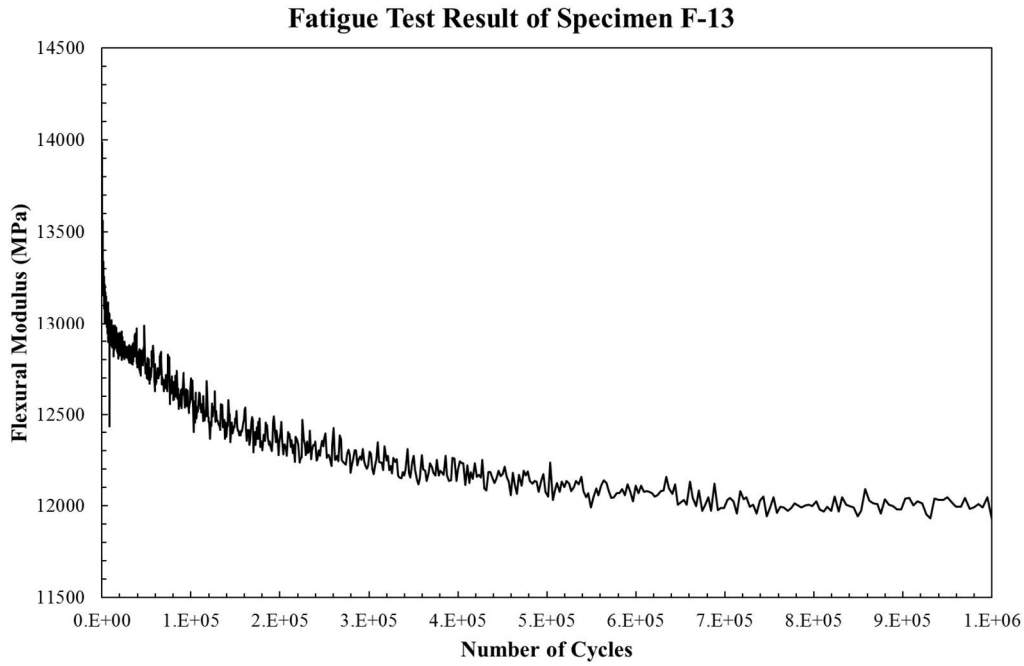
Fatigue Test Result of Specimen F-13
Flexural Modulus (MPa)
14500
14000
13500
13000
12500
12000
11500
0.E+00
1.E+05
2.E+05
3.E+05
4.E+05
5.E+05
6.E+05
7.E+05
8.E+05
9.E+05
1.E+06
Number of Cycles

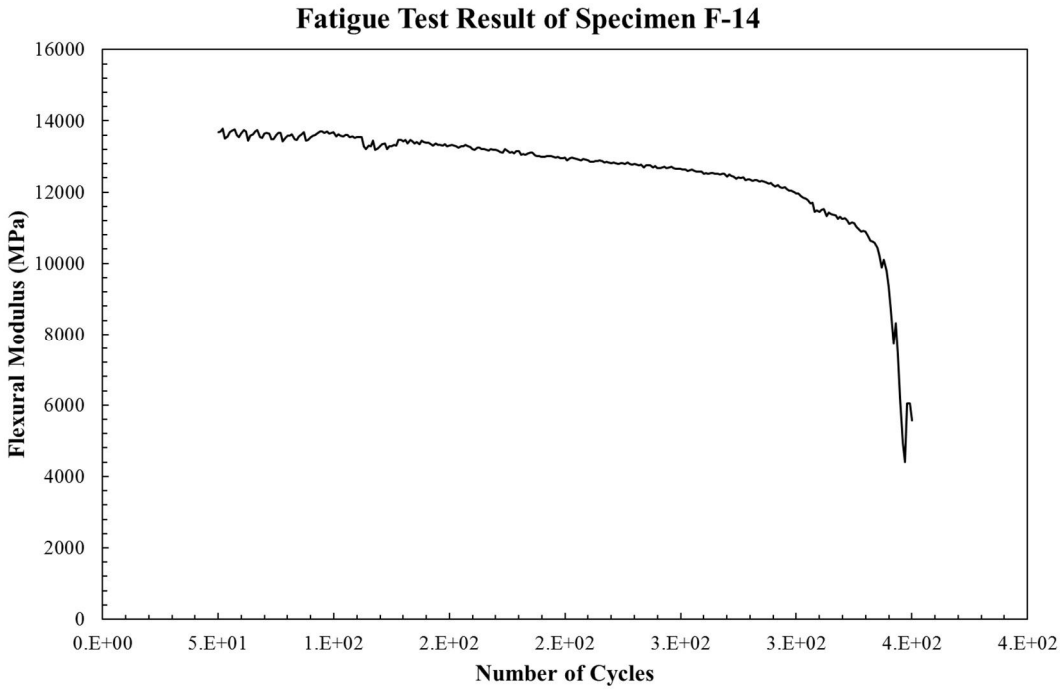
Fatigue Test Result of Specimen F-14
Flexural Modulus (MPa)
16000
14000
12000
10000
8000
6000
4000
2000
0
0.E+00
5.E+01
1.E+02
2.E+02
2.E+02
3.E+02
3.E+02
4.E+02
4.E+02
Number of Cycles

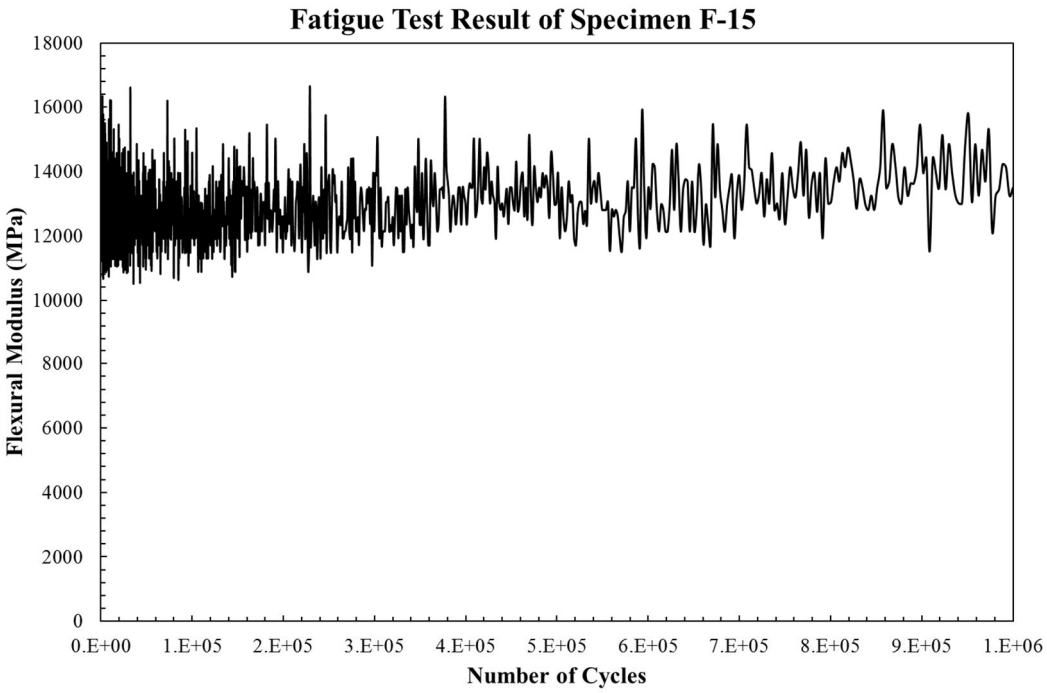
Fatigue Test Result of Specimen F-15
Flexural Modulus (MPa)
18000
16000
14000
12000
10000
8000
6000
4000
2000
0
0.E+00
1.E+05
2.E+05
3.E+05
4.E+05
5.E+05
6.E+05
7.E+05
8.E+05
9.E+05
1.E+06
Number of Cycles

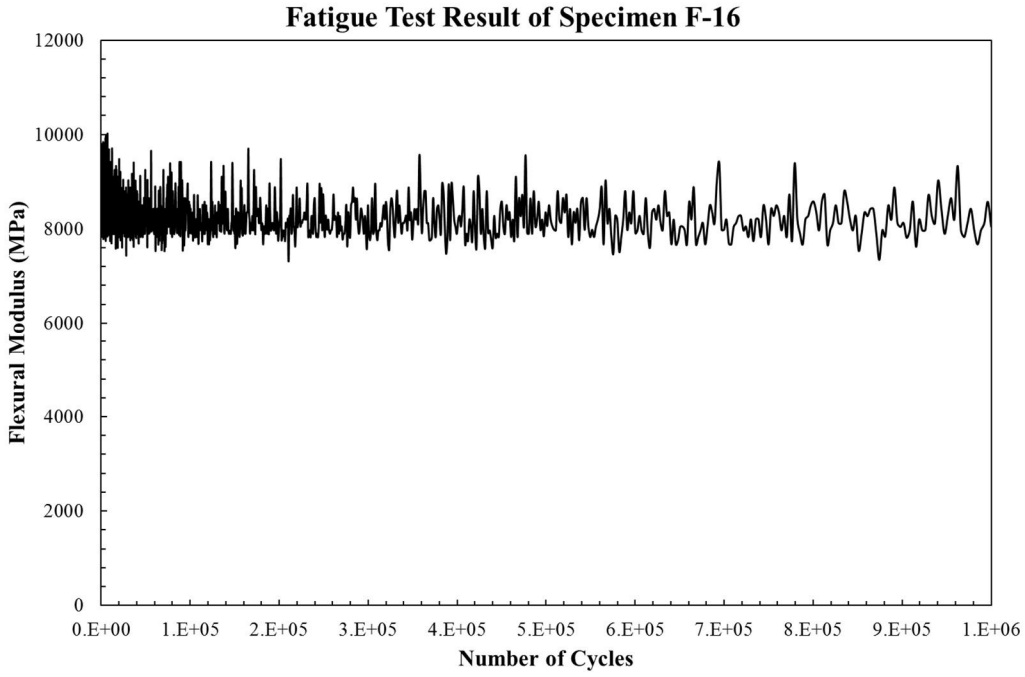
Fatigue Test Result of Specimen F-16
Flexural Modulus (MPa)
12000
10000
8000
6000
4000
2000
0
0.E+00
1.E+05
2.E+05
3.E+05
4.E+05
5.E+05
6.E+05
7.E+05
8.E+05
9.E+05
1.E+06
Number of Cycles

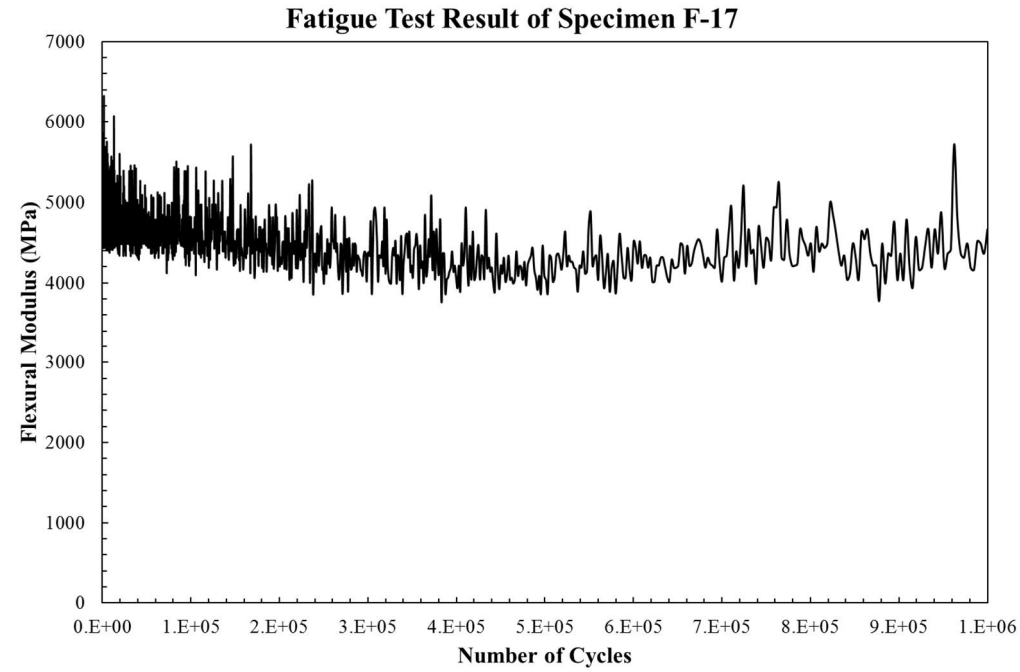
Fatigue Test Result of Specimen F-17
Flexural Modulus (MPa)
7000
6000
5000
4000
3000
2000
1000
0
0.E+00
1.E+05
2.E+05
3.E+05
4.E+05
5.E+05
6.E+05
7.E+05
8.E+05
9.E+05
1.E+06
Number of Cycles

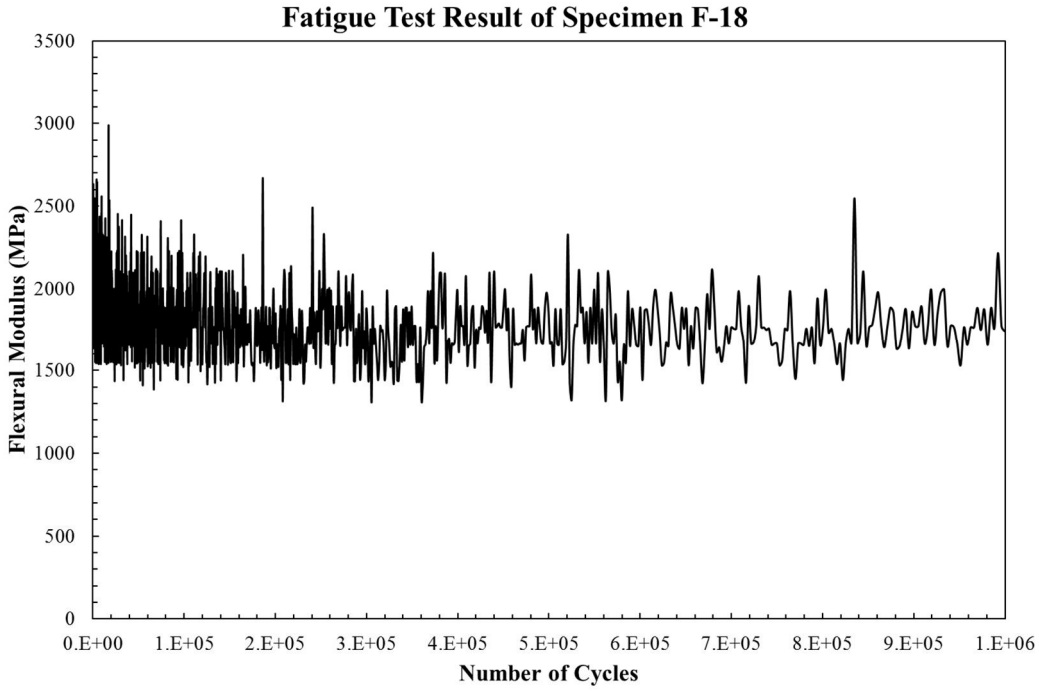
Fatigue Test Result of Specimen F-18
Flexural Modulus (MPa)
3500
3000
2500
2000
1500
1000
500
0
0.E+00
1.E+05
2.E+05
3.E+05
4.E+05
5.E+05
6.E+05
7.E+05
8.E+05
9.E+05
1.E+06
Number of Cycles

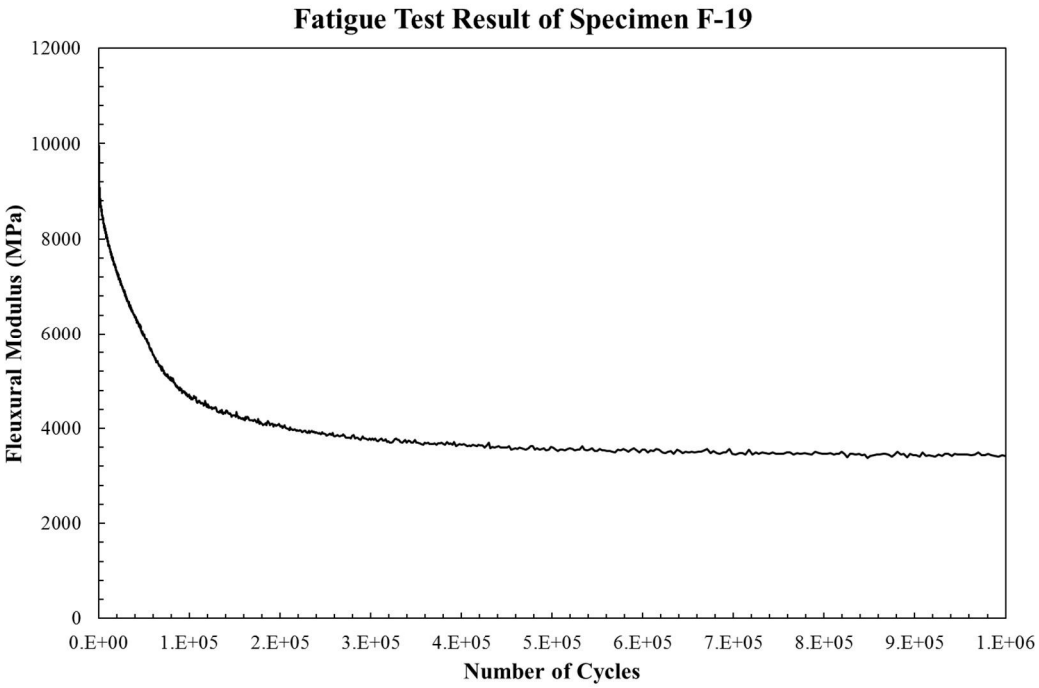
Fatigue Test Result of Specimen F-19
Fleuxural Modulus (MPa)
12000
10000
8000
6000
4000
2000
0
0.E+00
1.E+05
2.E+05
3.E+05
4.E+05
5.E+05
6.E+05
7.E+05
8.E+05
9.E+05
1.E+06
Number of Cycles

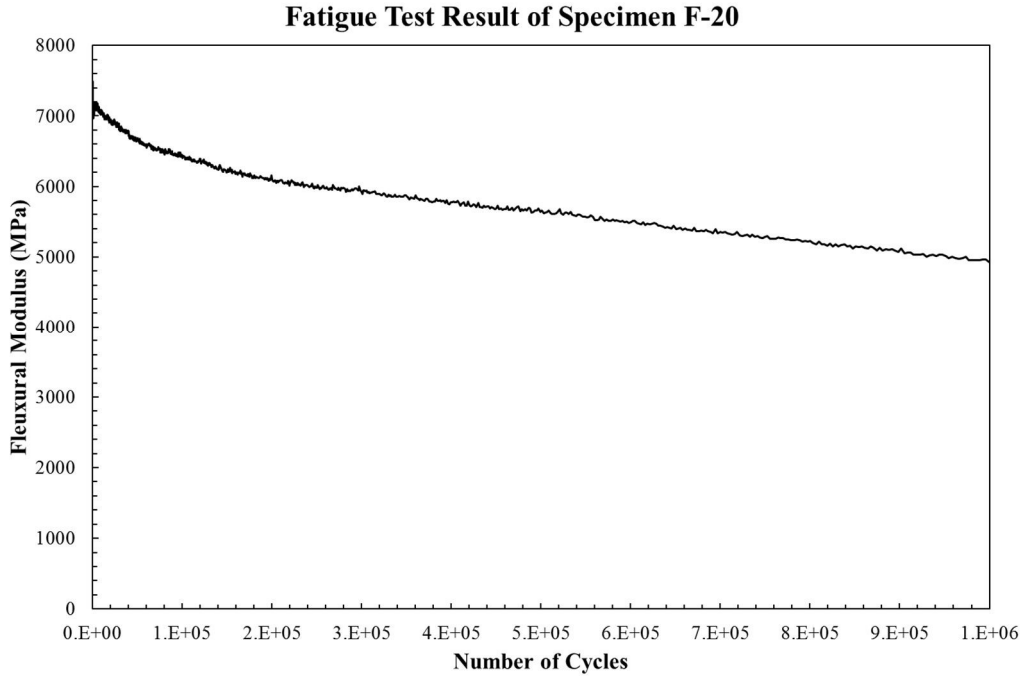
Fatigue Test Result of Specimen F-20
Fleuxural Modulus (MPa)
8000
7000
6000
5000
4000
3000
2000
1000
0
0.E+00
1.E+05
2.E+05
3.E+05
4.E+05
5.E+05
6.E+05
7.E+05
8.E+05
9.E+05
1.E+06
Number of Cycles

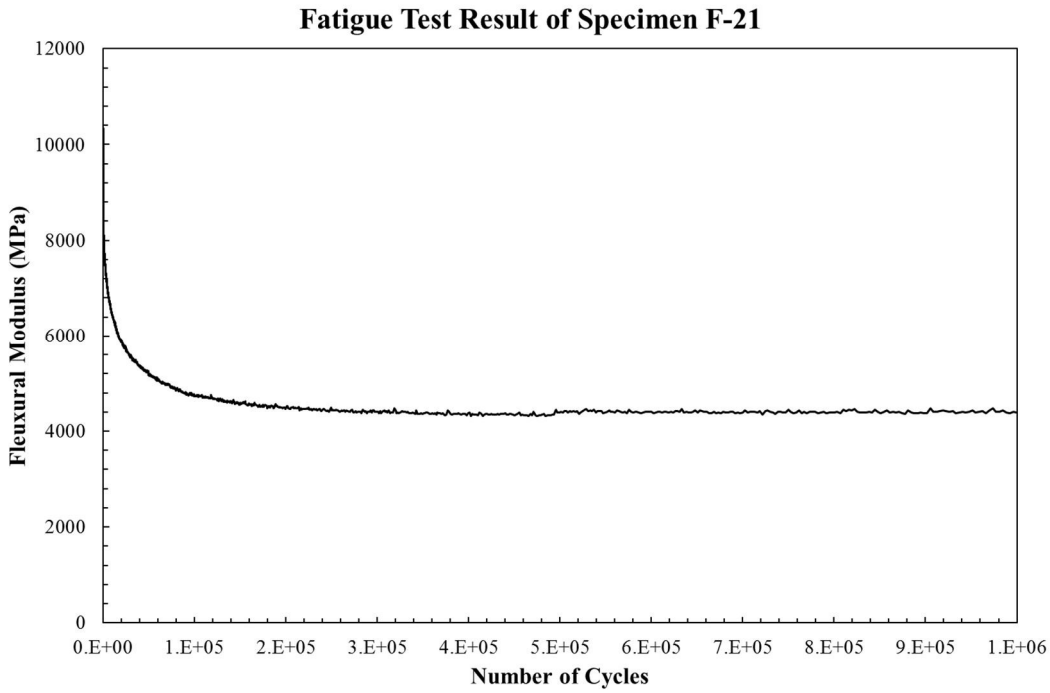
Fatigue Test Result of Specimen F-21
Fleuxural Modulus (MPa)
12000
10000
8000
6000
4000
2000
0
0.E+00
1.E+05
2.E+05
3.E+05
4.E+05
5.E+05
6.E+05
7.E+05
8.E+05
9.E+05
1.E+06
Number of Cycles

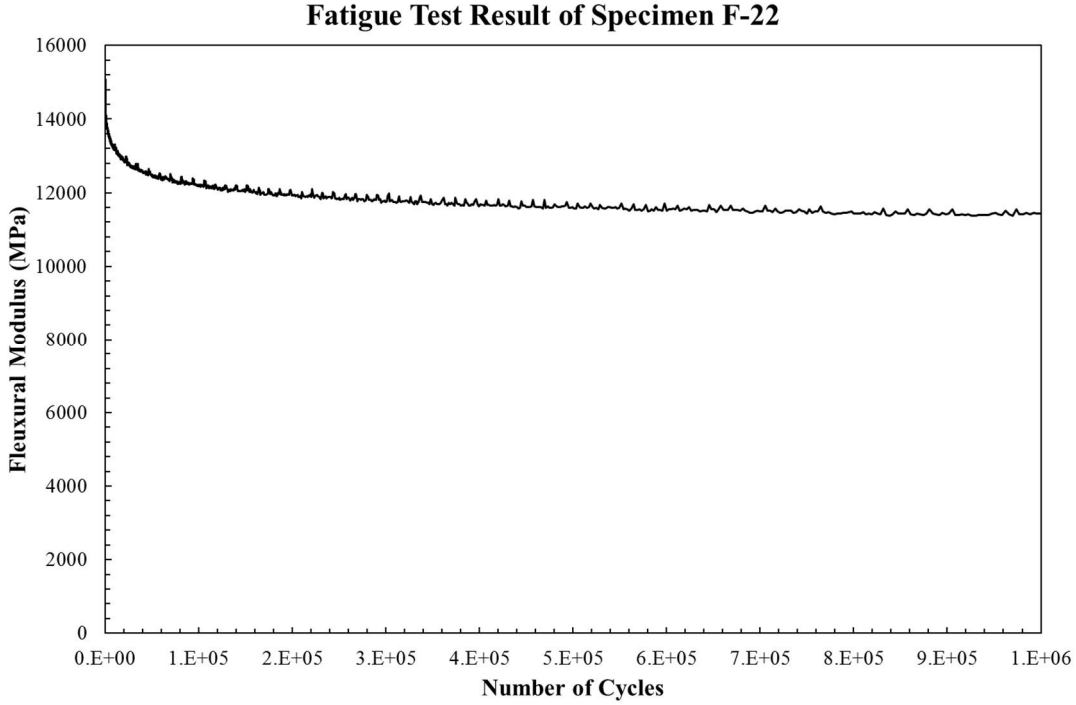
Fatigue Test Result of Specimen F-22
Fleuxural Modulus (MPa)
16000
14000
12000
10000
8000
6000
4000
2000
0
0.E+00
1.E+05
2.E+05
3.E+05
4.E+05
5.E+05
6.E+05
7.E+05
8.E+05
9.E+05
1.E+06
Number of Cycles

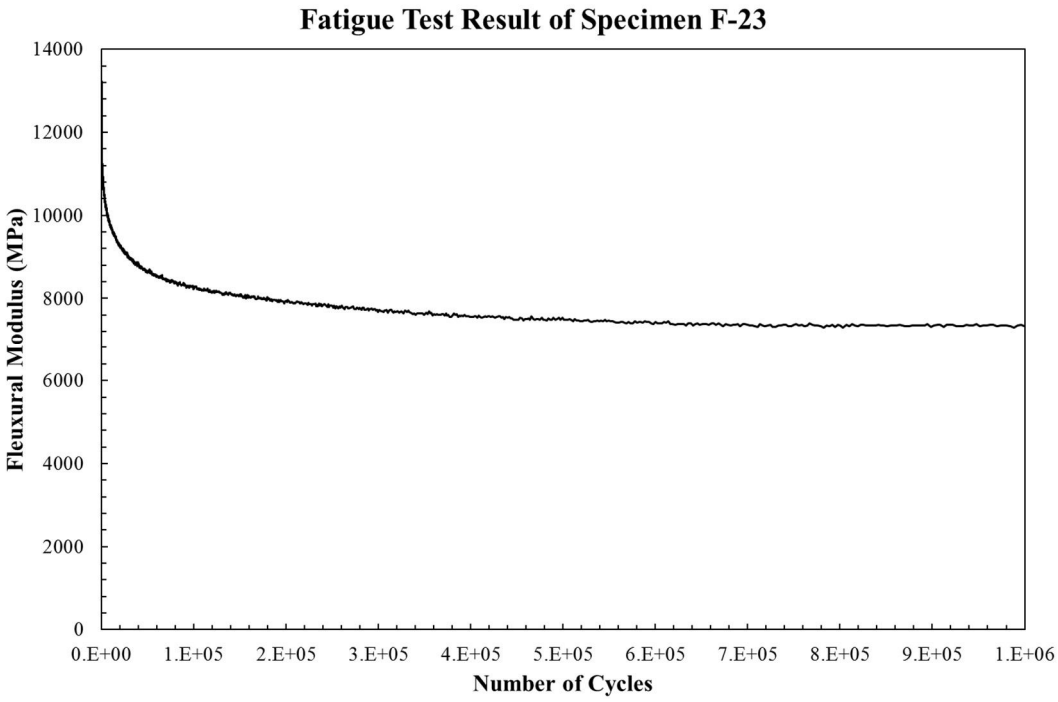
Fatigue Test Result of Specimen F-23
Fleuxural Modulus (MPa)
14000
12000
10000
8000
6000
4000
2000
0
0.E+00
1.E+05
2.E+05
3.E+05
4.E+05
5.E+05
6.E+05
7.E+05
8.E+05
9.E+05
1.E+06
Number of Cycles

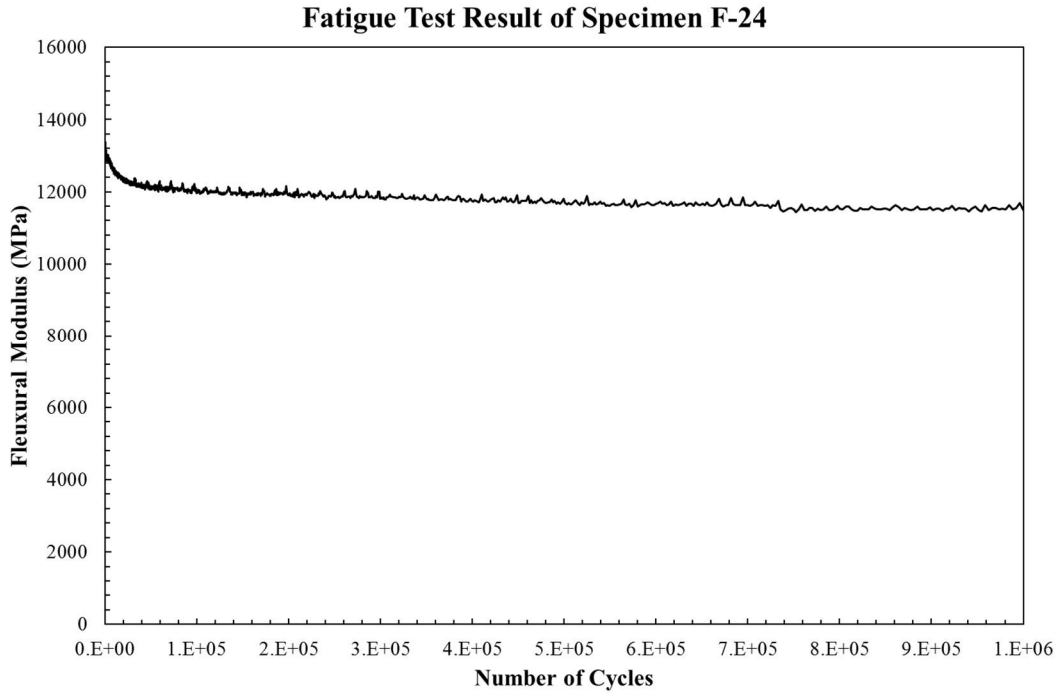
Fatigue Test Result of Specimen F-24
Fleuxural Modulus (MPa)
16000
14000
12000
10000
8000
6000
4000
2000
0
0.E+00
1.E+05
2.E+05
3.E+05
4.E+05
5.E+05
6.E+05
7.E+05
8.E+05
9.E+05
1.E+06
Number of Cycles

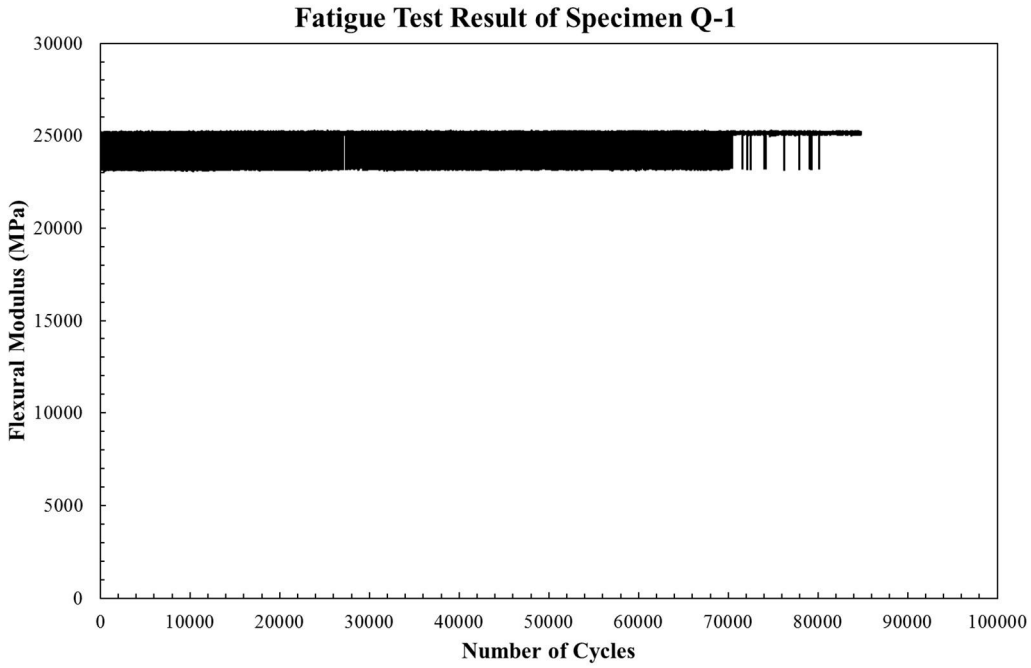
Fatigue Test Result of Specimen Q-1
Flexural Modulus (MPa)
30000
25000
20000
15000
10000
5000
0
0
10000
20000
30000
40000
50000
60000
70000
80000
90000
100000
Number of Cycles

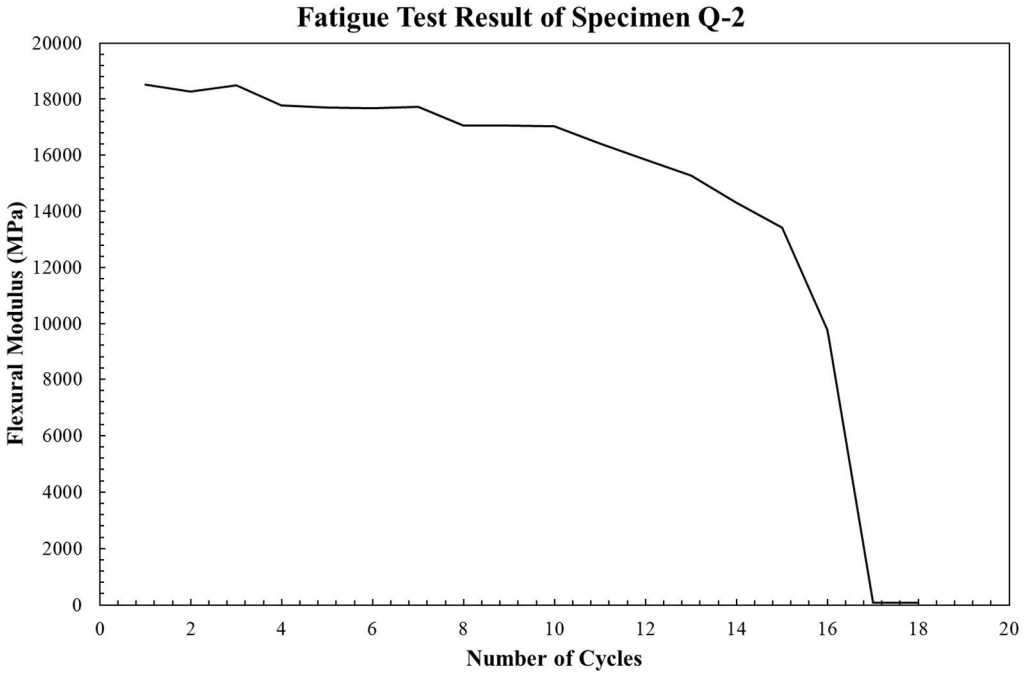
Fatigue Test Result of Specimen Q-2
Flexural Modulus (MPa)
20000
18000
16000
14000
12000
10000
8000
6000
4000
2000
0
0
2
4
6
8
10
12
14
16
18
20
Number of Cycles

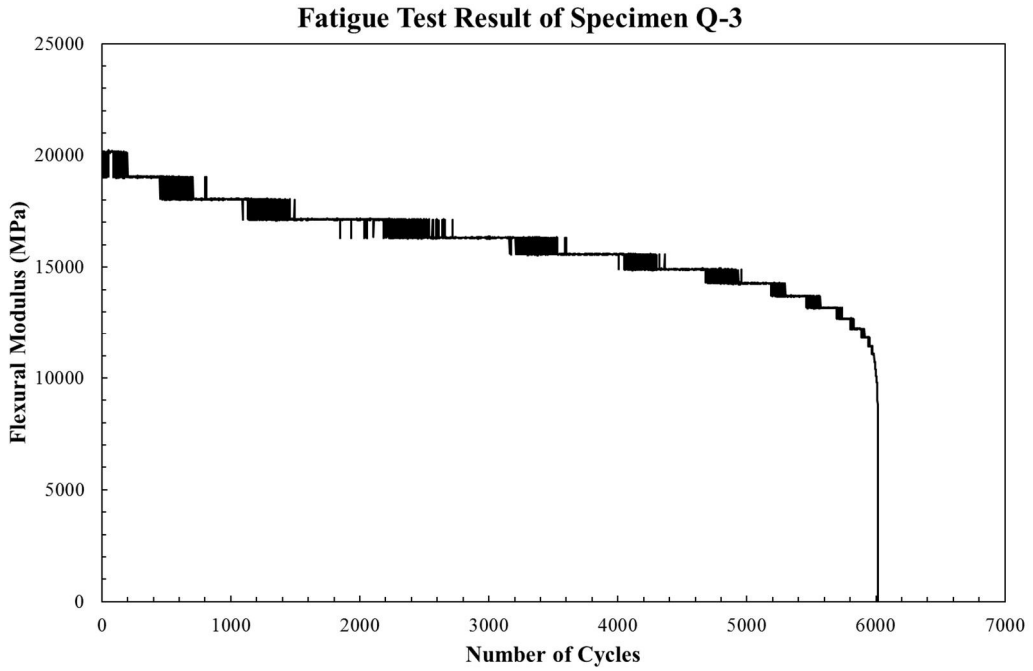
Fatigue Test Result of Specimen Q-3
Flexural Modulus (MPa)
25000
20000
15000
10000
5000
0
0
1000
2000
3000
4000
5000
6000
7000
Number of Cycles

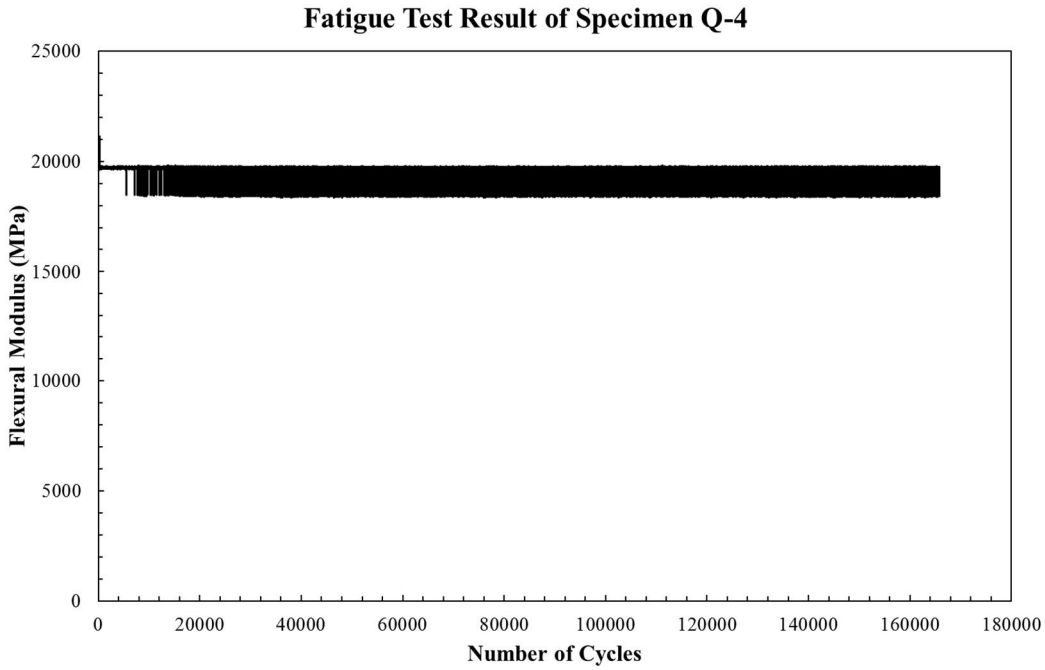
Fatigue Test Result of Specimen Q-4
Flexural Modulus (MPa)
25000
20000
15000
10000
5000
0
0
20000
40000
60000
80000
100000
120000
140000
160000
180000
Number of Cycles

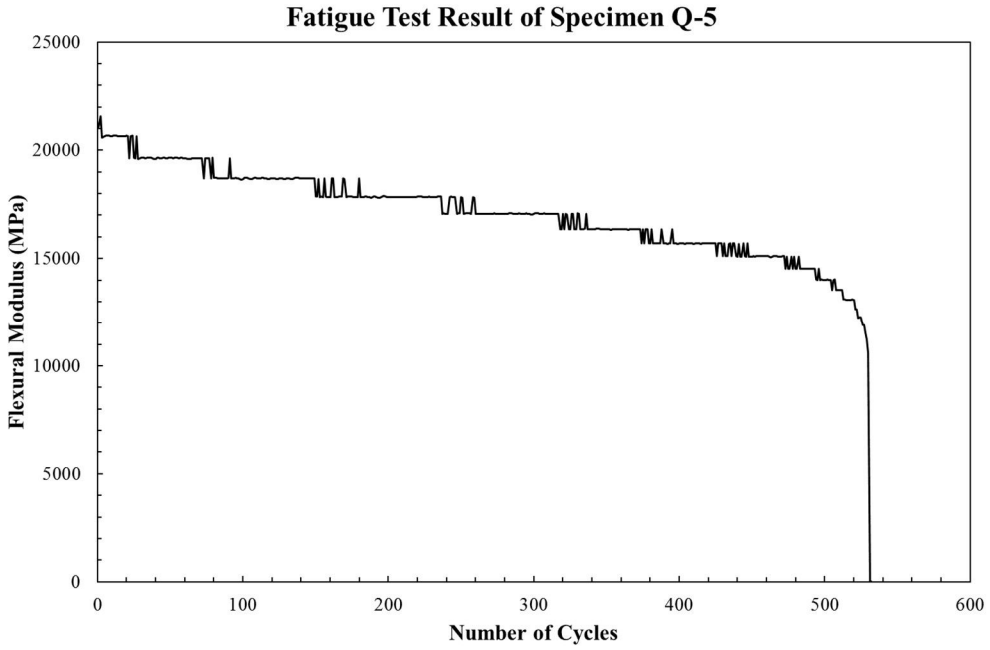
Fatigue Test Result of Specimen Q-5
Flexural Modulus (MPa)
25000
20000
15000
10000
5000
0
0
100
200
300
400
500
600
Number of Cycles

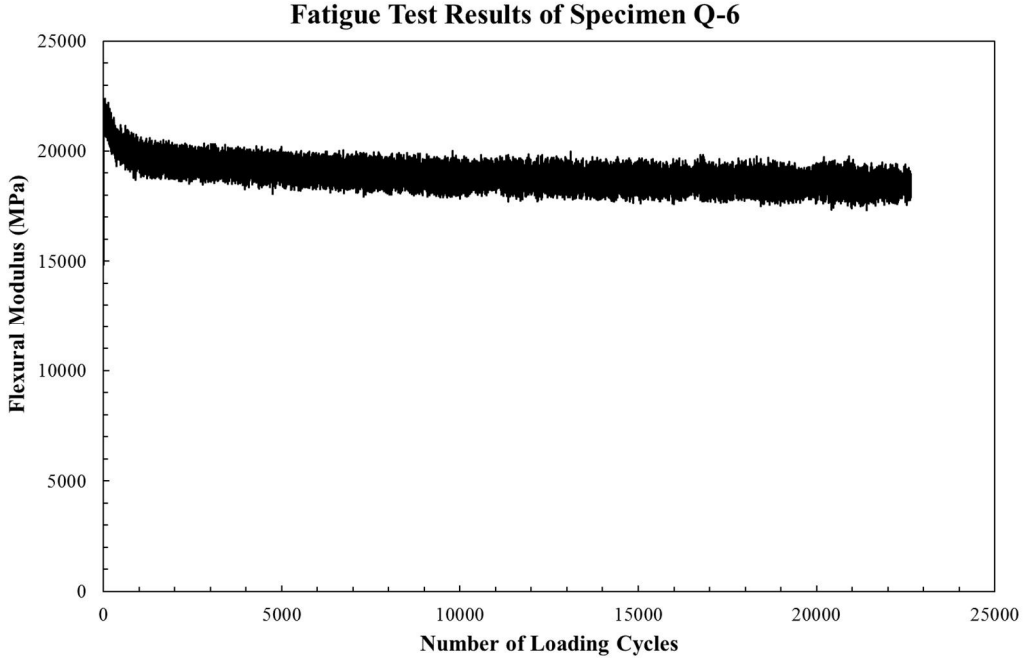
Fatigue Test Results of Specimen Q-6
Flexural Modulus (MPa)
25000
20000
15000
10000
5000
0
0
5000
10000
15000
20000
25000
Number of Loading Cycles

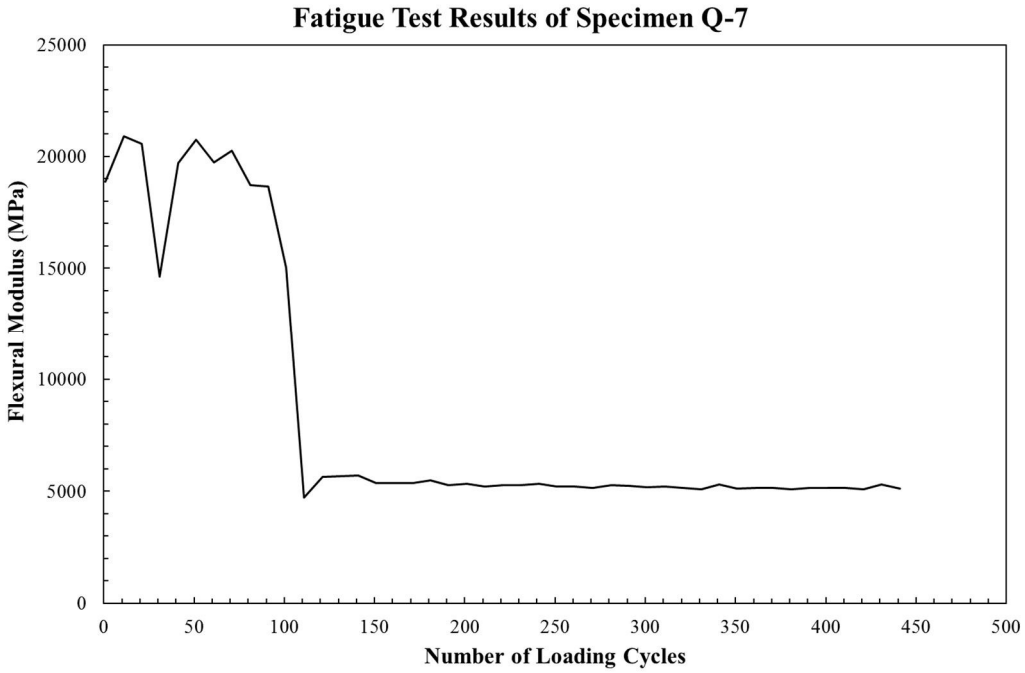
Fatigue Test Results of Specimen Q-7
Flexural Modulus (MPa)
25000
20000
15000
10000
5000
0
0
50
100
150
200
250
300
350
400
450
500
Number of Loading Cycles

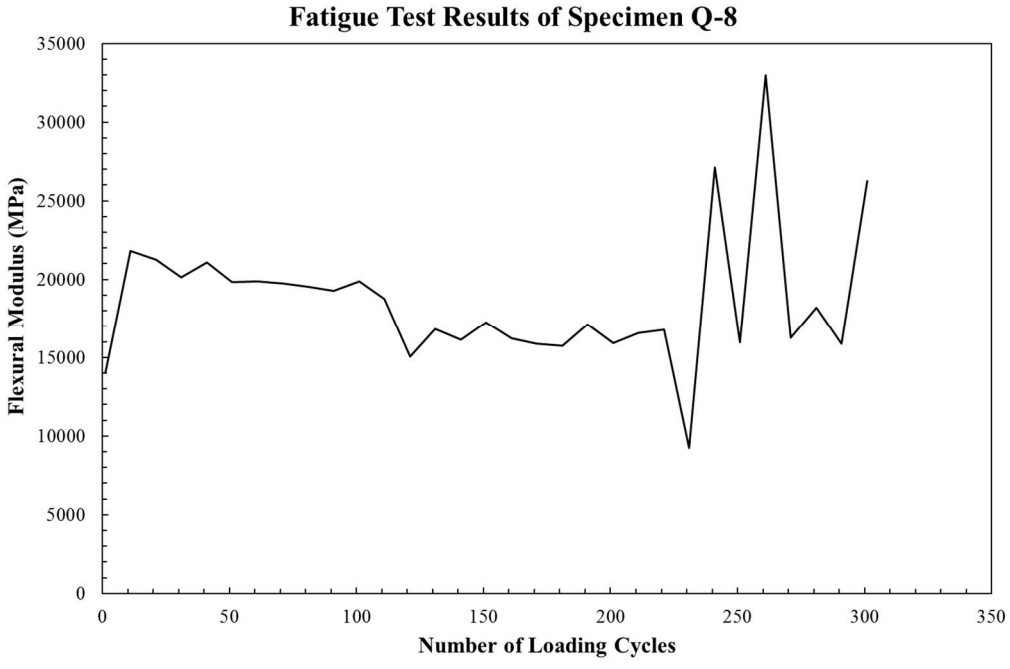
Fatigue Test Results of Specimen Q-8
Flexural Modulus (MPa)
35000
30000
25000
20000
15000
10000
5000
0
0
50
100
150
200
250
300
350
Number of Loading Cycles

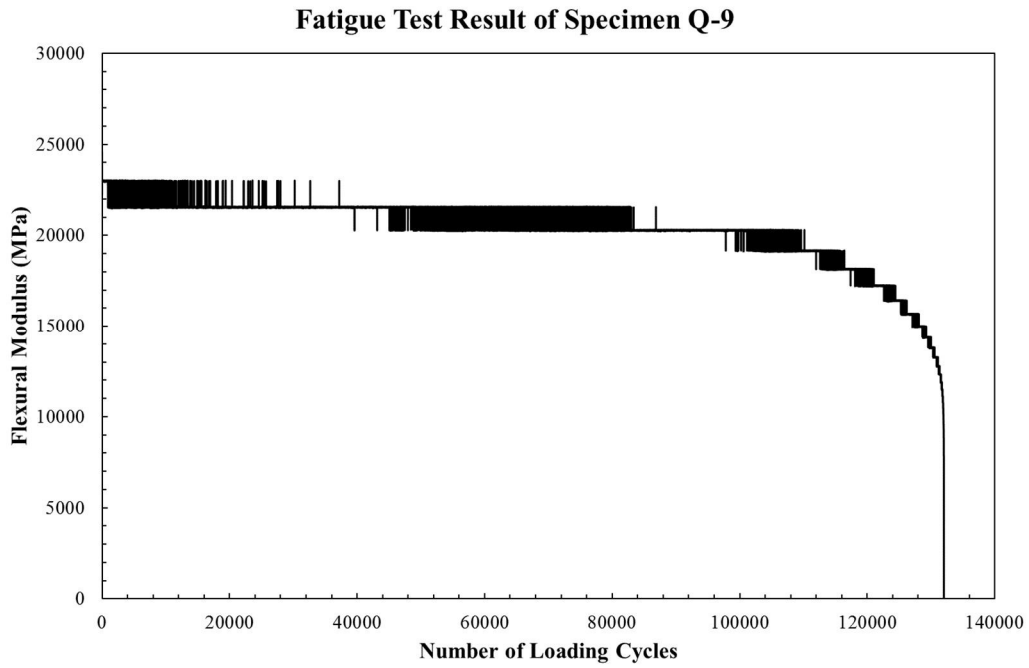
Fatigue Test Result of Specimen Q-9
Flexural Modulus (MPa)
30000
25000
20000
15000
10000
5000
0
0
20000
40000
60000
80000
100000
120000
140000
Number of Loading Cycles

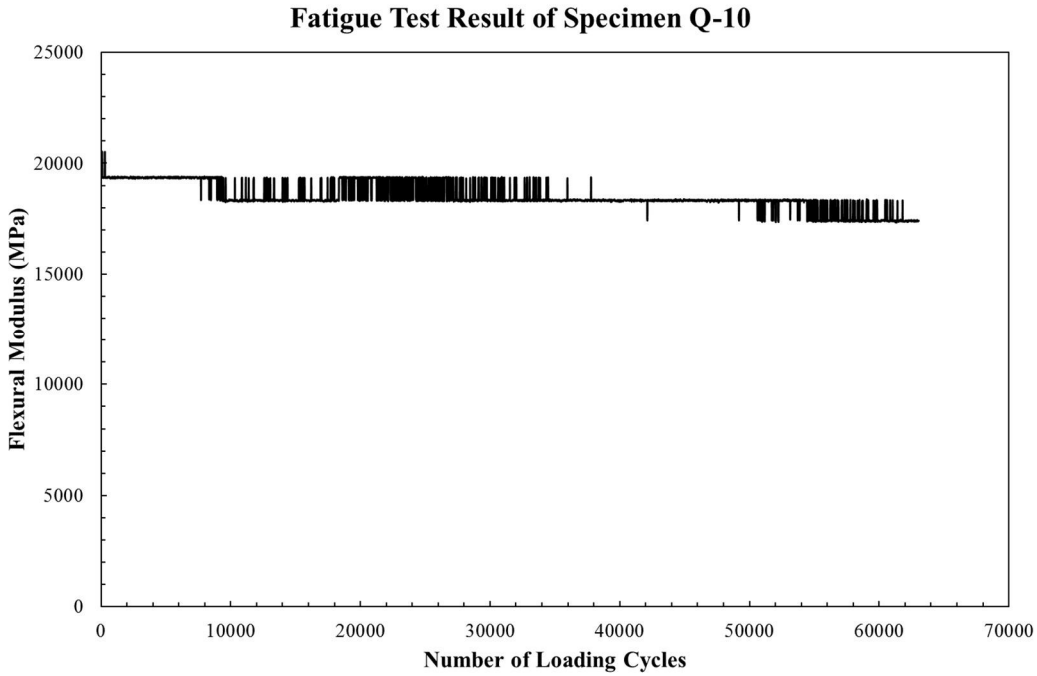
Fatigue Test Result of Specimen Q-10
Flexural Modulus (MPa)
25000
20000
15000
10000
5000
0
0
10000
20000
30000
40000
50000
60000
70000
Number of Loading Cycles

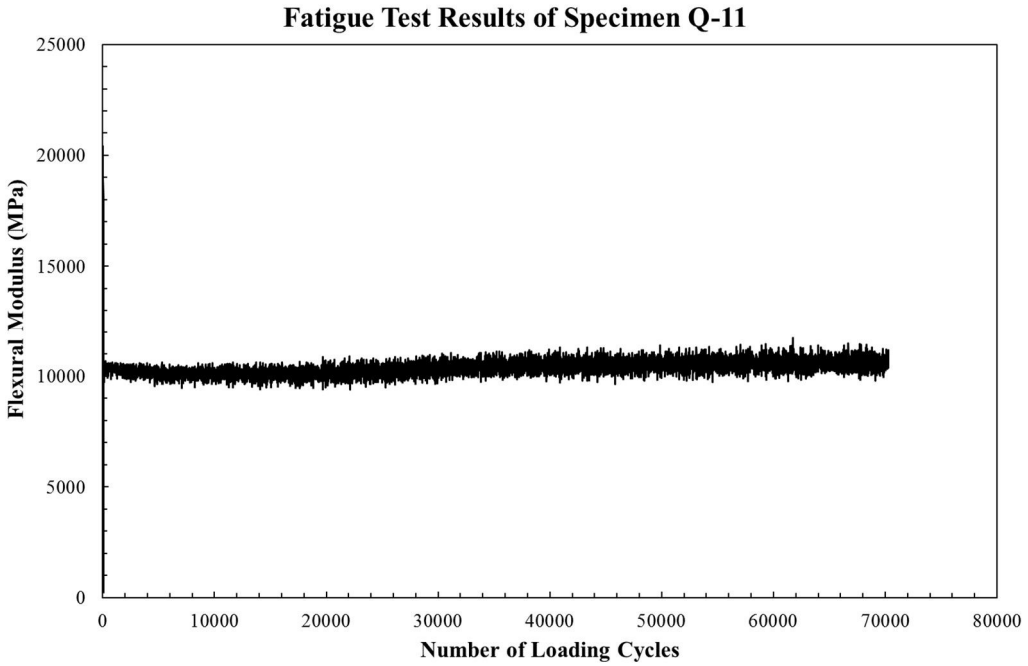
Fatigue Test Results of Specimen Q-11
Flexural Modulus (MPa)
25000
20000
15000
10000
5000
0
0
10000
20000
30000
40000
50000
60000
70000
80000
Number of Loading Cycles

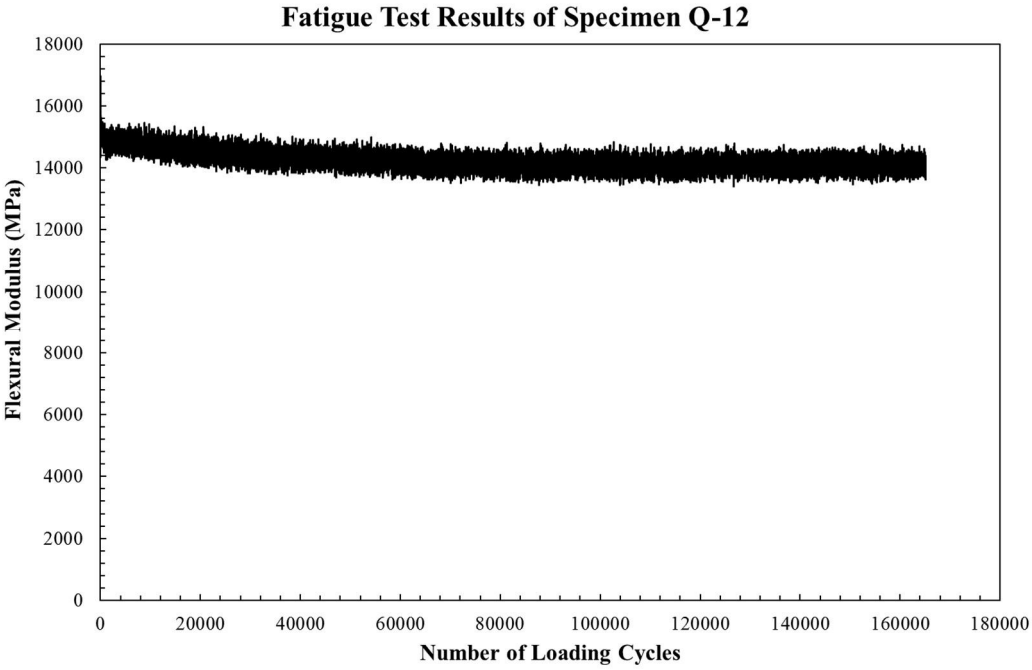
Fatigue Test Results of Specimen Q-12
Flexural Modulus (MPa)
18000
16000
14000
12000
10000
8000
6000
4000
2000
0
0
20000
40000
60000
80000
100000
120000
140000
160000
180000
Number of Loading Cycles

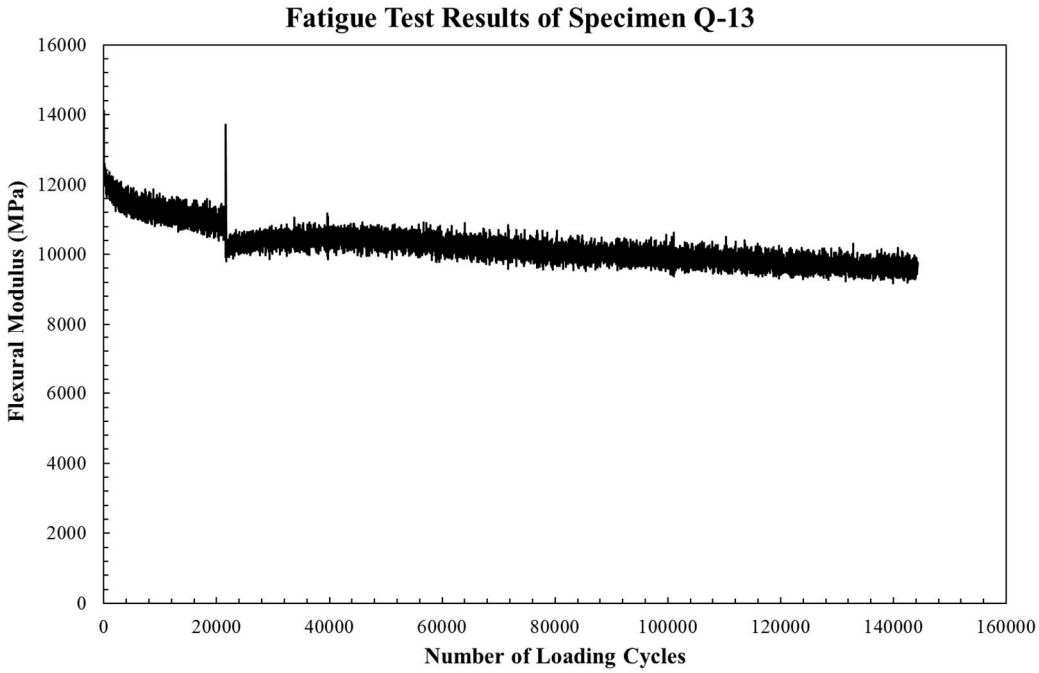
Fatigue Test Results of Specimen Q-13
Flexural Modulus (MPa)
16000
14000
12000
10000
8000
6000
4000
2000
0
0
20000
40000
60000
80000
100000
120000
140000
160000
Number of Loading Cycles

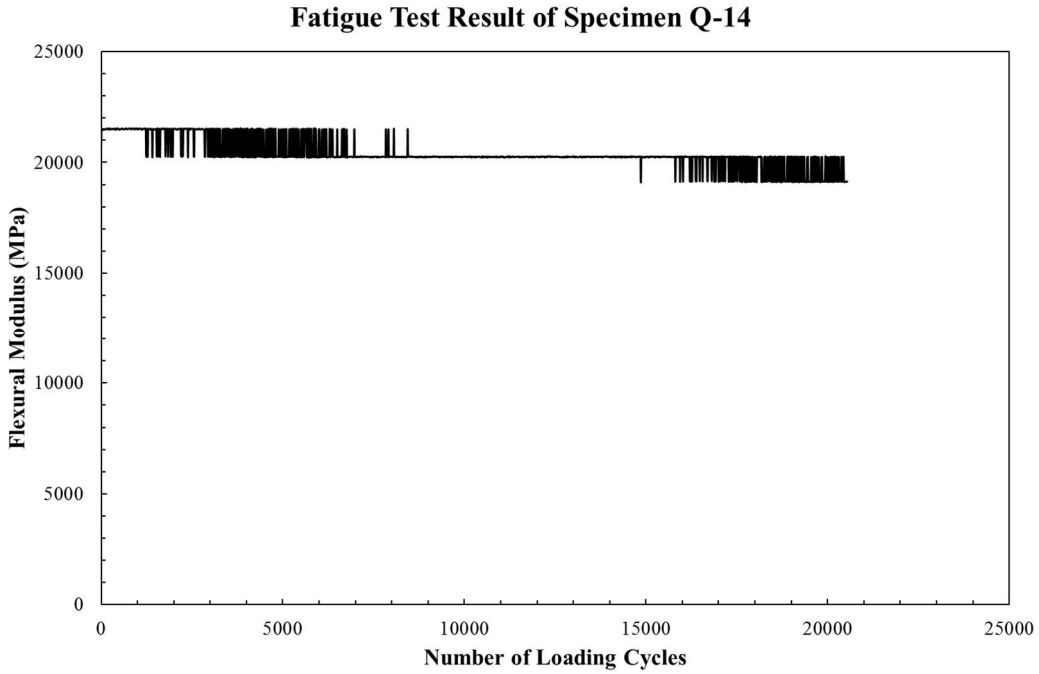
Fatigue Test Result of Specimen Q-14
Flexural Modulus (MPa)
25000
20000
15000
10000
5000
0
0
5000
10000
15000
20000
25000
Number of Loading Cycles

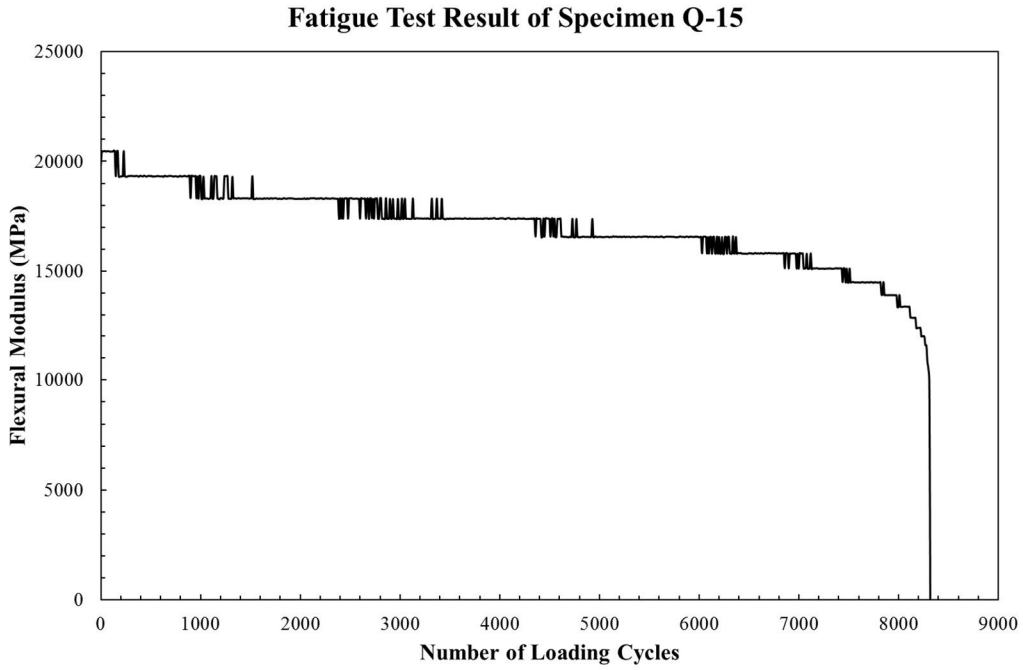
Fatigue Test Result of Specimen Q-15
Flexural Modulus (MPa)
25000
20000
15000
10000
5000
0
0
1000
2000
3000
4000
5000
6000
7000
8000
9000
Number of Loading Cycles

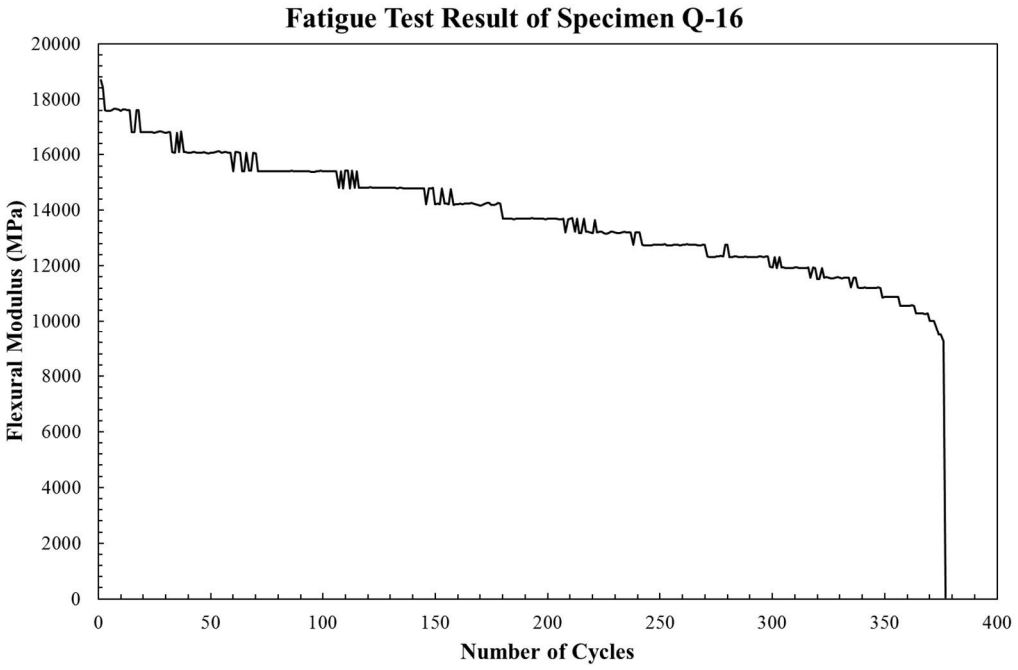
Fatigue Test Result of Specimen Q-16
Flexural Modulus (MPa)
20000
18000
16000
14000
12000
10000
8000
6000
4000
2000
0
0
50
100
150
200
250
300
350
400
Number of Cycles

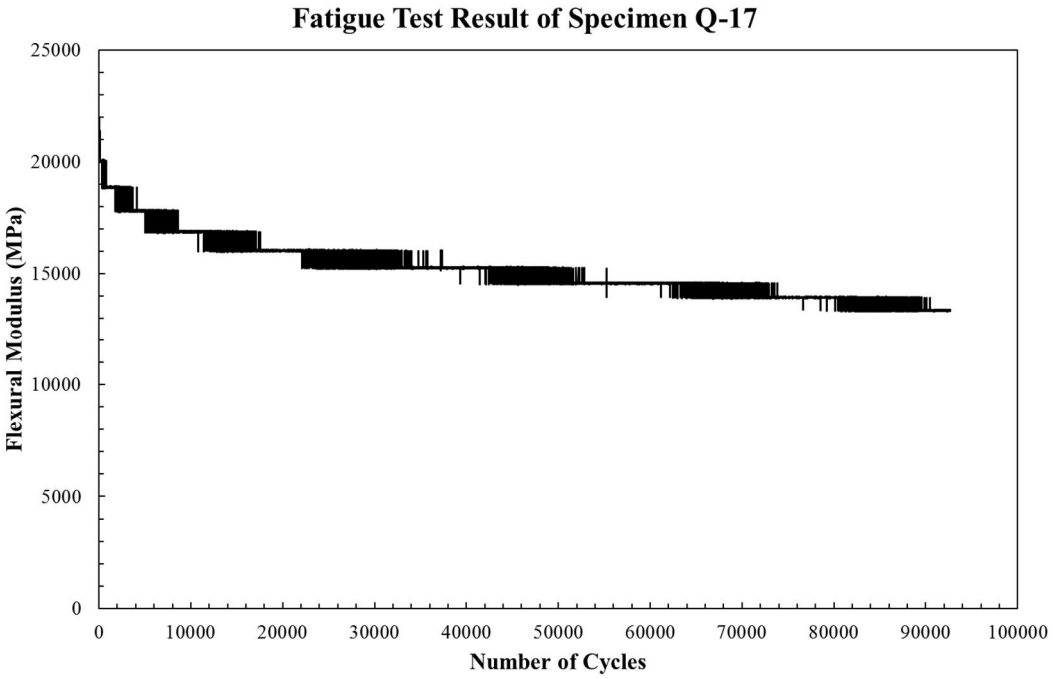
Fatigue Test Result of Specimen Q-17
Flexural Modulus (MPa)
25000
20000
15000
10000
5000
0
0
10000
20000
30000
40000
50000
60000
70000
80000
90000
100000
Number of Cycles

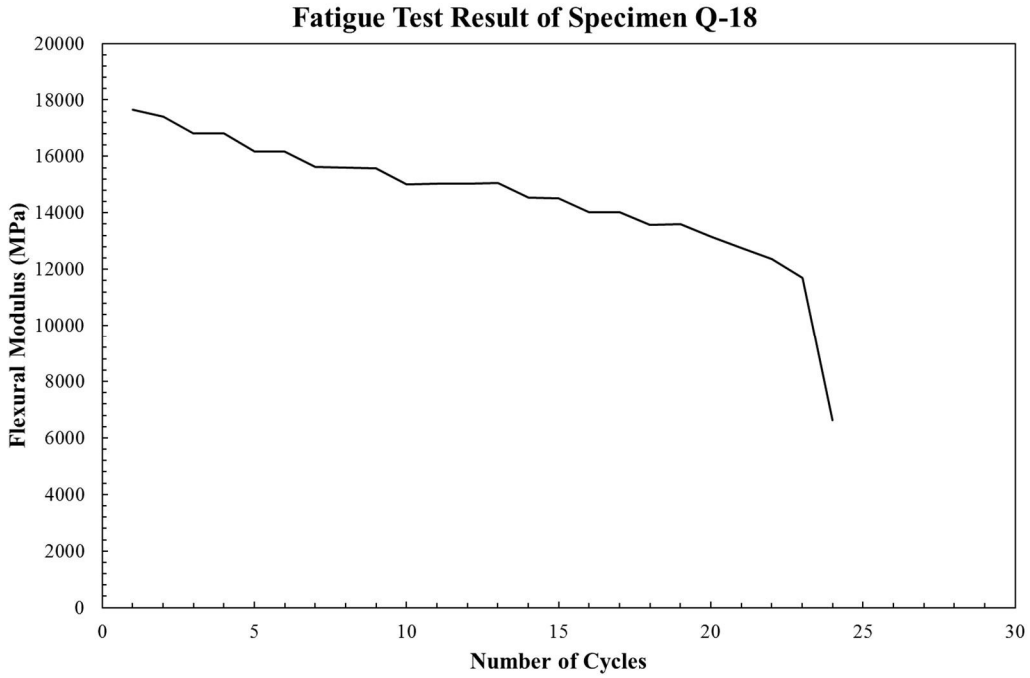
Fatigue Test Result of Specimen Q-18
Flexural Modulus (MPa)
20000
18000
16000
14000
12000
10000
8000
6000
4000
2000
0
0
5
10
15
20
25
30
Number of Cycles

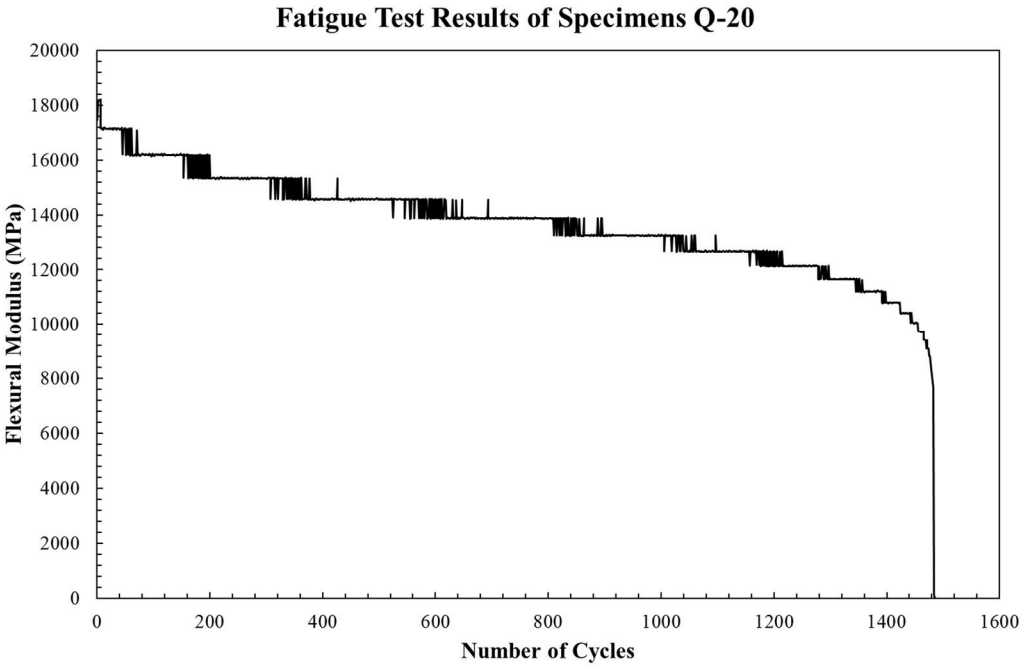
Fatigue Test Results of Specimens Q-20
Flexural Modulus (MPa)
20000
18000
16000
14000
12000
10000
8000
6000
4000
2000
0
0
200
400
600
800
1000
1200
1400
1600
Number of Cycles

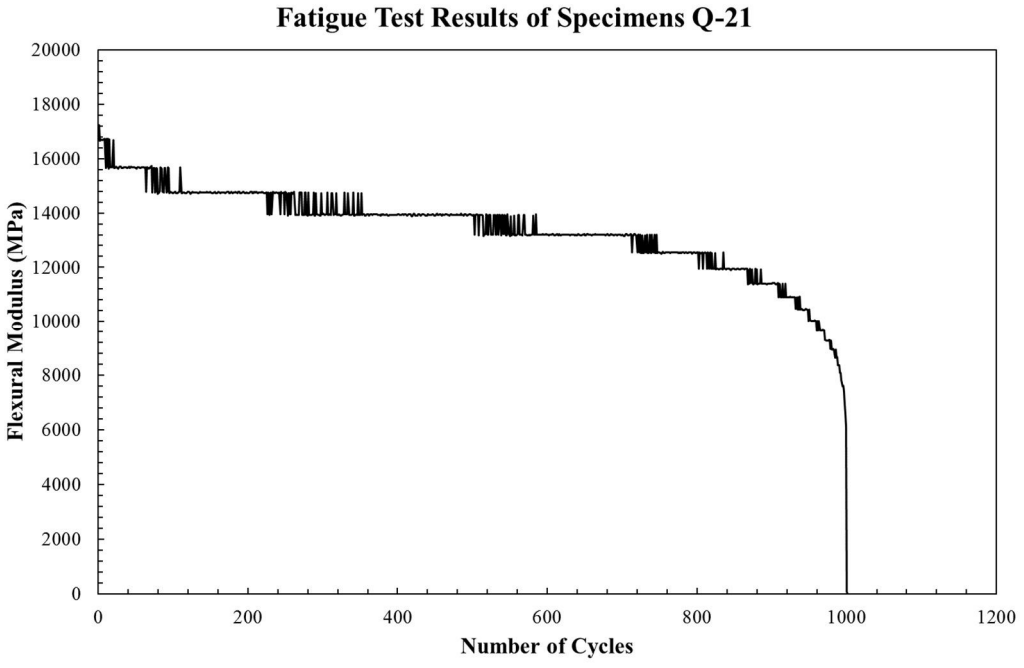
Fatigue Test Results of Specimens Q-21
Flexural Modulus (MPa)
20000
18000
16000
14000
12000
10000
8000
6000
4000
2000
0
0
200
400
600
800
1000
1200
Number of Cycles

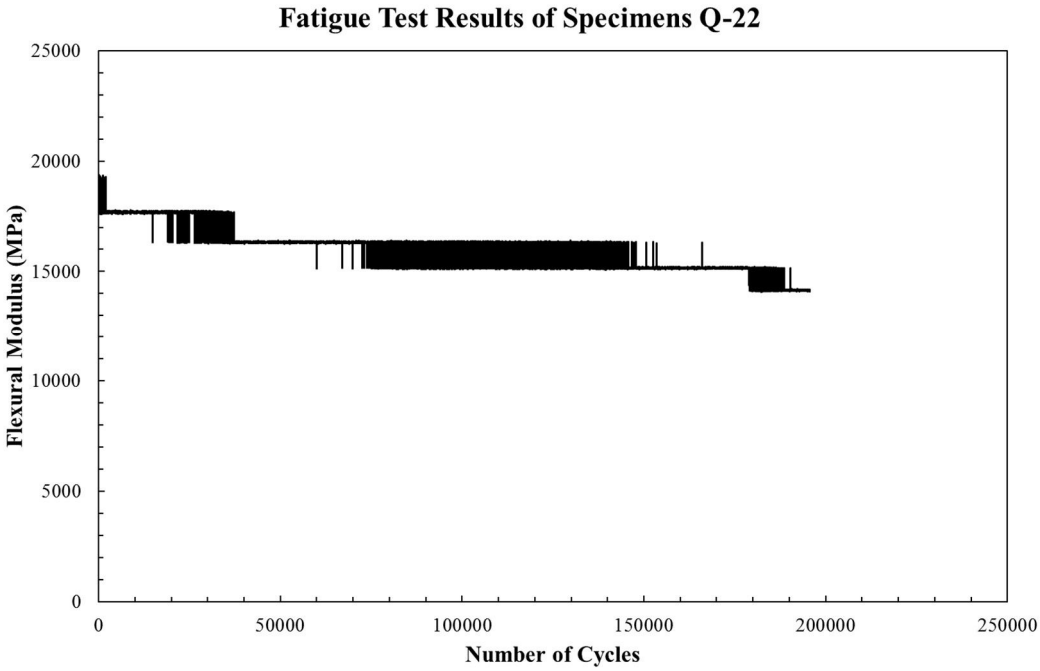
Fatigue Test Results of Specimens Q-22
Flexural Modulus (MPa)
25000
20000
15000
10000
5000
0
0
50000
100000
150000
200000
250000
Number of Cycles

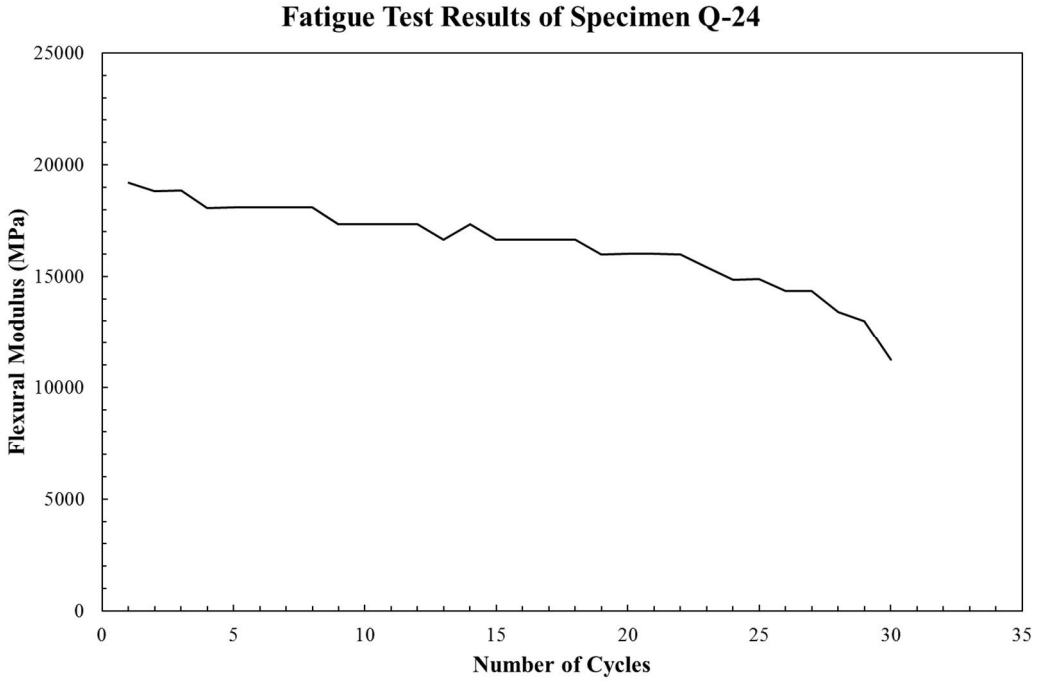
Fatigue Test Results of Specimen Q-24
Flexural Modulus (MPa)
25000
20000
15000
10000
5000
0
0
5
10
15
20
25
30
35
Number of Cycles

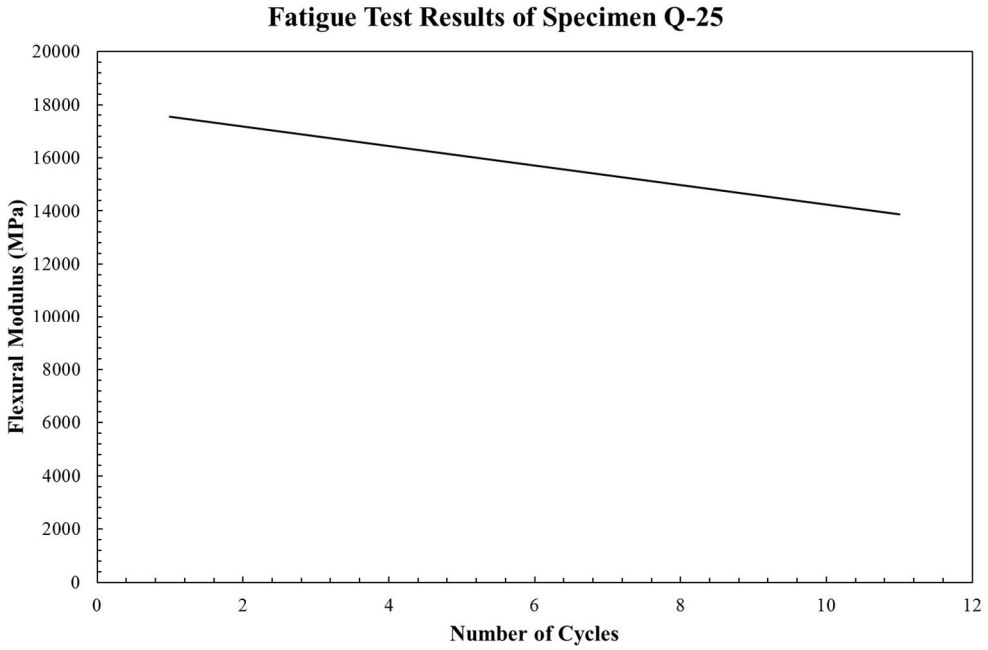
Fatigue Test Results of Specimen Q-25
Flexural Modulus (MPa)
20000
18000
16000
14000
12000
10000
8000
6000
4000
2000
0
0
2
4
6
8
10
12
Number of Cycles

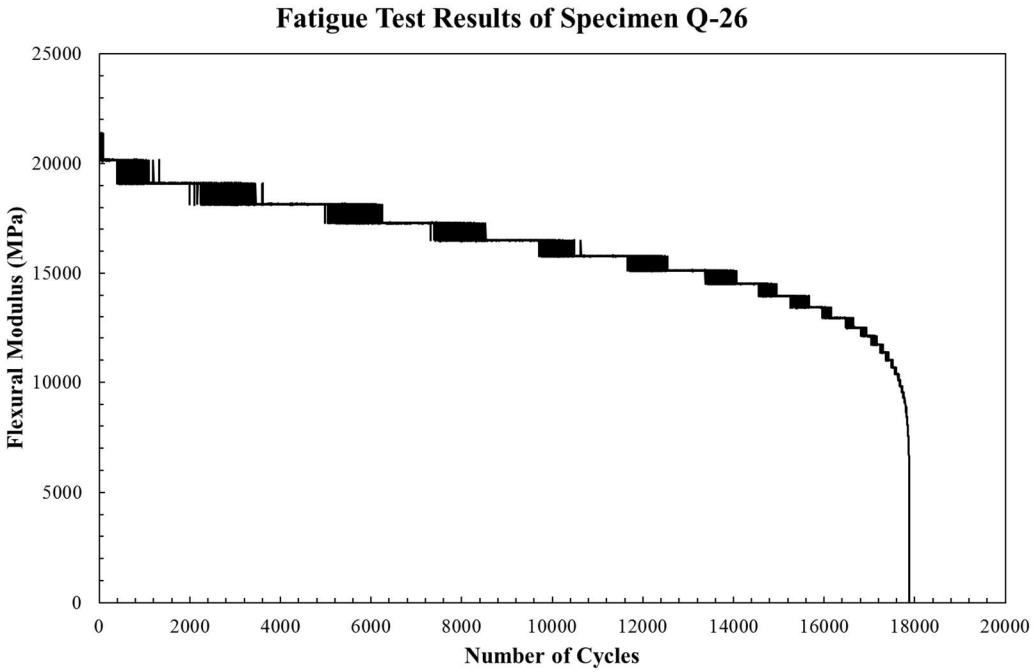
Fatigue Test Results of Specimen Q-26
Flexural Modulus (MPa)
25000
20000
15000
10000
5000
0
0
2000
4000
6000
8000
10000
12000
14000
16000
18000
20000
Number of Cycles

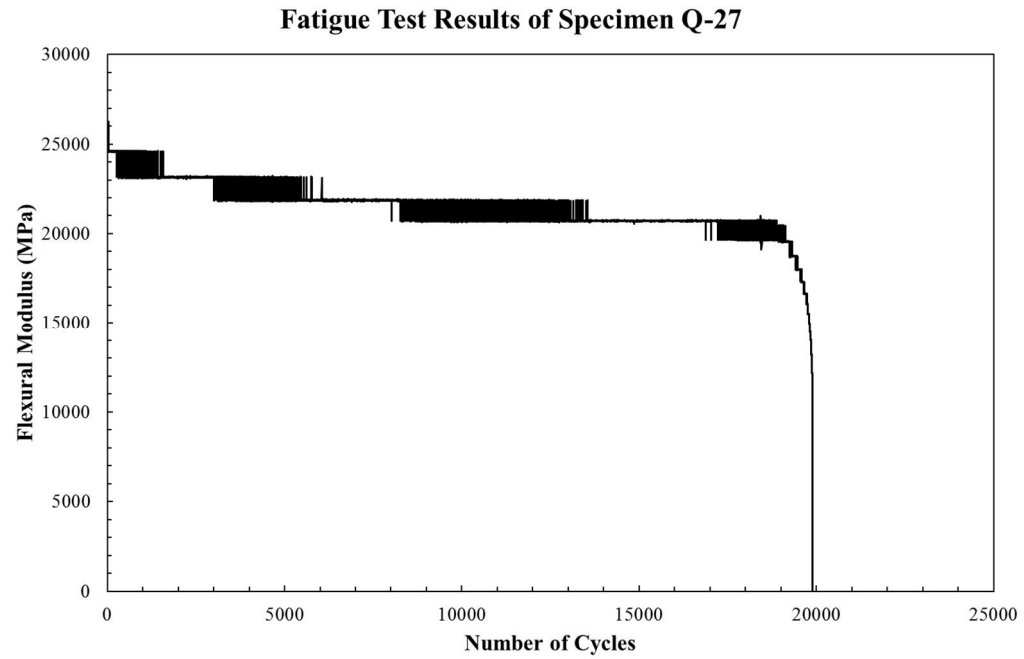
Fatigue Test Results of Specimen Q-27
Flexural Modulus (MPa)
30000
25000
20000
15000
10000
5000
0
0
5000
10000
15000
20000
25000
Number of Cycles

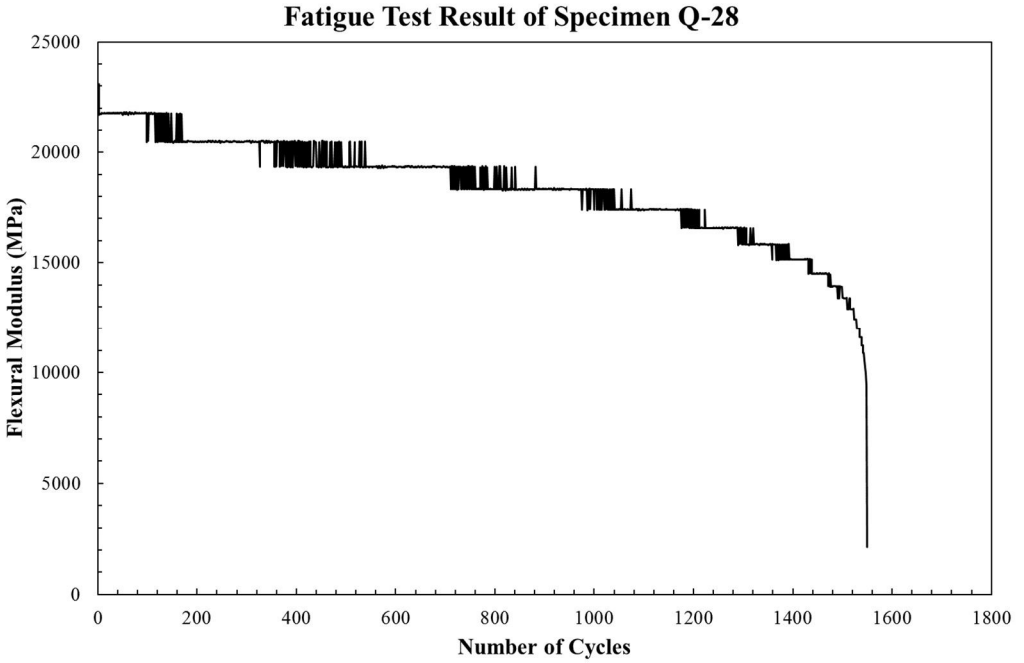
Fatigue Test Result of Specimen Q-28
Flexural Modulus (MPa)
25000
20000
15000
10000
5000
0
0
200
400
600
800
1000
1200
1400
1600
1800
Number of Cycles